**The Dissertation Committee for John Austin Mohan Certifies that this is the approved version of the following dissertation:**

# LINKING FISH MIGRATION AND HYPOXIA EXPOSURE TO TROPHIC ECOLOGY USING NATURAL CHEMICAL TAGS

**Committee:**

Benjamin D. Walther, Supervisor

James W. McClelland

G. Christopher Shank

Peter Thomas

Karin Limburg

# LINKING FISH MIGRATION AND HYPOXIA EXPOSURE TO TROPHIC ECOLOGY USING NATURAL CHEMICAL TAGS

**by**

**John Austin Mohan, B.S., M.S.**

**Dissertation**

Presented to the Faculty of the Graduate School of

The University of Texas at Austin

in Partial Fulfillment

of the Requirements

for the Degree of

**Doctor of Philosophy**

**The University of Texas at Austin**

**August 2015**

# Dedication

This work is dedicated to my parents, Francis and Stella Mohan, and my family who have always provided unending support, love, and encouragement throughout my life and academic career. I am truly honored to join the rank of doctors in my family including my father Francis, M.D., my sister Elizabeth, M.D., and brother David, Ph.D. I also dedicate this work to my friend, colleague and partner Stephanie Denise Smith for always keeping me well nourished, remaining patient and always listening, taking me on epic traveling adventures, and always believing in my scientific abilities.

# Acknowledgements

I am much obliged for the assistance provided by the numerous people that have made this research possible. My advisor, Dr. Benjamin Walther, thank you for your constant guidance, training and confidence in my abilities and for taking me as your first PhD student. Thanks to my committee members Dr. Peter Thomas, for letting me participate on your research cruises and laboratory experiments, Dr. Chris Shank for collecting water samples and always remaining excited about my research, and Dr. Jim McClelland and Dr. Karin Limburg, for your expert advice and direction. I am grateful for all the collaborators that inspired me to expand my research interests including Saydur Rahman, Nathan Miller, Sharon Herzka, Tara Connelly, Stephanie Smith, and Carlos Diaz-Gil. Many thanks to the entire FAML family past and present including Venus Mills, Cindy Faulk, Jeff Kaiser, Dr. Lee Fuiman, Dr. Joan Holt, Andreau Blanco, Avier Montalvo, Lisa Havel, Rick Kline, Rasmus Ern, and Matt Seeley. Many undergrad researchers were involved in various aspects of this research including Keya Jackson, Ben Staton, Brade Hendrickson, Joseph Ripley, Brandon Kohler, Victoria Leonard, and Ava Ibanez. Finally, I am very thankful for the many friends I have made in Port Aransas, especially the Board House Surf and Skate Shop/Team and Taco Tuesday Crew, for always maintaining the PhDude's stoke level. Texas Parks and Wildlife Department and NOAA SEAMAP provided additional samples for this work.

The Environmental Protection Agency Science to Achieve Results (EPA-STAR) fellowship (FP 91748701) and the Mission Aransas National Estuarine Research Reserve (MANERR) Graduate Research Assistantship provided funding for this research.

# Linking fish migration and hypoxia exposure to trophic ecology using natural chemical tags

John Austin Mohan, Ph.D.

The University of Texas at Austin, 2015

Supervisor: Benjamin D. Walther

Natural tags in fish reveal life history information that includes migration pathways and dietary sources. The chronological and geochemical properties of otoliths record changes in fish growth and reflect ambient salinity gradients, allowing reconstruction of coastal and estuarine movements. Stable isotopes of carbon and nitrogen in liver and muscle tissues provide dietary histories over short and long time scales, respectively. In order to apply natural tags, validation studies are needed that examine incorporation dynamics of elements and isotopes, such as the effects of physiology and growth on element uptake and isotope turnover, and describe chemical gradients of dissolved elements over time and space. Along the coast of Texas, dissolved Sr:Ca and Ba:Ca varied predictably with salinity over broad geographic and annual time scales. Tissue isotope turnover experiments revealed faster turnover of liver compared to muscle, offering short- and long-term dietary indicators. Using established estuarine ion gradients and tissue turnover rate estimates, estuarine ingress and habitat residence patterns were examined in Atlantic croaker collected from positive, metastable, and negative estuary types, encompassing the north-south Texas coast. Migration patterns varied depending on local salinity regimes, with strong regional gradients exhibited in both otolith elements and tissue isotopes. Fine scale between bay movements were

detected using differences in liver-muscle $\delta^{13}C$ values as indicators of tissue equilibrium status and time since habitat shift. In the northern Gulf of Mexico, the long-term sublethal effects of seasonal hypoxia on fish populations remain unclear, due to unknown exposure histories. Hypoxic redox conditions promote release of dissolved $Mn^{2+}$ from the sediment, thus otolith Mn:Ca profiles can reflect lifetime hypoxia exposure. Lab experiments demonstrated a minimal influence of physiology on element uptake in response to hypoxia. Field studies in the northern Gulf of Mexico quantified estuarine habitat use using otolith Ba:Ca and coastal hypoxia exposure using otolith Mn:Ca, and assessed isotope trophic niche area using muscle tissue $\delta^{15}N$ and $\delta^{13}C$ values. Isotope niche area was similar between coastal and hypoxia exposed fish, suggesting trophic resilience of Atlantic croaker to seasonal hypoxia. This research provides a novel multi-proxy approach; using lab and field validated natural tags for linking migration and environmental exposure histories to trophic ecology in a marine fish.

# Table of Contents

# List of Tables

# List of Figures

# PRELUDE

Natural tag approaches are frequently utilized to characterize major life history events in the lives of fishes. Migratory fish transverse geochemical and isotopic gradients and assimilate dissolved elements and isotopes in chronologically accreted calcified structures (i.e. otoliths), and regenerated soft tissues (i.e muscle and liver). These natural 'tags' offer important insight to lifetime salinity histories and recent dietary experiences. Information regarding habitat use and food web dynamics is critical for resource managers, conservation efforts and designation of Essential Fish Habitat (Rosenberg et al. 2000).

Many marine fish species exhibit bipartite life cycles, with juvenile life stages that rely on coastal and estuarine habitats as important nursery grounds (Able 2005). Understanding of nursery habitat value has evolved over the past few decades, with an initial attention on biomass transfer from discreet juvenile habitat areas to offshore adults habitats via migration (Beck et al. 2001). More recent attention has focused on ecosystem complexities (i.e. connectivity, food webs, resource dynamics) that involve spatial and temporal variation (Nagelkerken et al. 2013; Sheaves et al. 2014). Thus, emphasis has shifted from identifying discreet areas as nursery *habitat*, to a focus on characterizing nursery *function* and quantifying ecological processes. Understanding true nursery value is critically important, in face of increasing human pressure on coastal and estuarine habitats that includes changes in land use and cover, alteration of river flows, pollution and eutrophication (Greene et al. 2015).

Reconstructing environmental and dietary histories of fish can be achieved with natural tags including otolith chemistry and tissue stable isotope analysis. Natural tags are imparted on all individuals in populations and therefore do not suffer from limitations of

conventional tagging techniques that include tag loss, altered fish behavior, cost, or need for recapture. Otolith chemistry can provide information on natal origins (Walther et al. 2008), movement across salinity gradients (Elsdon et al. 2008), or exposure to hypoxic redox conditions (Limburg et al. 2014). Accurate interpretation of otolith chemistry proxies requires understanding potential vital effects, such as physiology (Izzo et al. 2015) or reproduction (Kalish 1991; Sturrock et al. 2014), which can be quantified using controlled laboratory studies. Stable isotopes of carbon provide information about dietary contributions from different sources of primary producers such as benthic versus pelagic production (France 1995) and terrestrial versus marine production (Fry 2002). Nitrogen stable isotopes are useful for identifying trophic level (Post 2002), but also can reveal anthropogenic nutrient enrichment in food webs (McClelland et al. 1997). Proper understanding of stable isotope trophic proxies also requires validation studies in the lab that constrain isotope assimilation rates (tissue turnover) and dynamics (lipid and diet quality effects). Additionally, using a multi-proxy approach increases reliability of individual proxies when agreement is detected between otolith elements and tissue isotopes.

This dissertation seeks to advance the applicability of natural tag approaches by *i*) characterizing physicochemical gradients over time and space in **Chapter 1**; *ii*) investigating element and isotope incorporation dynamics in controlled lab experiments in **Chapter 2** and **Chapter 4**; *iii*) apply information gathered from validation studies to investigate *iv*) juvenile Atlantic croaker nursery habitat use along the coast of Texas in **Chapter 3**, and *v*) the effects of seasonal hypoxia exposure on Atlantic croaker trophic dynamics, in the northern Gulf of Mexico in **Chapter 5**.

Atlantic croaker *Micropogonias undulatus* was chosen as a model species, because it is a ubiquitous estuarine dependent species found throughout Texas estuaries

and coastal Gulf of Mexico. Migration patterns of juvenile Atlantic croaker have been studied using otolith chemistry in estuaries along the northeast US coast (Thorrold et al. 1997; Thorrold and Shuttleworth 2000; Hoover et al. 2012) and croaker responses to hypoxia exposure has been previously examined in both lab and field based studies in the northern Gulf of Mexico 'Dead Zone' (Craig and Crowder 2005; Eby et al. 2005; Thomas and Rahman 2009a; Thomas and Rahman 2012; Craig 2012). Strong regional climatic gradients along the Texas coast generate various estuarine types ranging from positive in the north to negative and hyper saline in the south, representing a dynamic physicochemical environment upon which to examine fish migration and habitat use. This work employs a multi-proxy approach by combining otolith chemistry and tissue-specific stable isotope analysis, to link migration with trophic ecology to assess nursery habitat value in dynamic Texas estuaries, and examine trophic consequences of sub-lethal hypoxia exposure in the seasonally hypoxic 'Dead Zone'.

# CHAPTER 1: SPATIOTEMPORAL VARIATION OF TRACE ELEMENTS AND STABLE ISOTOPES IN SUBTROPICAL ESTUARIES: REGIONAL LOCAL AND SEASONAL SALINITY-ELEMENT RELATIONSHIPS

Published as: Mohan, J.A., and B.D. Walther. 2015. Spatiotemporal variation of trace elements and stable isotopes in subtropical estuaries: II. Regional, local, and seasonal salinity-element relationships. *Estuaries and Coasts* 38:769-781. Reprinted with permission.

Author contributions: J.A.M. collected and analyzed the data and wrote the manuscript; B.W.D. provided data interpretation and editorial advice.

## ABSTRACT

Trace elements and stable isotopes are commonly used in chronologically formed biominerals as proxies of temperature and/or salinity in estuarine and marine environments. To accurately use the chemistry of biominerals as salinity proxies, understanding the consistency of dissolved element-salinity relationships across spatiotemporal scales is essential. We examined relationships between dissolved Ba:Ca, Sr:Ca, Mg:Ca, Mn:Ca, $\delta^{18}O$ and salinity on regional, local, and seasonal scales in the lower portions of subtropical estuaries (salinities 15-42 ppt) of Texas, including locations where seasonal alternations between negative and positive estuaries can occur. Across all spatiotemporal scales, Ba:Ca displayed a negative linear relationship within the sampled salinity range and was elevated at sites furthest from the ocean and lowest at locations closest to the Gulf of Mexico. This pattern remained consistent as the metastable estuary switched from negative to positive after a rain event. On regional scales, $\delta^{18}O$ displayed a positive linear relationship with salinity and was strongly related to evaporation rates. On local and seasonal scales, evaporation enriched $\delta^{18}O$ at upper enclosed estuarine sites

and this pattern was consistent over time including periods of negative estuary conditions. Dissolved Sr:Ca and Mg:Ca varied linearly with salinity on regional scales, but displayed minimal variation across temporal scales within an estuary. High variability in dissolved Mn:Ca-salinity relations was found at all spatiotemporal scales, with localized episodic peaks of Mn:Ca possibly due to sediment disturbance. Although dissolved Ba:Ca and $\delta^{18}O$ were not predictably related to salinity on local scales, consistent up-estuary enrichment and lower-estuary depletion make these two constituents reliable proxies for animal movements across the ocean-estuary gradient as recorded in chronologically formed biominerals.

## 1.1 INTRODUCTION

The physicochemical properties of estuaries are often highly dynamic and can exhibit considerable temporal and spatial variation. The mixing of fresh river water and seawater results in gradients of salinity, ionic strength, pH, dissolved organic carbon (DOC), nutrient concentrations, and alkalinity, all which influence the distribution and behavior of many trace elements and isotope ratios (Benoit et al. 1994; Fry 2002). The concentrations of many trace elements in freshwater end members are controlled by the weathering of terrigenous minerals with rock composition and age influencing element type and abundance (Middelburg et al. 1988; Negrel et al. 1993). In the estuarine mixing zone, sorption-desorption processes may alter the concentrations of certain elements. Removal processes of trace elements include complexation of metals with organic ligands (Wen et al. 1999) while sediment resuspension due to tidal action, storms, or biological activity may supply elements to either dissolved or particulate pools (Zhang 1995; Zwolsman and van Eck 1999). While some elements display conservative

behavior across salinity gradients with linear salinity-element relationships that result from simple dilution between two end-members (Fry 2002), non-conservative (non-linear) salinity-element relationships may occur if estuarine mixing is influenced by a third end member or by biogeochemical processes and/or anthropogenic activities (Paucot and Wollast 1997) that supply or remove dissolved constituents resulting in uncoupling of predictive relationships to salinity (Morris et al. 1978).

Salinity-constituent relationships have been examined in several estuarine systems, and the behavior of individual constituents depends strongly on the degree to which additions, removals or isotopic fractionation alters constituent values across the estuarine gradient. Strontium, magnesium, and calcium often exhibit conservative behavior and increase linearly with salinity in most estuaries (Dorval et al. 2005; Gillanders and Munro 2012), however exceptions do occur where freshwater endmembers (i.e. strontium), may be higher in freshwater compared to marine endmembers (Kraus and Secor 2004). Curvilinear behavior for these constituents may also result when, for instance, groundwater addition introduces a third-endmember at intermediate salinities (Walther and Nims 2015). Dissolved barium typically displays non-conservative behavior with high concentrations at low salinities due to desorption from suspended particulate matter in the estuarine mixing zone, normally followed by linear mixing with salinity for the remainder of the gradient (Hanor and Chan 1977; Coffey et al. 1997). Manganese is redox-sensitive and the dissolved species ($Mn^{2+}$) shows high variability due to release from sediment reduction of organic matter in suboxic and anoxic conditions and vertical supply to the water column (Trefry and Presley 1982; Klinkhammer and McManus 2001). Decreases in pH and physical disturbances of the sediments affect release of Mn to a much greater degree than changes in dissolved oxygen or salinity (Atkinson et al. 2007) and this sensitivity to

environmental parameters often leads to high seasonal and spatial variability in concentrations (Shiller 1997; Dorval et al. 2005; Kowalski et al. 2012). Finally, $\delta^{18}O$ stable isotope values in estuarine waters are influenced by fractionation associated with precipitation and evaporation processes as well as the composition of the freshwater endmember, and often show strong linear relationships with salinity (Ingram et al. 1996; Cooper et al. 1997).

Estuary-to-ocean salinity gradients in subtropical Texas estuaries can fluctuate temporally due to seasonal differences in freshwater inputs associated with precipitation events (Flint 1985; Nielsen-Gammon et al. 2005). On a large spatial scale, the coast of Texas displays a north-south latitudinal climatic and hydrologic gradient. Increased rainfall and freshwater inflow occur in the northern estuaries, while southern estuaries experience half the amount rainfall and orders of magnitude less freshwater inflow compared to northern estuaries (Tolan 2007). Salinity regimes of estuaries along the north-south Texas coast are characterized as positive, metastable, and negative. North-Texas estuaries receive consistent rainfall and fluvial freshwater inputs and thus remain positive year-round, while in south-Texas estuaries, evaporation greatly exceeds freshwater inputs resulting in hypersaline conditions and negative estuaries, such as the Laguna Madre (Tolan 2007). Central-Texas estuaries, such as the Mission–Aransas, can alternate between positive and negative regimes throughout the year due to seasonal precipitation events and can be considered metastable estuaries (Head 1985).

Hypersaline conditions (salinity > 35 ppt) and reverse estuary behavior can potentially disrupt expected constituent-salinity relationships. For instance, Gillanders and Munro (2012) reported that dissolved barium concentrations within the Australian Coorong Lagoon decreased from fresh water to marine salinities, and then dramatically increased in hypersaline waters with salinities above 40 ppt, a previously undocumented

phenomenon. Therefore, more studies on constituent-salinity relationships in hypersaline conditions are necessary, especially for dissolved elements that are typically used in biogenic calcified structures as salinity proxies (Diouf et al. 2006; Gillanders and Munro 2012). If linear behavior was disrupted due to hypersalinity, then predictive relationships of dissolved elements to salinity would not hold, leading to inaccurate interpretations of salinity proxies, such as the calcified earstones of fish (otoliths) which are commonly used to estimate migratory fish movement across salinity gradients.

In this study, we investigated the consistency of element-salinity relationships across local, regional, and seasonal scales in subtropical Texas estuaries. This study examined constituent-salinity relationships in three contexts. First, relationships were evaluated across three separate estuaries across the entire Texas coast, including a positive, metastable and negative estuary to determine regional patterns. Second, relationships were evaluated within each of the three estuary types to determine local patterns. Third, constituents were monitored within the metastable estuary at several fixed stations over a span of 12 months to determine seasonal patterns. Over the duration of the 12-month study, the salinity regime in the metastable estuary reversed from a negative to a positive regime after heavy spring precipitation, allowing us to examine the consistency of element-salinity relationships after an elevated freshwater inflow period. In the metastable estuary, environmental and climatic time series were examined for correlations to dissolved elemental and isotopic constituents to explore possible mechanisms driving the observed seasonal patterns. This project focused on relationships observed for the lower estuarine regions with salinities >15 ppt given that the dynamics of the freshwater end members are addressed in a companion paper (Walther and Nims 2015).

## 1.2 METHODS

### 1.2.1 Study area and environmental data

To examine coast-wide geographic variation in dissolved chemistry, replicate samples were collected from five sites within Galveston Bay (GB, a positive estuary), the Mission-Aransas estuary (MA, a metastable estuary), and the Laguna Madre (LM, a negative estuary; Fig. 1.1). Each estuary was sampled in July 2012 within 10 consecutive days to reduce temporal variation and make spatial comparisons between estuaries. To assess temporal variation across the seasons, the Mission-Aransas estuary was sampled monthly from October 2011 through September 2012 at five fixed stations that form the Mission-Aransas National Estuarine Research Reserve System Wide Monitoring Program (MANERR SWMP; Fig. 1.1). At each station, a YSI 600XL sonde measured temperature, salinity, dissolved oxygen, pH, and water samples were collected for trace elements and isotopes as described below. The environmental parameters were measured to investigate alternative (i.e. other than salinity) influences on element behavior. For example, phytoplankton may influence dissolved element behavior through biological uptake or absorption/desorption processes (Stecher and Kogut 1999). Chlorophyll *a* samples were passed through Whatman GF/F filters and extracted with 90% acetone and concentrations were determined using a Turner Designs Trilogy Fluorometer as described by Mooney & McClelland (2012). Daily cumulative precipitation data recorded at the Copano East (CE) site were downloaded from the NOAA NERR Centralized Data Management Office website http://cdmo.baruch.sc.edu on 8/6/2013. Mean monthly precipitation values were calculated from these data for graphical display. Mean monthly discharge data was downloaded from U.S. Geological Survey website http://waterdata.usgs.gov/nwis for gauge station 8189500 in Refugio, TX on the Mission River that drains into Copano Bay, for gauge station 8188500 in the San Antonio River,

and gauge 8176500 in the Guadalupe River. These three river gauge stations were selected as they characterize the dominant contributors to water inflow in the Mission-Aransas estuary from the north (Mission River) and the east (San Antonio & Guadalupe rivers) (Ward 2010). Mean monthly lake evaporation data was downloaded from the Texas Water Development Board website (http://www.twdb.texas.gov/surfacewater/conditions/evaporation/index.asp) from indexed regions 813 (Galveston Bay), 910 (Mission-Aransas), and 1010 (Laguna Madre). Mean monthly evaporation rates were compared between the three regions from September 2011 through October 2012. July 2012 evaporation rates were then plotted against regional mean $\delta^{18}O$ values in July.

### 1.2.2 Water sample collection

Surface water samples were obtained using a portable sampler (Barnant Company) equipped with a peristaltic pump (Masterflex Easy Load L/S, Cole Parmer) and acid-washed tubing (Masterflex C-Flex L/S 17) deployed at approximately 0.5 m depth from the leeward side of a small fiberglass boat. Sample water was collected in 30 ml acid-washed polytetrafluorethylene (PTFE) syringes (Norm-Ject) that were rinsed with three sample volumes before being filtered into 30 ml acid-washed LDPE Nalgene bottles with acid-washed 0.45 μm and 0.2 μm PTFE filters (Sartorius Stedim Minisart SRP 25). Filtered water was fixed to pH <2 with trace metal grade nitric acid (Aristar Ultra) and refrigerated until analysis. Oxygen stable isotope samples were syringe filtered (0.45 and 0.2 μm) into 30 ml amber glass vials (Fisherbrand) that were filled to overflowing to eliminate headspace and refrigerated until analysis. Ultrapure (18.2

MΩ·cm) water was filtered in the field as described above to serve as method blanks during laboratory analysis.

### 1.2.3 Water sample analysis

All samples were analyzed at the University of Texas Jackson School of Geosciences. Trace elements $^{24}Mg$, $^{40}Ca$, $^{55}Mn$, $^{88}Sr$, and $^{137}$ Ba were quantified using an Agilent 7500ce quadrupole inductively coupled plasma mass spectrometer (ICP-MS) run in solution mode. Samples were diluted 100X by weight using 2% ultrapure trace metal grade nitric acid. A sub-set (N=12) of samples were spiked with an internal multi-element standard solution to assess mean spike recoveries (mean 98%) and monitor instrument drift. An external standard reference material NIST 1643e diluted 10x was used to determine accuracy and was between 5-10% for all elements. Elemental counts were converted to concentrations using internally spiked standards and then converted to molar element:Ca ratios. Stable oxygen isotopes were analyzed with a Thermo Electron 253 isotope ratio mass spectrometer (IRMS) coupled to a Gasbench II. One milliliter of sample water was equilibrated with 3000 ppmV $CO_2$ in helium for 24 hours at 25 °C and the equilibrated headspace $CO_2$ was sampled in continuous flow. Laboratory standards were calibrated against Vienna Standard Mean Ocean Water (VSMOW) and reported $\delta^{18}O$ values were reproducible within 0.05 ‰. Linear regression was used to investigate the strength of element-salinity relationships against the null hypothesis that the slope=0 at regional, local and seasonal scales. Local salinity-element regressions within a particular estuary represent small-scale mixing and dilution processes, which are different mechanisms compared to regional regressions, which depict larger-scale climatic controls, such as temperature, inflow, and evaporation. Regional lake evaporation data from July was plotted against $\delta^{18}O$ values to examine relationships. For the Mission-

Aransas annual dataset, Pearson correlations were compared between dissolved elements and physicochemical parameters (salinity, temperature, DO, Chl *a*) to investigate potential relationships. Evaporation rate data was excluded from the correlation analysis, because only a single regional value was available and not site-specific indices. The ship channel (SC) site was excluded from correlation analysis because it is primarily oceanic Gulf of Mexico water (Fig. 1.1C) and was missing data for January and February. Values of pH were missing from several sites and months and so were also excluded from correlations analysis.

## 1.3 RESULTS

### 1.3.1 Regional relationships

Water samples across all estuaries and locations sampled in July 2012 included salinities ranging from 15.7 to 43.8 ppt. Within each estuary, salinity ranges were Galveston Bay: 15.7-22.4, Mission-Aransas: 29-36.4, Laguna Madre: 42.2-43.8. For the regional scale comparison of constituents across all three estuaries, all element-salinity relationships were statistically significant and positive, except for expected negative relationship for Ba:Ca (Table 1.1; Fig. 1.2). Barium:Ca displayed the highest range in observed values across the salinity gradient, ranging from 5-150 μmol/mol, with a slope of -3.21±0.6 and an intercept of 175±21 μmol/mol (Table 1.1). The elemental ratios Sr:Ca and Mg:Ca exhibited minimal variation across the salinity range (~ 1 mmol/mol), but were strongly related to salinity and had similar slopes of approximately 0.03 (Table 1.1). Values of $\delta^{18}O$ ranged from -0.3 ‰ in Galveston Bay to 2.5 ‰ in Laguna Madre with a slope of 0.1±0.008 (Table 1.1). Notably, $\delta^{18}O$ values were most enriched at the southern Laguna Madre sampling sites, moderately enriched at Mission-Aransas, and

closer to typical Gulf of Mexico values (~0 ‰) in the northern Galveston Bay, corresponding to the average salinity ranges encountered during sampling within each estuary and regional evaporation rates in July (Fig. 1.3). Manganese:Ca showed high variability even within replicate samples, resulting in large error bars, but still displayed a significant positive relationship to salinity (Fig. 1.2).

### 1.3.2 Local relationships

Examining relationships on a local scale within each estuary, fewer elements displayed statistically significant linear relationships, likely due to restricted salinity ranges observed in each of the estuaries (Fig. 1.2). No significant relationships were detected in Laguna Madre, which was not surprising given that salinities only ranged from 42.2 to 43.8 ppt. Barium:Ca was significantly negatively related to salinity in both Galveston Bay (slope =-9.7±2.6; intercept=294±50) and Mission-Aransas (slope=-12.2±1.9; intercept=454±61 μmol/mol) (Table 1.1; Fig. 1.2). Strontium:Ca was not significantly related to salinity within any estuary, however Mg:Ca was significantly related to salinity in GB with a very similar slope and intercept compared to the regional regression (Table 1.1). Values of $\delta^{18}O$ displayed a negative statistically significant relationship to salinity in Mission-Aransas, however the negative relationship was driven by local evaporation and not salinity and thus the regression line is not plotted (Fig. 1.2). Significant relationships between Mn:Ca and salinity were negative in Galveston Bay and positive in Mission-Aransas (Table 1.1). Overall, the Mn:Ca - salinity regression parameters of slope and intercept were highly variable with large errors (SE) when comparing local to region regressions, and even local to local (Galveston Bay and Mission-Aransas) regressions (Table 1.1).

### 1.3.3 Seasonal relationships

Mean lake evaporation rates increased 3-fold from winter to summer, and regional evaporation rates consistently ranked Laguna Madre>Mission-Aransas>Galveston Bay during the summer (Fig. 1.3). From October to April, the Mission-Aransas was a negative estuary with higher salinities at Copano West, the site farthest inland from the ocean (Fig. 1.1; Fig. 1.4). Local precipitation gradually increased in the winter, after which a large rain event in April resulted in a 20-fold increase in Mission River discharge into Copano Bay (Fig. 1.5). Additionally the combined flow of the San Antonio and Guadalupe Rivers also peaked in February and March (Fig. 1.5). The earlier peak in flow from the San Antonio and Guadalupe Rivers was expected given their sensitivity to rainfall events across the entire watersheds that span significant portions of Texas. This punctuated rainfall and subsequent inflow effectively reversed Mission-Aransas back to a positive estuary from April through September (Fig. 1.4). Geographic differences in the influence of specific tributaries on salinity at certain sites were evident. For instance, salinity at the Mesquite Bay site began to decline in March concurrent with elevated inflow from the San Antonio and Guadalupe Rivers, whereas salinity at Copano East declined in April-May after the April peak in inflow from the Mission River. These patterns was expected given the close proximities of the Mesquite Bay and Copano East sites to the mouths of the Guadalupe or Mission river mouths, respectively. The elevated springtime discharge also increased pH from May to June at all sites except Ship Channel (Fig. 1.4). All sites had similar temperatures each month, with January exhibiting the lowest temperature of 15°C that increased each month until reaching a plateau in the summer at 29°C (Fig. 1.4). Dissolved oxygen was highest in December and gradually declined into the summer as temperatures increased (Fig. 1.4). Chlorophyll *a* displayed peaks in the following months and locations: January in Copano West, January and

March in Copano East; December and March in Mesquite Bay; April in all sites except Mesquite Bay. In May, Chl *a* deceased at all sites and remained low throughout the summer and fall compared to the winter and spring (Fig. 1.4).

Values of Ba:Ca showed a consistent up-estuary to ocean gradient, with rankings in Ba:Ca values of Copano West>Copano East>Mequite Bay>Aransas Bay>Ship Channel during all months of the year except January and February, when a distinct drop in values occurred at all sites (Fig. 1.6). Values of $\delta^{18}O$ were enriched above typical oceanic values and displayed an up-estuary to ocean gradient for all months except during May when values converged following the discharge event (Fig. 1.6). Strontium:Ca, Mg:Ca, and Mn:Ca exhibited limited variation throughout the year, except for a large spike in Mn:Ca in January at Copano East (Fig. 1.6). Seasonal consistency of element-salinity relationships was investigated by using linear regression analysis on the yearlong Mission-Aransas data set for all sites together and then for each site individually. For all sites combined across the year, Ba:Ca was negatively related to salinity and $\delta^{18}O$ was positively related to salinity, and the regression parameters (slope and intercept) were very similar to the regional regressions (Table 1.1; Fig. 1.7). Similarly, $\delta^{18}O$ was significantly positively related to salinity within each individual bay throughout the year, while Ba:Ca was significantly negatively related to salinity in Copano West and Mesquite Bay across the seasons (Table 1.1; Fig. 1.7). However, a single January data point largely drove the regression in Copano West and the relationship became insignificant if the January point was removed ($F$=1.15; $p$=0.319). The Ba:Ca-salinity relationship in MB became stronger with the $r^2$ increasing to 0.65 if the January data point was removed. Although there was a significant relationship found between Mn:Ca and salinity in Mesquite Bay, the regression parameters were inconsistent when compared to regional and local regressions (Table 1.1; Fig. 1.7).

Correlation analysis revealed that Ba:Ca was negatively correlated to salinity and positively correlated to temperature (Table 1.2). Oxygen stable isotopes were positively correlated to salinity, but no other elements displayed significant correlations to salinity, temperature, DO, or Chl *a* (Table 1.2).

## 1.4 DISCUSSION

Across the Texas coast, constituent-salinity regressions were significant and linear for dissolved Ba:Ca, Sr:Ca, Mg:Ca, Mn:Ca and $\delta^{18}O$ across large spatial scales. For these comparisons, salinity was considered a proxy for regional differences in climate, and the balance between evaporation and inflow, rather than representing a mixing relationship between fresh and marine end members as would occur within a given estuary. On finer local scales within individual estuaries and on temporal scales of one year, Ba:Ca and $\delta^{18}O$ displayed consistent up-estuary to down-estuary gradients, even though the Mission-Aransas estuary reversed from negative to positive after a rain event, uncoupling the direct relationship of Ba:Ca to salinity. Dissolved elements that display consistent up-estuary enrichment and lower-estuary depletion are reliable candidates for studying animal movements across the ocean-estuary gradient, by quantifying elemental changes in chronologically formed binominals.

### 1.4.1 Spatial patterns

In this study, dissolved Ba:Ca demonstrated the most consistent linear behavior across all scales of space and time over the salinity range sampled. Slopes of the Ba:Ca-salinity relationship was similar on regional ($b$=-3.2) and seasonal ($b$=-4.6) scales, but slightly higher on local ($b_{GB}$=-9.8; $b_{MA}$=-12.2) scales. In the Mission-Aransas Estuary,

only the Copano West and Mesquite Bay sites maintained significant Ba:Ca-salinity regressions on seasonal scales, possibly due the influence of the Mission River inflows on Copano West and the influence of the combined San Antonio plus Guadalupe River inflows on Mesquite Bay. The Misson-Aransas Ba:Ca-salinity relationship displayed the largest y-intercept=454 μmol/mol, which is within error of the mean freshwater end member value of 471 ± 106 (S.D.) μmol/mol measured in the neighboring Nueces estuary (Walther and Nims 2015). The linear nature of the observed Ba:Ca-salinity relationships was likely due to the high salinity range sampled (>15ppt). Non-linear curved behavior would be expected for Ba:Ca at lower salinities, but linear behavior is expected at higher salinities (Coffey et al. 1997; Walther and Nims 2015). If linear mixing of barium at low salinities is assumed, then the effective river end member (EREM) concentration can be estimated (Coffey et al. 1997; Sinclair and McCulloch 2004). The Ba EREM estimates the total effective flux of Ba from a river including dissolved Ba inputs and the contribution from desorption processes from the suspended particulate matter load (Sinclair and McCulloch 2004) and is useful for making comparisons between rivers. However, interpreting the y-intercept as effective river end member concentrations may not apply in the Mission-Aransas, where multiple tributaries with distinct Ba end members all contribute water masses that vary in relative magnitude geographically and temporally. Dorval et al. (2005) reported linear behavior of dissolved barium in the Chesapeake Bay across a salinity gradient (13-27 ppt) similar to our study. In contrast, Hanor & Chan (1977) describe highly non-linear behavior of dissolved Ba due to low-salinity desorption of particulate Ba in the mixing zone of the Mississippi River. Low-salinity peaks in dissolved Ba are commonly reported in estuaries across the world, but the location and magnitude of the peak along the salinity gradient varies depending on estuarine particle dynamics, riverine sediment delivery, and Ba storage/release in salt

marshes (Coffey et al. 1997). Barium ions adsorbed to suspended particular matter (SPM) in freshwater will be exchanged with major cations in seawater, resulting in mid-salinity peaks in dissolved Ba (Hanor and Chan 1977). Barium:Ca displayed consistent linear behavior across the range of salinities (15-43 ppt) we sampled, but non-linear behavior would most likely be detected if lower salinities were sampled (Hanor & Chan 1977, Coffey et al. 1997, Walther and Nims 2015). Novel behavior of dissolved Ba was found in the Coorong Lagoon of Australian, where the Ba-salinity relationship displayed expected negative slopes from salinities of 0 to 37 ppt, but switched to unexpected positive slopes from 37 ppt to 120 ppt (Gillanders and Munro 2012). Hypersalinities > 42 ppt did not disrupt the dissolved Ba:Ca-salinity relationships in the LM however, Gillanders & Munro (2012) sampled salinities > 100 ppt and these highly concentrated ion concentrations may be required to disrupt expected Ba:Ca-salinity relationships. Additional factors that may disrupt linear Ba - salinity relationships include submarine groundwater discharge (Shaw et al. 1998; Walther and Nims 2015) dissolution and diffusion from the sediment (Joung and Shiller 2014), and anthropogenic activities (i.e. drilling muds) (Joung and Shiller 2013)

Stable oxygen isotopes were consistently positively related to salinity over both regional and seasonal scales, but at local scales within the Mission-Aransas evaporation enriched $^{18}O$ at lower salinities, resulting in a negative linear fit. Several studies have found positive linear relationships between $\delta^{18}O$ and salinity (Ingram et al. 1996; Cooper et al. 1997). The $\delta^{18}O$ of estuarine water is both a mixture of ground water sources and precipitation (Stalker et al. 2009). Evaporative processes can lead to enriched $\delta^{18}O$ values due to preferential escape of light $^{16}O$ atoms (Stalker et al. 2009). In the Mission-Aransas, evaporative processes increased $\delta^{18}O$ values at Copano West and Copano East, the two sites furthest from the ocean, which resulted in the negative relationship between

$\delta^{18}O$ and salinity in Mission-Aransas during July (Stalker et al. 2009). This result contrasts that of (Walther and Nims 2015) who found no relationship of $\delta^{18}O$ to salinity (0-50 ppt) in the Nueces River in neighboring Corpus Christi Bay in 2011, potentially due to evaporative enrichment of $^{18}O$ atoms during the drought-dominated period that was sampled. We found a strong relationship between regional evaporation rates and $\delta^{18}O$, indicating that evaporation increasingly dominates $\delta^{18}O$ behavior in subtropical estuaries with decreasing latitude. It is therefore important to consider local evaporative effects that can disrupt predictable relationships of water $\delta^{18}O$ to salinity in some subtropical systems when choosing reliable salinity proxies.

On regional and local scales, both Sr:Ca and Mg:Ca exhibited very similar behavior. Neither dissolved constituent varied more than 1 mmol/mol (Sr:Ca) or mol/mol (Mg:Ca) and very similar slopes were detected ranging from 0.028 to 0.038 (Table 1), indicating minimal variation over the salinity ranges sampled. The underlying geology of this region of the Texas coast tends to be primarily carbonates, which are typically high in Sr, Mg, and Ca. Due to the limited range of variation, dissolved concentrations of Sr and Mg may provide limited information as salinity proxies along the Texas coast (Walther and Nims 2015).

The dissolved element ratio which exhibited the highest variability across all spatial and temporal scales was Mn:Ca. The behavior of the redox-sensitive element manganese is controlled mostly by redox potentials, in contrast to the other elements examined that tend to vary by salinity. In experimental conditions, changes in pH and physical disturbance of the sediments can influence dissolved Mn release more than changes in dissolved oxygen or salinity (Atkinson et al. 2007). On a coast-wide regional scale, dissolved Mn:Ca was significantly positively related to salinity, although on a local scale, only the Mission-Aransas showed a positive Mn:Ca-salinity relationship. Several

other studies have reported non-linear behavior of Mn:Ca across salinity gradients (Dorval et al. 2005; Gillanders and Munro 2012). Additionally, the slope and y-intercept of the Mn:Ca-salinty relationship was highly variable across spatial and temporal scales indicating less reliability as a salinity proxy. However, if the variation in dissolved Mn is influenced by redox potentials and DO levels, then Mn:Ca in calcified structures may provide information on dissolved oxygen exposure histories (Limburg et al. 2011; Mohan et al. 2012; Limburg et al. 2014).

### 1.4.2 Temporal patterns

Similar to observed spatial patterns, both Ba:Ca and $\delta^{18}O$ exhibited consistent temporal patterns over a 12 month sampling schedule. The sampling stations used in Mission-Aransas display a distinct distance-to-ocean gradients in Ba:Ca values, with values decreasing across sites ranking from farthest to closest to the Gulf of Mexico in order Copano West>Copano East>Mesquite Bay>Aransas Bay>Ship Channel. Interestingly, both Ba:Ca and $\delta^{18}O$ maintained this distinct gradient for every month except two distinct instances. In January, dissolved barium was depleted below detection at all sites, which coincided with lowest annual temperatures. Besides salinity, temperature was the only other environmental factor that was related to Ba:Ca. It is difficult to pinpoint the mechanism for decreased dissolved Ba:Ca in January, but potentially reduced freshwater inputs had influenced Ba:Ca behavior. There was minimal precipitation (<1 mm) and very low river discharge from November through January in the Mission-Aransas. Perhaps low freshwater inputs did not deliver much SPM to Copano Bay in the winter, resulting in less desorption of barium from SPM due to ion exchange and thus decreased dissolved pools of barium (Coffey et al. 1997). Although

we detected high variation in Ba on monthly time scales, Elsdon & Gillanders (2006) found large variation in dissolved Ba at small temporal scales of days and weeks in three different Australian estuaries. Stecher and Kogut (1999) reported rapid dissolved Ba removal in the Delaware estuary that was associated with the end of the spring bloom and barite precipitation and depletion of the dissolved Ba pool. Chl *a* data from the Mission-Aransas exhibits increases in April at all sites in response to the inflow event, but not in January. Thus dissolved Ba depletion due to phytoplankton-associated barite precipitation does not seem to account for the decrease in Ba:Ca in January at all Mission-Aransas sites.

Similar to Ba:Ca, stable oxygen isotopes did show distinct spatial separation between sites throughout the year ranking from most enriched to least enriched Copano West>Copano East>Mesquite Bay>Aransas Bay>Ship Channel. Values of $\delta^{18}O$ did converge in May in response to the elevated spring discharge, but sites returned to unique values the next month in June. In contrast to the seasonal and spatial variability of Ba:Ca and $\delta^{18}O$, Sr:Ca and Mg:Ca exhibited limited variation across all months at each site. As mentioned above, these patterns may be due to the limited range of salinities sampled (20 – 39 ppt) in the Mission-Aransas for the sampled year. Curvilinear mixing curves of both Sr:Ca and Mg:Ca have been reported in systems with salinities < 20, with both elemental ratios decreasing and low salinities (Walther and Nims 2015, Gillanders & Munro 2012, Mohan et al. 2012). Manganese:Ca also exhibited limited seasonal variation with values < 10 μmol/mol, except for one large spike in January only at Copano East when dissolved Mn:Ca reached 145 μmol/mol. A potential explanation for the spike may have been a sedimentary disturbance, which could have delivered reduced $Mn^{2+}$ from the sediments into the water column. Dissolved oxygen levels were above 5 mg/l throughout the year, indicating that a hypoxic event was not the source of elevated Mn at Copano East in

January. Many other studies have found high spatial (Statham et al. 2005) and temporal (Shiller 1997; Elsdon and Gillanders 2006) variation in dissolved Mn, which is not unexpected since Mn behavior is highly influenced by natural redox cycles and mediated by microbial activities (Thamdrup et al. 1994; Pakhomova et al. 2007; Richard et al. 2013).

### 1.4.3 Conclusion

We found that dissolved Ba:Ca displays consistent up-estuary to down-estuary concentration gradients in subtropical estuaries in Texas, suggesting Ba:Ca would be reliable for tracking animal movements across the ocean-estuary gradient even during periods of reverse estuary conditions. On seasonal scales, dissolved Ba:Ca decreased sharply in the winter, potentially related to decreased delivery of SPM and decreased ion exchange, depleting dissolved Ba pools. Stable oxygen isotopes displayed positive conservative behavior across regional and temporal scales, but the relationship was reversed in the Mission-Aransas due to local evaporation effects. Although dissolved Sr:Ca and Mg:Ca also exhibited conservative behavior, the minimal variation we detected in these ratios makes them less reliable proxies of salinity in south Texas estuaries. Although $\delta^{18}O$ values varied positively or negatively with salinity at regional and local scales, these dynamics were strongly driven by the importance of evaporative processes in driving local enrichment of $\delta^{18}O$ values. Together, these results suggest that dissolved Ba:Ca exhibits the most reliable gradient along the estuary-ocean continuum due to mixing between freshwater and marine endmembers, and this constituent holds the best promise for reconstructing movements of mobile fauna with calcified hard parts, such as fish otoliths.

**Table 1.1** Linear relationships between salinity and dissolved elemental and isotopic constituents at regional, local, and seasonal scales. Slope and intercept estimates are presented ± SE. Only statistically significant relationships testing the null hypotheses that slope=0 are reported.

| scale | bay | site | element | equation | $r^2$ | F | *p* |
|---|---|---|---|---|---|---|---|
| regional | all | all | Sr:Ca mmol/mol | Y = 0.033±0.003*X + 6.99±0.09 | 0.83 | 136.6 | < 0.0001 |
| | all | all | Ba:Ca µmol/mol | Y = -3.21±0.6*X + 175±21 | 0.65 | 24.67 | 0.0003 |
| | all | all | Mg:Ca mol/mol | Y = 0.028±0.002*X + 3.92±0.07 | 0.91 | 147.6 | < 0.0001 |
| | all | all | Mn:Ca µmol/mol | Y = 0.25±0.05*X - 4.63±1.7 | 0.64 | 23.42 | 0.0003 |
| | all | all | $\delta^{18}O$ per mil | Y = 0.10±0.008*X - 1.94±0.3 | 0.85 | 160.7 | < 0.0001 |
| local | GB | all | Ba:Ca µmol/mol | Y = -9.77±2.6*X + 294±50 | 0.63 | 13.89 | 0.0058 |
| | GB | all | Mg:Ca mol/mol | Y = 0.038±0.01*X + 3.73±0.2 | 0.54 | 9.37 | 0.0156 |
| | GB | all | Mn:Ca µmol/mol | Y = -0.0037±0.0005*X + 0.16±0.01 | 0.85 | 47.14 | 0.0001 |
| local | MA | all | Ba:Ca µmol/mol | Y = -12.2±1.9*X + 454±61 | 0.83 | 39.36 | 0.0002 |
| | MA | all | Mn:Ca µmol/mol | Y = 1.05±0.3*X - 29.21±8.5 | 0.65 | 15.04 | 0.0047 |
| | MA | all | $\delta^{18}O$ per mil | Y = -0.093±0.02*X + 4.34±0.7 | 0.67 | 16.54 | 0.0036 |
| seasonal | MA | all | Ba:Ca µmol/mol | Y = -4.60±1.1*X + 211±36 | 0.27 | 18.77 | < 0.0001 |
| | MA | all | $\delta^{18}O$ per mil | Y = 0.065±0.02*X - 0.72±0.7 | 0.18 | 11.13 | 0.0016 |
| seasonal | MA | CW | Ba:Ca µmol/mol | Y = -6.46±2.5*X + 307±84 | 0.42 | 6.51 | 0.0311 |
| | MA | CW | $\delta^{18}O$ per mil | Y = 0.090±0.03*X - 0.81±0.9 | 0.55 | 10.93 | 0.0091 |
| seasonal | MA | CE | $\delta^{18}O$ per mil | Y = 0.099±0.02*X - 1.56±0.6 | 0.77 | 29.31 | 0.0004 |
| seasonal | MA | MB | Ba:Ca µmol/mol | Y = -2.70±1.1*X + 145±35 | 0.42 | 6.453 | 0.0317 |
| | MA | MB | Mn:Ca µmol/mol | Y = 0.44±0.09*X - 8.46±10 | 0.74 | 26.15 | 0.0006 |
| | MA | MB | $\delta^{18}O$ per mil | Y = 0.076±0.02*X - 1.19±0.6 | 0.64 | 15.91 | 0.0032 |
| seasonal | MA | AB | $\delta^{18}O$ per mil | Y = 0.11±0.03*X - 2.56±1.1 | 0.58 | 12.52 | 0.0063 |
| seasonal | MA | SC | $\delta^{18}O$ per mil | Y = 0.11±0.03*X - 3.27±1 | 0.69 | 15.83 | 0.0053 |

**Table 1.2** Pearson correlation results between dissolved elements and environmental factors in the MA sampled for 12 months. Significant ($p$<0.05) correlations using Bonferroni probabilities indicated in bold. The Ship Channel site and pH was excluded due to missing data.

| element | salinity | temperature | DO | Chl *a* |
|---|---|---|---|---|
| Sr:Ca mmol/mol | -0.06 | -0.04 | -0.01 | 0.09 |
| Ba:Ca µmol/mol | **-0.494** | **0.45** | -0.35 | -0.03 |
| $\delta^{18}O$ per mil | **0.59** | -0.12 | -0.06 | -0.23 |
| Mg:Ca mol/mol | 0.129 | -0.196 | 0.2 | 0.03 |
| Mn:Ca µmol/mol | 0.19 | -0.32 | 0.18 | 0.19 |

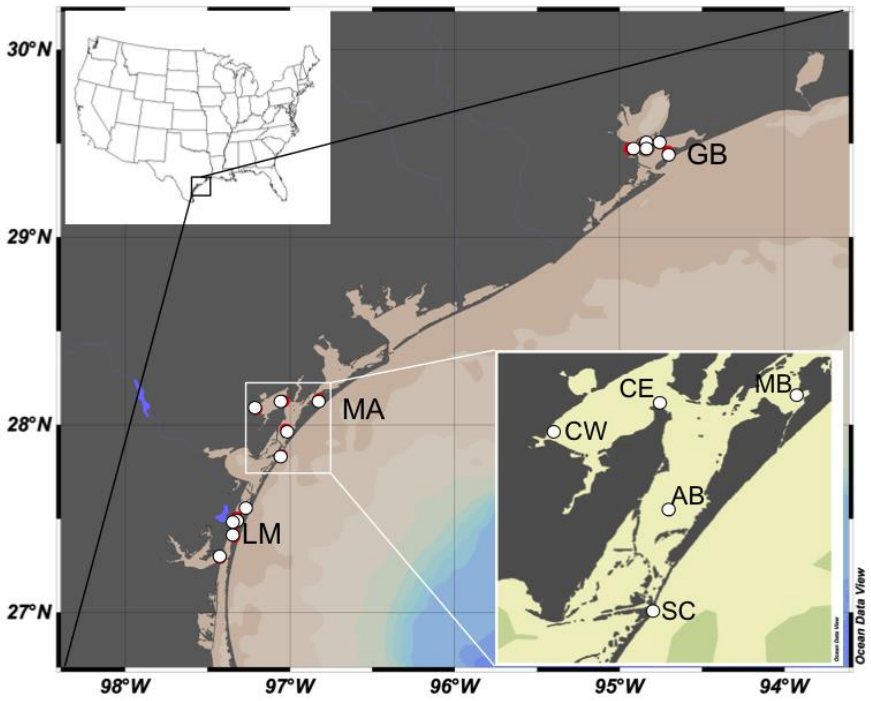


**Figure 1.1** Map of water sampling locations (white dots) in Galveston Bay (GB), Mission-Aransas (MA) and Laguna Madre (LM). Five fixed stations Copano West (CW), Copano East (CE), Mesquite Bay (MB), Aransas Bay (AB), and Ship Channel (SC) were sampled monthly in Mission-Aransas.

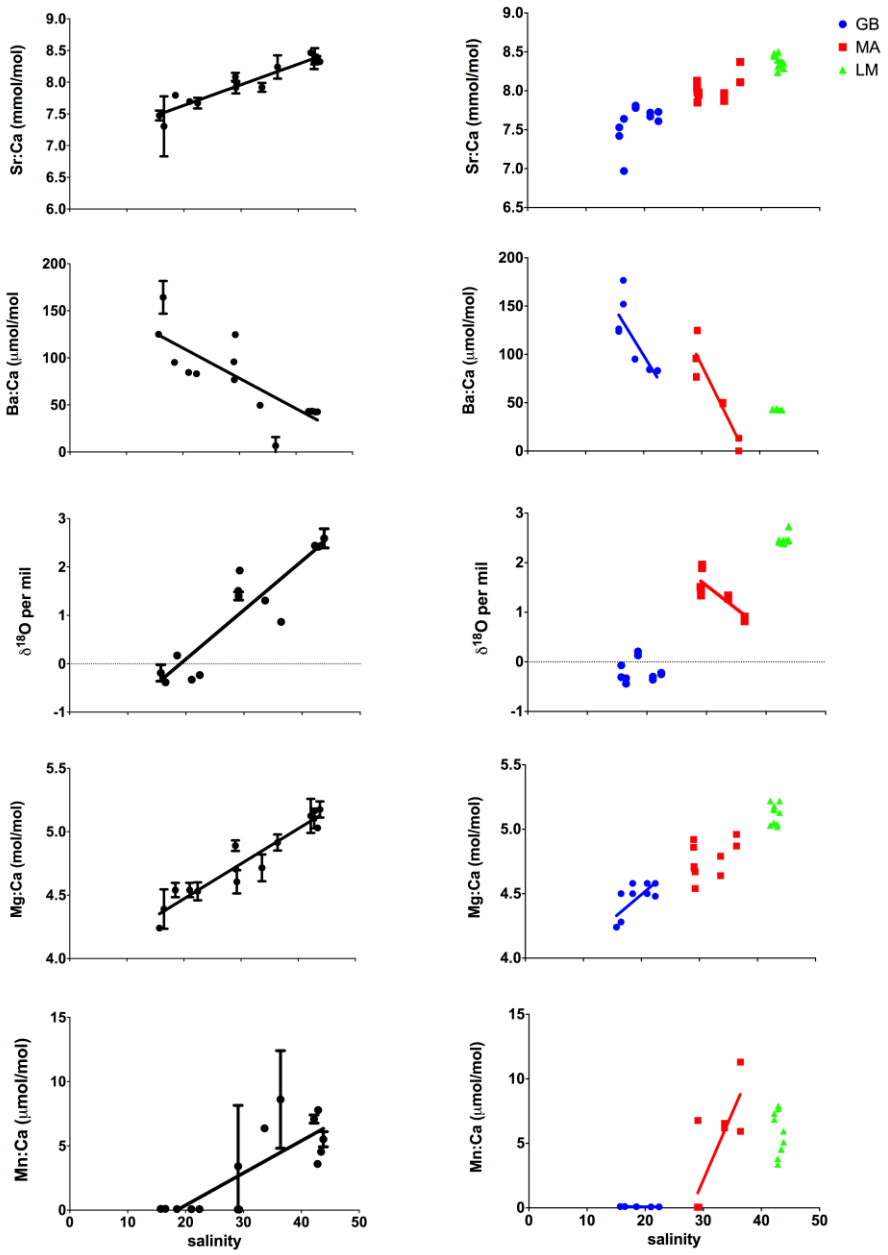


**Figure 1.2** Element-salinity relationships on regional (left column) and local (right column) scales from samples collected in July 2012. Plotted lines display significant linear regressions (excluding $\delta^{18}O$ in Mission-Aransas). Error bars indicate standard deviation from 2 replicate samples for regional data. Dotted lines indicate expected oceanic $\delta^{18}O$ value of 0‰.

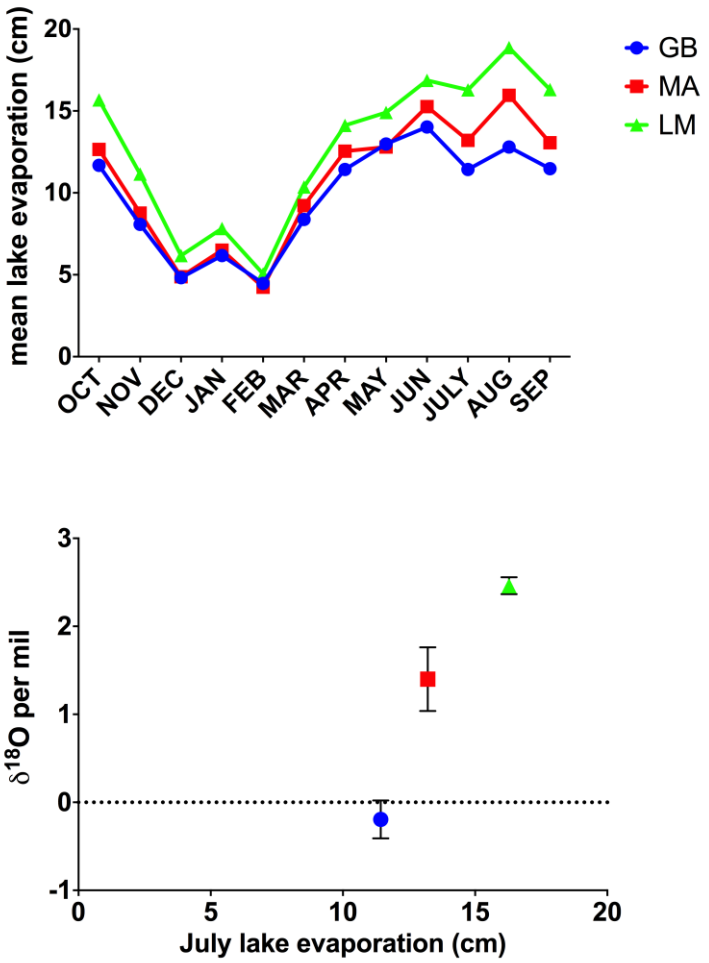


**Figure 1.3** Mean monthly lake evaporation rates for Galveston Bay (GB), Mission-Aransas (MA) and Laguna Madre (LM) and relationship to mean July $\delta^{18}O$ in each Bay.

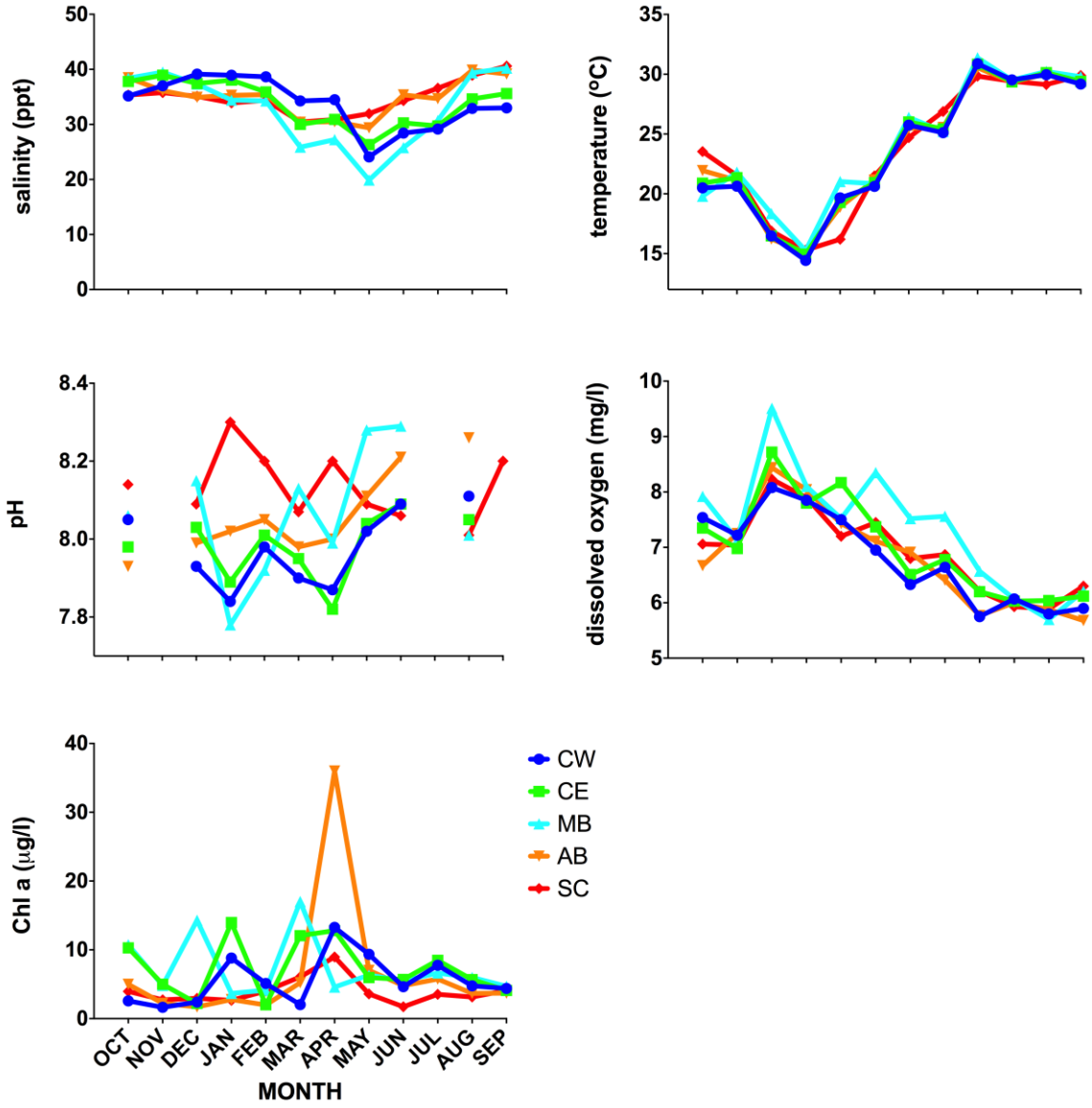


**Figure 1.4** Time series of physicochemical parameters and Chl *a* concentrations from October 2011 to September 2012 in the Mission-Aransas Estuary. Breaks in the pH time series lines represent missing data.

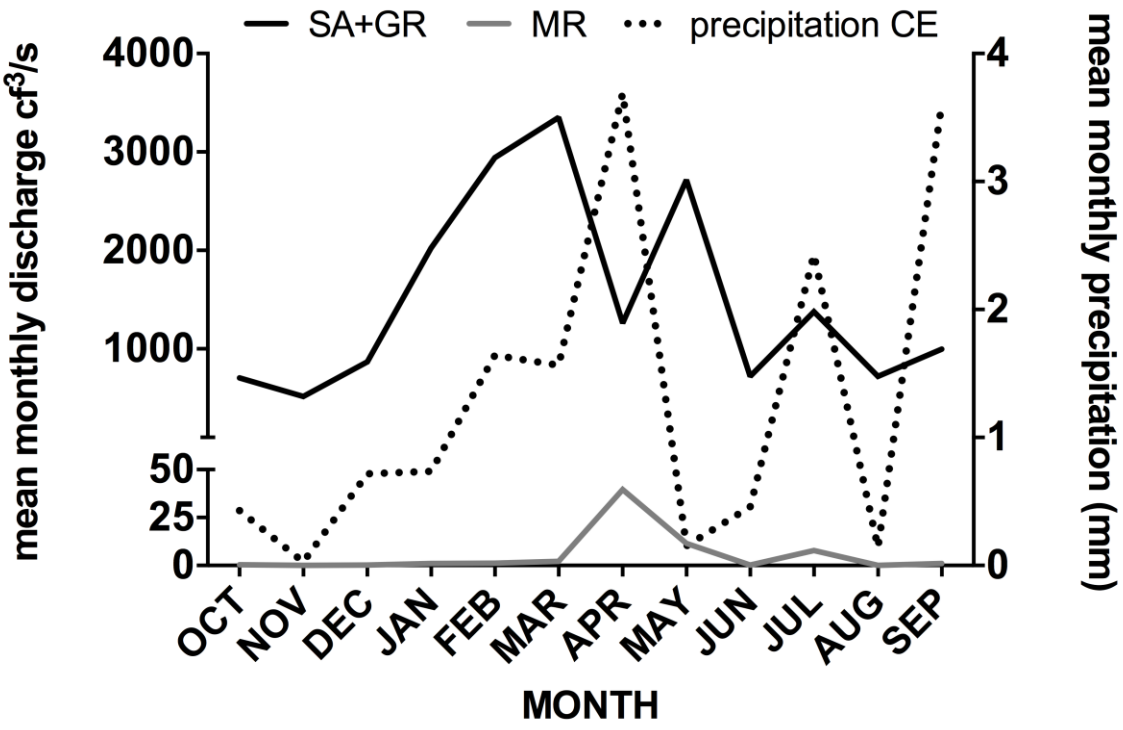


**Figure 1.5** Mean monthly discharge for the Mission River (MR) at USGS station gauge 8189500 in Refugio, TX, and summed discharge (USGS 8188500 + USGS 8176500) of the San Antonio (SA) and Guadalupe Rivers (GR). Daily cumulative precipitation data recorded at the Copano East (CE), the only site with meteorological data.

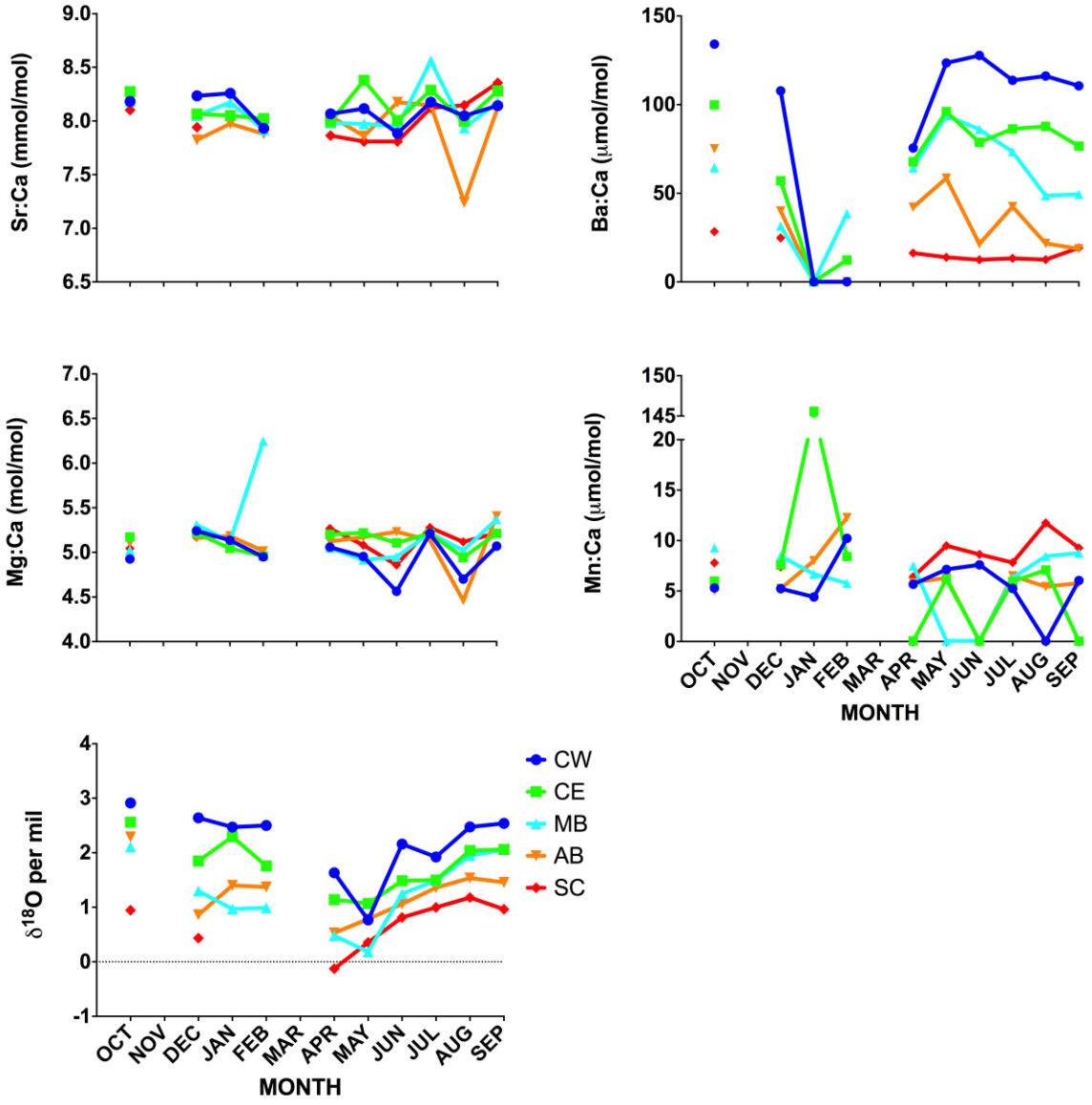


**Figure 1.6** Time series of dissolved elemental and isotopic constituents in the Mission-Aransas from October 2011 to September 2012. Different colors represent different sites. Note that sampling was not conducted in November and March (breaks in line). Note break in Y-axis for Mn:Ca. Dotted line in $\delta^{18}O$ plot indicates expected oceanic $\delta^{18}O$ value of 0‰.

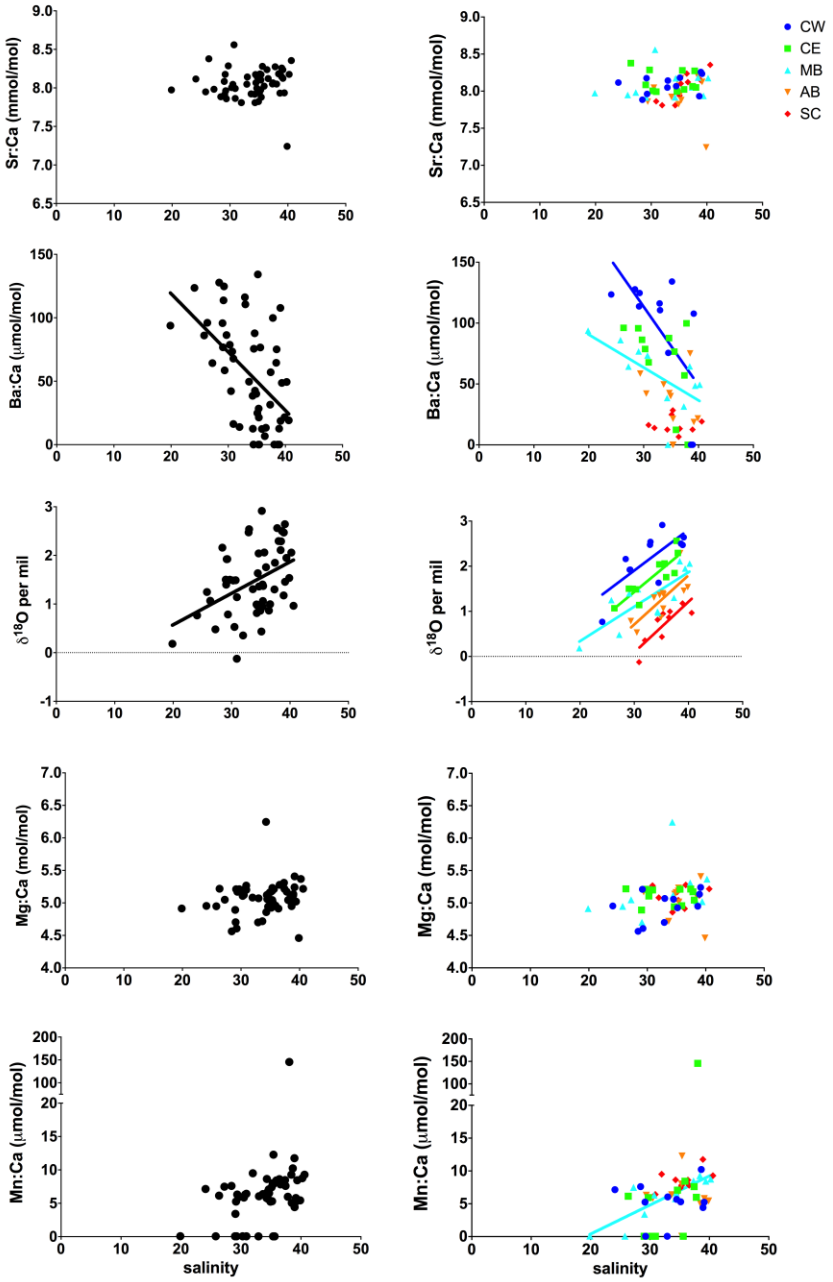


**Figure 1.7** Element-salinity relationships for all Mission-Aransas sites combined (left column) and for each site individually (right column) throughout the year. Different color lines represent different sites and plotted lines display significant linear regressions. Dotted lines indicate expected oceanic $\delta^{18}O$ value of 0‰.

# CHAPTER 2: TISSUE-SPECIFIC ISOTOPE TUNROVER AND DISCRIMINATION FACTORS ARE AFFECTED BY DIET QUALITY AND LIPID CONTENT IN AN OMNIVOROUS CONSUMER


## ABSTRACT

Tissue stable isotopes can be used for dietary reconstruction provided the factors influencing turnover rates and trophic discrimination factors (TDF) between consumer tissues and diet are known. We quantified $\delta^{13}C$ and $\delta^{15}N$ dynamics in muscle and liver tissues in lab-reared juvenile marine fish after a switch from a high quality control diet to medium and low quality diets with decreasing protein and lipid content. Turnover of $\delta^{15}N$ in the liver was strongly influenced by metabolism, equilibrating 3X faster compared to muscle for both diets. Nitrogen TDF were dependent on diet quality, with values ranging from 3.0-6.5‰ in muscle and 1.5-3.0‰ in liver. The effects of mathematical lipid correction on $\delta^{13}C$ turnover and discrimination were examined by developing novel empirical equations involving C:N ratios and lipid $\delta^{13}C$ values. Lipid correction affected estimates of isotope turnover in the low quality diet treatment, with lipid-corrected muscle carbon isotopes equilibrating to diet 2X faster than non-corrected muscle, due to lipid retention increasing turnover estimates for non-corrected values. Conversely, lipid-corrected liver half-lives were 4.4X slower than non-corrected liver because lipid metabolism increased turnover rates for non-corrected values. A shift in control fish liver carbon TDF of 2.1 and 1.7‰ for non-corrected and lipid-corrected values, respectively, between the beginning and end of the experiment was attributed to a 32% increase in lipid content. These results demonstrate that metabolic routing of lipid macromolecules

strongly influence tissue-specific turnover, and is important to consider when reconstructing trophic dynamics.

## 2.1 INTRODUCTION

Stable isotopes are powerful tools for tracing diets and studying food webs across a wide diversity of organisms, from butterflies and elephants on land, (Hobson et al. 1999; van der Merwe et al. 1990) to shrimp and tuna in the sea (Fry 1983; Graham et al. 2010). Unique isotope signatures at the base of the food web are passed to higher trophic levels (with some modifications), and thus provide a means of identifying trophic pathways. Many migratory species transit across dietary 'isoscapes,' that vary as a function of natural biogeochemical and anthropogenic sources and processes (Hobson et al. 2010). Examples of isoscapes include gradients in $\delta^{13}C$ values of dissolved inorganic carbon and primary producers, which differ regionally between the ocean and the coast (Fry et al. 1984), and locally between fresh water, estuarine and marine habitats (Fry 2002). Nitrogen isotope gradients are often due to the dominance of denitrification, nitrification or fixation processes transforming the pool of available N (Macko et al. 1984; McClelland et al. 1997; Holl et al. 2007; Sigman et al. 2009) or due to anthropogenic inputs of $^{15}N$ enriched nitrogen sources (McClelland et al. 1997; Schlacher et al. 2007). Provided turnover rates are known, isotopic clocks from tissues record migration timing, as movement between habitats with isotopically distinct food resources (isoscapes) are reflected in tissues of mobile consumers (Herzka 2005; Hobson et al. 2010).

Accurate interpretations of diet histories from tissue stable isotope ratios require a detailed understanding of the factors that affect 1) the time frame represented by the

tissue analyzed (i.e. turnover rate) and 2) the isotopic offset between the tissue and the diet, or trophic discrimination factor (Hobson et al. 2010). Tissue turnover rates are influenced by growth via the accumulation of new tissue through mass gain and metabolism via the breakdown and replacement of existing tissue (Fry and Arnold 1982; Hesslein et al. 1993; Herzka 2005). Models have been developed that estimate the relative contribution of growth (Fry and Arnold 1982) and metabolism (Hesslein et al. 1993) to isotope turnover (reviewed by Boecklen et al. 2011). In general, tissues with fast growth and high metabolism have quicker turnover rates. For instance, the high metabolic activity of liver tissue leads to more rapid turnover than muscle in birds (Hobson and Clark 1992), bony fishes (Suzuki et al. 2005; Logan et al. 2006; Buchheister and Latour 2010), elasmobranchs (MacNeil et al. 2006; Malpica-Cruz et al. 2012), and mammals (Sponheimer et al. 2006). Trophic discrimination factors ($TDF=\delta_{tissue} - \delta_{diet}$) are influenced by many variables including the element of interest (e.g. $^{13}C$ or $^{15}N$), taxonomic group (e.g. birds, fish, mammals), specific tissue (e.g. blood, liver, muscle), and diet (e.g. protein and lipid content) as reviewed by Martínez del Rio et al. (2009). Environmental temperature and the amount of food consumed can also affect TDF (Barnes et al. 2007). Even within an individual animal and tissue, TDF can vary as a function of growth rate (Trueman et al. 2005). Given the range of variables that influence both turnover rate and TDF, and the importance of both factors for accurately determining trophic relationships, there have been recent calls for more controlled laboratory experiments to explore the dynamics of turnover rates and TDF (e.g. Martínez del Rio et al. 2009, Boecklen et al. 2011).

A particular area of concern for trophic studies is the effect of lipid content on carbon isotope turnover and fractionation. Lipids are depleted in $^{13}C$ relative to protein and carbohydrates and many researchers address 'lipid bias' with chemical extraction or

mathematical correction techniques. Despite their wide use, lipid correction equations developed using a certain species are generally not applicable to other species or between tissues within the same species, and no universal lipid correction model exists (Post et al. 2007; Mintenbeck et al. 2008; Logan et al. 2008). Additionally, lipids such as essential fatty acids are important nutritional and source-specific components of food webs (Litzow et al. 2006) and so by extracting lipids before measuring $\delta^{13}C$ values, dietary information may be irretrievably lost. In contrast, correcting for 'lipid bias' using mathematical equations permits comparison between lipid-corrected and non-corrected carbon isotope values and preserves dietary information contained in the lipid fraction. Moreover, migratory omnivores will potentially feed on a large range of dietary items of variable qualities and lipid content that can introduce considerable complexity into isotope-based dietary reconstructions. Despite the importance of lipids, they are rarely addressed in controlled experiments that quantify isotope turnover rates and TDF.

We conducted a diet switch experiment on an omnivorous marine teleost, Atlantic croaker (*Micropogonias undulatus)*, with individuals that were reared in the laboratory with known diet and growth histories. The experiment was designed to achieve four primary objectives: 1) determine nitrogen and carbon isotope turnover rates of fish muscle and liver tissue using models that partition turnover to growth and metabolism; 2) estimate tissue-specific TDF and compare to other studies; 3) investigate the influence of diet quality on turnover and TDF; and 4) examine the influence of lipids on assimilation dynamics using empirically-derived correction equations for $\delta^{13}C$ values based on extracted-lipid $\delta^{13}C$ values and C:N ratios. Results of this study reveal the complex factors that affect tissue-turnover rates and isotopic discrimination, and will facilitate interpretation of tissue isotope data from migratory animals.

## 2.2 METHODS

### 2.2.1 Fish husbandry

Atlantic croaker eggs were collected from laboratory brood stock grown under simulated photoperiod and temperature regimes to induce natural spawning at the University of Texas Marine Science Institute (UTMSI), Port Aransas, Texas USA. Eggs were treated with 1-ppm formalin for 30 min to prevent bacterial and fungal infections and hatched in 150 L conical tanks. Rotifers were raised on *Isochrysis galbana* algae and enriched over 24 hours with RotiGrow Plus (Reed Mariculture Inc.) to increase essential fatty acid content and enriched rotifers were then fed daily to croaker larvae. Rotifers were added as needed to maintain densities of 5-10 rotifers·ml$^{-1}$. After 3 weeks, larvae were fed *Artemia* enriched with AlgalMac 3050 (Bio-Marine, Inc.) at starting densities of 0.25 artemia·ml$^{-1}$, which was increased to 2 artemia·ml$^{-1}$ as fish grew. Larvae were then gradually weaned onto an enriched marine dry feed Otohime EP3 (Reed Mariculture Inc.) that increased in pellet-size from 250 μm to 1.7 mm as fish reached juvenile size (60 d of age). On d 60, juveniles were transferred to circular 350 L grow-out tanks and fed Otohime pellets (2.3 mm). After 165 d, fish reached experimental size (110±10 mm total length, 17±5 g) and were transferred into 12 individual 450 L experimental tanks at densities of ~ 30 fish per tank. Each tank was equipped with an automatic feeder that dispensed pellet food at 09:00, 12:00, 15:00 and 18:00 h daily. After one week of acclimation, all fish were anesthetized with MS-222 (150 mg·L$^{-1}$), measured for length and mass and tagged individually with Visual Implant Alpha (VIA) IV tags (Northwest Marine Technologies, Inc.). The tags contained unique codes and were inserted into the snout cavity to monitor individual growth rates. Tagged fish were further acclimated for 10 d before initiating the diet switch.

### 2.2.2 Experimental protocol

Experimental diets ("medium" quality and "low" quality) were selected to be a similar pellet size to the control diet but had different protein and fat content and source (terrestrial versus marine), resulting in distinct isotope values (Table 2.1; Fig. 2.1). The low quality feed contained 5% lipid and 32% protein, primarily from terrestrial sources and was below the optimal protein level of 45% recommended for Atlantic croaker (Davis and Arnold 1997). The control feed contained 15% lipid and 48% protein and was primarily from marine sources, while the medium quality diet had 12% lipid and 45% protein from a mixture of terrestrial and marine sources, according to manufacturer information. The isotopic shift in experimental diets was comparable to natural diet shifts a coastal migratory fish could experience following a movement between offshore and upper estuarine habitats. Each diet was randomly assigned to 4 tanks, resulting in 4 replicate tanks per treatment. On experiment d 0, immediately before the diet switch, 12 fish were sacrificed to obtain initial equilibrium isotope values and estimate TDF for both muscle and liver tissues (Fig. 2.1). Food was withheld 24 hours before sampling to ensure clearance of stomach contents. Random samples of 2 fish per tank were collected on d 7, 18, 32, 52, and 104, resulting in 8 fish per time point per diet treatment. Fish were euthanized with a lethal dose of MS-222 and placed on ice until dissection. The Institutional Animal Care and Use Committee (AUP-2013-0083) at the University of Texas at Austin approved all experimental procedures.

### 2.2.3 Sample analysis

Each fish was patted dry, weighed (0.01 g) and measured for standard length (SL; mm) and total length (TL; mm). The VIA tag was removed from the snout and fish identification was recorded. The liver and a fillet of dorsal white muscle tissue was

collected, rinsed with deionized water, weighed, placed in 2 ml vials and frozen at -80°C. Samples were then freeze dried for 36 hours, re-weighed, and ground into a fine powder using a ceramic mortar and pestle. One (±0.2) mg of dried tissue was then packed into tin capsules and sent to the Stable Isotope Facility of the University of California Davis for bulk C and N content and isotope analysis using a PDZ Europa ANCA-GSL elemental analyzer interfaced to a PDZ Europa 20-20 isotope ratio mass spectrometer (Sercon Ltd., Cheshire, UK). A replicate tissue was included every 16th sample to assess precision. Mean standard deviation (SD) of 13 replicates was 0.08‰ for $\delta^{13}C$ and 0.12‰ for $\delta^{15}N$ values. Four certified standards Bovine Liver, USGS-41 Glutamic Acid, Nylon 5, and Glutamic Acid were also analyzed to assess accuracy and the mean SD across two analytical days ranged from 0.05-0.08‰ for $\delta^{13}C$ and 0.06-0.14‰ for $\delta^{15}N$ values.

### 2.2.4 Lipid correction of $\delta^{13}C$ values

Lipid-rich tissues are depleted in $^{13}C$ values relative to whole organisms (DeNiro and Epstein 1977), and we accounted for this effect by developing tissue-specific mathematical lipid correction equations based on empirical data (Sweeting et al. 2006; Mintenbeck et al. 2008; Logan et al. 2008). We measured C content (µg mg-dry weight $(DW)^{-1}$) and the $\delta^{13}C$ values of extracted lipids from all three diets ($n$=4 per diet) and from freeze-dried liver (~10 mg) and muscle (~20 mg) of a subset of two fish from each time point and diet treatment (muscle $n$=35; liver $n$=34). Total lipids were extracted in chloroform:methanol:water (2:1:0.5) according to Parrish (1999; modified from Folch et al., 1957) and were suspended in 500 µL of chloroform. From the chloroform-lipid extract, 50 µL was transferred to a pre-weighed tin capsule containing a small piece of pre-combusted glass fiber filter. The extract was absorbed onto the filter and kept under

the fume hood for at least five hours to allow the excess chloroform to evaporate. The tin capsules containing the dried filters were weighed using a microbalance to obtain lipid dry weight (mg) and total % lipid measurements. Prepared samples were analyzed using a Finnigan MAT Delta Plus stable isotope mass spectrometer coupled to a Carlo Erba 1500 elemental analyzer (CE Instruments, NC 2500) at UTMSI. Lipid stable isotope values are reported in relation to conventional standards Casein (114859) and USGS Isotopic Reference Material Standard 20192 L-Glutamic Acid with a mean SD of 0.12‰. Relationships between % lipid measurements, bulk $\delta^{13}C$ values and molar C:N ratios were investigated (Fig. 2.2)

A simple mass balance model was used to calculate the stable isotope value of the non-lipid (NL) portion ($\delta^{13}C_{NL}$): $\delta^{13}C_{Bulk} = (\delta^{13}C_L * f_L) + (\delta^{13}C_{NL} * f_{NL})$, where $\delta^{13}C_L$ is the measured stable isotope value of the lipid extract, $f_L$ is the measured fraction of carbon in the bulk tissue that came from lipids, and $f_{NL}$ is the fraction of carbon that came from non-lipids ($f_{NL}= 1- f_L$). The mass-balance derived $\delta^{13}C_{NL}$ values of diet and tissue samples were used directly as the "lipid-corrected" values for developing lipid correction equations (described below) and calculating non-lipid TDF. To develop a mathematical correction to be applied to the entire bulk $\delta^{13}C$ dataset, relationships between the known subset of $\delta^{13}C_{NL}$ values using mass balance described above, and bulk tissue C:N molar ratios were explored (Fig. 2.3). For liver samples, a linear model including C:N and the subset of calculated $\delta^{13}C_{NL}$ values (derived from a mass balance equation) was used to correct each liver sample for lipid-bias: $\delta^{13}C_{NL} = -0.135 * C:N – 18.6$; $r^2 = 0.49$. Bulk muscle values were corrected using the following linear equation: $\delta^{13}C_{NL} = \delta^{13}C_{Bulk} + 0.56 * C:N – 1.3$; $r^2 = 0.60$. Both the bulk carbon data and mathematically lipid-corrected carbon data were used in non-linear models described below in order to compare the

effects of including or excluding the lipids on tissue-specific estimates of isotope turnover.

### 2.2.5 Non-linear curve fitting

Tissue-specific isotopic turnover was modeled as a function of both growth and time after the diet switch. The Fry & Arnold (1982) growth-based model was used to determine the relative contribution of growth and metabolic turnover to isotope turnover in muscle and liver tissues: $\delta_t = \delta_f + (\delta_i - \delta_f)*(M_t/M_i)^c$, where $\delta_i$ is the mean initial isotope value before the diet was switched, $\delta_f$ is the final isotope value at equilibrium with the diet, $\delta_t$ is the isotope value at time t, $M_i$ is the mean initial fish mass before the diet switch, and $M_t$ is the mass of an individual fish at time t, and *c* is the coefficient of isotopic turnover. When $c = -1$, isotope turnover is attributed to growth alone, or dilution of the initial isotope value by mass gain. When $c < -1$, then a more negative the value of *c* indicates a greater contribution of metabolism to isotope turnover through the loss and replacement of existing body tissues (a function of the balance of catabolism and anabolism).

To estimate tissue turnover rates, the data were fit to the time-based Hesslein et al. (1993) model: $\delta_t = \delta_f + (\delta_i - \delta_f)e^{-(k+m)t}$, where $\delta_t$, $\delta_f$, and $\delta_i$ are the same as above, *k* is the exponential growth constant, and *m* is the coefficient of isotopic turnover. The growth constant *k* was estimated by curve-fitting the data to an exponential growth model $w_t = w_i*e^{kt}$, where $w_t$ is the mass of fish at time t, $w_i$ is the initial mass of the fish, and t is time (Fig. 2.4). When curve-fitting the Fry & Arnold (1982) and Hesslein et al. (1993) models, the tissue-specific initial value ($\delta_i$) was constrained as the mean isotope value (N=12) at d 0, when both muscle and liver tissues were in isotopic equilibrium with the high quality

control diet after being fed the control diet for 5 months prior to the experiment. Equilibrium trophic discrimination factors (TDF = $\delta_{tissue} - \delta_{diet}$) for the muscle and liver tissues of the diet-switched fish at the beginning of the experiment were calculated using $\delta_i$ of d 0 fish, and the δ values of the medium and low quality diets. Using the equilibrium TDF calculated for the fish at the beginning of the experiment and the isotope ratios of the medium and low quality diets, the final equilibrium tissue isotope value ($\delta_f$) for both the medium and low quality diet fish were predicted and used as 'initial values' during the curve fitting procedure. To compare model-derived parameter estimates, t-tests were used on estimates of *c* and *m* to test the null hypotheses $h_o$: $c = -1$ and $h_o$: $m = 0$ (Table 2.2).

### 2.2.6 Turnover rate estimates and TDFs

The length of time required to achieve a specific percent isotope turnover following a change in diet can be estimated using the equation presented by Tieszen et al. (1983): $T_{\alpha/100} = \ln (1 - \alpha/100)/(k+m)$, where T is time in days, α is the percent turnover, and $k+m$ are model parameters estimated using the Hesslein et al. (1993) time-based model described above. The $t_{50\%}$ and $t_{95\%}$ turnover rates were estimated by setting $\alpha = 50$ and 95, respectively (Table 2.2). The error for each turnover estimate was determined by including the upper and lower SE for *k* and *m* parameters and recalculating $t_{50\%}$ and $t_{95\%}$. The percent contribution of metabolic turnover (MTO) to overall turnover was determined using: MTO = $m/k+m$ only when *m* was statistically greater than zero (Table 2.2). Tissue-specific TDF were calculated for the control fish on d 0 and d 104. For the medium and low quality diet reared fish, TDF were calculated using $\delta_f$ for bulk $\delta^{15}N$ and $\delta^{13}C$ values and on the subset of extracted lipid $\delta^{13}C$ values. For comparison, TDF were

also calculated based on the lipid-correction equation-derived $\delta^{13}C_{non\text{-}lipid}$ final values, and for the predicted equilibrium muscle and liver δ values that resulted from non-linear growth-based (Fry and Arnold 1982) and time-based (Hesslein et al. 1993) models (Table 2.4). To compare the TDF calculated at d 104 to the equilibrium TDF predicted by curve fitting the isotope turnover models, $TDF_{difference}=TDF_{observed} - TDF_{predicted}$ was calculated. Standard error estimates for the observed TDF were calculated by propagating the errors of $\delta_{tissue}$ and $\delta_{diet}$ : $SE_{TDF} = \sqrt{(SE_{\delta tissue}^2 + SE_{\delta diet}^2)}$.

## 2.3 RESULTS

### 2.3.1 Growth

Growth rate constants (*k*) were highest in control fish (*k*=0.013), followed by fish fed the medium (*k*=0.011), and low (*k*=0.006), quality diets (Fig. 2.4). Fish fed the low quality diet achieved a mean relative mass gain (final fish mass / initial fish mass) of only 2 by d 104, while fish fed the medium and control diet achieved mean relative mass gains of 3.5 and 4, respectively. Mean daily growth rates (mm $d^{-1}$±SEM) over the 104 day experiment ranked 0.37±0.03 <0.67±0.04 <0.84±0.04 for the low, medium, and high quality diets, respectively.

### 2.3.2 Nitrogen turnover

Nitrogen isotope turnover in muscle was primarily driven by growth, as indicated by *c* values that were not statistically different than -1 for the medium and low quality diets (Fig. 2.5 & 2.6; Table 2.2). Liver $\delta^{15}N$ turnover was highly influenced by metabolic turnover with *c*= -5.3±0.8 for the medium quality diet (Fig. 2.4) and *c*= -5.5±1.1 for the

low quality diet (Fig. 2.6). The time-based model yielded $t_{50\%}$ estimates ranging from 27-54 d for muscle tissue and 9-18 d for liver tissue. Fish fed the low quality diets took twice as long to reach $t_{50\%}$ than those fed the medium quality diet. Regardless of diet, liver nitrogen turnover was 3-fold faster than muscle tissue, due to the combined influence of growth and metabolism on liver tissue. The curve-fitted values of *m* parameters in the time-based model were all significantly different from zero, indicating at least some influence of metabolic turnover in muscle and liver tissues. The percent contribution of metabolic turnover (MTO) was 85% for liver tissues of fish fed both diet treatments. Muscle MTO ranged from 53-57%, and the muscle data tended to have higher $r^2$ values, indicating better curve fits (Table 2.3).

### 2.3.3 Carbon turnover

According to the growth-based model, turnover of carbon isotopes in muscle and liver tissue was dominated by growth processes, with metabolic turnover playing a minor role. Estimates of Fry and Arnold's (1982) coefficient of isotopic turnover (*c*) were not significantly different from -1; however, the estimates had low precision due to large standard error (Table 2.2) and a high dispersion in the data (Fig. 2.7). Similarly, *m* parameter estimates were not significantly different than zero except for bulk liver ($m$=0.044±0.009) and non-lipid fractions in muscle ($m$=0.009±0.003) of fish fed the low quality diet (Table 2.3). Bulk liver also had the most negative *c* estimate (c=-2.4±1.2‰), although this estimate did not differ significantly from -1.

Bulk and non-lipid carbon turnover differed between tissues and between experimental diet treatments. For the medium quality diet, $t_{50\%}$ for bulk muscle was estimated as 30±11 d, which was comparable to the non-lipid fraction of muscle (36±12

d; Fig. 2.7). Likewise, $t_{50\%}$ was similar for the bulk and non-lipid fraction of liver tissue for fish fed the medium quality diet. When accounting for the high error in *m*, these estimates of $t_{50\%}$ ranged from 30-50 d (Fig. 2.7). In contrast, when fish were fed the low quality diet, $t_{50\%}$ of bulk liver was >4x shorter than the non-lipid fraction (Fig. 2.8). Bulk muscle tissue of fish fed the low quality diet showed the slowest turnover ($t_{50\%}$=79±38 d; $t_{95\%}$=343±163 d), and the estimates decreased by almost 2-fold when considering solely the mathematically corrected non-lipid fraction ($t_{50\%}$=43±8 d; $t_{95\%}$=188±33 d).

### 2.3.4 Trophic discrimination factors

Muscle tissue showed greater TDF than liver tissue for both carbon and nitrogen isotopes (Fig. 2.9; Table 2.4). Nitrogen TDF for both muscle and liver tissue tended to increase as diet quality decreased (low diet TDF>medium>control), which was related to the larger isotopic difference between the control diet and the low quality diet (control diet – low diet=7‰) compared to the medium quality diet (control diet – medium diet=4.8‰). Observed nitrogen TDF on d 104 ranged from 2.3 to 6.5‰ in muscle and 0.8 to 3‰ in liver (Fig. 2.9; Table 2.4).

Bulk carbon TDF between treatments displayed less variation in muscle (range 1.3-2.3‰) than in liver tissue (-0.9 to -3‰). $\delta^{13}C$ values (both bulk and non-lipid carbon) of liver in the control fish changed by -2‰ between d 0 and d 104, while liver $\delta^{15}N$ values increased by 0.68‰. Muscle $\delta^{15}N$ and $\delta^{13}C$ values of fish fed the control diet remained similar between d 0 and 104, and between bulk and non-lipid fractions (Fig. 2.9). Non-lipid fractions of both the muscle and liver tissues for all diets showed a mean increase of 1‰ (range 0.3 – 1.9‰), relative to bulk carbon isotope values (Table 2.4). The lowest TDF occurred in the lipid fractions of the muscle samples, ranking -0.14‰<-

0.25‰<-0.72‰ for the control<medium<low quality diets and similarly ranking -0.3‰<-0.8‰<-1.74‰ for the lipid-only fraction of the liver (Table 2.4). For the medium quality diet, $TDF_{difference}$ ($TDF_{observed}$ - $TDF_{predicted}$) were all < 1‰ (except one value), suggesting that the final observed δ tissues were very close to reaching isotopic equilibrium. For the low quality diet, 8 of 12 estimates of were > 1‰ suggesting that final δ values of the tissues had not reached equilibrium. Bulk carbon isotopes in the liver of fish fed the low quality diet displayed the lowest $TDF_{difference}$ of -0.25‰ and exhibited the shortest half-life, providing evidence that bulk liver $\delta^{13}C$ values had reached equilibrium.

## 2.4 DISCUSSION

In this controlled diet-switch experiment, nitrogen isotope turnover was 3-fold faster in the liver compared to muscle, due to the strong influence of metabolic turnover. Carbon isotope turnover was primarily driven by growth, but lipids both increased turnover in muscle tissue and decreased turnover in liver tissue in the slow growing fish fed the low quality diet. TDF also varied by tissue type, diet type and carbon pools (lipid versus non-lipid), including some unexpected changes in the control fish that were kept on a high quality diet throughout the experiment. This study is the first to directly quantify and compare bulk and non-lipid tissue-specific carbon isotope turnover rates and trophic discrimination factors in a marine fish and reveals that lipid dynamics can potentially complicate carbon isotope interpretations.

### 2.4.1 Nitrogen turnover

Fish fed the low quality diet exhibited low mean growth rates (0.37 mm $d^{-1}$) that resulted in tissue turnover rates that were twice as long compared to fish fed the medium

quality diet, which displayed faster growth (0.67 mm $d^{-1}$). Initially, some fish did not consume the low quality diet and lost mass during the first 2 weeks, and there was a lack of change in the stable isotope ratios of the liver between days 0 to 18 (Fig. 2.6). In contrast, observed growth rates for fish fed the medium quality diet were similar to the natural juvenile Atlantic croaker growth rates of 0.5-0.99 mm $d^{-1}$ reported by Knudsen and Herke (1978). Control fish did exhibit the highest growth rates of 0.84 mm $d^{-1}$, confirming the diets were of high quality.

Nitrogen isotope half-lives of Atlantic croaker muscle tissue ranged from 27-54 days, which was within the range of the half-life for juvenile sand goby muscle of 28 d (Guelinckx et al. 2007), slightly longer than the half-life of muscle of juvenile Japanese temperate sea bass of 19 d (Suzuki et al. 2005), and shorter than those of muscle of juvenile grass carp of 68 d (Xia et al. 2013b). Atlantic croaker liver tissue turned over rapidly with $\delta^{15}N$ isotopic half-lives ranging from 9-18 d, which is approximately 1X to 3X faster than liver tissues of juvenile sea bass or carp, respectively (Suzuki et al. 2005; Xia et al. 2013b), but 3X slower than the half-life of sand goby liver tissue of 3 d (Guelinckx et al. 2007). We attribute faster turnover rates of liver compared to muscle tissues to greater protein synthesis and degradation rates in liver, and thus greater contribution of metabolic turnover to tissue turnover (Martínez del Rio et al. 2009).

A strong contribution of metabolic turnover to nitrogen isotope turnover was detected with the Fry and Arnold (1982) model yielding *c*-values of -5 for the liver and the Hesslein et al. (1993) model yielding *m* parameters that were significantly different from zero for both muscle and liver. Our results are consistent with other diet switch experiments on fishes that have reported *c* values ranging from -4 to -5 for $\delta^{15}N$ liver, and -1 to -2.3 for $\delta^{15}N$ muscle (Logan et al. 2006; Guelinckx et al. 2007; Buchheister and Latour 2010; Xia et al. 2013b). The percent contribution of metabolic turnover to total

isotope turnover (MTO) was consistently estimated to be 53-58 % for muscle and 85% for the liver tissue, regardless of growth rate or diet, which is similar to MTOs reported for carp (Xia et al. 2013b) and summer flounder (Buchheister and Latour 2010). The strong influence of metabolic turnover in the liver resulted in half-lives that were 3X faster than muscle half-lives, which is within the range of other studies that found liver half-lives to be 1.3X (Suzuki et al. 2005), 2.3X (Xia et al. 2013b), or 8-10X (Guelinckx et al. 2007; Buchheister and Latour 2010) faster than muscle half-lives in juvenile fishes. The studies mentioned above examined juvenile fishes in the size range of 6-50g, within the size range of fish in this study. However, in older slow-growing fishes with lower metabolism, differences in turnover between tissues may be less apparent and occur on the order of years (Hesslein et al. 1993; Madigan et al. 2012).

### 2.4.2 Carbon turnover and lipid correction

To our knowledge, this is the first study to directly compare bulk and non-lipid carbon isotope tissue-specific turnover rates and TDF using empirically derived mathematical lipid correction equations. We developed tissue-specific lipid correction equations because applying lipid corrections based on different species can be problematic (Mintenbeck et al. 2008). Instead of measuring the isotopic composition of the lipid-free portion of tissues, as is commonly done (e.g. Post et al. 2007), in this study lipids were extracted and their $\delta^{13}C$ values used in a mass balance mixing model to estimate the non-lipid fraction of the carbon pool and its isotopic composition ($\delta^{13}C_{NL}$). Although Folch-based lipid extraction techniques (Folch et al. 1957) are more complex than lipid removal methods commonly used in isotope studies, extraction techniques yield measurements of lipid dry weight and percent lipid composition, which were

essential variables used in developing lipid correction models. Non-lipid portions of muscle tissue were on average about 1‰ enriched in $^{13}C$ compared to bulk samples, which has been reported in other studies (Sotiropoulos et al. 2004; Elsdon et al. 2010). Lipids are depleted in $^{13}C$ compared to protein and carbohydrates due to kinetic isotope fractionation that occurs during lipid synthesis (DeNiro and Epstein 1977). The degree of $^{13}C$ depletion in tissues is strongly correlated to the lipid content and C:N ratio of the tissue (Post et al. 2007; Logan et al. 2008). We found a linear relationship between C:N ratios and bulk $\delta^{13}C$ values for both the muscle and liver tissues, which supported using a simple linear lipid-correction equation. The effect of lipid correction on tissue turnover rate and its influence on growth versus metabolic turnover varied according to diet type and our lipid correction approach allowed us to make important inferences about the dynamics of carbon assimilation.

### 2.4.3 Growth versus metabolism

Our results suggested that turnover of carbon isotopes in both liver and muscle tissue was almost completely driven by growth because the curve-fitted values of the *c* parameters were not significantly different from -1 for both bulk and the non-lipid carbon pools in both tissue types from both experimental diets. For the medium quality diet, the *c* parameter for the non-lipid carbon pools in liver was more negative than that for the low quality diet (-2.1±1.8), but the estimate had the poorest model fit ($r^2$=0.19). In addition, for the medium quality diet the values of all *m*-parameters were not statistically different than zero. In contrast, the *m*-parameter estimates for non-lipid muscle and bulk liver tissue for fish fed the low-quality diet were statistically different from zero with MTOs of 62% for non-lipid fraction of muscle and 88% for bulk liver. Other studies have

reported primarily growth-based carbon isotope turnover in muscle (Watanabe et al. 2005; Zuanon et al. 2006; Buchheister and Latour 2010; Malpica-Cruz et al. 2012) but few studies have quantified growth-based isotope turnover for liver. We expected to find a stronger influence of metabolic turnover on liver carbon turnover than for muscle tissue, based on the importance of metabolic turnover indicated by the analysis of the nitrogen isotope turnover in our study and results for other juvenile fishes (Guelinckx et al. 2007; Buchheister and Latour 2010; Xia et al. 2013a). Instead, we found growth to be the predominant driver of carbon isotope turnover in all tissue and diet treatments, except for livers of low quality diet fish. This deviation from a growth-driven turnover to metabolism-driven turnover may be due to the significantly slower growth rates of fish fed the low quality diet

The limited difference in the isotopic composition between the initial and experimental diets may have caused reduced precision and accuracy in our model parameter estimates when fitting the carbon isotope data. For instance, the $\delta^{13}C$ values of the medium and low quality diets only differed from the control diet by 1.1‰ and 2‰, respectively, while $\delta^{15}N$ values varied by 4.8‰ and 7‰, respectively. The small isotopic difference between the control and medium quality diet (only 1‰) resulted in high dispersion of the data (low signal-to-noise ratio), large error in *c* and *m* parameter estimates, and low $r^2$ values (ranging 0.25-0.52) indicating poor model fits. The larger difference of 2‰ between the control and low quality diet resulted in better model fits with higher $r^2$ values (0.56-0.88). These results suggest that larger isoscape gradients (differences in end-member isotope values) should allow for better resolution of detecting natural diet switches. Additionally, we found differences in tissue-specific turnover rates of fish fed the medium quality diet compared to the low quality diet, mostly due to

differences in protein and lipid content of the diet and retention or catabolism of lipids in specific tissues.

### 2.4.4 Isotope half-lives ($t_{50\%}$)

Fish tissues have more variable stable isotope half-lives compared to birds and mammals, and a recent review found isotope half-lives in fishes to range between 1-7 weeks in liver tissue and 2-8 weeks in muscle (Boecklen et al. 2011), which concurs with our results. Carbon half-lives for fish fed the medium quality diet ranged 4-5 weeks for bulk muscle and 6-7 weeks for bulk liver. There was a minor difference between non-lipid and bulk fractions in liver half-lives of medium diet fish (only 1 week), even though liver lipid content (46±3%) was twice that of muscle (23±2% lipid of DW) (Table 2.5). In contrast, carbon isotope turnover in muscle and liver tissues of fish fed the low quality diet varied between non-lipid and bulk fractions, potentially related to the large difference in lipid content (37% of DW) between muscle and liver tissues as well as variations in the carbon metabolism of the non-lipid and lipid fractions.

In muscle tissue of the fish fed the low quality diet, the bulk carbon isotope ratios were variable and the half-life therefore had a high error (79±38 d), while the lipid-corrected values were more consistent, leading to a greater precision in the half-life estimate (43±8 d). The carbon isotope half-life of bulk muscle was 1.8X slower than the non-lipid fraction. This likely reflects either rapid lipid accumulation, given that lipid content was substantially higher in fish fed the low-quality diet at d 104 (24±6% per DW) compared to day 0 (12±2%), or retention of lipids from the previous high quality control diet. A companion study by Smith et al. (*In Review*) analyzed the fatty acid composition of a subset of fish (N=49) from this experiment, and found that a terrestrially derived

fatty acid (18:2n-6) increased proportionally from 3% of total fatty acids at d 0 to 16% at d 104 in muscle tissue of fish fed the low quality diet. The incorporation of terrestrially-derived fatty acids due to the nutritionally-deficient diet led to slower growth rates and hence longer turnover times in bulk muscles of low-diet fish. The faster turnover of the non-lipid muscle was driven by both growth and metabolic turnover (MTO=62%), indicating protein catabolism occurred during the course of the experiment. However, the opposite was true for the liver tissue, in which the bulk fraction had a shorter half-life of 14±2 d than the non-lipid fraction (61±21 d). Livers from fish fed the low quality diet had higher lipid content (60±2%) and MTO was very high (88% of isotopic turnover was attributed to metabolic turnover). This suggests that lipid metabolism contributed to the faster carbon isotope turnover of bulk livers of fish fed the low quality diet compared with those fed the medium quality diet or when considering the non-lipid carbon fraction. Thus, fish feeding on a nutritionally poor diet with low growth rates may increase the storage of lipids in muscle tissue resulting in increased half-lives, while the metabolism of lipids in liver tissues would decrease half-life estimates. Overall, comparing lipid corrected values to bulk values allowed differentiation between lipid retention and lipid metabolism, which had opposite effects on turnover estimates.

### 2.4.5 Trophic discrimination factors

To accurately interpret diet from tissue-specific stable isotope analysis requires knowledge of TDF, which are often assumed to remain constant for nitrogen at approximately 3-4‰ and 0-1‰ for carbon (DeNiro and Epstein 1977; DeNiro and Epstein 1981; Minagawa and Wada 1984; Peterson and Fry 1987). However, recent studies have demonstrated that TDF can vary widely depending on diet quantity and

quality (Adams and Sterner 2000; Caut et al. 2009; Robbins et al. 2010; Elsdon et al. 2010), and tissue type (Suzuki et al. 2005; Buchheister and Latour 2010; Malpica-Cruz et al. 2012; Xia et al. 2013b; Xia et al. 2013a).

### 2.4.6 Nitrogen TDF

The experimental 'low-quality' diet with a low protein content, low $\delta^{15}N$ values, and high C:N ratios resulted in lower TDF in the muscle tissue, which concurs with several other studies (Adams and Sterner 2000; Caut et al. 2009; Robbins et al. 2010; Elsdon et al. 2010). In this study, TDF of Atlantic croaker muscle estimated for fish at the end of the experiment ranged from 3‰ (in control fish fed the diet with the highest protein quality) to 6.5‰ (in the lowest quality diet). The TDF values reported for summer flounder of 2.1-2.5‰ (Buchheister and Latour 2010), Japanese temperate sea bass of 2.4‰ (Suzuki et al. 2005), neonate leopard sharks of 2.3‰ (Malpica-Cruz et al. 2012), Pacific blue-fin tuna of 1.9‰ (Madigan et al. 2012), and grass carp of 3-3.9‰ (Xia et al. 2013b) are comparable to the values we found for fish fed the control and medium quality diets. The high TDF calculated for muscle (6.5‰) in the low quality diet fish likely resulted from muscle tissue not reaching equilibrium with the diet by d 104, as indicated by both the long half-lives ($t_{50\%}$= 79±38; $t_{95\%}$= 343±163) and large $TDF_{difference}$ (1.2-1.7). Liver $\Delta^{15}N$ of Atlantic croaker ranged from 1.5-3‰, which was similar to liver $\Delta^{15}N$ in grass carp of 3.1‰ (Xia et al. 2013b), and summer flounder ranging 1.5-2.3‰ (Buchheister and Latour 2010), but higher than liver $\Delta^{15}N$ values in other marine fishes (Suzuki et al. 2005; Madigan et al. 2012) and elasmobranchs (Malpica-Cruz et al. 2012). The difference in $\delta^{15}N$ enrichment (muscle>liver) could be related to differing levels of essential versus non-essential amino acids, with livers containing more essential amino

acids that exhibit less fractionation (Pinnegar and Polunin 1999; Martínez del Rio et al. 2009; Bloomfield et al. 2011).

### 2.4.7 Carbon TDF

Carbon TDF exhibited consistent trends, where TDF of muscle were always positive and enriched relative to diet, while TDF of livers were mostly negative and depleted compared to diet. TDF of non-lipid pools in muscle were about +1‰ higher compared to TDF of bulk muscle, for both the medium and low quality diets. In contrast, TDF of non-lipid pools in liver increased by +1.8 and +2.2‰ compared to bulk liver for the medium and low quality diets, respectively. TDF calculated based on the $\delta^{13}C$ values of the lipid-extracts from muscles and livers and lipid-extracts from diets were -0.3 and -0.8‰ for the medium quality diet and -0.7 and -1.4‰ for the low quality diet, respectively. The small fractionation between lipid only portions of the diet and tissues suggests that lipid $\delta^{13}C$ values in tissues may accurately reflect $\delta^{13}C$ values of lipid pools in diet and thus be used to trace lipid flux through food webs, given that lipid pools often derive from isotopically distinct sources. Unexpectedly, significant shifts were detected in liver $\Delta^{13}C$ of control fish between d 0 and d 104, for the bulk, non-lipid, and lipid fractions. Liver TDFs became more negative by 2, 1.7, and 0.8‰ for bulk, non-lipid, and lipid fractions, respectively. The decrease in bulk liver $\Delta^{13}C$ between d 0 and 104 can be attributed to an increase in lipid content from 40% to 72% and thus depleted $\delta^{13}C$ tissue values over the experiment. However, that both non-lipid and lipid TDF also changed over the course of the experiment suggests that other factors besides lipid accumulation could be responsible and requires further study. Researchers that do not account for the influence of lipids and assume constant TDF for tissues that vary substantially in lipid

content may misinterpret estimates of trophic linkages and the proportional contribution of different carbon sources.

### 2.4.8 Application of stable isotope half-lives to field studies

Although isotopic half-lives are most commonly reported in diet switch studies, they only estimate time required for 50% equilibrium with diet. A more ecologically relevant turnover estimate is the time to 95% equilibrium ($t_{95\%}$) because it represents the amount of time for near complete isotopic equilibrium. The estimated $t_{95\%}$ are consistently 4.3X greater than for both diets and tissues. For example, for fish fed the medium quality diet that experienced growth rates more similar to natural populations, the muscle tissue $t_{95\%}$ was approximately 4 months. Over a seasonal time scale of 4 months, changes in food abundance and lipid content would be expected that would complicate application of laboratory turnover estimates, especially for an opportunistic omnivorous fish such as Atlantic croaker (Overstreet and Heard 1978). Future controlled feeding studies should estimate $t_{95\%}$ in order to be applicable to field studies of this nature.

### 2.4.9. Conclusions

Understanding stable isotope assimilation dynamics with controlled laboratory experiments is fundamental for interpreting isotope-inferred trophic relationships in natural settings. Combining multiple animal tissues with different isotopic 'clocks' provides important information on the timing of animal migration across isoscapes, such as identifying early versus late migrants and the ecological consequences of variable migration histories on individual and population levels. In this controlled experiment

nitrogen isotopes in liver tissues equilibrate with diet 3X faster than muscle tissue and thus can act as short-term dietary 'clocks' while muscle tissues equilibrate with diet over longer temporal scales. Carbon isotope turnover depended on the magnitude of the isotopic diet shift and the effect of lipids including tissue-specific lipid retention, which decreased muscle turnover, and lipid metabolism, which increased liver turnover. Therefore, we recommend that future studies consider the influence of lipids on carbon isotope values of specific species and specific tissues, and where feasible develop tissue- and species-specific lipid-correction equations to accurately estimate tissue half-lives and precisely constrain the effect of lipids. Furthermore, we advocate that lipids are essential dietary resources, and thus removing lipids for food web studies biases interpretation in favor of a protein or non-lipid driven food web. This may be a suitable approach for specific ecosystems (i.e. tropical and subtropical) where lipids are not highly conserved, but other ecosystems like polar and temperate regions are highly dependent on lipid dynamics (e.g., Falk-Petersen et al. 2007) and their trophic effects should not be overlooked. Likewise, the trophic transfer of lipid-soluble organic pollutants often mirrors the flow of lipids through a food web (Kainz and Fisk 2009). Thus, tracing lipid pathways through food webs can elucidate dietary sources of contaminants in consumers. To derive accurate turnover and TDF estimates from laboratory diet switch experiments that can be applied to field situations, we recommend designing experiments with multiple diet types (including controls) that reflect natural diets, and directly examining the influence of lipids on tissue-specific turnover and fractionation, by developing empirical mathematical correction equations.

**Table 2.1** Diet composition, mean C:N molar ratios and mean stable isotope values (N = 4 ± SE) for three treatment diets used in the experiment. The lipid $\delta^{13}C$ values were directly measured, while the non-lipid $\delta^{13}C$ values were estimated using mixing models.

| diet | % protein | % fat | % fiber | % ash | C:N | $\delta^{15}N$ | $\delta^{13}C$ | $\delta^{13}C$ non-lipid | $\delta^{13}C$ lipid |
|---|---|---|---|---|---|---|---|---|---|
| control[a] | 48 | 14.5 | 2 | 14 | 6.3±0.1 | 10.7±0.3 | -21.7±0.11 | -20.5±0.23 | -25.44±0.16 |
| medium[b] | 45 | 12 | 3.5 | | 7.4±0.2 | 5.9±0.35 | -22.6±0.41 | -22.2±0.02 | -24.26±0.20 |
| low[c] | 32 | 5 | <5 | <7 | 9.5±0.5 | 3.7±0.21 | -23.7±0.16 | -23.5±0.03 | -25.25±0.23 |

[a] Otohime EP3, dry pellet (Reed Mariculture Inc.).

[b] Aquafeed 4512 (FK), dry pellet (Cargill Animal Nutrition).

[c] Production 32, dry pellet (Rangen Connatural Products).

**Table 2.2** Growth-based tissue turnover model parameter estimates (± SE) based on the model of Fry & Arnold (1982). Estimates of *c* parameters in bold are significantly different from -1 as determined by a t-test ($p<0.05$). Predicted final δ values are derived from the curve fitting procedure, while observed final δ values (mean ± SE) were measured at the end of the experiment on d 104.

| | | | | | Fry & Arnold 1982 | | |
|---|---|---|---|---|---|---|---|
| diet | element | tissue | initial $\delta_{observed}$±SE | final $\delta_{observed}$±SE | *c* ± SE | $r^2$ | final $\delta_{predicted}$±SE |
| | | muscle | 13.0±0.04 | 10.6±0.1 | -1.00±0.15 | 0.95 | 9.39±0.35 |
| | $\delta^{15}N$ | liver | 11.5±0.13 | 8.0±0.3 | **-5.27±0.81** | 0.88 | 7.34±0.16 |
| MED | | muscle | -19.7±0.14 | -20.7±0.14 | -1.1±0.93 | 0.4 | -21.2±0.79 |
| | $\delta^{13}C$ | muscle non-lipid | -18.6±0.09 | -19.3±0.05 | -1 | 0.49 | -19.6±0.48 |
| | | liver | -22.6±0.23 | -24.3±0.12 | -0.99±0.88 | 0.29 | -24.7±1.15 |
| | | liver non-lipid | -20.7±0.09 | -22.2±0.29 | -2.09±1.84 | 0.19 | -21.9±0.49 |
| | $\delta^{15}N$ | muscle | 13.0±0.04 | 10.2±0.09 | -1.48±0.45 | 0.89 | 8.45±0.88 |
| | | liver | 11.5±0.13 | 6.7±0.19 | **-5.51±1.1** | 0.75 | 5.66±0.45 |
| LOW | | muscle | -19.7±0.14 | -21.3±0.22 | -1 | 0.66 | -23.2±2.4 |
| | $\delta^{13}C$ | muscle non-lipid | -18.6±0.09 | -20.1±0.11 | -1 | 0.79 | -21.7±1.4 |
| | | liver | -22.6±0.23 | -25.8±0.15 | -2.35±1.2 | 0.24 | -26.6±1.1 |
| | | liver non-lipid | -20.7±0.09 | -23.5±0.4 | -1 | 0.62 | -26.1±3.5 |

**Table 2.3** Time-based tissue turnover model parameter estimates (± SE) based on the model of Hesslein et al. (1993). Estimates of *m* in **bold** are significantly different from 0, as determined by t-test ($p<0.05$). MTO is the percent contribution of metabolic turnover to total isotope turnover, $t_{50\%}$ is the time in days for 50% isotope turnover, and $t_{95\%}$ is the time in days for 95% isotope turnover. Predicted final δ values are derived from the curve fitting procedure, while observed final δ values (mean ± SE) were measured at the end of the experiment on d 104.

| | | | | | Hesslein et al. 1993 | | | | | | | |
|---|---|---|---|---|---|---|---|---|---|---|---|---|
| diet | element | tissue | initial $\delta_{observed}$±SE | final $\delta_{observed}$±SE | *k* | *m* ($d^{-1}$)±SE | *k*+*m* | MTO | $t_{50\%}$ (d) | $t_{95\%}$ (d) | $r^2$ | final $\delta_{predicted}$±SE |
| MED | $\delta^{15}N$ | muscle | 13.0±0.04 | 10.6±0.1 | 0.0112±0.0004 | **0.015±0.003** | 0.026 | 57.7 | 27±3 | 115±12 | 0.93 | 10.4±0.13 |
| | | liver | 11.5±0.13 | 8.0±0.3 | | **0.069±0.012** | 0.081 | 85.2 | 9±1 | 37±5 | 0.69 | 7.3±0.17 |
| | $\delta^{13}C$ | muscle | -19.7±0.14 | -20.7±0.14 | | 0.012±0.013 | 0.023 | n/a | 30±11 | 129±47 | 0.41 | -20.9±0.33 |
| | | muscle non-lipid | -18.6±0.09 | -19.3±0.05 | | 0.0083±0.009 | 0.019 | n/a | 36±12 | 154±50 | 0.52 | -19.5±0.22 |
| | | liver | -22.6±0.23 | -24.3±0.12 | | 0.0027±0.0092 | 0.014 | n/a | 50±20 | 216±88 | 0.38 | -24.8±0.85 |
| | | liver non-lipid | -20.7±0.09 | -22.2±0.29 | | 0.005±0.013 | 0.0162 | n/a | 43±20 | 185±85 | 0.25 | -22.5±0.83 |
| LOW | $\delta^{15}N$ | muscle | 13.0±0.04 | 10.2±0.09 | 0.00607±0.0004 | **0.0069±0.003** | 0.013 | 53.1 | 54±11 | 232±48 | 0.89 | 9±0.58 |
| | | liver | 11.5±0.13 | 6.7±0.19 | | **0.033±0.0093** | 0.039 | 84.6 | 18±3 | 76±15 | 0.75 | 5.74±0.51 |
| | $\delta^{13}C$ | muscle | -19.7±0.14 | -21.3±0.22 | | 0.0027±0.0075 | 0.009 | n/a | 79±38 | 343±163 | 0.56 | -22.7±1.8 |
| | | muscle non-lipid | -18.6±0.09 | -20.1±0.11 | | **0.0099±0.003** | 0.016 | 61.9 | 43±8 | 188±33 | 0.88 | -20.6±0.22 |
| | | liver | -22.6±0.23 | -25.8±0.15 | | **0.044±0.0092** | 0.05 | 88.0 | 14±2 | 60±10 | 0.78 | -25.6±0.19 |
| | | liver non-lipid | -20.7±0.09 | -23.5±0.4 | | 0.0052±0.0056 | 0.011273 | n/a | 61±21 | 265±91 | 0.69 | -24.8±1.3 |

**Table 2.4.** Trophic Discrimination Factors (TDF) for each diet treatment, isotope ratio, and tissue calculated from observed mean tissue values at days 0 and 104 and for predicted final isotope values. Model predicted TDF were estimated using the growth-based Fry and Arnold (1982) and time-based Hesslein et al. (1993) model outputs.

| diet | isotope | tissue | observed TDF | | model predicted TDF | | | |
|---|---|---|---|---|---|---|---|---|
| | | | | | Fry and Arnold 1982 | | Hesslein et al. 1993 | |
| | | | day 0 | day 104 | $TDF_{pred}$ | $TDF_{diff}$ | $TDF_{pred}$ | $TDF_{diff}$ |
| CON | $\delta^{15}N$ | muscle | +2.34 | +2.98 | | | | |
| | | liver | +0.77 | +1.45 | | | | |
| | $\delta^{13}C$ | muscle | +1.98 | +1.36 | | | | |
| | | liver | -0.94 | -2.97 | | | | |
| | $\delta^{13}C_{non\text{-}lipid}$ | muscle | +1.87 | +1.71 | | | | |
| | | liver | -0.24 | -1.92 | | | | |
| | $\delta^{13}C_{lipid}$ | muscle | +0.02 | -0.14 | | | | |
| | | liver | +0.52 | -0.30 | | | | |
| MED | $\delta^{15}N$ | muscle | | +4.67 | +3.5 | 1.17 | +4.46 | 0.21 |
| | | liver | | +2.11 | +1.45 | 0.66 | +1.41 | 0.70 |
| | $\delta^{13}C$ | muscle | | +1.79 | +1.33 | 0.46 | +1.59 | 0.20 |
| | | liver | | -1.77 | -1.22 | -0.55 | -2.23 | 0.46 |
| | $\delta^{13}C_{non\text{-}lipid}$ | muscle | | +2.87 | +2.56 | 0.31 | +2.72 | 0.15 |
| | | liver | | -0.01 | +0.21 | -0.22 | -0.31 | 0.30 |
| | $\delta^{13}C_{lipid}$ | muscle | | -0.25 | | | | |
| | | liver | | -0.84 | | | | |
| LOW | $\delta^{15}N$ | muscle | | +6.49 | +4.79 | 1.70 | +5.34 | 1.15 |
| | | liver | | +3.01 | +2.0 | 1.01 | +2.08 | 0.93 |
| | $\delta^{13}C$ | muscle | | +2.3 | +0.41 | 1.89 | +1.01 | 1.29 |
| | | liver | | -2.18 | -2.97 | 0.79 | -1.95 | -0.23 |
| | $\delta^{13}C_{non\text{-}lipid}$ | muscle | | +3.34 | +1.75 | 1.59 | +2.84 | 0.50 |
| | | liver | | -0.01 | -2.62 | 2.61 | -1.33 | 1.32 |
| | $\delta^{13}C_{lipid}$ | muscle | | -0.72 | | | | |
| | | liver | | -1.38 | | | | |

**Table 2.5** Percent lipid (mean±SEM) for muscle and liver tissues and extracted lipid $\delta^{13}C$ value over experimental time. 'Total' represents the mean of each treatment for all time points.

| tissue | time (d) | control | | | | medium | | | | low | | | |
|---|---|---|---|---|---|---|---|---|---|---|---|---|---|
| | | % lipid | N | $\delta^{13}C$ lipid | N | % lipid | N | $\delta^{13}C$ lipid | N | % lipid | N | $\delta^{13}C$ lipid | N |
| muscle | 0 | 12±2 | 8 | -25.4±0.22 | 4 | | | | | | | | |
| | 7 | 20±4 | 5 | -25.9±0.31 | 2 | 15±4 | 5 | -25.5±0.32 | 2 | 30±13 | 5 | -25.8±0.07 | 2 |
| | 18 | 15±2 | 5 | -25.8±0.23 | 2 | 23±6 | 4 | -25.2±0.19 | 2 | 16±3 | 5 | -26.3±0.04 | 2 |
| | 32 | 24±5 | 6 | -25.8±0.23 | 3 | 24±4 | 5 | -25±0.07 | 2 | 19±6 | 5 | -25.8±0.07 | 2 |
| | 52 | 43±7 | 5 | -25.5±0.03 | 2 | 31±6 | 5 | -24.5±0.01 | 2 | 24±5 | 5 | -25.7±0.17 | 3 |
| | 104 | 25±6 | 5 | -25.6±0.02 | 2 | 22±3 | 5 | -24.5±0.001 | 2 | 24±6 | 5 | -26±0.05 | 2 |
| | total | 23±4 | 6 | -25.7±0.18 | 6 | 23±2 | 5 | -25.0±0.12 | 5 | 23±3 | 5 | -25.9±0.08 | 5 |
| liver | 0 | 40±5 | 8 | -24.9±0.22 | 4 | | | | | | | | |
| | 7 | 31±3 | 5 | -24.6±0.19 | 2 | 40±3 | 5 | -24.8±0.10 | 2 | 66±2 | 4 | -25.9±0.06 | 2 |
| | 18 | 49±8 | 6 | -24.5±0.03 | 3 | 43±9 | 5 | -24.9±0.29 | 2 | 58±2 | 5 | -25.5±0.25 | 2 |
| | 32 | 52±4 | 4 | -25±0.10 | 2 | 40±10 | 4 | -24.5±0.02 | 2 | 52±11 | 5 | -25.7±0.03 | 2 |
| | 52 | 59±8 | 5 | -25±0.40 | 2 | 52±4 | 6 | -24.7±0.27 | 3 | 62±3 | 6 | -25.9±0.31 | 3 |
| | 104 | 72±8 | 4 | -25.7 | 1 | 54±2 | 4 | -25.1±0.35 | 2 | 62±5 | 5 | -26.6±0.12 | 2 |
| | total | 51±6 | 6 | -25±0.19 | 6 | 46±3 | 5 | -24.8±0.21 | 5 | 60±2 | 5 | -25.9±0.15 | 5 |

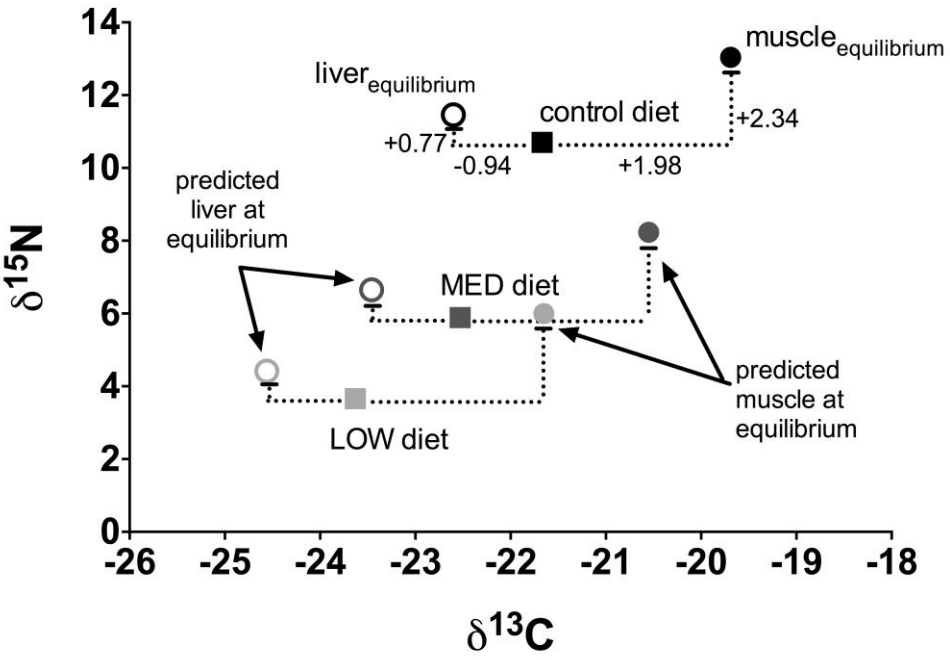


**Figure 2.1**. Bulk $\delta^{13}C$ and $\delta^{15}N$ values of experimental diets (squares) and day 0 equilibrated liver tissue (open black circle) and muscle tissue (filled black circle) of Atlantic croaker used to estimate trophic discrimination factors (TDF). Estimated TDF were used to calculate 'predicted' equilibrium liver values (open gray circles) and 'predicted' equilibrium muscle values (filled gray circles) for fish fed the experimental diets (medium (MED) and LOW quality) used during modeling of isotope turnover rates. Mathematically corrected non-lipid $\delta^{13}C$ data not shown.

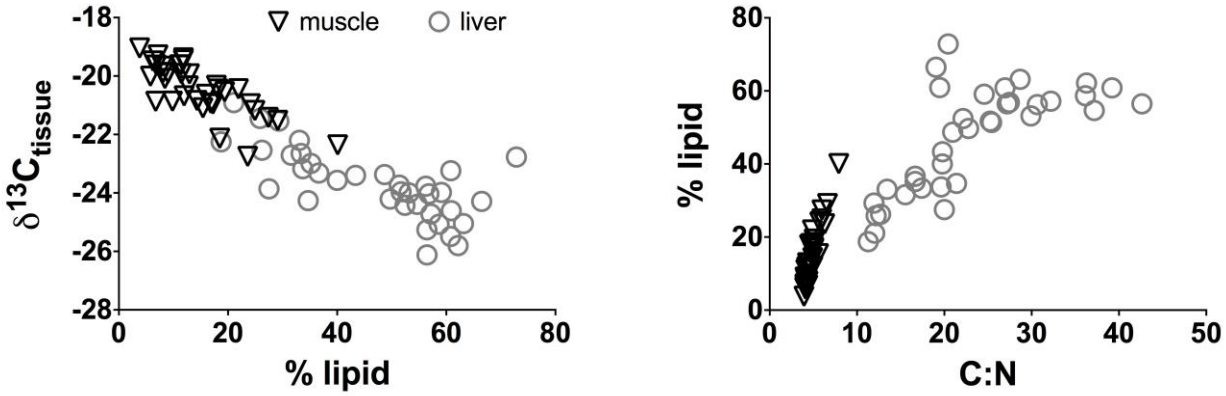


**Figure 2.2** Relationships between measured percent lipid and bulk muscle (black inverted triangles) and liver (gray open circles) tissue $\delta^{13}C$ values (left) and molar C:N ratios (right).

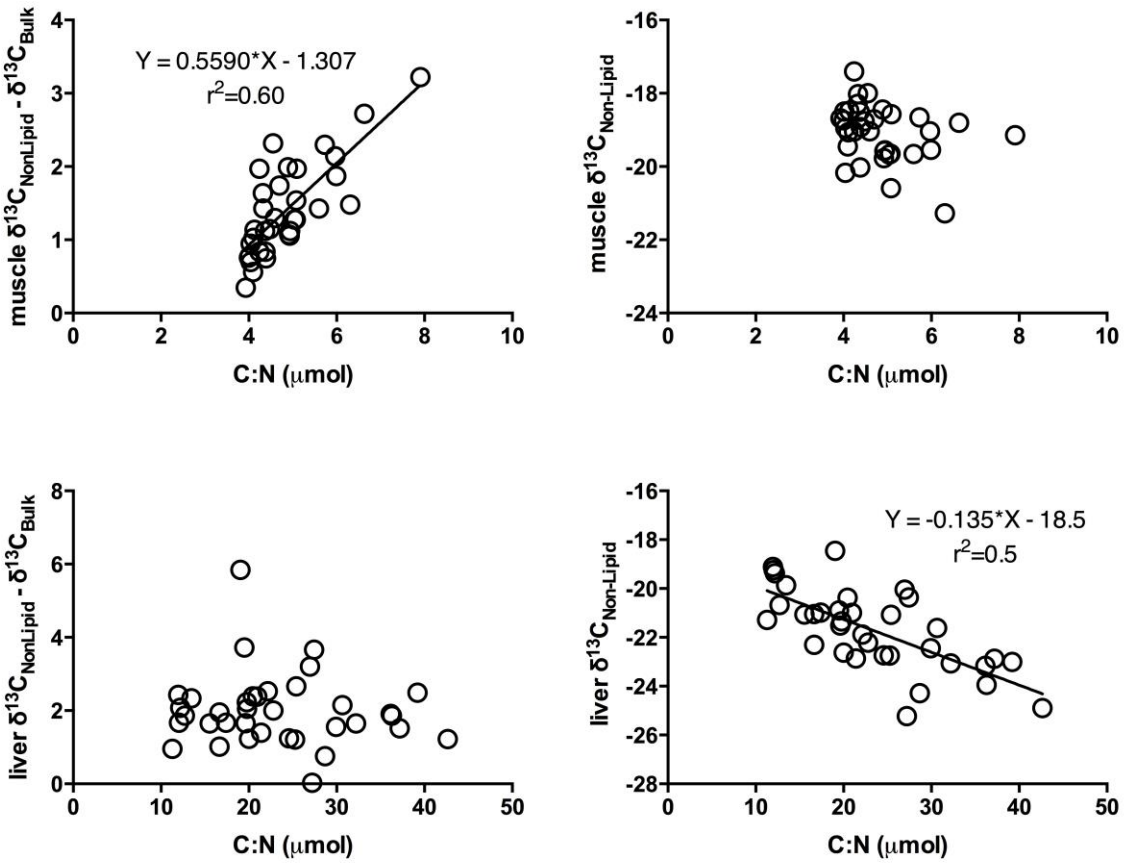


**Figure 2.3** Relationships between C:N molar ratios and the difference between mass balance estimated $\delta^{13}C_{\text{non-lipid}}$ values and $\delta^{13}C_{\text{bulk}}$ values (left panels), or between mass balance estimated $\delta^{13}C_{\text{non-lipid}}$ values for muscle (top panels) and liver (bottom panels) tissues. Solid lines indicate significant linear regressions.

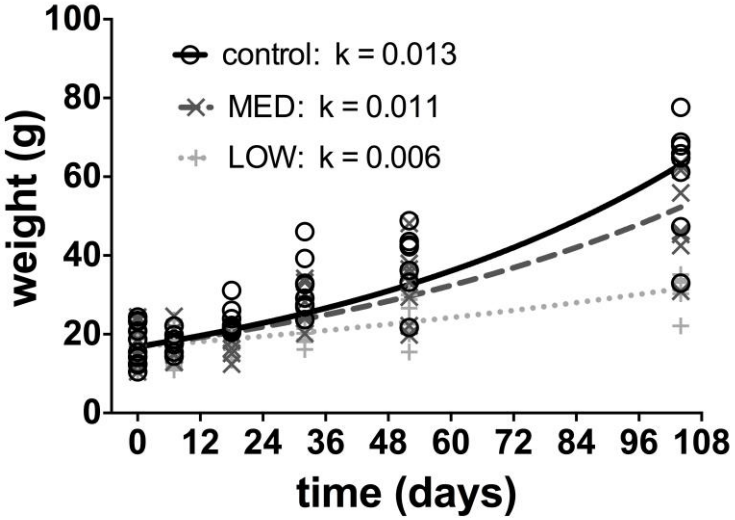


**Figure 2.4** Exponential curve fits for weight gain over time used to estimate the exponential growth constant *k* for Atlantic croaker fed control, medium quality (MED) or low quality (LOW) diets.

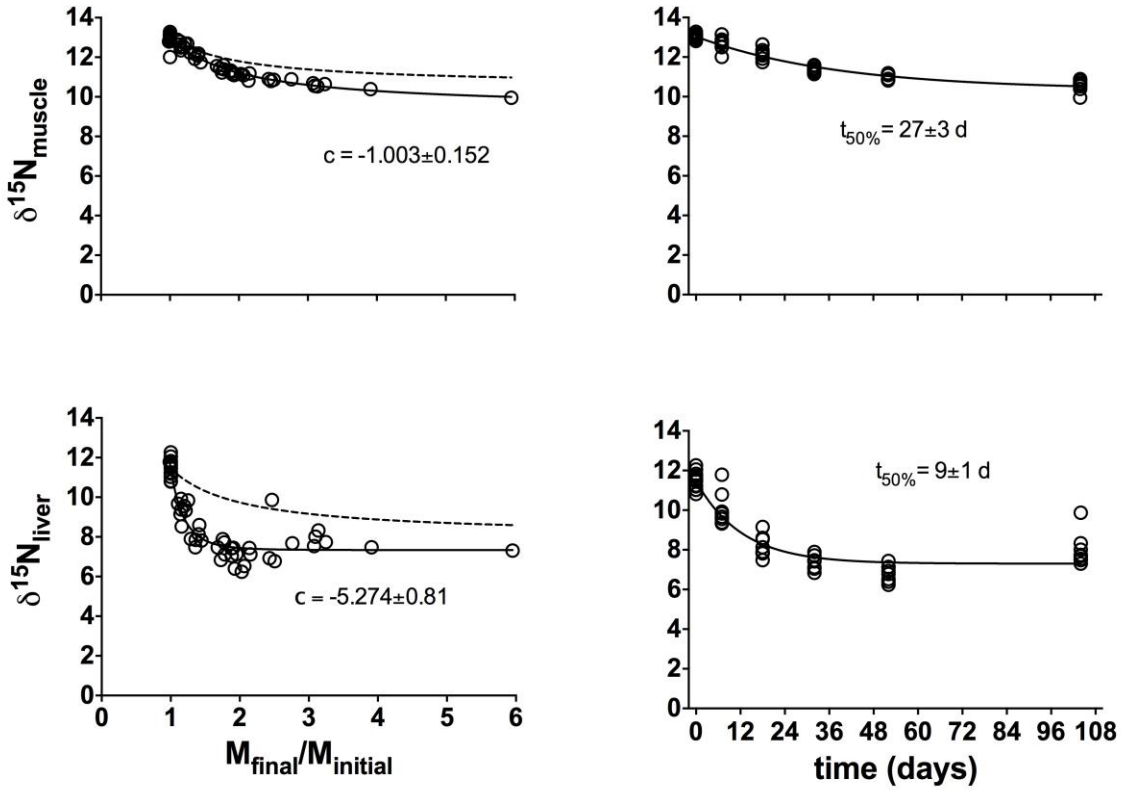


**Figure 2.5** Non-linear curve fits of $\delta^{15}N$ for Atlantic croaker fed a **medium quality** diet using growth based (left panels) and time based (right panels) models for muscle tissue (upper panels) and liver tissue (bottom panels); dashed lines on left panels represent curve fit when *c*=-1 and therefore turnover is due to growth alone. $M_{final}/M_{intial}$= mass of an individual fish at time sampled / initial mass of an individual fish; *c*=coefficient of isotopic turnover; $t_{50\%}$=time (in days) for tissues to reach 50% equilibrium with diet.

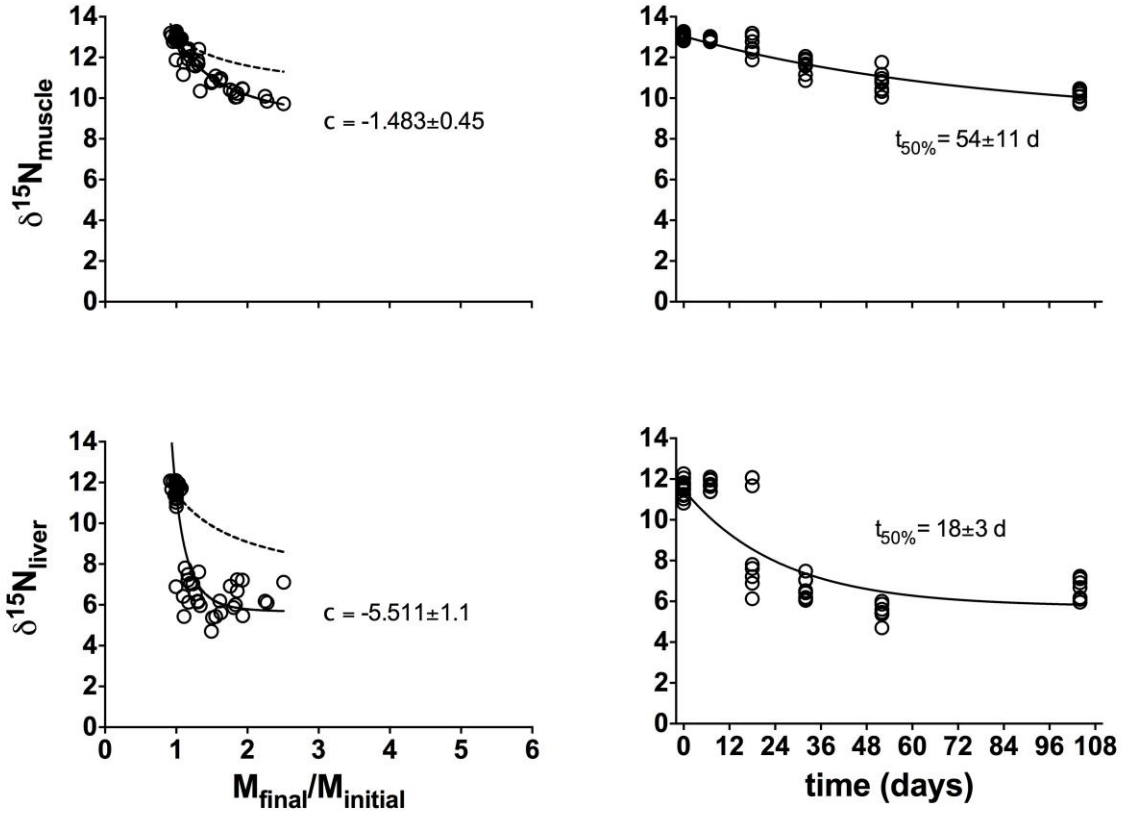


**Figure 2.6** Non-linear curve fits of $\delta^{15}N$ for Atlantic croaker fed a **low quality** diet using growth based (left panels) and time based (right panels) models for muscle tissue (upper panels) and liver tissue (bottom panels); dashed lines on left panels represent curve fit when *c*=-1 and therefore turnover is due to growth alone. The parameters $M_{final}/M_{intial}$, *c*, and $t_{50}$ are defined in **Fig 2.5**.

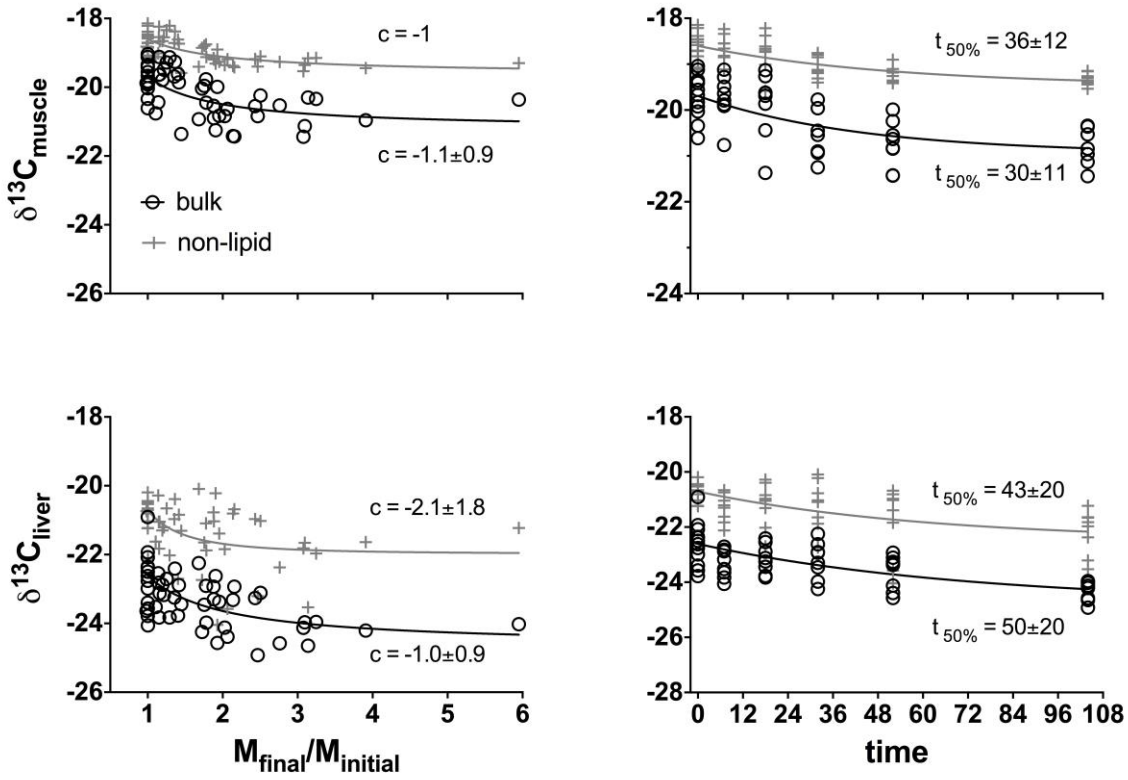


**Figure 2.7** Non-linear curve fits of $\delta^{13}C$ for Atlantic croaker fed a **medium quality** diet using growth-based (left panels) and time-based (right panels) isotope turnover models applied to muscle tissue (upper panels) and liver tissue (bottom panels). Black open circles = bulk $\delta^{13}C$; gray crosses=mathematically corrected non-lipid $\delta^{13}C$. The parameters $M_{final}/M_{intial}$, $c$, and $t_{50}$ are defined in **Fig 2.5**.

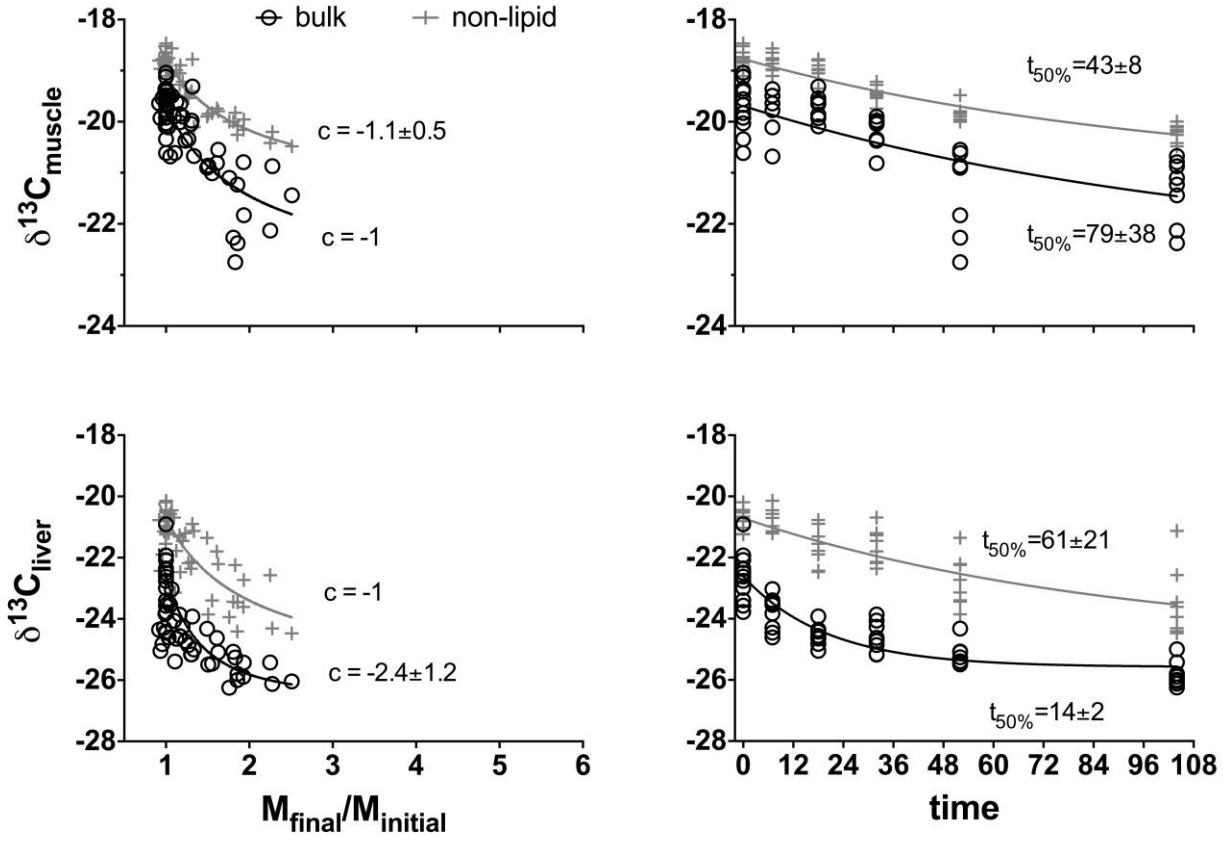


**Figure 2.8** Non-linear curve fits of $\delta^{13}C$ for Atlantic croaker fed a **low quality** diet using growth based (left panels) and time based (right panels) models for muscle tissue (upper panels) and liver tissue (bottom panels). Black open circles = bulk $\delta^{13}C$; gray crosses=mathematically corrected non-lipid $\delta^{13}C$. The parameters $M_{final}/M_{intial}$, *c*, and $t_{50}$ are defined in **Fig 2.5**.

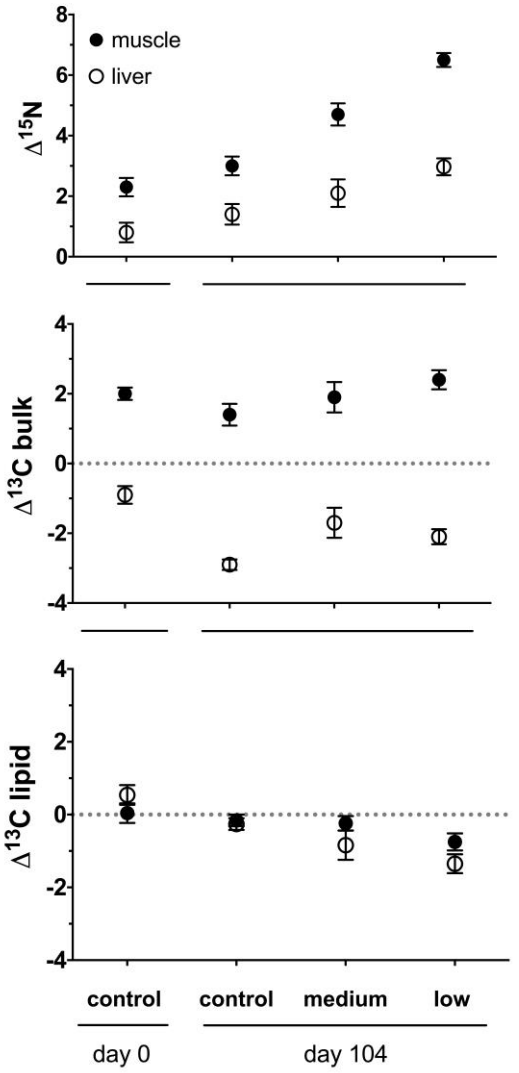


**Figure 2.9** Trophic discrimination factors (TDF) for nitrogen (top panel), bulk carbon (middle panels) and lipid carbon (bottom panel) stable isotopes. TDF for muscle (filled circles) and liver (open circles) were calculated using the observed $\delta_{initial}$ for the control on d 0 and observed $\delta_{final}$ for control, medium or low quality diet treatments at d 104.

# CHAPTER 3: A MULTI-PROXY APPROACH FOR ESTIMATING ESTUARINE HABITAT RESIDENCE ACROSS A GEOGRAPHIC CLIMATIC GRADIENT


## ABSTRACT

Understanding the true value of estuarine nurseries requires information on habitat connectivity and trophic interactions. A novel multi-proxy natural tag approach was developed to estimate estuarine immigration of juvenile Atlantic croaker in subtropical estuaries of the western Gulf of Mexico. Juvenile age-0 fish were collected along a latitudinal gradient that included positive (PS), metastable (MS), and negative (NG) estuary types to test the hypothesis that estuarine ingress timing and habitat residence would vary along climatic and physicochemical gradients. Otolith elemental chronologies of Sr:Ca and Ba:Ca were used to detect fish movement across salinity gradients, while tissue-specific stable nitrogen and carbon isotope ratios revealed time since very recent (liver) and moderately recent (muscle) diet shifts. Nitrogen isotope values in both liver and muscle tissues in fish from all sampling sites were highly correlated ($r^2$=0.98), suggesting both tissues were in isotopic equilibrium and fish were estuarine residents for at least 3 months prior to capture. Anthropogenic nutrient enrichment was reflected in increased $\delta^{15}N$ values in fish in northern positive estuaries that receive high freshwater input. Deviations from the equilibrated muscle-liver $\delta^{13}C$ relationship (residuals) in both the PS and NG suggested recent diet shifts and fish movement between adjacent bays. Otolith edge Sr:Ca and Ba:Ca were related to positive carbon isotope residuals, indicating movement from high to low salinities in the PS, and low to high salinities in the NG. Strong regional gradients in natural tag signatures

suggests local adaptation to environmental conditions and supports bay-specific spatial management of estuarine dependent species along the Texas coast.

## 3.1 INTRODUCTION

Estuaries encompass the land-sea interface and are highly productive systems that provide economically valuable ecosystem services. Importantly, estuaries serve as juvenile nursery habitats by providing a complexity of habitat types that confer predation refuge and prey diversity, factors that promote growth and survival of early life stages (Beck et al. 2001). Current techniques used to estimate the 'value' of nurseries relies on quantifying areas that contribute the most juvenile recruits to offshore adults stocks through ontogenetic migrations (Beck et al. 2001; Vasconcelos et al. 2011). However, defining nursery value as simple biomass transfer overlooks the complex nature of the 'true value' of nurseries, which includes complex ecological interactions and resource dynamics (Le Pape and Bonhommeau 2013; Sheaves et al. 2014). Recent emphasis has shifted from concentrating on discreet areas to focusing on the processes that underlie nursery function and can vary in both space and time (Sheaves et al. 2014). For example, Sheaves et al. (2014) described the variety of components that determine nursery value, such as: 1) connectivity, for both ontogenetic and seascape migrations; 2) ecophysiological factors, such as food webs and predation trade-offs; and 3) resource dynamics, including ontogenetic diet shifts and allochthonous inputs. These nursery functions are not static and change over regional and local scales (Nagelkerken et al. 2013). Therefore, examining nursery functions in diverse estuarine types over broad geographic scales will increase understanding of true nursery value. In order to accomplish this, however, individual-based histories of nursery habitat occupancy and

ecological interactions such as food web participation must be reconstructed to fully evaluate nursery function for mobile species.

In the northern and western Gulf of Mexico, a continuum of estuary 'types' occurs from the Mississippi River delta down to south Texas. The Texas coast is dominated by barrier islands, which enclose estuaries and thus limit seawater exchange to very discreet inlets. Additionally, the arid climate of south Texas causes evaporation to exceed precipitation resulting in inverse estuaries with salinities higher than the ocean, especially during periods of drought (Mohan and Walther 2014). If these enclosed and hypersaline environments pose osmotic challenges to fish ingressing to estuarine embayments, then the nursery function of enclosed estuaries may vary geographically (Able 2005). Currently, there is a lack of information on the degree of estuarine dependency in hypersaline lagoons, or variation in estuarine use over broad geographic scales (Able 2005).

Quantifying the degree of estuarine habitat use and connectivity in marine fish may be achieved by utilizing the geochemical and chronological properties of fish ear stones, or otoliths (Albuquerque et al. 2012). Elements such as strontium and barium have been studied extensively and used to track fish movements between fresh and saltwater environments (reviewed in Walther and Limburg 2012). The relationships between otolith chemistry and water chemistry for Sr and Ba have also been investigated in the laboratory with numerous species (Secor et al. 1995, Bath et al. 2000, Milton and Chenery 2001, Martin and Thorrold 2005; Walther and Thorrold 2006). However, recent work has demonstrated complex physiological influences on otolith element uptake, that may uncouple direct relationships to ambient levels (Sturrock et al. 2014; Izzo et al. 2015). The elemental chemistry of Atlantic croaker otoliths has been measured in numerous studies, and in fact some of the first work using laser ablation ICP MS was

conducted on Atlantic croaker in experimental conditions (Fowler et al. 1995). In those early studies, croaker were held at constant salinities and temperature for 71 days to examine relationships between water characteristics and otolith chemistry. Temperature was found to have a primary effect on otolith Sr, but this effect was confounded by otolith size and growth rate (Fowler et al. 1995). Thorrold et al. (1997) used laser ablation to measure Sr:Ca, Mg:Ca, and Ba:Ca at the otolith core and otolith edge of juvenile croaker collected in brackish rivers in NC and VA. Strontium:Ca was elevated at the otolith core and decreased toward otolith periphery, and the opposite pattern was seen for Ba:Ca. It was suggested these elemental patterns were reflecting the offshore to inshore migration of this estuarine dependent species, with elements reflecting movement across dissolved ion (salinity) gradients. The negative correlation between otolith Sr:Ca and Ba:Ca was again validated in croaker collected in the Chesapeake Bay and Pamlico Sound (Thorrold and Shuttleworth 2000), also reflecting estuarine ingress across salinity gradients. Although these studies found consistent elemental patterns across sectioned otoliths that were hypothesized to originate from variable ambient water chemistries due to salinity gradients, none of them have been based on direct field quantifications of variations in dissolved elemental water chemistry across salinity gradients (Mohan and Walther 2014). These studies also used discrete laser spots on regions of the otolith instead of continuous laser scans that can increase resolution of detecting life-history transitions that can then be coupled to fish growth histories (Hoover et al. 2012). If multiple cohorts can be collected by sampling over many months, it may be possible to identify both early and late migrants (Warlen and Burke 1990; Nixon and Jones 1997).

Retracing fish movements based on dietary changes can be examined using tissue stable isotopes of carbon and nitrogen (Trueman et al. 2012). Nitrogen isotopes reflect trophic level, but also increase due to inputs of anthropogenic wastewater nitrogen

(McClelland et al. 1997). Isotopes of carbon trace autotrophic sources at the base of the food web, and vary between benthic versus pelagic (France 1995) and terrestrial versus marine primary production (Peterson 1999). Few studies to date have employed a multi-proxy approach to investigate estuarine habitat use by combining otolith chemistry to tissue stable isotopes to trace movements across salinity gradients or between food webs (Limburg 1998; Dierking et al. 2012; Fodrie and Herzka 2013). Analyzing multiple tissues that have both high and low growth, and thus fast or slow turnover, may permit detailed understanding of equilibrium conditions in tissues regarding water or diet, and may reveal recent migratory history (Fry et al. 2003; Dierking et al. 2012; Fodrie and Herzka 2013).

This study aims to answer the following research questions: 1) Do estuarine immigration and habitat residence patterns differ along a regional geographic gradient between positive, metastable, and negative estuarine types? 2) Does estuarine habitat use differ within local estuaries, across salinity gradients (using otolith chemistry) and between trophic end members (using tissue isotopes)? 3) What suite of natural proxies can best describe individual migratory patterns? Variation in immigration timing is assessed by comparing muscle and liver isotope values given experimentally validated equilibrium tissue turnover rates (Chapter 2). Linking migratory behavior and habitat connectivity to trophic dynamics in estuarine dependent species can be achieved by utilizing dual natural biogeochemical tags, and contributes to the understanding of nursery habitat value.

## 3.2 METHODS

### 3.2.1 Fish collection

Juvenile young-of-year Atlantic croaker were collected by bottom trawls during Texas Parks and Wildlife Department (TPWD) bi-monthly random stratified fishery-independent sampling from April 2012 through September 2012 in Galveston Bay, the Mission Aransas Estuary, and north Laguna Madre (Figure 3.1; Table 3.1). These regions were selected to represent 3 different estuary types: Galveston Bay - positive (PS) estuary; Mission-Aransas – metastable estuary (MS); and Laguna Madre – negative estuary (NG) and will be referred to as such throughout this chapter. At each station where croakers were collected, measurements of temperature (°C), salinity, and dissolved oxygen (mg/l) were recorded. Fish were humanely euthanized, and placed on ice until frozen in the laboratory.

In the lab, fish were thawed, patted dry, and weighed to the nearest 0.01 g (W) and measured for standard and total length (TL) to the nearest mm. Fulton's condition factor was calculated for each fish using $K= W/TL^3$. Sagittal otoliths were removed, cleaned of adhering tissue with ultrapure water and stored in 1.5 mL vials to air-dry under a class 100 laminar flow hood. Muscle and liver tissues were removed, rinsed with ultrapure water, and freeze dried (-80°C for 48 h) for tissue stable isotopes analysis (described below).

Left otoliths were embedded in Buehler epoxi-cure resin doped with Indium (30ppm) and sectioned in the transverse plane containing the otolith core using an Isomet low speed diamond blade saw (Buehler). Sections were mounted to petrographic slides and polished to the core using 30 μm and 3 μm lapping film and ultrapure water. Individually polished otolith sections were transferred to single petrographic slides (*n*=12

otolith sections/slide) to be ultrasonically cleaned with ultrapure water (5 m cleanse x3) and dried in a class 100 laminar flow hood.

### 3.2.2 Otolith analysis

Otoliths were analyzed for $^{40}Ca$, $^{88}Sr$, $^{138}Ba$ using an Aligent 7500ce ICP-Q-MS coupled to a New Wave UP 193-FX laser with a 26-μm laser spot diameter and 5-μm $s^{-1}$ scan speed at the University of Texas Jackson School of Geoscience, Austin TX. An initial pre-ablation pass (75x75 μm square; 30% power; 25 μm $s^{-1}$) removed surface contamination before acquiring data. Laser transects were run from the otolith core to the outer edge along the longest growth axis of the otolith that exhibits the widest growth increments to improve resolution and detectability of elemental patterns (Mohan et al. 2014). Otolith elemental intensity (counts) data were processed using Iolite (Paton et al. 2011) Trace Element IS data reduction scheme, with calcium (as 37.69 wt % in aragonite) as the internal standard and matrix matched MACS -3 USGS certified calcium carbonate as the reference material. Certified NIST 610 and 612 glass standards ($n$=42) were analyzed every hour during each analytical run, and average RSD's calculated over three analytical days were 6-8% for $^{88}Sr$ and 7% for $^{138}Ba$.

### 3.2.3 Tissue stable isotope analysis

Freeze-dried muscle and liver tissue were ground into a fine powder using a ceramic mortar and pestle. Approximately 1 mg of dried tissue was packaged into tin capsules and shipped to the University of California Davis Stable Isotope Facility for dual $\delta^{15}N$ and $\delta^{13}C$ analysis. A duplicate sample was included every $16^{th}$ sample ($n$=9) and mean standard deviation (SD) between duplicates was 0.08 for $\delta^{15}N$ and 0.07 for

$\delta^{13}C$. Mean SD between certified laboratory standards for $\delta^{15}N$ and $\delta^{13}C$ were: Bovine liver = 0.15 and 0.02; USGS-41 Glutamic Acid = 0.13 and 0.12; Nylon 5 = 0.14 and 0.06; Glutamic Acid = 0.10 and 0.06. Muscle tissue C:N ratios were very consistent (range: 3.7-3.9) and low, and thus were not corrected for lipids. Liver tissue C:N ratios were more variable (range: 5-8), but values were much lower than experimental fish (Chapter 2) and thus liver carbon values were not corrected for lipid content.

### 3.2.4 Long –term regional salinity data

In order to determine the consistency and/or variation of salinity gradients within each estuary and characterize each estuarine type, annual salinity data (1/1/2012-1/1/2013) was gathered from multiple sources. In the positive estuary Galveston Bay (Trinity-San Jacinto Estuary), salinity data was obtained by request from the Texas Water Development Board (www.twdb.texas.gov) at five stations spanning the entire bay: BAYT, FISH, TRIN, MIDG, BOLI. In the metastable Mission-Aransas Estuary, salinity data was downloaded from the National Estuarine Research Reserve Centralized Data Management Office (http://cdmo.baruch.sc.edu) from the following System Wide Monitoring Platform Stations: Copano West (CW), Copano East (CE), and Aransas Bay (AB). Salinity data from the negative hypersaline estuary Laguna Madre was obtained from the Texas Coastal Ocean Observatory Network (TCOON: http://www.cbi.tamucc.edu/cbi/data) station 170 National Park Service-Baffin Bay (mouth of Baffin Bay), and station 171 National Park Service – Bird Island (Upper Laguna Madre). Monthly averages were calculated for each station and plotted from Jan 2012-Dec 2012 (Figure 3.2).

### 3.2.5 Data analysis

Fish were classified into migratory groups based on similarities in otolith chemistry profiles based on both Sr:C and Ba:Ca values as salinity proxies (Figure 3.3). Individual profiles were visually inspected to determine predominant patterns of increase or decrease over the entire transect. Fish that displayed similar characteristics in Sr:Ca and Ba:Ca patterns were grouped together. For example, fish that displayed high Sr:Ca in the otolith core that decreased throughout the primordium as Ba:Ca increased (i.e. Type A Figure 3.3), were grouped together. Spatial and temporal occurrence of otolith-based migratory groups was examined using frequency plots by collection site and collection month (Figure 3.4).

Linear regression was used to examine relationships between muscle and liver tissue carbon and nitrogen isotope values (Fig. 3.5) and also to calculate liver-muscle residuals (Fig. 3.6). Individual migratory behavior was estimated by plotting liver $\delta^{13}C$, the 'fast' isotopic clock (95% turnover in 1-2 month), versus muscle $\delta^{13}C$, the 'slow' clock (95% turnover 3-4 month) and calculating the muscle-liver residuals ($r_i = X_i - \bar{X}$) from the $\delta^{13}C$ liver versus $\delta^{13}C$ muscle linear regression (Fig. 3.6). A positive residual would indicate that slow turnover muscle tissue is lagging behind fast turnover liver tissues after a fish migrated down an isoscape gradient from increased-to-decreased $\delta^{13}C$ values (i.e. ocean-to-estuarine movement). In contrast, a negative residual would occur when a fish migrated across a decreased-to-increased isoscape (i.e. up estuary-to-down estuary). Tissue-specific turnover rates were determined from a controlled laboratory diet-switch experiment (Chapter 2). Individual carbon isotope muscle-liver residuals were regressed against otolith edge chemistry, to determine congruence between diet (tissue isotopes) and water (otolith chemistry) proxies (Fig. 3.7).

Local patterns in stable isotopes and otolith chemistry patterns were examined by plotting $\delta^{13}C$ against $\delta^{15}N$ for muscle (Fig. 3.8a) and liver (Fig. 3.8b) and a biplot of

otolith edge (outer 25 μm) Sr:Ca versus Ba:Ca (Fig. 3.8c), which represented the most recent few days to weeks of past habitat residence.

## 3.3 RESULTS

### 3.3.1 Fish collections

In each bay system, juvenile Atlantic croaker were collected from a variety of locations and sampling dates (Fig. 3.1; Table 3.1), with total of 81 fish examined (PS=27, MS=26, NG=28). Even though sample sizes and collection dates were uneven, fish displayed similar mean TL in the PS (range: 120-145 mm) and NG (range: 110-139 mm), but were significantly smaller in the MS (range: 114-115) that was only sampled in the month of July (Table 3.2). In the NG, fish came from a variety of dates and locations; therefore samples were pooled based on similar geographic location to increase local sample sizes (Fig. 3.1).

### 3.3.2 Regional salinity gradients

Mean monthly salinity in each bay maintained a consistent regional gradient from January to December 2012 (Fig. 3.2), with the PS estuary remaining positive throughout the year, the MS estuary switching from negative (Jan-Mar) to positive (May-Oct), and the NG estuary remaining hypersaline across all months (Fig. 3.2). There was a pattern of decreasing mean monthly salinity in the PS and MS from Jan until May, after which salinities steadily increased in all regions from May to Dec. Although the regional mean monthly salinity gradients were consistent, there was some fine scale daily variation in local salinities as revealed by measurements taken during fish collections (Table 3.1). For example, in NG salinities were approximately 10 ppt higher at the upper estuarine sites

(NG 1 & 2: Laguna Salada and Baffin Bay) compared to sites in the outer Laguna Madre (NG 3 & 4: mouth of Baffin Bay and Outer Laguna Madre). However, this trend was not reflected in long term data stations located in outer Laguna. The upper estuarine sites (PS 1 & 2: Trinity Bay) in the PS varied over 18 ppt between May and Sep (Table 3.1).

### 3.3.3 Otolith chemistry

Six major otolith chemistry types were identified based on lifetime patterns of Sr:Ca and Ba:Ca (Fig. 3.3). The two dominant types that were present in all regions were Type A and Type B comprising 36% and 33% of all fish, and showed strong regional patterns in otolith Sr:Ca. Type A was characterized by high Sr:Ca values in the otolith core that gradually decreased with a concomitant increase in otolith Ba:Ca within the first 1000 μm of the laser transect for the PS and MS. For PS Type A fish, Ba:Ca decreased sharply around 1500 μm, then remained low, while otolith Sr:Ca increased. For MS Type A fish, there was also a sharp decrease in otolith Ba:Ca occurring around 1000 μm, but Sr:Ca remained constant. Interestingly, the Ba:Ca 'hump' that occurred in early life (approximately springtime) of Type A fish, corresponds with springtime related drops in salinity that occurred exclusively in the MS and PS (Fig. 3.2). In contrast, the NG Type A fish were characterized by high overall Sr:Ca and low Ba:Ca, but sharp increases in Ba:Ca and Sr:Ca near the otolith edge. Type B, the second most common type also exhibited a strong regional gradient in otolith Sr:Ca that started elevated in the core, then decreased to steady levels after 1000 μm. Ba:Ca in Type B fish was consistently low throughout the otolith. Type C was the rarest otolith type (only 3/81 = 4%) and was characterized by high Ba:Ca in the otolith core that remained high and decreased towards the edge, with otolith Sr:Ca displaying low values in the PS, but high variation in the MS. Type D, the second rarest type only found in the MS, displayed high core Sr:Ca that

decreased then leveled off, with Ba:Ca starting high and gradually decreasing throughout otolith. Type E was only present in the PS and exhibited unique high Sr:Ca in otolith core, that gradually and continually decreased throughout the entire otolith to low values < 1 mmol/mol at the edge, with Ba:Ca remaining low and stable throughout. Otolith Type F was only present in the NG and it was the most common type in that system (46%), and displayed high Sr:Ca and low Ba:Ca that remained consistent and stable throughout the otolith (Fig. 3.3).

The occurrence of otolith types showed unique spatial and temporal patterns (Fig. 3.4). In the PS, Type E only occurred at location PS_1 and during May, while Type B was found at sites PS_2-4 and was present in both July and Sep. Otolith Type D was only present in the MS, and there was about equal representation of each type at both sampling locations (MS_1&2), but sampling only occurred in July. All of the fish collections in the NG occurred in the spring (Apr, May, June), and only 3 otolith types were present. Type F, which was unique to NG and the most common type, was present at all sampling locations and was most common in Apr and at up-estuary sites (NG_1&2). Otolith Type A was only present at outer Laguna Madre sites NG_3&4, and was absent from up-estuary sites (Baffin Bay NG_1&2) (Figure 4).

### 3.3.4 Tissue stable isotopes

*Regional patterns:* Nitrogen stable isotopes showed a very strong regional gradient, with no overlap in $\delta^{15}N$ values of liver or muscle tissues between fish collected from the PS, MS, or NG (Figure 5). The strong linear 1:1 relationship between $\delta^{15}N$ liver and $\delta^{15}N$ muscle ($\delta^{15}N_{muscle} = 1.00 \pm 0.02 * \delta^{15}N_{liver} + 1.79$; $df=79$, $r^2=0.98$) was highly significant ($p<0.0001$) suggesting that the tissues were in isotopic equilibrium with

respect to nitrogen. There was also a significant relationship between $\delta^{13}C$ liver and $\delta^{13}C$ muscle ($\delta^{13}C_{muscle} = 0.889 \pm 0.05 * \delta^{13}C_{liver} - 0.15$; df=79, $r^2=0.79$, $p<0.0001$), but there was much more spread in the data and overlap in tissue $\delta^{13}C$ values between the estuaries, suggesting the tissues were not in carbon isotope equilibrium due to individually variable immigration timing across different basal carbon sources (Fig. 3.5).

*Local scale patterns:* $\delta^{13}C_{tissue}$ –to– $\delta^{15}N_{tissue}$ and $Sr:Ca_{otolith\ edge}$ –to– $Ba:Ca_{otolith\ edge}$ biplots were created to examine patterns on a local spatial scale (Fig. 3.8). Most of the variation in these plots occurred along the x-axis (carbon for isotopes and Sr:Ca for otoliths). For muscle tissue, there was grouping between locations in the PS and MS, but separation of sites NG_3 and NG_4 from sites NG_1&2 (Fig. 3.8 top). For liver tissue, sites PS_1 and PS_4 separated from PS_2&3 in opposite directions, while site NG_3 clustered with sites (NG_1&2) (Fig 3.8 middle). There was no difference or variation in MS muscle or liver tissue $\delta^{13}C$ values. Similarly, otolith edge Sr:Ca and Ba:Ca for MS did not display variation but was intermediate between the PS and NG (Fig. 3.8 bottom). Otolith edge Sr:Ca was highest in the NG, intermediate in the MS, lower at estuarine PS sites (3-4), and lowest at PS_1. Fish collected from the Laguna Madre (NG_3&4) had the highest otolith Ba:Ca, while those collected within Baffin Bay (NG_1&2) had low Ba:Ca levels similar to the PS. Levels of Ba:Ca in MS fish otolith edges were intermediate between the PS and NG fish (Fig. 3.8 bottom).

*Individual migration patterns:* The strong 1:1 agreement between $\delta^{15}N$ tissue isotope values (Fig. 3.5) indicates that muscle and liver tissues are both in isotopic equilibrium relative to dietary nitrogen. The nitrogen-tissue relationship suggests that fish were resident for at least ~3 months, according to experimentally validated tissue isotope

turnover in this species (Chapter 2). Additionally, slower carbon isotope turnover in croaker suggests that disequilibrium between muscle and liver carbon isotopes may reveal estuarine immigrants that arrived more than 3 months prior to capture, such that muscle $\delta^{15}N$ had sufficient time to equilibrate but muscle $\delta^{13}C$ did not (Chapter 2).

In the PS, most residuals were positive and occurred at the furthest up-estuarine site (PS_1), but some negative residuals were also observed (Fig. 3.9 top). Most fish in the MS had tissues that were in equilibrium and fell on the tissue equilibrium line, with only a few positive residuals (Figure 3.9 middle). In the NG, there were two separate groups: fish from NG_4 had increased tissue carbon values and fell on the equilibrium line; while fish from the middle sites (NG_2&3), had both positive and negative residuals (Fig. 3.9 bottom). Relationships between individual fish $\delta^{13}C_{muscle\text{-}liver}$ residuals and otolith edge Sr:Ca and Ba:Ca reveals some interesting patterns (Fig. 3.7). There was a significant ($p$=0.0015) negative relationship ($\delta^{13}C_{muscle\text{-}liver}$ residual = -0.97±0.27*Sr:Ca $_{otolith\ edge}$ + 1.52±0.46; $r^2$=0.34) between tissue residuals and otolith Sr:Ca in the PS (Fig. 3.7 top left). No significant relationships between tissue residuals and otolith chemistry were detected in the MS. In the NG, both otolith edge Sr:Ca and Ba:Ca were significantly positively related to tissue residuals: $\delta^{13}C_{muscle\text{-}liver}$ residual = 1.03±0.40*Sr:Ca $_{otolith\ edge}$ – 2.75±1.02; $r^2$=0.21; $p$=0.016, and $\delta^{13}C_{muscle\text{-}liver}$ residual = 0.038±0.012*Ba:Ca $_{otolith\ edge}$ – 0.78±0.23; $r^2$=0.29; $p$=0.003.

### 3.3.5 Condition and tissue C:N ratios

Biological parameters (morphometrics and tissue C:N ratios) were examined for each otolith type in each region, however, due to limitations on sample sizes for individual otolith types, only regions were statistically compared using 1-way ANOVA

with Holm-Sidak multiple comparisons test (Table 3.2). Mean fish condition (K factor) was lowest in the MS (0.89±0.02), but similar between the PA (1.02±0.02) and NG (0.99±0.02); these patterns also applied to TL (Table 3.2). Otolith mass was significantly higher in the PS, but lower and comparable between the MS and NG. Muscle tissue C:N ratios were strikingly similar (~3.7) between all regions, but liver tissue C:N ratios were lower in the PS (5.42±0.09) compared to the MS (5.99±0.2), and highest in the NG (6.38±0.1) (Table 3.2).

## 3.4 DISCUSSION

In this study, strong regional gradients in otolith Sr:Ca and Ba:Ca chronologies and muscle and liver nitrogen isotopes were detected that integrated chemical information from water and diet over long time scales (otolith=entire life; nitrogen isotopes=past 3.5 months). Fish movement between local scale (between-bay) salinity gradients and carbon isotope pathways were also detected, utilizing residuals of liver-muscle $\delta^{13}C$ linear relationships, and otolith edge chemistry, representing more recent (~weeks) habitat residence. Across a broad geographic scale encompassing positive, metastable, and negative estuarine types, we detected unique otolith chemistry profiles, suggesting migratory contingents within each salinity regime. The maintenance of diverse migratory tactics under environmental gradients suggests phenotypic plasticity in response to climatic forcing (Ray 2005). Using a multi-proxy approach can enhance interpretations of each individual proxy, such as diet histories based on tissue isotopes or ambient waters based on otolith chemistry.

### 3.4.1 Estuarine ingress and residence of Atlantic croaker

Croaker display a typical 'estuarine dependent' life history with a protracted offshore spawning season that extends from September to March, with peak spawning occurring in October in the Gulf of Mexico (White and Chittenden 1977). Larvae are transported by wind driven transport to inshore coastal areas, where larvae and early juveniles enter estuarine nurseries after 2-3 months post hatch transport (Warlen and Burke 1990). Distinct temporal partitioning between similar estuarine-dependent Sciaenid species occurs in the Aransas Estuary (MS), with peak abundance of postsettlement croaker (10-14 mm) appearing in early and late winter (Rooker et al. 1998). However, it was suggested that croaker only used the seagrass transiently as abundance decreased over time (Rooker et al. 1998), and other studies have found croaker to make ontogenetic habitat shifts (White and Chittenden 1977). A recent study used North Carolina juvenile croaker otolith Sr:Ca and Ba:Ca profiles, daily increment enumeration, and spectral analysis to estimate the timing of ingress (Hoover et al. 2012). Strontium profiles estimated 68 days and barium profiles 85 days to estuarine ingress, and growth rate had no effect on ingress timing (Hoover et al. 2012). It was hypothesized that Sr:Ca represented entry into the estuary, while Ba:Ca indicated up estuary (low salinity) movements. However, Hoover et al (2012) examined a limited cohort of fish ($n$=14) that were on average 120 d (4 month) old, with corresponding core-to-edge otolith laser transects ~1700 μm in length. The Type A fish collected in PS and MS displayed similar decreasing Sr:Ca and increasing Ba:Ca patterns within the first 1500-1700 μm, as described by Hoover et al. (2012). Other studies have reported similar high-to-low otolith Sr:Ca patterns in wild collected congeners red drum (*Sciaenops ocellatus*) and black drum (*Pogonias cromis*), suggesting comparable patterns of estuarine ingress (Rooker et al. 2004). However, Atlantic croaker total lengths and laser transects used in this study where twice as long (~30 mm TL greater and 3000 μm longer transect length) compared

to croaker examined in Hoover et al. (2012), indicating that TX fish where twice as old (8+ months). Both element profile data and nitrogen isotope values (3+ month equilibration time) concur with our age approximation (8+ months), and suggest fish were resident near collection sites for at least 3-4 months prior to capture (Chapter 2). In contrast to Hoover et al. (2012) and Rooker et al. (2004) that characterized ingress on a fine scale (days old) or residence in transient habitats (post settlement seagrass), we examined larger juvenile croaker, that survived ingress population bottlenecks of high mortality (Fodrie and Herzka 2013). Examining older fish allowed for identifying a large range of migratory timing, including very late migrants into the estuary. However, the data suggested that most fish were resident in the habitat of capture for at least 3 months prior to collection with few late migrants detected. Thus, despite the protracted spawning season of Atlantic croaker migration timing was similar between the systems, with fish displaying estuarine ingress at least 3 months prior to capture.

### 3.4.2 Regional scale patterns

Coastal climatic gradients in Texas (temperature, precipitation, evaporation) result in geographic salinity regimes and a diversity of estuarine types (Tolan 2007). In northern estuaries, such as Galveston Bay, increased urban and industrial development results in high nutrient inputs and water quality degradation, while in the southern estuaries (Laguna Madre) nutrient inputs are minimal and water residence times are longer. The nitrogen tissue isotope signatures directly reflect this strong regional gradient and ranged from 9-22‰, with no overlap in $\delta^{15}N$ values between bays. Variation in tissue isotopes was not related to trophic level, and although fish were slightly smaller in MS, there were no significant relationships between total length and tissue isotopes (data not shown). The strong regional gradient was also reflected in otolith Sr:Ca patterns, with low values in

the PS, intermediate values in the MS, and high values in the NG that where consistent across entire life histories. This pattern correlates with salinity, temperature and dissolved Sr:Ca (Fig. 3.10) gradients along the coast of Texas (Mohan and Walther 2014), and all of these factors are known to affect otolith Sr:Ca (Secor et al. 1995; Kraus and Secor 2004; Izzo et al. 2015).

Additional regional gradients included condition factor (*K* lowest in MS), otolith mass (highest in PS) and C:N liver ratios (lowest in PS). Salinity is known to affect croaker growth and behavior (Moser et al. 1989; Peterson et al. 1999). Croaker held for 3 weeks at salinities of 5‰ experienced relative increases in wet weight (WW) 4X greater than initial weight, compared to a 2-fold increase for fish held at 20‰. Otolith diameter was also significantly increased at low salinities (Peterson et al. 1999). We found that croaker collected from the low salinity PS estuary had significantly larger otolith mass compared to the MS and NG, suggesting higher growth (Nixon and Jones 1997). Otolith Type E that was only found at the lowest salinity (4.4 ppt) PS_1 location also displayed the largest size (TL=145±7) compared to all other fish, suggesting higher growth at low salinity. Moser and Gerry (1989) suggested there was a high energetic cost in Atlantic croaker associated with highly fluctuating salinities, and hypothesized that croaker accumulate in areas with stable salinities and avoid variable conditions. The fluctuating salinities in the MS from winter though the summer could have influenced the significantly lower condition factor (K=0.9±0.02) detected in MS fish.

### 3.4.3 Local gradients

*Positive Estuary:* In Galveston Bay (PS), fish were collected across the salinity gradient and during the spring summer and fall. Water quality gradients in PS caused by urbanization and industrial pollution have caused reduced growth and condition in

Atlantic croaker collected at up-estuarine locations according to previous work (Burke et al. 1993). In contrast, evidence of higher growth was detected at the most up-estuarine sites with lower salinities in this study. Carbon isotope values in the muscle ranged from 19.5 to 21‰, which approximates isotope signatures between benthic macroalgae, particulate organic matter (POM), and marsh plants (Herzka et al. 2002; Connolly et al. 2005). While the mean muscle carbon isotope values of croaker collected at each site grouped together, the mean liver carbon isotope values separated by site, with the further up-estuarine site having the most decreased value (~23.5‰) approaching marsh plant values. Additionally otolith edge Sr:Ca was significantly decreased, compared to other sites, suggesting residence in low salinity water. The decreasing otolith and liver $\delta^{13}C$ values suggests that PS_1 fish (also otolith type E) more recently migrated to that location, since muscle tissue still grouped with the other locations.

*Metastable Estuary:* Fish in the Mission-Aransas (MS) were only collected on one day in July and at two locations in Copano Bay (MS_1) and Aransas Bay (MS_2). Even though sampling was limited in MS, there was still a high diversity of otolith types that were equally represented at both locations. Isotopic signatures and otolith edge elemental values where tightly grouped, suggesting these fish were residents for 4+ months since muscle and liver carbon isotopes were in equilibrium. Carbon isotope values were more enriched compared to other regions and locations, suggesting either seagrass, marsh grass (Fry et al. 1977; Fry 1983; Herzka et al. 2002; Connolly et al. 2005) or benthic carbon (France 1995; Fodrie and Herzka 2013) sources were contributing to fish production in the MS.

*Negative Estuary:* In the hypersaline Laguna Madre (NG), unexpected otolith Ba:Ca patterns were detected, in addition to large separation in carbon isotopes. Higher otolith edge Sr:Ca (>2 mmol/mol) was exhibited in all NG fish as expected, but unexpectedly increased otolith edge Ba:Ca was found in fish from the Upper Laguna Madre sites NG_3 and NG_4. The abrupt increase in otolith edge Ba:Ca may be related to submarine groundwater discharge, which has been reported to be highly variable in the NG (Uddameri et al. 2014). Site NG_4 also had the highest carbon signature, most likely related to known seagrass beds occurring there and transfer of enriched $^{13}C$ through the food web (Fry et al. 1977). Fish at NG_3 displayed liver carbon values that grouped with Baffin Bay locations (in equilibrium), but the muscle tissue lagged behind liver, suggesting recent migration from the outer Laguna Madre, where there was also increased Ba:Ca in NG_4 fish. Interestingly, a sampling transect that occurred in June 2012 across salinities ranging from 35ppt to 52ppt detected a positive relationship between dissolved Ba:Ca and salinity (Fig. 3.10). A positive salinity-dissolved Ba:Ca relationship has only been reported in one other study in an Australian hypersaline lagoon (Gillanders and Munro 2012). Even though dissolved Ba:Ca unexpectedly increased at high salinities (up to 120), otolith Ba:Ca increased linearly with water Ba:Ca but otolith Sr:Ca did not respond to hypersalinity (Gillanders and Munro 2012). However, Diouf et al. (2006) reported increased dissolved Sr:Ca and otolith Sr:Ca in tilapia *Sarotherodon melanotheron* collected from a West African hypersaline estuary (salinity >50). The otolith Sr:Ca in tilapia revealed that the fish did not make large scale migrations under hypersaline conditions (Diouf et al. 2006). If hypersaline environments pose energetic and osmotic stress in Atlantic croaker (Moser et al. 1989) resulting in reduced growth (smaller otoliths), then fish would limit movements and display high site fidelity, as detected in the majority of NG fish. Higher C:N ratios were also detected in the MS and

NG with highly variable salinities, potentially indicating storage of more lipid molecules needed for increased osmoregulatory machinery at the cellular level. Tissue C:N ratios can be used as reliable proxies of lipid content in Atlantic croaker (Chapter 2) and other estuarine dependent species (Woodland and Secor 2011).

### 3.4.4 Individuals

Fish were qualitatively categorized into six different groups based on lifetime patterns of Sr:Ca and Ba:Ca. Although this grouping technique is subjective, there was agreement between independent measures of natural trophic stable isotope tags and natural salinity otolith chemistry tags. Additionally, the liver-muscle residual was calculated for each fish as a measure of individual tissue equilibrium status. In the PS, lower otolith edge Sr:Ca (low salinity) was related to positive $\delta^{13}C_{\text{liver-muscle}}$ residuals, indicating recent up-estuarine (increased $\delta^{13}C$ → decreased $\delta^{13}C$) movement. Conversely, in the NG hypersaline estuary, positive $\delta^{13}C_{\text{liver-muscle}}$ residuals were related to higher otolith Sr:Ca and Ba:Ca (hypersalinities). The difference in otolith patterns between the PS and NG estuaries reflected the climate driven salinity gradients. The muscle-liver tissue residuals responded similarly to movements from enriched to depleted $^{13}C$ food webs. Minimal variation in liver-muscle carbon residuals in the MS suggests either limited inter-bay movement, or limited differences in basal carbon sources between Copano Bay (CB) and Aransas Bay (AB), two subsystems of the metastable estuary. Salinity differences between CB and AB were only ~4ppt, and previous work has demonstrated small difference in POM $\delta^{13}C$ or $\delta^{15}N$ over such salinity range in the MS (Bishop 2012). In the hypersaline NG, the most common otolith Type F (46%) displayed high constant Sr:Ca and low constant Ba:Ca. These element profiles suggest either settlement into coastal areas and later estuarine ingress at larger size (Fodrie and Herzka

2013), or that ingress into a hypersaline estuary would not be detected as a decrease in otolith Sr:Ca, as predicted for Sciaenid spp. in the MS (Rooker et al. 2004), or croaker in NC (Hoover et al. 2012).

### 3.4.5 Summary

Even though adult Atlantic croaker exhibit a protracted spawning season, similar early estuarine immigration was detected in each system and late estuarine migrants were not detected, in agreement with previous studies of Atlantic croaker ingress (Rooker et al. 1998; Hoover et al. 2012). Previous studies on estuarine Atlantic croaker movements focused on earlier life (larval and post-larval ingress), while this study examined later juvenile habitat residence and found a high degree of site fidelity, but also finer scale inter-bay movements, based on otolith and tissue natural tags. This multi-proxy approach was able to identify inter-bay connectivity and diverse resource use, which are essential components for estimating nursery habitat function (Nagelkerken et al. 2013; Sheaves et al. 2014). Increased Ba:Ca was detected in otoliths and water from the hypersaline estuary, contradicting expected elemental behavior across salinity gradients that has only been reported in one other study (Gillanders and Munro 2012). Over broad geographic scales, croaker inhabited a diversity of habitat types, suggesting this common estuarine-dependent species has non-specific nursery habitat requirement. Strong regional signals in natural tags from each estuary suggest local adaptation to environmental gradients, and limited population mixing on broad geographic scales. These results support spatial management of estuarine dependent species along the Texas coast.

**Table 3.1** Number of Atlantic croaker (N) and mean total length (TL± SE) collected from each bay and date, including physicochemical parameters recorded at each station. See Figure 3.1 for locations of each Site.

| Region | Bay | Site | Date | N | TL (mm) | Temperature (C°) | Salinity | DO (mg/l) | depth (m) |
|---|---|---|---|---|---|---|---|---|---|
| Galveston Bay (PS) | Trinity Bay | PS 1 | 5/4/12 | 6 | 145±7 | 26.5 | 4.4 | 8.7 | |
| | Trinity Bay | PS 2 | 9/18/12 | 4 | 120±5 | 27.9 | 22.4 | 6.6 | |
| | Dickinson Bay | PS 3 | 7/18/12 | 8 | 121±4 | 29.3 | 16.5 | 5.1 | |
| | East Bay | PS 4 | 7/18/12 | 9 | 132±10 | 28.6 | 18.5 | 6.3 | |
| Mission-Aransas (MS) | Copano Bay | MS 1 | 7/7/12 | 20 | 114±2 | 30.0 | 26.2 | 6.3 | 3.0 |
| | Aransas Bay | MS 2 | 7/7/12 | 6 | 115±2 | 29.0 | 30.5 | 5.6 | 3.2 |
| Laguna Madre (NG) | Laguna Salada | NG 1 | 4/24/12 | 3 | 120±8 | 25.5 | 56.4 | 8.6 | 1.9 |
| | Baffin Bay | NG 2 | 4/24/12 | 7 | 118±4 | 24.3 | 53.3 | 7.5 | 2.3 |
| | Baffin Bay | NG 2 | 5/17/12 | 1 | 132 | 27.2 | 53.2 | 5.9 | 2.5 |
| | Outer Laguna Madre | NG 3 | 4/19/12 | 1 | 119 | 25.0 | 38.7 | 8.9 | 2.3 |
| | Baffin Bay | NG 3 | 5/29/12 | 2 | 115±5 | 29.4 | 44.4 | 6.6 | 2.6 |
| | Baffin Bay | NG 3 | 6/7/12 | 6 | 139±6 | 29.4 | 44.4 | 6.6 | 2.6 |
| | Upper Laguna Madre | NG 4 | 5/8/12 | 7 | 124±3 | 29.5 | 43.6 | 7.9 | 1.1 |
| | Upper Laguna Madre | NG 4 | 5/10/12 | 1 | 110 | 25.3 | 46.5 | 5.8 | 1.8 |

**Table 3.2** Biological parameters of each otolith type including total length (TL), Fulton's condition factor (K), otolith mass (mg), muscle liver residuals, and molar carbon:nitrogen ratios for the muscle and liver. A one-way ANOVA was used to compare regional TL, K, otolith mass, and tissue C:N ratios with different lower case letters representing significant differences (Holm-Sidak multiple comparisons).

| Region | type | N | TL | K | otolith mass | muscle-liver residual | C:N muscle | C:N liver |
|---|---|---|---|---|---|---|---|---|
| Galveston Bay (PS) | A | 8 | 121±6 | 0.98±0.02 | 59±7 | -0.43±0.10 | 3.75±0.01 | 5.34±0.06 |
| | B | 12 | 129±7 | 1.05±0.03 | 72±9 | -0.23±0.17 | 3.73±0.01 | 5.43±0.18 |
| | C | 2 | 134±7 | 1.08±0.10 | 69±2 | -0.58±0.24 | 3.75±0.03 | 5.74±0.57 |
| | E | 5 | 145±9 | 1.01±0.03 | 69±10 | 1.15±0.29 | 3.71±0.01 | 5.39±0.14 |
| | **total** | **27** | **130±4** [a] | **1.02±0.02** [a] | **68±5** [a] | | **3.74±0.007** [a] | **5.42±0.09** [a] |
| Mission-Aransas (MS) | A | 12 | 111±2 | 0.94±0.04 | 50±2 | 0.44±0.16 | 3.74±0.01 | 6.32±0.37 |
| | B | 9 | 119±4 | 0.84±0.03 | 56±5 | -0.03±0.15 | 3.75±0.02 | 5.69±0.31 |
| | C | 1 | 112 | 0.93 | 47 | 0.32 | 3.74 | 5.51 |
| | D | 4 | 115±3 | 0.82±0.02 | 51±4 | 0.12±0.09 | 3.73±0.01 | 5.8±0.29 |
| | **total** | **26** | **114±2** [b] | **0.89±0.02** [b] | **52±2** [b] | | **3.74±0.009** [a] | **5.99±0.2** [b] |
| Laguna Madre (NG) | A | 9 | 131±5 | 1.06±0.02 | 59±6 | 0.37±0.14 | 3.74±0.01 | 6.40±0.21 |
| | B | 6 | 127±2 | 0.97±0.05 | 49±4 | -0.70±0.38 | 3.76±0.02 | 6.06±0.29 |
| | F | 13 | 117±3 | 0.94±0.02 | 39±2 | -0.26±0.19 | 3.76±0.01 | 6.51±0.24 |
| | **total** | **28** | **124±2** [a] | **0.99±0.02** [a] | **47±3** [b] | | **3.75±0.009** [a] | **6.38±0.14** [b] |

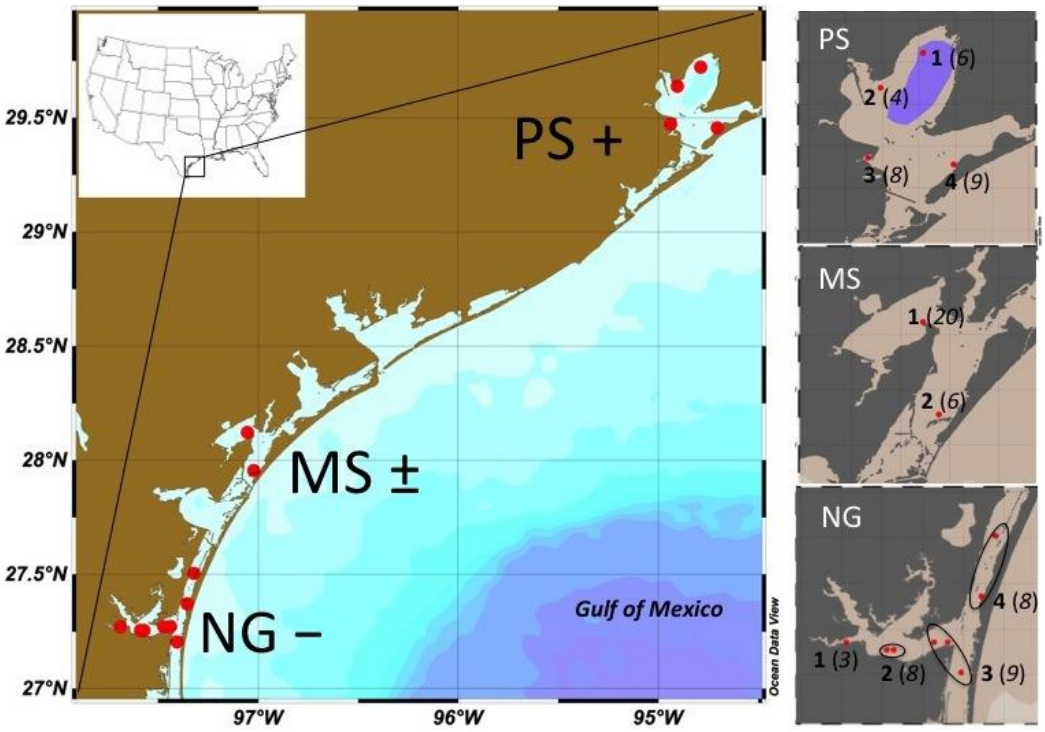


**Figure 3.1** Map of sampling locations along the southeast Texas coastline (left). Regional estuaries include: Galveston Bay – positive (PS+); Mission-Aransas – metastable (MS±); and Laguna Madre – negative (NG-). Within each local estuary (right) fish were collected from sites farther up within the bay (sites numbered **1** and **2**) and at sites closer to ocean inlets (sites numbered **3** and **4**). The negative (NG) estuary, sites that where close to each other were pooled together in increase sample size (in *italics*).

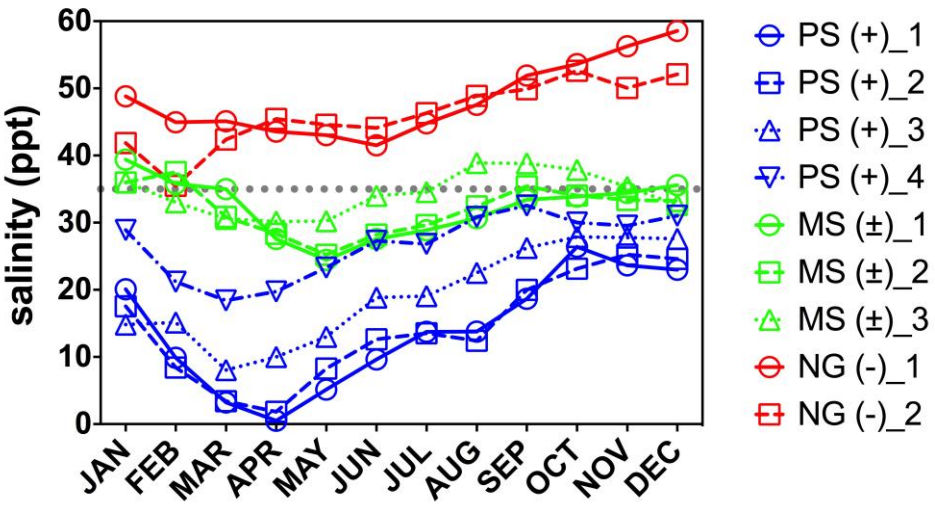


**Figure 3.2** Annual salinity patterns in the PS (blue), MS (green) and NG (red) regional estuaries. Different shapes indicate fixed sampling locations (described in text), with lower numbers indicating locations far from the ocean and higher numbers representing sites closer to the ocean. Fish were collected monthly from April to July, as well as September (see Table 3.1).

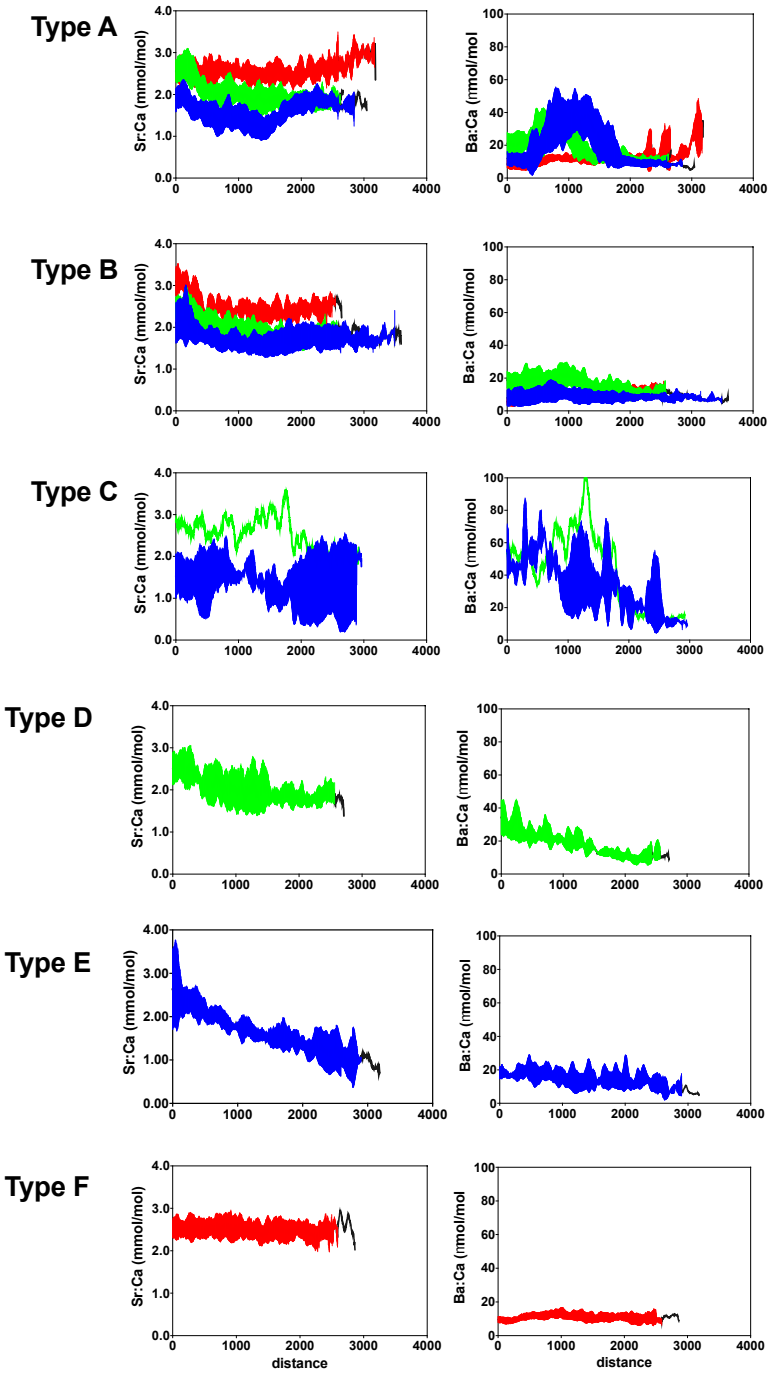


**Figure 3.3** Lifetime juvenile Atlantic croaker otolith chemistry patterns observed in the positive (blue), metastable (green) and negative (red) estuary types. Dark line = mean otolith values and colored whiskers = standard deviation.

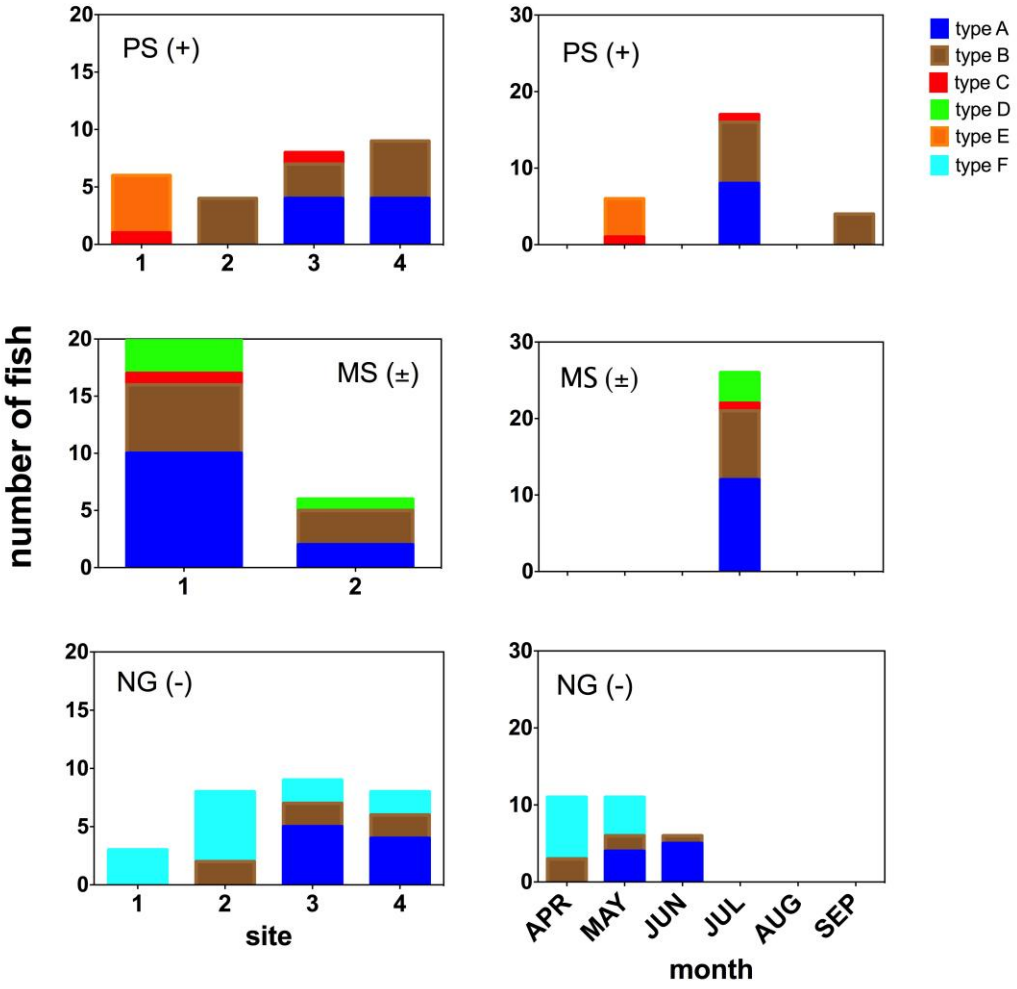


**Figure 3.4** Spatial and temporal occurrence of each otolith chemistry type in the positive (PS – top), metastable (MS – middle) and negative (NG – bottom).

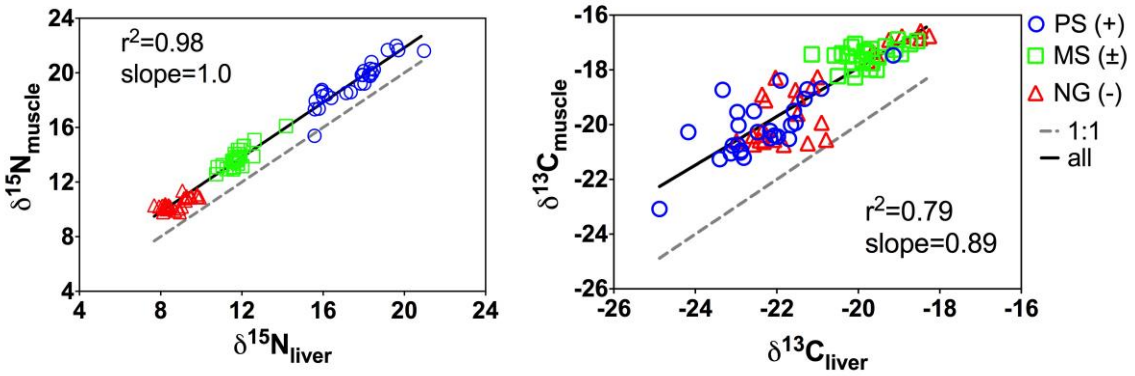


**Figure 3.5** Muscle versus liver tissue biplot for nitrogen (left) and carbon (right). Solid line indicates fitted linear regression; dotted grey line indicates 1:1 relationship.

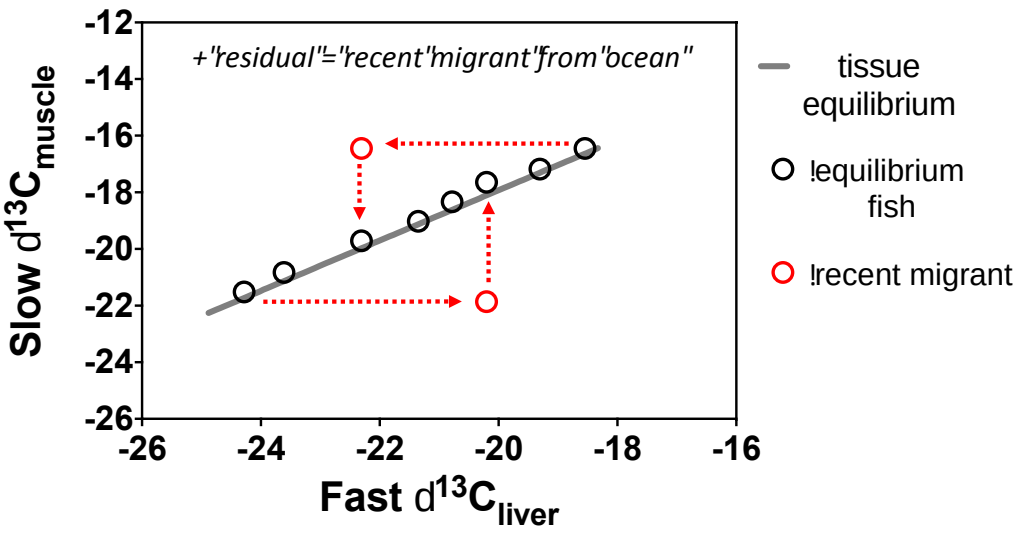


**Figure 3.6** Linear regressions between 'fast' liver carbon isotopes and 'slow' muscle carbon isotopes with example tissue equilibrium line (gray solid line), fish with tissues in isotopic equilibrium (open black circles), and recent migratory fish (red open circles), with muscle tissue lagging behind liver tissue isotope values (red dashed line).

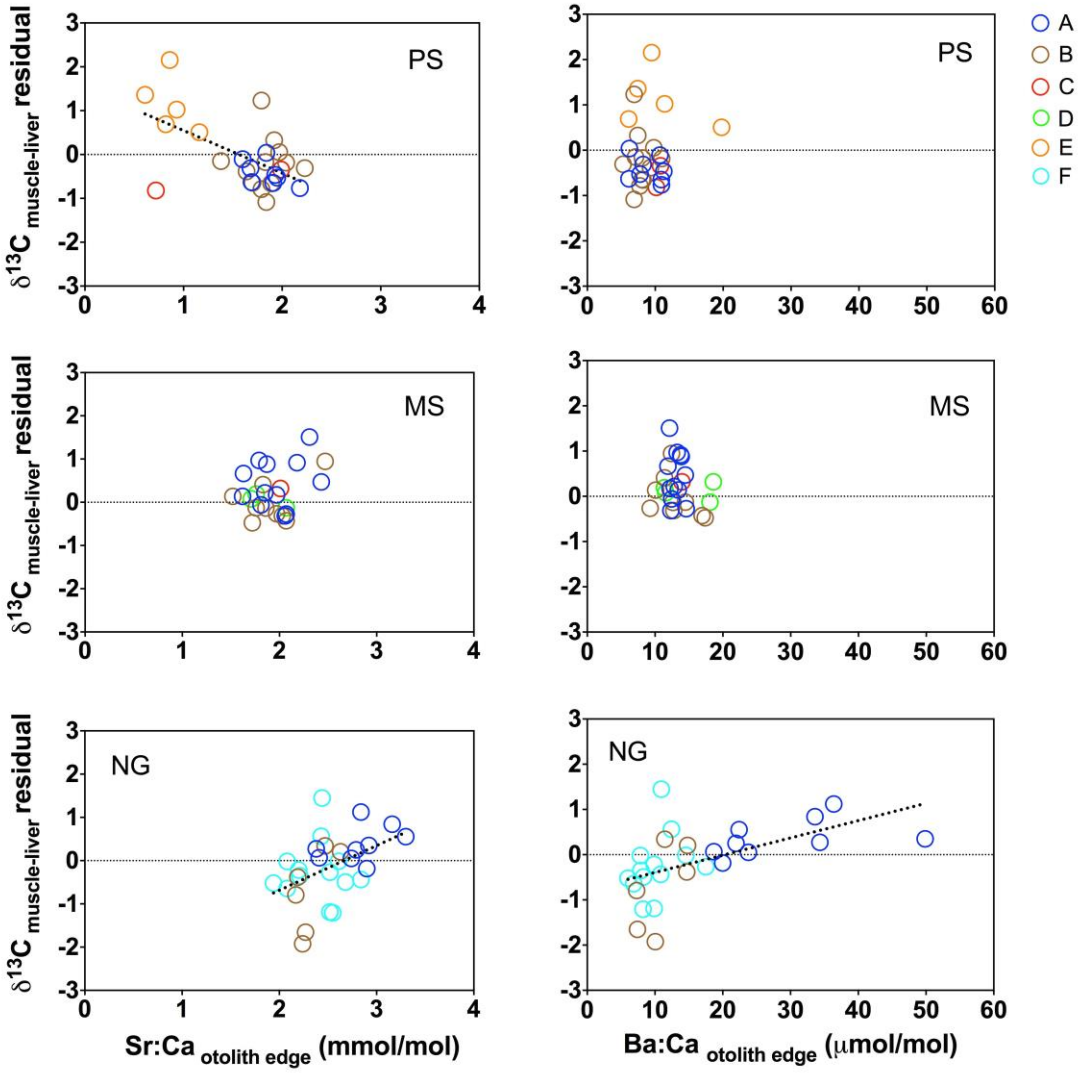


**Figure 3.7** Carbon isotope tissue residuals versus otolith edge chemistry in the PS (top) MS (middle) and NG (bottom). Black dashed line indicates significant linear regressions.

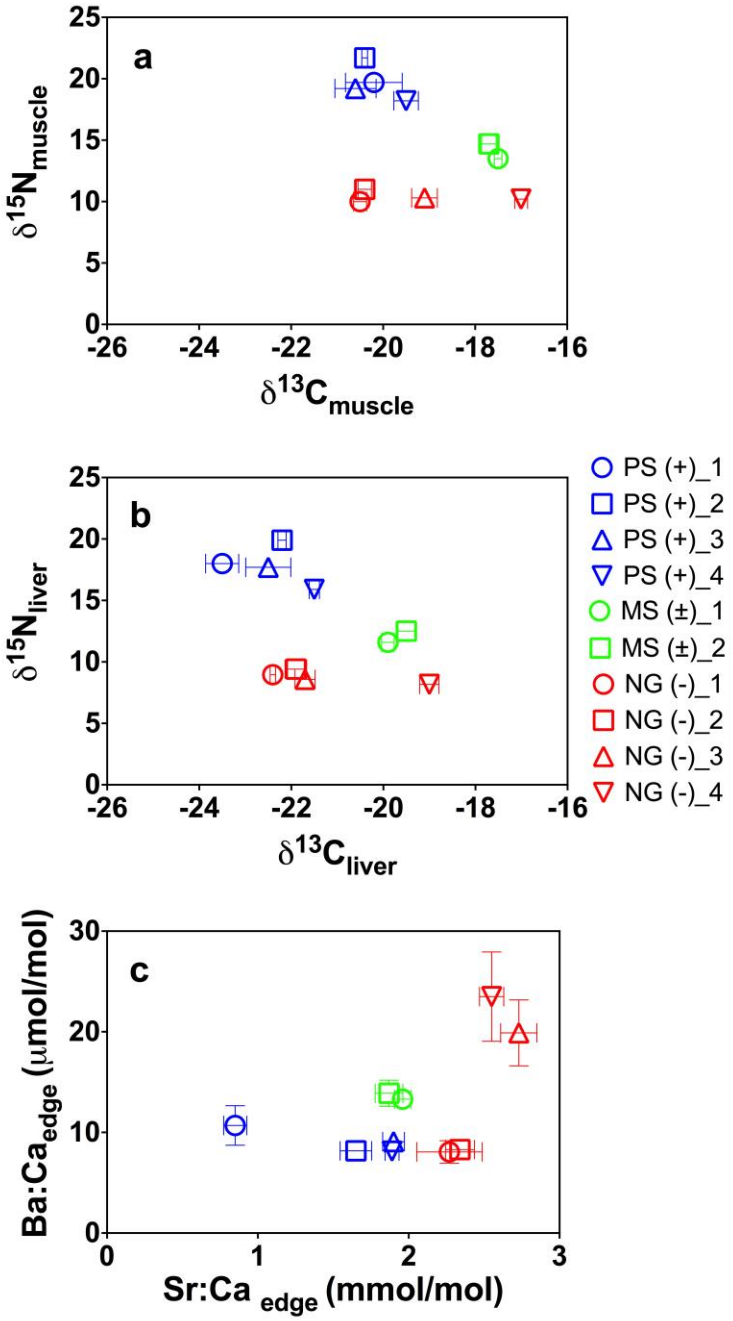


**Figure 3.8** Biplots of mean (±SEM) carbon-to-nitrogen tissue stable isotopes for muscle (a), liver (b) and otolith edge chemistry (c) grouped by collection location (symbols) and region (color). Outer otolith edge of otoliths (25 microns) represents recent few days to 1-week.

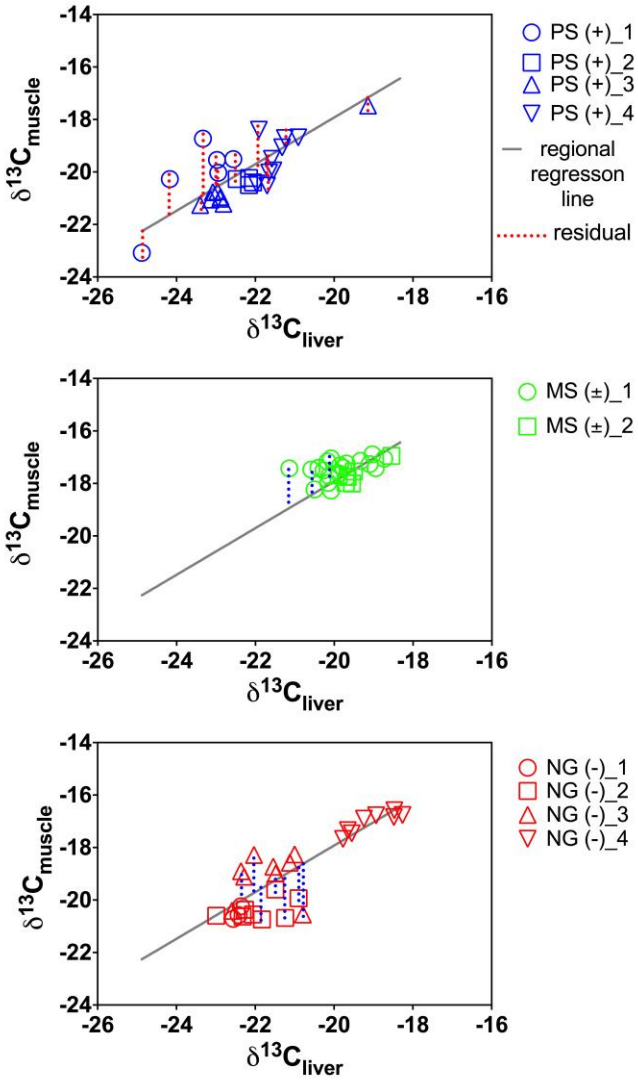


**Figure 3.9** Linear regressions between liver and muscle carbon isotopes in the PS (top), MS (middle), and NG (bottom). Gray line indicates overall linear regression, blue dashed line indicate residual.

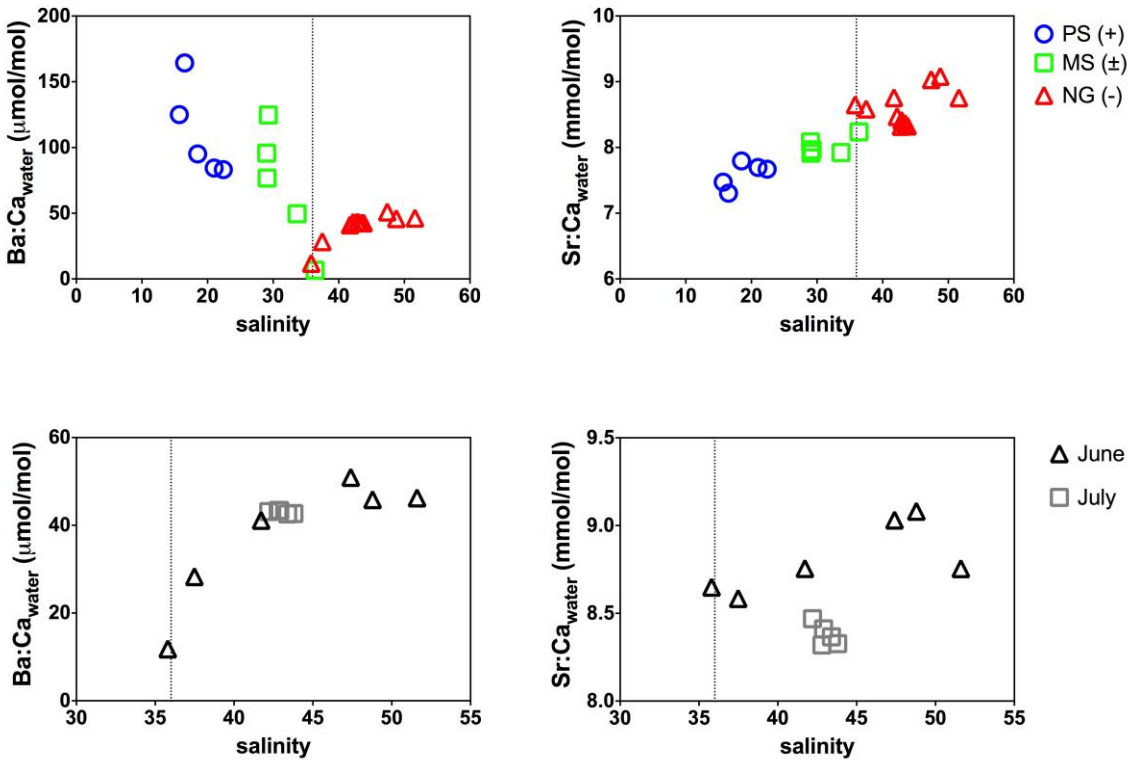


**Figure 3.10** Regional dissolved Ba:C and Sr:Ca versus salinity (top panels) in the PS (blue), MS (green) and NG (red) estuaries during the summer, and in the NG in June (black triangle) and July (gray square) of 2012 (bottom panels). In the NG, samples were collected in June and July across a hyper saline gradient.

# CHAPTER 4: INFLUENCE OF CONSTANT AND PERIODIC EXPERIMENTAL HYPOXIC STRESS ON ATLANTIC CROAKER OTOLITH CHEMISTRY

Published as: Mohan, J.A., M.S. Rahman, P. Thomas, B.D. Walther. 2014. Influence of constant and periodic experimental hypoxic stress on Atlantic croaker otolith chemistry. *Aquatic Biology* 20:1-11. Reprinted with permission.

Author contributions: J.A.M. collected and analyzed the data and wrote the manuscript; M.S.R. and P.T. designed and conducted the experiments; B.D.W. provided data interpretation and editorial advice.

## ABSTRACT

The chemical composition of fish otoliths may provide information on the environmental exposure histories of fishes if "vital effects" on element incorporation are minimal. In order to use redox-sensitive geochemical proxies in otoliths such as manganese to quantify sublethal exposure to hypoxia, the relative influence of endogenous and exogenous controls on otolith composition must first be validated. Controlled laboratory experiments were conducted on Atlantic croaker (*Micropogonias undulatus*) to examine the response of otolith Sr:Ca, Ba:Ca, Mg:Ca, Mn:Ca, and Na:Ca ratios to either constant or periodic hypoxia treatments for 4 and 10 weeks, respectively. Although fish somatic growth and condition were affected by constant hypoxia, no difference in otolith chemistry relative to normoxic control treatments was detected. Similar to the 4-week study, there was no difference in otolith chemistry between fish (males and females combined) exposed 10-weeks to constant hypoxia and control normoxic fish. Periodic hypoxia significantly decreased otolith Ba:Ca and Mg:Ca in both males and females, reduced Sr:Ca in males, and there was a slight effect of sex on otolith

Mn:Ca. Significant interactions between treatment and sex were detected for otolith Sr:Ca and Na:Ca, possibly related to combined stresses of gonadal development and periodic hypoxic stress. Although responses to treatments were observed for some elements, the magnitudes of responses were minimal compared to exogenous variation driven by water chemistry composition reported in previous laboratory and field investigations. The otolith chemistry of Atlantic croaker is therefore minimally influenced by endogenous factors in response to hypoxic stress, which has important implications for interpreting otolith chemical chronologies of wild fish collected within natural hypoxic regions.

## 4.1 INTRODUCTION

Hypoxia (dissolved oxygen < 2 mg $O_2$ $l^{-1}$) is increasing in frequency and severity in coastal ecosystems worldwide due to human activities (Diaz and Rosenberg 2008). Fish exposed to hypoxia have exhibited negative sublethal physiological effects including reduced growth (McNatt and Rice 2004), shifts in habitat (Craig 2012), and reproductive disorder (Thomas and Rahman 2012), yet less is known about natural exposure levels that elicit damaging organismal and ecological responses, especially for mobile species capable of sensing, tolerating, and avoiding hypoxia (Froeschke and Stunz 2011). A validated chronological geochemical proxy indicating hypoxia exposure in fishes is needed to assess the long-term sublethal effects of hypoxic exposure on aquatic communities.

Fish respond to an oxygen challenge by first attempting to extract more oxygen from the water using strategies of increasing gill ventilation rates, red blood cell counts, and hemoglobin $O_2$ binding capacity (Wu 2002). If the oxygen challenge persists, they will depress metabolism and 'turn down the pilot light' (Hochachka et al. 1996) and

initiate energy conserving pathways by down regulating protein synthesis and modifying enzymes to decrease ATP use (Wu 2002; Bickler and Buck 2007). Many hypoxia responsive pathways are turned on via the 'master switch,' the hypoxia inducible factor HIF-α, a heterodimeric transcription factor (Rahman & Thomas 2007, Nikinmaa & Rees 2005). HIF-α is expressed in a wide range of fish tissues and codes for genes related to red blood cell production, vascularization, apoptosis, and carbohydrate metabolism. Under normoxic conditions, the HIF protein is degraded, but expression will occur under hypoxic exposure. Short-term biomarkers, such as HIF-α, provide reliable molecular indicators of exposure to hypoxia in several fish (Thomas & Rahman 2009) and crustacean (Kodama et al. 2012) species on time scales of hours to days. However, HIF-α mRNA expression returns to basal levels within 24 hours after recovery from hypoxia, offering no information on lifetime patterns of exposure and the potential for long-term sublethal effects (Rahman & Thomas 2007, Kodama et al. 2012).

Fish otoliths are calcium carbonate structures that deposit permanent daily growth bands offering detailed information on age and growth. Otoliths are metabolically inert and not subject to resorption, even during periods of stress (Campana 1983) or starvation (Maillet and Checkley 1990). Although much otolith chemistry research has focused on chemical identifiers of migratory movements and stock discrimination (Walther & Limburg 2012), there is significant potential for geochemical indicators of hypoxia exposure to be recorded in otoliths. In particular, otolith manganese (Mn) is a viable geochemical hypoxia proxy (Limburg et al. 2011). Hypoxia alters redox conditions such that Mn oxides are reduced; the reduced forms (primarily $Mn^{2+}$ but also $Mn^{3+}$) are soluble, and under suboxic/hypoxic conditions dissolved Mn can be released into the water column (Thamdrup et al. 1994, Slomp et al. 1997) and remain dissolved for several days (Pakhomova et al. 2007). If elevated dissolved Mn leads to increased incorporation

of Mn in otoliths, a direct link between residence in hypoxic waters and otolith composition could be employed. However, in order to effectively interpret potential hypoxia proxies such as Mn/Ca, it is important to validate whether hypoxic stress alone, in the absence of ambient chemical differences, could alter otolith chemistry.

During otolith accretion, aragonite is crystallized onto an organic protein matrix, and dissolved elements from the ambient environment that have passed through several biological barriers (i.e. gill, intestine, blood, and endolymph interfaces) are incorporated into the crystal structure (Campana 1999). While the concentration of some elements may directly reflect water concentrations, there is significant opportunity for physiological regulation of uptake and transport of certain ions at each barrier. Sturrock et al. (2012) employed hard/soft acid-base theory to describe the behavior of certain metals in seawater and in the blood and endolymph of marine fish. Hard acid cations, such as Mg, Sr, Ca, and Ba, exist as free hydrated ions in seawater and in the blood of the fish, so they are more likely to passively diffuse across blood-endolymph membranes, and are more readily accepted into the crystal lattice by substituting for Ca during otolith precipitation. Soft acid cations such as Cu, Pb and Zn are strongly bound to organic ligands in seawater and strongly bind proteins in the blood and thus require more active transport across biological membranes and are susceptible to being rerouted to the liver or actively excreted. The soft acid cations are more likely incorporated with the organic protein matrix of the otolith, or in interstitial spaces of crystal defects. The behavior of intermediate cations, such as Mn, may depend on the environmental or physiological context (Sturrock et al. 2012). The potential influences on blood-endolymph chemistry variation include both environmental (salinity, temperature, dissolved oxygen) and physiological (ontogeny, sex, growth rate) factors (Walther et al. 2010). Understanding whether endogenous (physiological) or exogenous (environmental) processes dominate

otolith elemental incorporation is essential for effective interpretations of biogenic proxies.

Here, we examine the elemental chemistry of Atlantic croaker *Micropogonias undulatus* otoliths in response to hypoxia exposure using both short-term (4-week) and long-term (10 week) hypoxia exposure laboratory experiments. This species was chosen because of its extensive use as a model for identifying individual (Thomas and Rahman 2009a; Thomas and Rahman 2012) and population-level effects (Craig and Crowder 2005; Creekmore 2011) of hypoxia exposure. We hypothesize that hypoxic stress will affect element incorporation into the otolith, potentially driven by physiological alteration of blood chemistry through changes in protein and ion content. Experiments were performed in seawater with unmanipulated chemical composition to test the degree of endogenous alteration of otolith chemistry after exposure to hypoxic stress. In the first experiment, fish were exposed for 4-weeks to constant hypoxia or normoxia (controls) and otoliths were analyzed along the sulcul axis by laser ablation ICP MS. For the second experiment, fish were exposed for a longer duration of 10-weeks to normoxia, constant hypoxia, or periodic alternating hypoxia/normoxia and otoliths were analyzed along the ventral axis. Investigating the influence of internal physiological effects on otolith chemistry is essential to discern exogenous environmental signals from endogenous chemical signals contained in otoliths.

## 4.2 METHODS

### 4.2.1 Laboratory hypoxia experiments

*Experimental fish:* Atlantic croaker (100-110 mm total length, TL; 25-35 g wet mass, M), were caught by shrimp trawl in the Texas gulf coast by local fisherman and transported to fish holding facilities at the University of Texas Marine Science Institute.

Fish were treated with Paracide-F at 170 ppm in seawater for 1 h to minimize parasite infections and transferred in large indoor recirculating seawater tanks (4,727 L) under ambient temperature (22-23$^{o}$C) and photoperiod (13D:11L) conditions for at least 1 month prior to experimentation. Fish were fed chopped shrimp once a day (3% M/day). At the end of the experiments fish were sacrificed following guidelines approved by the Institutional Animal Care and Use Committee of the University of Texas at Austin.

*4-week constant hypoxia experiment*: Details of the experimental set-up are described by (Rahman and Thomas 2012). Briefly, in the hypoxia exposure tanks, the flow of air was reduced through the air flow meter gradually from 100-80% to 60, 40, 20, and finally adjusted until the dissolved oxygen (DO) level reached 1.7 mg $l^{-1}$, which was achieved within 2 days. A YSI multiprobe was used to monitor DO, pH, and temperature three times daily (Table 1., ESM Fig. 1). Sodium bicarbonate buffer was added as needed to adjust and maintain pH between 7.7-7.9 during the experiment. At the end of the study, fish total length (TL) in mm and wet mass (M) in g were measured, and the heads of the experiment subjects containing the otoliths were separated by treatment and frozen until analysis. Total length and mass data were used to calculate Fulton's condition index, $K = (M/TL^3)*100$.

*10-week constant and periodic hypoxia experiment:* Identical experimental methods as described above were used for the 10-week hypoxia study, however an additional treatment of periodic hypoxia exposure was produced by adjusting air flow to the tanks at weekly intervals to expose fish to hypoxia and normoxic conditions every other week. Salinity, temperature, dissolved oxygen concentration, oxygen saturation, and pH, were recorded daily for each of three replicate tanks for each treatment (ESM

Fig. 1). At the end of the experiment, fish were measured for total length. Fish sex was determined by examining the gonads and sagittal otoliths were immediately removed, cleaned with ultrapure water and stored in 1.5 ml polyethylene vials to air dry.

### 4.2.2 Otolith preparation and chemical analysis

*4-week exposure study*: Otoliths were weighed to the nearest 0.001 g and no difference in mass was detected between left and right otoliths (paired t-test, df=57, $t$=0.097, $p$=0.9225). Therefore, one was randomly chosen for analysis. Otoliths (N=46) were embedded in Epoxi-Cure resin, sectioned in the transverse plane using a low speed diamond blade saw, mounted on petrographic slides with Crystal Bond thermoplastic cement, then polished with lapping film (30µm and 3µm) to expose the core. Polished sections were then transferred to new petrographic slides (6-7 sections per slide) and sonicated in ultrapure water (18.2 mΩ) three times for 5 min and dried in a class 100 laminar flow hood before analysis.

*10-week exposure study*: Indium chloride (30 ppm) was added to the Epoxi-Cure resin and Crystal Bond embedding/mounting media to serve as an elemental indicator during the laser analysis, thus allowing precise determination of the otolith edge/resin interface in the data set. Left otoliths (N=72) were weighed, embedded, sectioned, polished, cleaned, and air-dried as described above.

Laser ablation inductively coupled plasma mass spectrometry (LA-ICP-MS) analyses were conducted at the University of Texas Jackson School of Geosciences, Austin, TX. An Aligent 7500ce ICP-Q-MS coupled to a New Wave UP 193-FX laser with a 26-µm laser spot diameter, 30% power (mean±SD: 4.37±0.16 J/cm$^2$), and 5-µm s$^{-1}$

scan speed was used to quantify $^{43}Ca$, $^{88}Sr$, $^{55}Mn$, $^{24}Mg$, $^{23}Na$, and $^{137}Ba$ from transects ablated across otoliths following an initial pre-ablation (35-µm spot diameter, 10% power, 25-µm $s^{-1}$ scan speed) to remove potential surface contamination. MACS-3 calcium carbonate and NIST 612 glass certified standards were run at the beginning and after every 60 minutes of analysis to convert raw intensity counts to molar concentrations (using MACS-3), correct for instrument drift and assess analytical precision (with NIST 612). Elemental intensity count data was converted to concentrations using the Trace Elements IS Data Reduction Scheme in the software Iolite that uses calcium (as 37.69 wt % in aragonite) as an internal standard (Paton et al. 2011) and then converted to molar ratios. Relative Standard Deviations (RSDs) based on repeated measurements of the NIST 612 standard for the 4-week data collected October 2010 over 2 days were: Sr=3.0%, Ba=5.4%, Mn=7.3%, Mg=7.5%, Na=12.9%; while the RSDs for the 10-week experiment fish analyzed December 2012 over 4 days were: Sr=10.2%, Ba=11%, Mn=19.6%, Mg=10.7%, Na=15.7%.

For the 4-week study otoliths, laser transects were initiated at the otolith core and run parallel to the sulcal groove to the otolith edge, obtaining a lifetime elemental profile for each otolith. For the 10-week study, the laser was run from the core to edge along the ventral otolith axis, which displays wider growth increments than the sulcal axis (APPENDIX A. Fig. 4.2a). Elemental concentrations were only compared within a given experiment using similar laser transect paths (treatments versus controls), given the potential for different concentrations obtained from different ablation axes. To estimate otolith precipitation rates, a subset of fish (N=4) were bathed 24 hrs in calcium staining Alizarin red solution (400 mg $l^{-1}$) and held for 4 or 10-weeks in the same size tank and fed the same food as experimental fish in normoxic conditions. At the end of the holding

period, the fish were sacrificed and otoliths were embedded, sectioned, and polished as described above. The stained otolith sections were then viewed with fluorescent light to capture digital images to measure the distance between stained growth increment and otolith edge using ImageJ software to estimate otolith precipitation rates (μm $day^{-1}$) along the sulcal and ventral growth axes (APPENDIX A: Fig 4.2b,c; Table 4.1). Mean otolith precipitation rates for the fish held 4-weeks and analyzed along the sulcal groove was 1.17 μm $d^{-1}$, while those otoliths from the 10 week study lasered along the ventral axis display mean precipitation rates of 1.35 μm $d^{-1}$ (APPENDIX A. Fig 4.1d). All fish tagged in the Alizarin study lost between 6-14% body weight due to poor feeding and thus our estimates of otolith precipitation are conservative estimates to ensure no pre-experimental aragonite was included in treatment comparisons (APPENDIX Table 4.1). The otolith chemistry data that was precipitated during the experiment was extracted from each fish otolith time series and averaged together for analysis.

*Collection and analysis of water samples:* During the 10-week experiment, water samples were collected from experimental tanks at 2-weeks and 4-weeks into the study to assess variation in water chemistry during the study. Samples were pumped from the bottom of a control and hypoxic tank using acid washed Teflon tubing and a peristaltic pump (Masterflex). The sample water was filtered with 0.45 and 0.2 μm PTFE filters in sequence with acid-washed 30 ml syringes and to remove any particulate matter and retain dissolved fractions and immediately acidified to pH<2 with trace metal grade nitric acid into acid-washed 30ml LDPE Nalgene bottles to be stored at 4°C until analysis. Water samples were analyzed for trace elements using solution based ICP-MS at the University of Texas Jackson School of Geosciences. Samples were diluted 100X with 2% trace metal grade $HNO_3$ and a subset of samples was spiked with matrix-matched

solutions to assess recoveries. Replicated blanks and certified reference standards were used to convert isotopes counts to concentrations and then converted to element:calcium ratios. Mean spike recoveries (N=6 spiked samples) were: Sr=95.9±0.4%, Ba=95.4 ± 0.4, Ca=97.0±1.7 Mn= 93.8 ±0.3, Mg=87.9±8.7, Na=67.9±23.7.

*Data analysis:* Student *t*-tests were used to compare condition factor (K) and otolith mass between control and constant hypoxia exposed fish from the 4-week and 10-week experiment. Elemental otolith data was examined for normality and homoscedasticity and a log transformation was performed for those elements that did not meet assumptions (Ba:Ca, Mg:Ca, and Mn:Ca). There was a significant difference in otolith mass between control and hypoxia-exposed fish in the 4-week exposure study (*t*-test, $t$=2.596, df=56, $p$=0.012), therefore a one-way ANCOVA was used to compare elemental ratios between control and hypoxia exposed fish, with otolith mass as a covariate.

Similarly, for the 10-week exposure study, mean experimental otolith elemental ratios were log (Ba:Ca, Mn:Ca) transformed to meet assumptions of normality and equal variance. Initially, a generalized linear model was performed to test the effect of treatment, sex, treatment*sex interaction, with tank nested within treatment*sex. There was no significant effect of tank on otolith elemental ratios, therefore, the three replicate tanks per treatment where pooled together to run a two-way ANOVA to examine the effect of treatment, sex, and treatment*sex on otolith elemental ratios and otolith mass. When a significant factor effect was detected with the two-way ANOVA, Holm-Sidak multiple comparison methods were used to determine which treatment or sex was

different by pooling data within a treatment (for Ba:Ca and Mg:Ca) or sex (for Mn:Ca). All statistical analyses were performed using SYSTAT 12.

## 4.3 RESULTS

### 4.3.1 Four-weeks exposure

The condition (K) factor and otolith mass of hypoxia-exposed fish were significantly reduced compared to control (K factor: $t$=4.207, df=61, $p$<0.001; otolith mass: $t$=2.596, df=56, $p$=0.012) (Fig. 4.1). However, no significant difference in otolith Sr:Ca, Ba:Ca, Mn:Ca, Mg:Ca, or Na:Ca ratios were detected between control and hypoxia exposed fish when accounting for otolith mass variation using ANCOVA (Fig. 4.1; Table 4.3).

### 4.3.2 Ten-weeks exposure

The dissolved elemental chemistry of the experimental tank water displayed limited variability for all elements except Ba:Ca and Mn:Ca. Barium:Ca molar ratios increased almost 2-fold from week 2 to week 4 in both control and hypoxia treatment tanks, which was accompanied by a decrease in salinity of approximately 5 ppt (Table 4.1). The Mn:Ca ratio was elevated in the hypoxic tanks which had 50% less dissolved $O_2$ than the control tanks by 6.6 μmol $mol^{-1}$ at 2 weeks and 2.5 μmol $mol^{-1}$ at 4 weeks (Table 4.1). In contrast to the 4-week study, otolith mass was not different between control or hypoxia exposed fish (Table 4.2). The condition (K) factor of fish exposed to constant hypoxia was significantly decreased compared to control (K factor: $t$=3.234, df=45, $p$=0.0023)(Fig. 4.1). Similar to the results of the 4-week exposure study, there were no significant differences in otolith Sr:Ca, Ba:Ca, Mn:Ca, Mg:Ca, or Na:Ca ratios

between control and fish exposed to constant hypoxia for 10 weeks (Fig 4.1). Only minor treatment and sex differences in the molar ratios of elements were observed in the periodic hypoxia treatment, varying less than 20%, whereas molar ratios of Sr:Ca, Ba:Ca, Mg:Ca and Zn:Ca in Atlantic croaker otoliths have been found to vary 60 to 90% in environmental samples collected from Chesapeake Bay and the Pamlico Sound, NC (Thorrold et al. 1997; Thorrold and Shuttleworth 2000). Interestingly, a significant treatment effect was detected for otolith Ba:Ca and Mg:Ca (Table 4.4), with post-hoc tests revealing that Ba:Ca and Mg:Ca was significantly reduced in the periodic treatment when males and females were pooled (Fig. 4.2). A significant interaction between treatment and sex was detected for both otolith Sr:Ca and Na:Ca (Table 4.4). For otolith Sr:Ca, females had decreased ratios in the control treatment, but males had decreased ratios in the periodic hypoxia treatment and there were no sex differences in the constant hypoxia treatment (Fig. 4.2). Otolith Na:Ca was significantly lower in males in the periodic hypoxia treatment, but there were no sex differences in the control or constant hypoxia treatments (Fig 4.2). Sex had a significant effect on otolith Mn:Ca when all treatments were pooled (Table 4.4), with females having higher ratios than males (Fig 4.2).

## 4.4 DISCUSSION

We have demonstrated with two independent controlled laboratory experiments that physiological stress associated with short and long-term constant sub-lethal hypoxic exposure has minimal influence on the otolith chemistry of the hypoxia tolerant teleost Atlantic croaker. In the first experiment, after 4-weeks of constant hypoxia exposure, fish condition was significantly reduced indicating that somatic growth was impaired, however there was no difference in the elemental ratios between control and hypoxia

exposed fish. Similarly, after 10-weeks of constant hypoxia exposure, the otolith chemistries of both male and female croakers were not different from controls yet condition factors of hypoxic fish were decreased, which lends further support to our initial finding. The variation in otolith Sr:Ca, Ba:Ca, Mg:Ca, and Na:Ca that was detected in response to the periodic hypoxia treatment was small compared to variation seen in field studies. In our study, the variation in otolith element ratios, between control and periodic hypoxia treatments was only 2 μmol/mol for Ba:Ca, 0.25 mmol/mol for Sr:Ca, 20 μmol/mol for Mn:Ca, and 0.5 mmol/mol for Na:Ca. In contrast, Thorrold & Shuttleworth (2000) reported 2-10 times the variation found in our study of 4 μmol/mol for Ba:Ca, 2.5 mmol/mol for Sr:Ca, 40 μmol/mol for Mn:Ca in otoliths of Atlantic croaker collected from northeastern estuaries. These data suggest that environmental factors dominate element incorporation with minimal influence from physiological stress.

The most promising geochemical proxy for hypoxia, Mn:Ca, did not show statistically significant variation by treatment. The experimental tank water from the constant hypoxic tanks did contain higher dissolved Mn:Ca, perhaps due to lower oxygen saturation allowing $Mn^{2+}$ to remain dissolved, but these differences were relatively small compared to field observations of dissolved Mn:Ca, which can vary over orders of magnitude in both space and time (Slowey and Hood 1971; Statham et al. 2005). Only two controlled laboratory studies have directly examined otolith composition following addition of dissolved Mn to water and neither reported positive relationships (Elsdon & Gillanders 2003, Miller 2009). In contrast, several field studies have reported positive correlations between ambient dissolved Mn:Ca and otolith Mn:Ca (Forrester 2005; Dorval et al. 2007; Mohan et al. 2012). Additional field studies have attributed elevated otolith Mn to hypoxic redox conditions in the Pamlico Sound (Thorrold and Shuttleworth 2000), Chesapeake Bay (Dorval et al. 2007), and Baltic Sea (Limburg et al. 2011). The

mechanism of Mn incorporation into otoliths is unclear but substitution with $Ca^{2+}$ ions in the aragonite crystal lattice has been suggested, as Mn has not been detected bound to proteins in cod otoliths (Miller et al. 2006). As discussed by Sturrock et al. (2012) the chemical behavior of $Mn^{2+}$ is intermediate between hard acids/bases and soft acids/bases, meaning it can exist in the plasma and endolymph in both free and bound forms. We did detect a slight statistically significant effect of sex ($p$=0.047) on otolith Mn:Ca, with higher ratios in females, but both males and females in the constant hypoxia treatment were similar. Unlike the other elements we investigated that tend to vary with salinity, dissolved Mn:Ca will flux out of sediments in dissolved form during low oxygen events, thus the non-effect of hypoxia on otolith Mn:Ca observed in this experiment, is perhaps due to lack of sedimentary supply of $Mn^{2+}$. The small variation in dissolved Mn:Ca between control and hypoxic experimental tank water was not enough to induce changes in otolith chemistry, as neither was the physiological effect of hypoxic stress. These results, along with other field studies that have measured ambient dissolved Mn (Dorval et al. 2007; Limburg et al. 2011; Mohan et al. 2012) support the hypothesis that variation in otolith Mn:Ca is strongly driven by exogenous, environmental dissolved ambient $Mn^{2+}$ variability that may be linked to sediment redox biogeochemistry.

Many studies have documented intrinsic vital effects on otolith chemistry, but few have examined differences between male and female fish. Kalish (1991) examined seasonal variation in the chemistry of the blood plasma, endolymph, and otoliths of male and female bearded rock cod, and also investigated changes in the protein content of the blood. Seasonal variation in the trace element chemistry of the endolymph was related to changes in the protein content of the blood plasma in response to gonad development. It was hypothesized that as fish invest energy into reproduction, more calcium-binding

proteins, such as the egg-yolk precursor vitellogenin, will be present in the blood and endolymph, which reduces the amount of free calcium available for otolith accretion resulting in increases in other trace metal impurities such as Sr (Kalish 1991). Earlier studies related otolith Sr:Ca to changes in temperature (Radtke 1989) or somatic growth rate (Sadovy and Severin 1992) without considering the effect of gonad development that is initiated by temperature changes and results in reduced somatic growth (Kalish 1991). The significant interaction between sex and treatment we detected for Sr:Ca and Na:Ca may have been the product of differential gonad investment in addition to the stress of the periodic hypoxia treatment.

Few other studies have examined the effects of stress on otolith chemistry (Kalish 1992) or blood and endolymph chemistry (Payan et al. 2004a). Thermal and osmotic stress resulted in low condition factors, a decrease in otolith Na/Ca, and an increase in otolith Sr/Ca in Australian salmon (Kalish 1992). Rainbow trout that were stressed with $Cl_2$ gas exhibited decreased $Na^+$ and $Cl^-$ in the blood plasma and endolymph, increased proteins in the proximal endolymph, but no changes in total Ca (Payan et al. 2004b). The stress-induced changes in endolymph chemistry also produced a 'check' mark and caused a reduction in otolith growth rate. Growth rate effects on otolith chemistry have been regarded as kinetic or physiological (Walther et al. 2010). Kinetic effects are controlled by the calcification rate of the otolith and can either result in increased element:Ca ratios if more trace elements get entrapped within the crystal during rapid calcification due to increased crystal defects (Gaetani and Cohen 2006) or decreased element:Ca if higher supplies of $Ca^{2+}$ in the endolymph dilutes the concentration of other trace elements in the calcifying fluid (Sinclair 2005). Physiological effects are mediated by metal-binding protein levels in the endolymph, which is coupled to somatic growth and affects the availability of free ions to be incorporated into the otolith. Otolith Mg:Ca was correlated

with somatic growth and otolith precipitation rates in spot (Martin and Thorrold 2005), Chinook salmon (Miller 2011) and Mg is subject to strong physiological regulation in fish (Woodcock et al. 2012). The stressful periodic hypoxia decreased otolith Mg:Ca as would be expected if Mg is under endogenous control, but otolith Ba:Ca also decreased. In many euryhaline species, otolith Ba:Ca typically displays positive relationships with ambient dissolved barium, as observed in both controlled lab experiments (Bath et al. 2000, Elsdon & Gillanders 2002, 2003, 2004, 2005, Bath Martin & Thorrold 2005, Miller 2009, Walther & Thorrold 2006), and field studies (Dorval et al. 2007, Mohan et al. 2012, Walther & Thorrold 2008). Some studies have found an effect of somatic/otolith growth on otolith Ba:Ca (Miller 2011, Walther et al. 2010), or temperature effects which can be related to growth (Elsdon and Gillanders 2002; Elsdon and Gillanders 2004), while others have detected no growth/temperature effects (Bath et al. 2000; Martin and Thorrold 2005; Martin and Wuenschel 2006). More work is needed to assess the potential effects of stress and growth on otolith Mg:Ca and Ba:Ca ratios.

Interestingly, the periodic hypoxia treatment did result in significant sex*treatment interactions for otolith Sr:Ca and Na:Ca and also decreased both otolith Ba:Ca and Mg:Ca, perhaps because alternating between hypoxic and normoxic conditions is more physiologically stressful than remaining in constant hypoxic conditions. Hypoxia tolerant species exhibit three specialized adaptations when they encounter low oxygen conditions that include 1) metabolic suppression, 2) tolerance of pH and ionic disturbances, and 3) ability to avoid free-radical injury during reoxygenation (Bickler and Buck 2007). Fish exposed to constant hypoxia would only need to enact the first two defense mechanisms, but those fish exposed to alternating weeks of hypoxia and normoxia would need to utilize all 3 mechanisms and at weekly intervals. The periodic hypoxia treatment did not significantly inhibit somatic growth,

since condition factors were not different than control fish, but otolith Ba:Ca and Mg:Ca was decreased. Dissolved Mg:Ca, Sr:Ca, Ba:Ca, and Na:Ca ratios were similar between control and constant hypoxia tanks throughout the experiment. Only dissolved Mn:Ca was different between control and hypoxic tanks, but a difference of 7 μmol $mol^{-1}$ is very minor compared to field observations of dissolved Mn:Ca in the northern Gulf of Mexico, which can vary over 100 μmol $mol^{-1}$ at low $O_2$ levels (J. Mohan, unpublished data), and Mn can be elevated several orders of magnitude in coastal regions compared to offshore Gulf waters (Slowey and Hood 1971).

We found differences in elemental chemistry between the sulcal and ventral axes of the croaker otoliths, as expected. The longer ventral axis exhibited approximately 1.5x Ba:Ca, 4x Mg:Ca and 40x Mn:Ca higher values compared to the sulcal axis. Only Na:Ca was increased 2-fold on the sulcal axis, while Sr:Ca was similar between both axes. These patterns may have arisen simply due to differences in precipitation rates and therefore incorporation dynamics of elemental impurities (Strasser et al. 2008; Walther et al. 2010). In addition, other studies have quantified the elemental composition of the endolymph fluid from which the otolith is mineralized and found heterogeneity between dissolved elements and proteins in the proximal and distal regions of the endolymph (Payan et al. 1999, Payan et al. 2004b). The endolymph fluid in trout was found to contain 20% higher $Na^+$ concentration on the proximal side, which is the same side that the sulcus is formed (Payan et al. 1999). Consistent with our results, Sr/Ca ratios displayed a uniform distribution along the proximo-distal axis in turbot otoliths that was related to homogeneous dissolved [$Sr^{2+}$] in the endolymph (Payan et al. 1999).

### 4.4.1 Conclusions

This is the first controlled laboratory study to examine the effects of hypoxic stress on otolith chemistry and one of the few studies to investigate the influence of sex on otolith elements. Constant hypoxia exposure over 4 or 10 weeks did not affect element incorporation in the otoliths of Atlantic croaker. Periodic hypoxia did influence element incorporation in complex and interactive ways and the exact mechanism of the hypoxic stress and sex influence is unclear. Otolith Mn:Ca was the only element ratio not affected by endogenous hypoxic stress, and thus may serve as a promising environmental indicator of hypoxic redox conditions.

**Table 4.1** Ambient physicochemical parameters of the experimental tanks from the 4-week study (mean ± standard deviation). Dissolved elemental chemistry data and ambient physicochemical parameters for both control and hypoxia tanks sampled at 2-weeks and 4-weeks in the 10-week experiment study. Time series for experimental tank conditions monitored daily can be found in Appendix A.

| Experiment | physicochemical parameter | experimental tank/sampling time | |
|---|---|---|---|
| | | control | hypoxia |
| 4 weeks | salinity (ppt) | 32.50±0.04 | 32.55±0.07 |
| | temperature (°C) | 21.87±0.12 | 21.85±0.07 |
| | DO (%) | 99.84±1.17 | 26.56±0.81 |
| | DO (mg $l^{-1}$) | 7.27±0.12 | 1.80±0.06 |
| | pH | 7.69±0.02 | 7.55±0.01 |

| | | 2 weeks | | 4 weeks | |
|---|---|---|---|---|---|
| | | control | hypoxia | control | hypoxia |
| 10 weeks | Sr:Ca (mmol $mol^{-1}$) | 8.21 | 8.21 | 8.04 | 8.07 |
| | Ba:Ca (µmol mol-1) | 12.52 | 13.16 | 27.9 | 28.89 |
| | Mn:Ca (µmol mol-1) | 6.8 | 13.4 | 7.02 | 9.53 |
| | Mg:Ca (mol mol-1) | 5.12 | 5.14 | 5 | 5.06 |
| | Na:Ca (mmol mol-1) | 45.07 | 45.19 | 43.88 | 44.63 |
| | salinity (ppt) | 39.04 | 39.08 | 34.49 | 34.79 |
| | temperature (°C) | 22.3 | 22.3 | 22.1 | 22 |
| | DO (%) | 76 | 23.3 | 82.4 | 26.4 |
| | DO (mg $l^{-1}$) | 5.34 | 1.64 | 5.97 | 1.85 |
| | pH | 7.35 | 7.44 | 7.53 | 7.45 |

**Table 4.2** Sample size (N), total length (TL), and otolith mass of Atlantic croakers exposed 4-weeks or 10-weeks to control, constant hypoxia, or intermittent hypoxia experimental treatments (mean ± standard deviation), with * indicating significant difference by Student t-test.

| Treatment | N | 4-week | | N | 10 week | |
|---|---|---|---|---|---|---|
| | | TL (cm) | otolith mass (mg) | | TL (cm) | otolith mass (mg) |
| control | 28 | 15.18±0.58 | 115.89±9.25 | 24 | 15.69±0.54 | 125.92±10.45 |
| constant hypoxia | 30 | 15.00±0.56 | 109.88±8.38* | 23 | 15.50±0.60 | 124.26±10.26 |
| periodic hypoxia | - | - | - | 24 | 15.796±0.59 | 126.42±9.151 |

**Table 4.3** One-way ANCOVA results with otolith mass as covariate for fish exposed 4-weeks to control or hypoxic conditions.

| Variable | Effect | Type III SS | df | MS | F | p |
|---|---|---|---|---|---|---|
| Sr:Ca | treatment | 0.054 | 1 | 0.054 | 1.659 | 0.205 |
| | otolith mass | 0.006 | 1 | 0.006 | 0.176 | 0.677 |
| logBa:Ca | treatment | 0.000 | 1 | 0.000 | 0.049 | 0.827 |
| | otolith mass | 0.003 | 1 | 0.003 | 0.299 | 0.588 |
| logMn:Ca | treatment | 0.020 | 1 | 0.020 | 0.345 | 0.560 |
| | otolith mass | 0.073 | 1 | 0.073 | 1.256 | 0.269 |
| logMg:Ca | treatment | 0.012 | 1 | 0.012 | 0.794 | 0.378 |
| | otolith mass | 0.000 | 1 | 0.000 | 0.011 | 0.918 |
| Na:Ca | treatment | 0.901 | 1 | 0.901 | 0.534 | 0.469 |
| | otolith mass | 0.160 | 1 | 0.160 | 0.095 | 0.759 |

**Table 4.4** Two-way ANOVA table investigating effects of treatment (control, constant hypoxia, periodic hypoxia) sex (male, female), and the interaction of treatment*sex in 10-week hypoxia study. Significant effects ($\alpha<0.05$) in bold.

| Variable | Effect | df | MS | F | p |
|---|---|---|---|---|---|
| otolith mass | treatment | 2 | 32.871 | 0.323 | 0.725 |
| | sex | 1 | 125.343 | 1.232 | 0.271 |
| | treatment*sex | 2 | 6.123 | 0.0602 | 0.942 |
| logMn:Ca | treatment | 2 | 0.0369 | 0.628 | 0.537 |
| | sex | 1 | 0.242 | 4.117 | **0.047** |
| | treatment*sex | 2 | 0.0247 | 0.42 | 0.659 |
| Mg:Ca | treatment | 2 | 0.0131 | 4.334 | **0.017** |
| | sex | 1 | 0.00311 | 1.032 | 0.313 |
| | treatment*sex | 2 | 0.00104 | 0.346 | 0.709 |
| Sr:Ca | treatment | 2 | 0.0564 | 0.729 | 0.487 |
| | sex | 1 | 0.00167 | 0.0215 | 0.884 |
| | treatment*sex | 2 | 0.451 | 5.822 | **0.005** |
| logBa:Ca | treatment | 2 | 0.0823 | 5.717 | **0.005** |
| | sex | 1 | 0.00655 | 0.455 | 0.503 |
| | treatment*sex | 2 | 0.0101 | 0.702 | 0.499 |
| Na:Ca | treatment | 2 | 0.0357 | 0.105 | 0.9 |
| | sex | 1 | 0.312 | 0.919 | 0.341 |
| | treatment*sex | 2 | 1.228 | 3.621 | **0.032** |

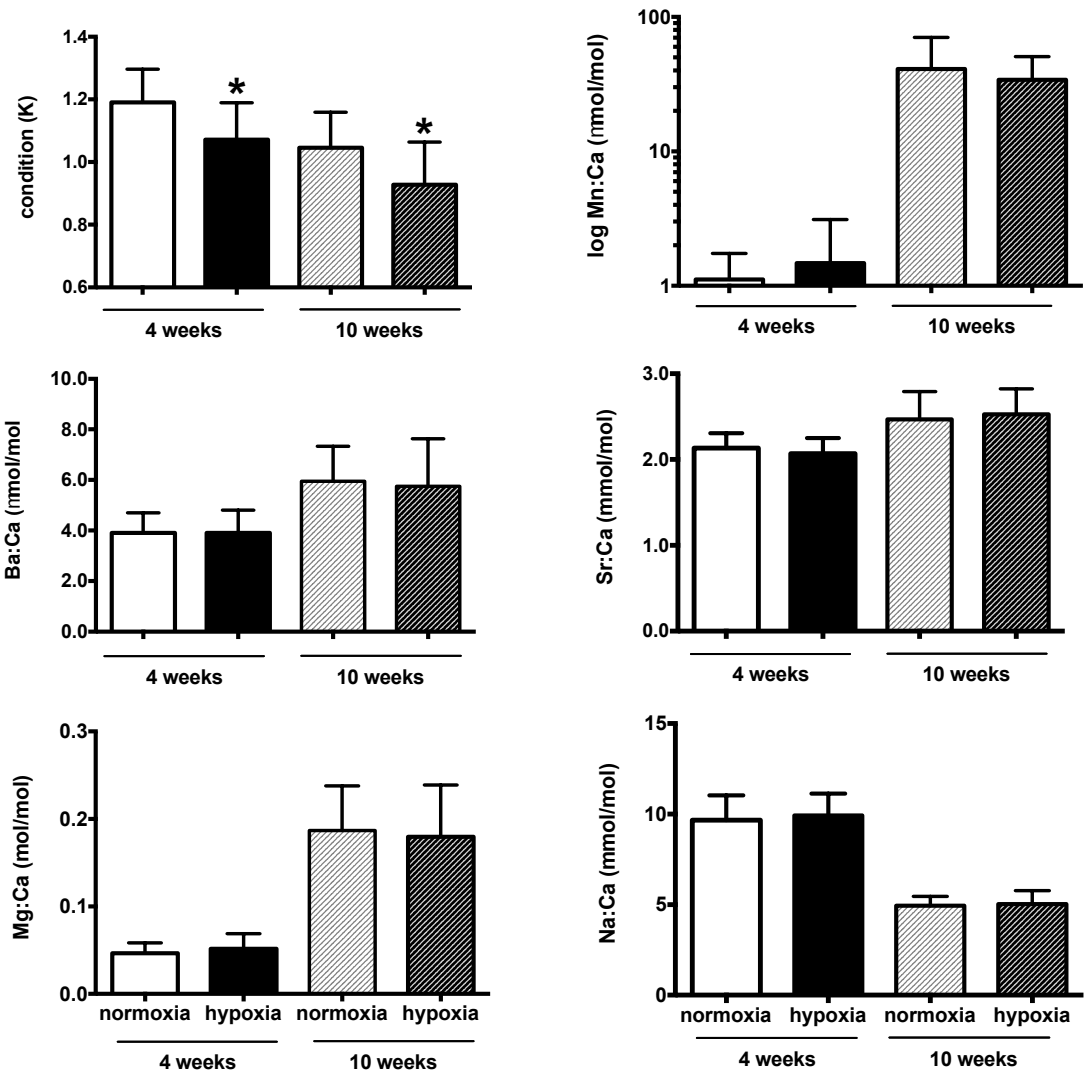


**Figure 4.1** Condition factor and otolith element:Ca ratios of Sr:Ca, Ba:Ca, Mn:Ca, Mg:Ca, and Na:Ca for Atlantic croaker exposed to either 4-weeks or 10-weeks to normoxia (control) or constant hypoxia. Error bars indicate standard deviation and * indicates significant difference by Student t-test. Note that differences in elemental concentrations between the 4- and 10-week experiments were due to ablations on different otolith growth axes.

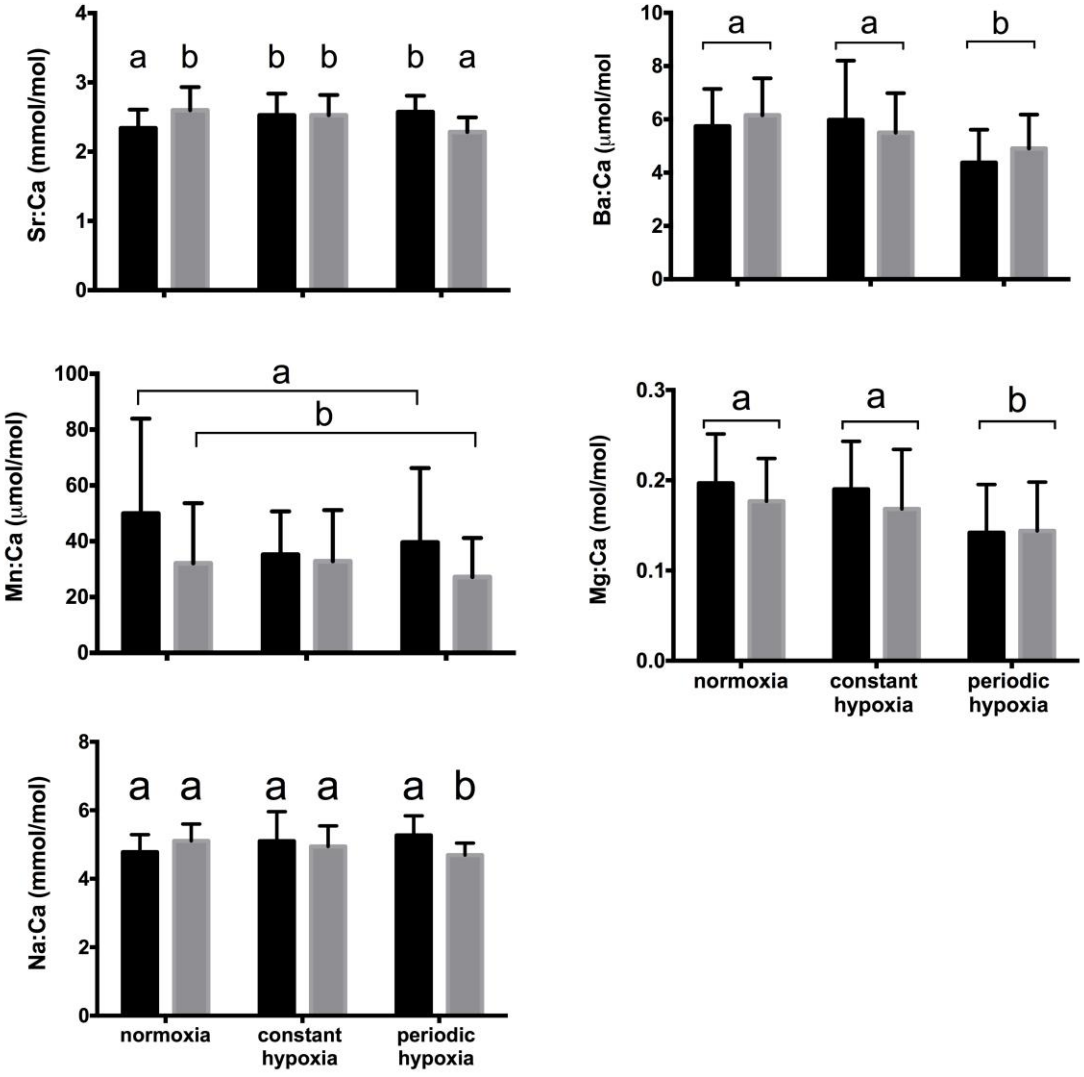


**Figure 4.2** Otolith element:Ca ratios of Sr:Ca; Ba:Ca; Mn:Ca; Mg:Ca; Na:Ca of females (black bars) and males (gray bars) exposed 10-weeks to normoxia (control), constant hypoxia, or periodic hypoxia. Error bars indicate standard deviation, with different lowercase letters above bars indicating significant post-hoc comparisons using Holm-Sidak methods after 2-way ANOVA examining main effects, with brackets above bars indicating pooled data.

# CHAPTER 5: DOES HYPOXIA EXPOSURE AFFECT TROPHIC NICHE AREA OF ATLANTIC CROAKER? AN OTOLITH CHEMISTRY AND TISSUE ISOTOPE APPROACH


## ABSTRACT

Seasonal hypoxia affects benthic ecosystems by altering feeding behaviors and trophic relationships. Identifying the sublethal effects of hypoxia on mobile fishes is difficult without long-term chronological geochemical records of individual exposure histories. In this study, trace element profiles in otoliths of demersal Atlantic croaker collected from the "Dead Zone" region of the northern Gulf of Mexico were used to quantify environmental exposure histories over the 2-3 months prior to capture. Otoliths were analyzed to quantify profiles of manganese (Mn) as a proxy of redox conditions and barium (Ba) as a proxy of estuarine habitat use. Estuarine and hypoxia exposure indices based on these proxies clustered fish into four recent exposure groups that included: late estuarine migrants, early estuarine migrants, offshore normoxic, and offshore hypoxic fish. Muscle tissue stable isotope values of carbon and nitrogen that also reflected 2-3 months of recent dietary history were used to estimate isotope niche area using standard ellipses. Fish demonstrating more estuarine habitat use displayed larger niche areas, while offshore normoxic and hypoxic fish exhibited small and statistically similar niche areas. These results suggest trophic resilience of demersal croaker to seasonal hypoxia in the northern Gulf of Mexico. A combination of otolith chemistry and tissue stable isotopes further enhances our understanding of responses to sublethal hypoxia and the potential consequences for ecosystem functioning.

## 5.1 INTRODUCTION

Hypoxia (dissolved oxygen (DO) < 2 mg/L) is a widespread phenomenon and occurs naturally world-wide, however the frequency and severity of hypoxic events are predicted to increase due to climate change, nutrient inputs and warming oceans (Diaz and Rosenberg 2008; Alteri and Gedan 2015). Currently, severe seasonal hypoxia and anoxia are developing in unprecedented open-coast locations, including the upwelling systems in the northeast Pacific where evidence suggests these events had not occurred in the past tens to thousands of years (Grantham et al. 2004; Chan et al. 2008; Erhardt et al. 2014) and signal modern oceanographic changes.

In shallow coastal systems such as in the northern Gulf of Mexico (nGoM), increasing eutrophication has contributed to the expansion of hypoxic zones in recent decades (Rabalais and Turner 2001). In the nGoM, hypoxia develops when thermo-haline stratification intensifies due to seasonal freshwater input, and subsequent nutrient enrichment fuel phytoplankton and zooplankton blooms. The seasonal pulse of sinking organic matter increases benthic respiration and microbial consumption of DO in bottom waters (Bianchi et al. 2010). Although hypoxia is common in the Gulf of Mexico, the magnitude and size of hypoxic regions varies both spatially and temporally for any given year (Rabalais & Turner 2001). Detecting measurable effects of hypoxia on coastal fishes has been difficult (Breitburg et al. 2009), but several studies have documented sub-lethal and indirect effects on diverse species and ecosystems, from both experimental and field-based approaches.

Research has demonstrated direct negative effects of hypoxia on benthic sessile burrowing species, such as increased predation during or shortly after episodic hypoxia (Long and Seitz 2008) and mortality due to prolonged exposure (Diaz and Rosenberg 1995; Baustian et al. 2009). However, in contrast to sessile organisms, mobile species such as fish may avoid hypoxia through lateral and vertical movements (Taylor et al.

2007; Roberts et al. 2009; Switzer et al. 2009; Zhang et al. 2009; Prince et al. 2010; Brady and Targett 2013; Brown et al. 2015). Laboratory studies have demonstrated that many species can detect and avoid hypoxia (Wannamaker and Rice 2000). Species that do not move away from oxygen stress may respond to hypoxia by reducing feeding and metabolic rates (Petersen and Pihl 1995; Brandt et al. 2009). In areas where hypoxia occurs episodically for short durations, mobile species may aggregate on the edges of hypoxic regions (Craig 2012). However, energetic consequences may result if available habitats are suboptimal in terms of preferable temperature (Coutant 1985; Craig and Crowder 2005) and availability of resources (Eby et al. 2005), which may alter trophic structure. Reduction of favorable habitat available to populations and concomitant reduced growth rates can result in decreased fitness of individuals. Disruption of reproductive endocrine function in Atlantic croaker *Micropogonias undulatus* exposed to hypoxia in the Gulf of Mexico (Thomas and Rahman 2012) and in controlled laboratory experiments (Thomas and Rahman 2009b) has been reported. Croaker collected from hypoxic sites displayed reduced gametogenesis related to increased expression of hypoxia-inducible factors (HIFs), which served as a reliable short-term (scale of 1-2 days) biomarkers of exposure to hypoxia (Thomas et al. 2007). It remains uncertain whether mobile species, such as croaker, reside in hypoxic environments for sufficient durations to generate reproductive impairment capable of affecting populations. Additionally, hypoxia may either enhance foraging by making benthic prey more vulnerable (Long and Seitz 2008) or decrease benthic prey availability and cause shifts to pelagic food webs (Nye et al. 2010). A lack of understanding natural hypoxia exposure levels in individuals is limiting the development of predictive models to estimate population-level affects (Rose et al. 2009). Quantifying individual exposure histories requires a long-term chronological recorder of lifetime hypoxia exposure.

Fish ear stones, or otoliths, have been used extensively as chronological geochemical records of the environments that fish encounter (Campana 1999). Recently, otolith manganese (Mn) has been used as an indicator of exposure to hypoxic water masses (Limburg et al. 2011; Limburg et al. 2014). Under low-oxygen conditions, the redox-sensitive $Mn^{2+}$ will flux out of the sediments and persist in the overlaying water column as dissolved species (Statham et al. 2005; Pakhomova et al. 2007). Fish inhabiting waters with elevated $Mn^{2+}$ would exhibit elevated otolith Mn:Ca, as demonstrated in several field studies (Forrester 2005; Dorval et al. 2007; Mohan et al. 2012). Elevated Mn:Ca in Atlantic croaker otoliths collected in the Neuse River Estuary was speculated to result from hypoxic redox conditions (Thorrold and Shuttleworth 2000). However, experimental studies that have attempted to spike water with dissolved manganese have failed to detect relationships to otolith chemistry (Elsdon and Gillanders 2003; Miller 2009), possibly due to lack of reduced oxygen saturation levels needed to keep manganese in dissolved and bioavailable form. In a recent controlled experiment, Atlantic croaker were exposed to constant or periodic hypoxia for up to 10-weeks and displayed reduced somatic growth but minimal difference in otolith chemistry (Mohan et al. 2014), suggesting that physiological stress has minor influence on otolith Mn:Ca. Results from the aforementioned field and lab studies suggest that environmental processes, such as sediment redox, dominate variability in otolith manganese. Otolith chemistry thus provides an opportunity to quantify hypoxic exposure histories on longer time scales than molecular biomarkers.

Stable isotopes are useful for tracing dietary pathways including diet source and trophic positioning. Unlike stomach content analysis, stable isotopes provide a time integrating signal of diet. Carbon isotope signatures in fish tissues reflect basal carbon sources (differential photosynthetic pathways), while stable nitrogen signatures reflect

trophic position with enrichment of $^{15}N$ occurring at higher trophic levels (reviewed by: Boecklen et al. 2011). Stable carbon isotope ratios are enriched in benthic versus pelagic food webs (France 1995) and depleted in terrestrial versus marine food webs (Peterson 1999). Measuring both $\delta^{13}C$ and $\delta^{15}N$ isotopes simultaneously, and plotting the values against each other reveals information on the overall trophic diversity of resources consumed, represented as an isotopic niche area (i.e. convex hull) (Layman et al. 2007b) that can be used to compare trophic relationships across populations or communities. For instance, isotopic niche areas were significantly reduced in grey snapper populations collected from fragmented habitats with lower prey diversity compared to unfragmented habitats (Layman et al. 2007a). Thus, fish participating in both benthic and pelagic food webs due to hypoxia would be expected to have larger isotope niche area, compared to fish feeding only on benthic sources. However, isotopic niche area comparisons can be biased by variable sample sizes between populations, therefore more robust Bayesian standard ellipse area estimates have been developed (Jackson et al. 2011) that are not biased by sample size.

The objectives of this study included: 1) using otolith chemistry to quantify hypoxia exposure levels and inshore habitat use for individual demersal Atlantic croaker; 2) based on the findings of 1), cluster fish into similar life-history groups based on recent (past 3 months) hypoxia exposure and inshore habitat residence and; 3) determine if hypoxia exposure affects feeding behavior and isotopic niche width using tissue stable isotopes. It was hypothesized that hypoxia could potentially: 1) limit foraging opportunities by restricting diets to stressed benthic prey items of lower trophic levels, resulting in small isotopic niches areas; or 2) enhance foraging opportunities by feeding on both benthic and pelagic prey items, resulting more diverse diets and larger isotopic niche areas; or 3) have no effect on croaker trophic dynamics. This study identifies

diverse migratory tactics and hypoxia histories in croaker using otolith chemistry and describes differences in isotopic niche area using a novel multi-proxy approach.

## 5.2 METHODS

### 5.2.1 Fish and water sample collections

Demersal Atlantic croaker were collected in the northern Gulf of Mexico on two separate cruises aboard the RV *Pelican* in the fall (8 October 2011 to 11 October 2011) and in the summer (30 July 2012 to 4 August 2012) at known hypoxic and normoxic sites using a bottom trawl (Fig 5.1). During the 2011 fall cruise, 10 fish per site were collected, measured in total length (TL), and dissected on board to collect both sagittal otoliths and a small filet of dorsal muscle tissue (Table 5.1). In the summer of 2012, about 10 fish where frozen whole and brought back to the lab for length and weight measurements, otolith removal, and collection of both muscle and liver tissues (Table 5.1).

At each site where fish were captured, a bottom water sample was collected using a CTD equipped with rosette sampling bottles and instruments to measure temperature, salinity, and dissolved oxygen at about 1 m from the bottom. Additional bottom water samples were collected opportunistically on separate cruises in June and August of 2012. Seawater was filtered on board the ship with 0.45µm and 0.2µm PTFE filters (Satorius Stedim Minisart SRP 25) attached to 30-ml PTFE syringes and collected in 30-ml LDPE Nalgene sample bottles – all filters, syringes, and bottles were acid washed. Water samples where fixed to pH<2 using trace metal grade nitric acid (Aristar) and chilled (~3°C) until analysis.

### 5.2.2 Otolith and water chemistry analysis

Sagittal otoliths were rinsed with ultrapure water, dried under a Class 100 laminar flow hood, and weighed to the nearest mg. Otoliths were embedded in Epoxi-cure resin that was spiked with indium (30 ppm) in order to differentiate the edge of the otolith from epoxy during laser ablation analysis. Embedded otoliths were thin sectioned in the transverse plane to extract the core region using a low-speed Isomet diamond blade saw. Thin sections were then mounted onto petrographic slides and polished using 30, 3 and 1 micron lapping film to expose the otolith core and elucidate the longest ventral growth axis. Individually polished otoliths were then transferred to new petrographic slides, digitally scanned, cleaned with ultrapure water bath, and then dried under a Class 100 laminar flow hood until analysis. Fish age was determined by counting annuli on scanned otolith images.

Elemental water and otolith data were collected using an Aligent 7500ce solution-based and laser-based ICP-Q-MS coupled to a New Wave 193-FX laser. Details of water and otolith chemistry analysis can be found in (Mohan and Walther 2014; Mohan et al. 2014). Laser scan transects were run from the otolith core to the edge along the longest dorso-ventral axis, using a 26-µm laser spot diameter at 5-µm $s^{-1}$ speed. Targeting the longest growth axis allowed optimal resolution of lifetime movements or exposure histories along the widest otolith growth bands. Otolith elemental intensity (counts) data was processed using Iolite (Paton et al. 2011) Trace Element IS data reduction scheme, with calcium (as 37.69 wt % in aragonite) as the internal standard and matrix matched MACS -3 USGS certified calcium carbonate as the reference material. Mean RSD for NIST 612 certified standards ($n$=67) analyzed over 4 analytical days was 13% for $^{55}$Mn and 14% for $^{138}$Ba. Concentration data were converted to molar ratios, and each transect was smoothed with a 7-point moving average.

### 5.2.3 Tissue stable isotope analysis

Muscle tissue samples were prepared as described in Chapter 2, and sent to UC Davis for carbon and nitrogen analysis. A duplicate tissue sample was included every 20$^{th}$ sample to determine precision. Mean SD of 10 duplicates was 0.042‰ and 0.037‰ for $\delta^{13}C$ and $\delta^{15}N$, respectively. Five certified standards Bovine Liver, USGS-41 Glutamic Acid, Nylon 5, and Glutamic Acid, and Peach leaves were also analyzed to assess accuracy and the mean SD was 0.07 ‰ for $\delta^{13}C$ and 0.12‰ for $\delta^{15}N$ values. Muscle tissue C:N molar ratios were low (mean±SD=3.93±0.2; range=3.7-4.9) indicating no need for lipid correction (Chapter 2). Differences in $\delta^{13}C$ and $\delta^{15}N$ values between cluster groups (described below) were compared using Kruskal-Wallace and Dunn's multiple comparison tests.

### 5.2.4 Otolith thresholds

Otolith element values above or below threshold values of Ba:Ca and Mn:Ca were used as indicators of estuarine habitat duration and coastal hypoxia exposure levels, respectively. Observations from controlled laboratory experiments and natural field measurements were used to establish conservative otolith threshold values (Table 5.2). First, partition coefficients *(D*=[element:Ca otolith]/[element:Ca water]) were determined based on water and otolith chemistry data from Mohan et al. (2014a) (Table 5.2). Second, the experimentally derived mean partition coefficient was multiplied by measured water chemistry values of inshore estuarine and coastal hypoxic environments measured in the field, to predict otolith chemistry values indicative of estuarine habitat residence and coastal hypoxia exposure (Table 5.2). For example, dissolved Ba:Ca in northern Gulf water does not exceed 30 μmol/mol until salinities are less than 20 ppt (APPENDIX B. Fig. 5.1), and dissolved Mn:Ca does not exceed 20 μmol/mol, until DO < 1mg/l when it

ranges 30-80 μmol/mol (Figure 5.2). Using these aforementioned field observations coupled with lab-derived *D* estimates allows prediction of otolith chemistry Ba:Ca values and Mn:Ca values that reflect estuarine habitat use and coastal hypoxia exposure (Table 5.2). An otolith Ba:Ca value <20 μmol/mol was considered coastal habitat use, while otolith Ba:Ca values >20 μmol/mol indicated inshore estuarine habitat residence. Exposure to coastal hypoxia only occurred when otoliths indicated coastal residence (Ba:Ca <20 μmol/mol) and otolith Mn:Ca was above the threshold (Mn:Ca>100 μmol/mol) (Table 5.2). To account for variation that exists in calculating *D* and natural water chemistry variation, a conservative approach was used to determine hypoxia and inshore levels. Otolith element values exceeding the threshold were assigned a value of 1, otolith values more than 2X the threshold were assigned a value of 2 and those 3X where equal to 3 (Figure 5.3). This categorized and binned values of inshore and hypoxia levels given geographic differences in chemical maxima driven by variable end members. Inshore residence and hypoxia exposure levels were calculated across entire fish otolith transects from core to edge (APPENDIX B Figs 5.2-5.6).

The most recent three months in otoliths was chosen to standardize otolith data to ecologically relevant time scales of muscle tissue stable isotope turnover rates (~ 3 months; Chapter 2) and limited to age 0 and age 1 year classes with similar growth and isotope turnover rates, for all subsequent comparison. Furthermore, focusing on early juvenile individuals with similar growth rates (ages 0 to 1), ensured there were minimal confounding effects of stage-specific otolith Mn uptake dynamics (Limburg et al. 2014). Estuarine and coastal hypoxia levels were summed over the last 1000 otolith microns (Figure 3), representing approximately 3 months of growth in juvenile croaker as determined from laboratory fish raised under controlled conditions (Chapter 2). A subset of fish (N=3) from experimental day 256 (~ 8.5 month), had otoliths prepared and

analyzed as detailed above. Mean (SE) laser distance for the three experimental fish of known age (8.5 months) was 3050±450μm, revealing that the most recent 1000 μm of otolith material represented the most recent two-three months for each fish.

### 5.2.5 Cluster analysis

Fish in the age 0 and 1 year classes (n=87) were grouped into clusters based on recent estuarine and hypoxia levels, using Wards distance and hierarchical cluster methods (SYSTAT). Hierarchical clustering groups individuals that are maximally similar (Ward 1963). Four major groups were defined: A, B, C, and D (Figure 5.4). For each group identified in the cluster analysis, recent hypoxia and estuarine levels, and muscle $\delta^{13}C$ and $\delta^{15}N$ where compared using Kruskal-Wallace nonparametric tests to control for unequal variance. Significant differences were further compared using Dunn's post hoc multiple comparison on mean ranks, with an adjusted p-value based on the number of comparisons.

### 5.2.6 Stable isotope standard ellipse comparison

A standard ellipse area (SEA) approach was used to compare cluster groups isotopic niche areas following Jackson et al. (2011) contained in the Stable Isotope Bayesian Ellipses package in R (SIBER). A conservative Bayesian estimate of isotope niche area that accounts for sample size differences was used to compare isotopic niches areas among cluster groups, with 10,000 posterior draws. Statistical significance between groups was considered when there was at least 99% probability that the standard ellipse area differed between groups.

## 5.3 RESULTS

### 5.3.1 Fish collections and site descriptions

*Fall 2011:* During the Fall 2011 cruise, samples were collected from the eastern, central, and western regions (Fig 5.1). The western region contained less young age-0 fish and older age-1 and age-2 fish, while the central and eastern sites exhibited higher numbers of age 0 and age 1 fish (Table 5.1). Environmental water quality (temperature, DO) and dissolved element (Sr:Ca and Mn:Ca) patterns were less variable in the fall, with the exception of the eastern sites (E1 and E2) that displayed lower salinities and higher dissolved Ba:Ca, as well as lower $\delta^{18}O$ values (Fig 5.5). The relationship between salinity and dissolved Ba:Ca was linear in the fall (Fig 5.2), but dissolved Mn:Ca was low (<10 μmol/mol) at high DO concentration (>6 mg/l). The linear relationship between salinity ranging 30-37 ppt and dissolved Ba:Ca was similar to relationships reported in Shim et al. (2012) (APPENDIX B. Fig. 5.1).

*Summer 2012:* During the summer 2012 cruise, fish were only collected from the eastern, central, and inshore central hypoxic regions (C1 and C2, Fig. 5.1). The majority of fish (*n*=10) collected from the eastern region were older, with only 2 fish that were age 0 and 7 fish age 1+ (Table 5.1). The central region contained the highest range of fish ages, from 0 to 5 years, with most fish being between 1+ and 2+ years (Table 5.1). The hypoxic sites closest to shore exhibited the youngest fish age 0 to 1. Hypoxia (DO<2 mg/l) was only detected at the most inshore shallow central sites (C1 and C2), which also contained the most elevated levels of dissolved Mn:Ca (Fig. 5.2 and 5.5). The shallow inshore sites (C1 and C2) also displayed the highest temperatures, but temperatures decreased as depth increased (Fig. 5.5).

### 5.3.2 Tissue isotopes

Carbon and nitrogen stable isotope values of muscle tissues (all ages pooled) displayed both seasonal and spatial variation. In the fall, muscle $\delta^{13}C$ values were similar in western and central regions, but were lowered and showed greater variation in the east (Fig. 5.6). Muscle $\delta^{15}N$ values were also lower in the eastern region during the fall, but highest in the western region. Relationships between total length and tissue isotope values also varied by season (Fig. 5.7). In the summer, muscle $\delta^{15}N$ and $\delta^{13}C$ values were linearly and positively related to TL by the equations: $\delta^{15}N=0.037*(TL)+8.5$; $r^2=0.39$; $p<0.001$ and $\delta^{13}C=0.039*(TL)-24.3$; $r^2=0.50$; $p<0.001$, respectively. However, there was no relationship between tissue isotopes and TL during the fall, or when considering only age 0 and age 1 fish that were used in the cluster analysis. Thus the slight effect of fish size on stable isotope values was accounted for by removing fish older than age 2+ from cluster and isotope niche analysis.

### 5.3.3 Cluster analysis

The cluster analysis revealed that four major groups existed based on recent (~past 3 months) hypoxia level and estuarine level (Fig. 5.8). Group A exhibited the highest recent estuarine levels, with Group B showing intermediate estuarine use and both Groups C and D showing low inshore estuarine levels. Only Group D had high recent non-estuarine hypoxia exposure levels (Fig. 5.8). Nitrogen and carbon tissue isotope showed similar patterns between groups, with groups A and B exhibiting significantly lower values compared to group C, and group D displaying intermediate values between other groups (Fig. 5.8).

Seasonal and spatial patterns in the occurrence of each group type were also apparent (Table 5.3). Group C (offshore residents) was the most common type found at

each location, except at the eastern region during the summer, when group D (high hypoxia exposure) was most prevalent (Table 5.3). There was an even distribution in the occurrence of group types B and D (n=8) between the fall and summer. Group A which displayed the highest inshore levels, showed the highest occurrence (n=5) in the eastern region during the fall.

### 5.3.4 Isotope niche

Isotopic niche width was compared between the cluster groups using a muscle tissue $\delta^{13}C$ and $\delta^{15}N$ biplot and convex hull (Layman et al. 2007b) and standard ellipse area methods (Jackson et al. 2011). Standard ellipse niche area estimates were 10, 7, 3, 2 per $mil^2$ for groups A, B, C, and D respectively. Bayesian estimated 99% credible intervals revealed groups A and B were significantly larger than groups C and D, and there was no significant difference between groups A and B or between groups C and D (Fig. 5.9).

## 5.4 DISCUSSION

This study links migration and environmental exposure histories to trophic dynamics in the seasonally hypoxic northern Gulf of Mexico and reveals trophic resilience of Atlantic croaker to sublethal hypoxia. Using otolith chemistry and tissue stable isotopes as environmental and dietary proxies, we found no effect of hypoxia exposure on isotope niche area in Atlantic croaker in the nGoM. Fish that displayed higher levels of inshore habitat residence (increased otolith Ba:Ca), had larger isotope niche areas, indicating larger overall trophic diversity.

A trophic shift in isotope niche area due to hypoxia exposure in Atlantic croaker was not detected in this study. Demersal croaker have demonstrated shifts in habitat use in response to hypoxia, occupying shallow waters and exhibiting density dependent reductions in growth due to decreased prey availability (Eby et al. 2005) and altered energy budgets due to increased variance in occupied temperature (Craig and Crowder 2005). Although these aforementioned studies have demonstrated fish escaping and movement away from hypoxia areas, croaker exhibited low avoidance thresholds to hypoxia (1-3 mg/l) in field surveys (Craig 2012) and will remain in low oxygen waters (1 mg/l) to avoid predation in laboratory experiments (Froeschke and Stunz 2011). Baustian et al. (2009) found that benthic infaunal prey densities did not differ between inshore, hypoxic, and offshore regions in the northern Gulf. Hypoxic sites were absent of oxygen-sensitive crustacean species, resulting in decreased prey community diversity compared to offshore sites, however no difference in croaker prey selectivity was detected at any location using stomach content analysis (Baustian et al. 2009). Other studies have documented dietary changes due to hypoxia, including optimal foraging on larger, weak prey (Pihl et al. 1992), and shifts from bivalves to less nutritious plant and detrital material diets (Powers et al. 2005). However, these studies have used stomach content analysis, which is limited to recent feeding history. Stable isotopes represent a time-integrated signal of diet, and croaker muscle tissues assimilate dietary changes over monthly time scales (Chapter 2). If croakers continue to strategically feed on stressed benthic prey during or immediately following hypoxia (Pihl et al. 1992), then isotope tissue signatures would not be expected to change, as reported in this study. We did not find evidence to support the hypothesis that croaker shift to pelagic food webs in response to summer hypoxia (Hazen et al. 2009; Nye et al. 2010). Enhanced foraging on stressed benthic prey on the edges of hypoxic zones in a Chesapeake Bay estuary has

been demonstrated in croaker (Long and Seitz 2008). Lake Erie yellow perch have been demonstrated to make brief forays into hypoxic water to forage on benthic prey, without exhibiting negative energetic consequences (Roberts et al. 2012). Anchovies will also make foraging dives into hypoxic hypolimnion to encounter higher prey densities (Taylor et al. 2007). Results of these studies have demonstrated the low-oxygen tolerant species may capitalize on lower trophic level benthic species that become vulnerable to predation during hypoxia, potentially experiencing an energetic tradeoff between increased consumption rates and suboptimal oxygen conditions (Brady and Targett 2013).

Lab experiments have demonstrated reduced feeding and growth under constant hypoxia determined from both physiological and molecular responses (reviewed Wu 2002), but field studies suggest complex behaviors including avoidance but also enhanced foraging (Long and Seitz 2008; Roberts et al. 2012; Brady and Targett 2013). Physiological effects of hypoxic stress on reproduction as indicated by increased HIF expression occurred on the scale of two to four weeks in laboratory Atlantic croaker (Thomas and Rahman 2009a). Exposing fish to periodic alternating hypoxic conditions is more stressful than constant exposure (Mohan et al. 2014), probably related to constant up- and down-regulation of molecular pathways. The tissue stable isotope trophic markers record diet on the order of three months, much longer than molecular markers or stomach contents, and thus may explain the lack of observed effects of hypoxia on trophic dynamics on these time scales.

Fish that exhibited high levels of inshore habitat residence, also had larger isotopic niche areas compared to offshore croaker. The increased niche area was primarily driven by deceased $\delta^{13}C$ values that ranged from -20 to -25 ‰. Bianchi et al. (2002) reported that sediments from the lower Mississippi river were more depleted (range: -21.9 to -24.6 ‰) compared to sediments collected off the Louisiana shelf (range:

-21 to -22 ‰) supporting the observation of more terrestrial-derived organic carbon at lower salinity, in congruence with this data set. Fry (1983) examined fish and shrimp migration patterns in the northern Gulf of Mexico using muscle carbon isotopes. A less marked convergence of tissue isotopes to offshore values indicated a continued reliance of adult croaker on estuarine foods due to close proximity with estuarine habitats. In contrast, pink and brown shrimp that migrate offshore as early juveniles and remain resident offshore during fast early growth, displayed sharp isotope convergence curves (Fry 1983). We found that 29% of croaker collected offshore recently occupied the inshore estuary. The strong relationship between muscle $\delta^{13}C$ and otolith Ba:Ca reveals that the inshore estuarine proxies agreed, providing evidence that both the diet (isotopes) and water (otoliths) proxies were responding to inshore estuarine movements. Several other studies have verified that otolith barium can reliably record fish movements into low salinity, inshore habitat (Nims and Walther 2014; Mohan et al. 2015). Also relationships between TL and muscle $\delta^{13}C$ and $\delta^{15}N$ follow expected patterns, but only in fish collected from the summer. Relationships between TL and isotope values of both age 0 and 1 pooled were not significant, suggesting minor influence of TL on subsequent analysis. Additionally, lower $\delta^{15}N$ was detected in the youngest fish (mostly age 0) collected closest inshore in the summer (sites C1 and C2), whereas higher $\delta^{15}N$ was measured in the oldest fish (age 1+ to 2+) farthest offshore in the fall (cites W1 and W2), following expected patterns related to ontogenetic offshore movements of croaker (Yakupzack et al. 1977).

The use of otolith chemistry as a record of hypoxia exposure relies on the assumption that hypoxia promotes an increased flux of dissolved $Mn^{2+}$ from the sediments into the water column. We characterized the relationship between dissolved oxygen and dissolved Mn in nGoM bottom waters, finding elevated dissolved $Mn^{2+}$ only

at DO < 2 mg/l, similar to several other studies on Mn behavior (Lewis and Luther 2000; Statham et al. 2005). We conservatively estimated otolith element thresholds, above which residence in estuarine waters or offshore hypoxic waters was inferred. Hypoxia exposure was only estimated for fish displaying offshore residence, to avoid any potential alternative sources of terrigenous Mn that could obscure benthic hypoxic redox conditions (Shim et al. 2012). There were spatial differences in behaviors of dissolved Mn:Ca and Ba:Ca, potentially related to the different riverine influence between the central and eastern regions. The central regions are strongly influenced by the Mississippi and Atchafalaya River outflows, which have well-characterized dissolved Ba and Mn end members (Hanor and Chan 1977; Shim et al. 2012; Joung and Shiller 2014). In contrast, the eastern region would be more influenced by the Pearl River, which exports twice the amount of organic carbon (Duan et al. 2007) and 2-8 times more dissolved and colloidal manganese (Stolpe et al. 2010) compared to the Mississippi or Atchafalaya Rivers. We found that the majority of the hypoxic groups occurred in the western and eastern regions (Table 3). Although hypoxia does not typically occur in the eastern nGoM, in 2010 there were expansive areas of hypoxia in the east related to increased river diversion in response to the Deepwater Horizon oil spill in the eastern regions (APPENDIX B. Fig.5.7; Limburg et al. 2014). We detected more hypoxia exposed fish in the eastern regions, where there is high delivery of Mn from the Pearl River (Stolpe et al. 2010), but not as many as expected in the central hypoxic regions as expected. These results suggest that absence of sedimentary manganese pools and organic matter supply may uncouple hypoxia – otolith Mn relationships and would require extensive sediment sampling to validate, which was beyond the scope of this study. Future studies that attempt to relate hypoxia exposure to otolith manganese patterns should sample sediments and potential infaunal prey to quantify bioavailable Mn pools.

The precise mechanism of manganese incorporation into fish otoliths is unclear. Some early experimental work has demonstrated that diet constitutes the major pathway of Mn accumulation in plaice soft tissue and bone, with minor uptake from water (Pentreath 1973; Pentreath 1976). The lack of relationships between dissolved Mn in water and otolith Mn from lab experiments (Elsdon and Gillanders 2003; Miller 2009) further supports the hypothesis of dietary Mn transfer. If stressed benthic prey becomes enriched with dissolved Mn from sedimentary pore waters during hypoxia, then fish predation and dietary transfer could represent a significant portion of otolith Mn variability. Benthic feeding fish have displayed increased otolith Mn that was correlated to enriched Mn levels in seagrass and detrital prey items (Sanchez-Jerez et al. 2002). However, lab experiments have demonstrated that dissolved Mn uptake in crustacean primarily occurs from the water (Baden et al. 1995; Baden et al. 1999) and that lobster tissue Mn levels could be used as biomarkers of hypoxia exposure (Baden and Neil 2003). Further work is needed to determine the role diet plays in Mn accumulation in fish otoliths.

### 5.4.1 Conclusions

A novel multi-proxy approach was used to examine the effects of long-term hypoxia exposure on trophic diversity of a common demersal marine fish. Trophic diversity, as represented by isotope niche area, was small between offshore fish and hypoxia-exposed fish, suggesting no change in long term feeding behavior due to hypoxia. The areal extent of hypoxia was small in 2012 due to drought conditions, which may have limited our ability to detect trophic effects. Fish that more recently migrated from the estuary to offshore habitats, displayed larger trophic niche areas suggesting a larger diversity of prey types consumed. These results suggest trophic resilience of

demersal croaker to hypoxia in the northern Gulf of Mexico, and increases knowledge of the ecological effects of seasonal hypoxia on fish populations.

**Table 5.1** Total numbers of fish (*n*) collected and mean total length (± standard error (SE) of each age class at each Site, Region, and Season. Totals in **bold** represent mean TL (±SE) for each age class in each season.

| Season | Region | Site | Age (yr) | | | | | | | | | | | |
|---|---|---|---|---|---|---|---|---|---|---|---|---|---|---|
| | | | 0 | | 1+ | | 2+ | | 3+ | | 4+ | | 5+ | |
| Fall 2011 | WEST | W1 | *4* | 153±2 | *3* | 175±11 | *3* | 178±5 | | | | | | |
| | | W2 | | | *7* | 162±3 | *3* | 186±15 | | | | | | |
| | CEN | C3 | *8* | 149±4 | *1* | 166 | *1* | 173 | | | | | | |
| | | C4 | *5* | 158±5 | *1* | 160 | *3* | 177±3 | *1* | 200 | | | | |
| | EAST | E1 | *6* | 153±3 | *4* | 194±25 | | | | | | | | |
| | | E2 | *2* | 138±2 | *7* | 186±12 | *1* | 177 | | | | | | |
| | | **total** | ***25*** | **150±2** | ***23*** | **174±8** | ***11*** | **178±5** | ***1*** | **200** | | | | |
| Summer 2012 | CEN_HYP | C1 | *10* | 139±2 | | | | | | | | | | |
| | | C2 | *7* | 140±2 | *3* | 154±8 | | | | | | | | |
| | CEN | C5 | *1* | 143 | *5* | 164±7 | *2* | 166±2 | *1* | 190 | *1* | 202 | | |
| | | C6 | *1* | 129 | *3* | 167±8 | *4* | 176±10 | *1* | 170 | | | *1* | 205 |
| | EAST | E3 | *2* | 144 | *3* | 163±7 | *5* | 167±3 | | | | | | |
| | | E4 | | | *4* | 160±3 | *5* | 165±4 | *1* | 182 | | | | |
| | | **total** | *21* | **139±2** | ***18*** | **161±2** | ***16*** | **169±3** | ***3*** | **181±6** | ***1*** | **202** | ***1*** | **205** |

**Table 5.2** Experimental data from Mohan et al. (2014) used to calculate mean partition coefficients *(D*=[element:Ca otolith]/[element:Ca water]) for Mn:Ca and Ba:Ca under constant dissolved oxygen (DO) and salinity regimes. Experimental otolith values were averaged between 3 treatments (n= 24 fish/treatment) from the 10-week study (Mohan et al. 2014). Predicted water quality and chemistry parameters from the field were derived from Figure 5.3 and Appendix B Fig. 5.1.

| Observed in laboratory | | | | | | | Predicted in field | | | |
|---|---|---|---|---|---|---|---|---|---|---|
| Element:Ca ratio | DO (mg/l) | salinity (ppt) | observed experimental water (µmol/mol) | mean experimental otolith (µmol/mol) | ***D*** | mean ***D*** (±SD) | predicted water quality | predicted field water (µmol/mol) | predicted field otolith (µmol/mol) | Otolith threshold (µmol/mol) |
| Mn:Ca | 1.7 | | 11.5 | 36±5 | 3.13 | 4.17 ±1.5 | DO <1.5 mg/l | 30 | 125 | hypox > 100 |
| | 5.7 | | 6.9 | | 5.22 | | | 50 | 209 | |
| | | | | | | | | 80 | 334 | |
| Ba:Ca | | 39 | 12.84 | 5.5±0.1 | 0.43 | 0.31 ±0.17 | S: 20 ppt | 50 | 16 | inshore > 20 |
| | | 34.6 | 28.4 | | 0.19 | | S: 10 ppt | 100 | 31 | coastal < 20 |
| | | | | | | | S: 5 ppt | 200 | 62 | |

**Table 5.3** Seasonal and spatial occurrences of each cluster group.

| Group | Type | N | Fall | | | | Summer | | | |
|---|---|---|---|---|---|---|---|---|---|---|
| | | | WEST | CEN | EAST | Total | CEN HYP | CEN | EAST | Total |
| A | High inshore | *9* | 0 | 1 | 5 | 6 | 2 | 0 | 1 | 3 |
| B | Inshore | *16* | 3 | 2 | 3 | 8 | 5 | 2 | 1 | 8 |
| C | Offshore | *46* | 10 | 9 | 7 | 26 | 10 | 7 | 3 | 20 |
| D | Hypoxia | *16* | 1 | 3 | 4 | 8 | 3 | 1 | 4 | 8 |
| Total | | ***87*** | **14** | **15** | **19** | **48** | **20** | **10** | **9** | **39** |

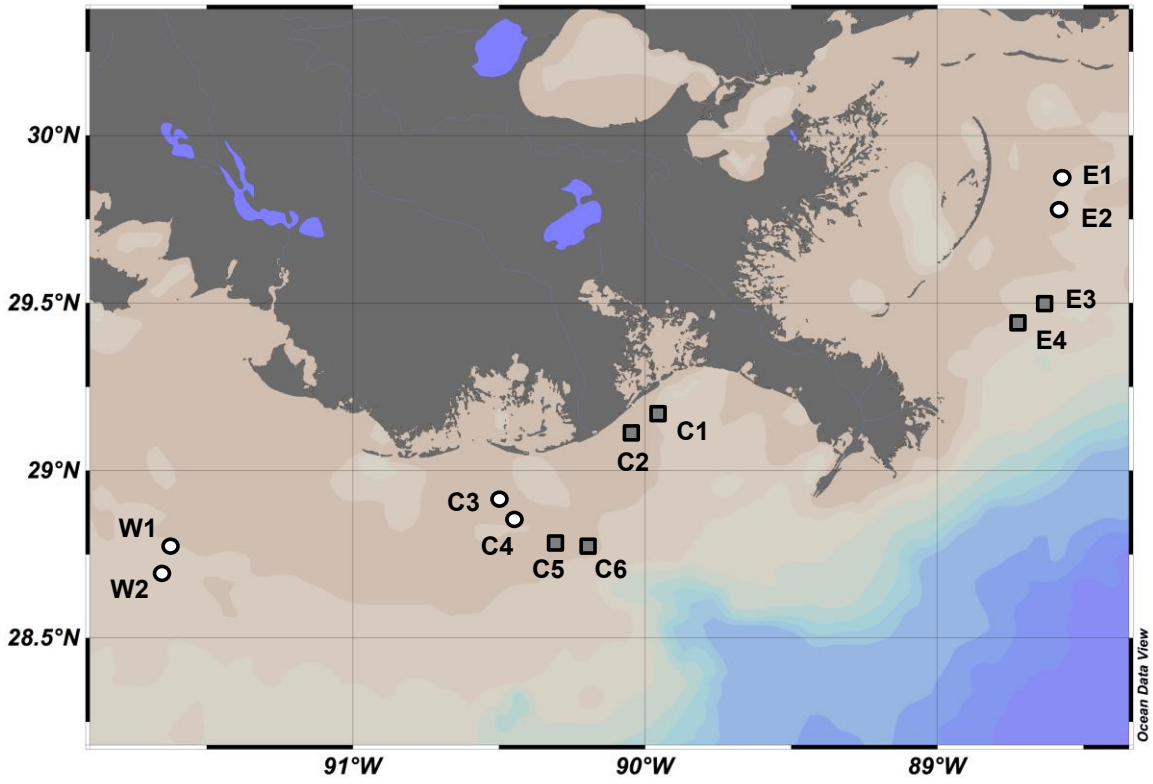


**Figure 5.1** Map of locations sampled in the northern Gulf of Mexico in the fall of 2011 and summer of 2012. White circles = fall stations; gray squares = summer stations. E = eastern sites; C = central sites; W = western sites.

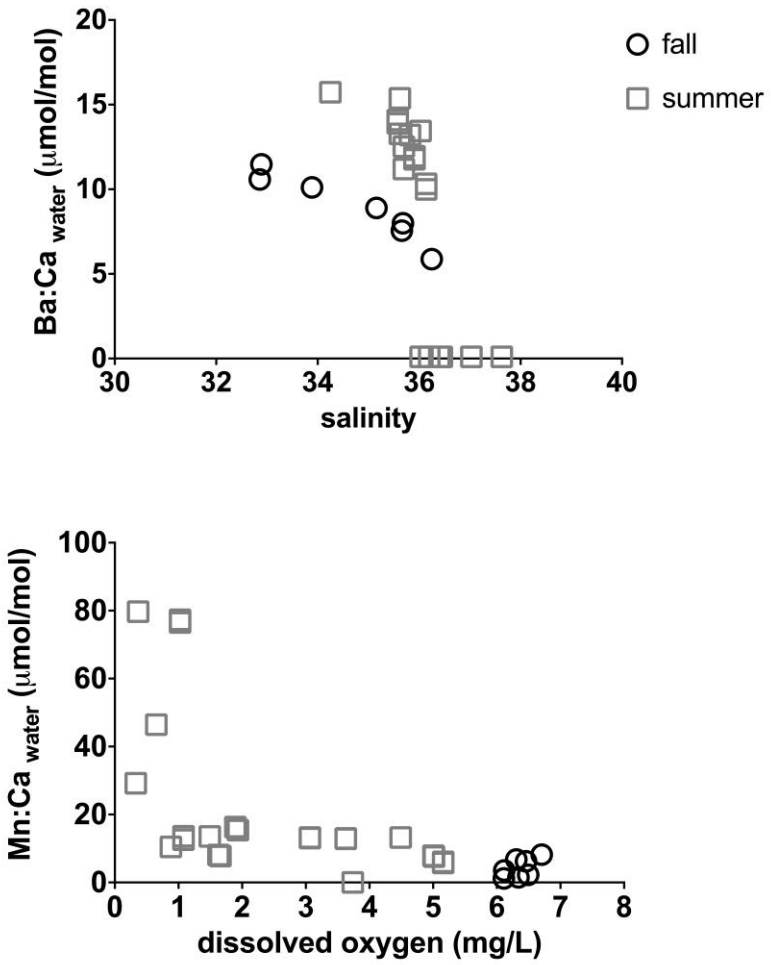


**Figure 5.2** Relationship between bottom water (~1 m above bottom) dissolved Ba:Ca and salinity (top panel) and dissolved Mn:Ca and dissolved oxygen (bottom panel) during the fall (black circles) and summer (gray squares).

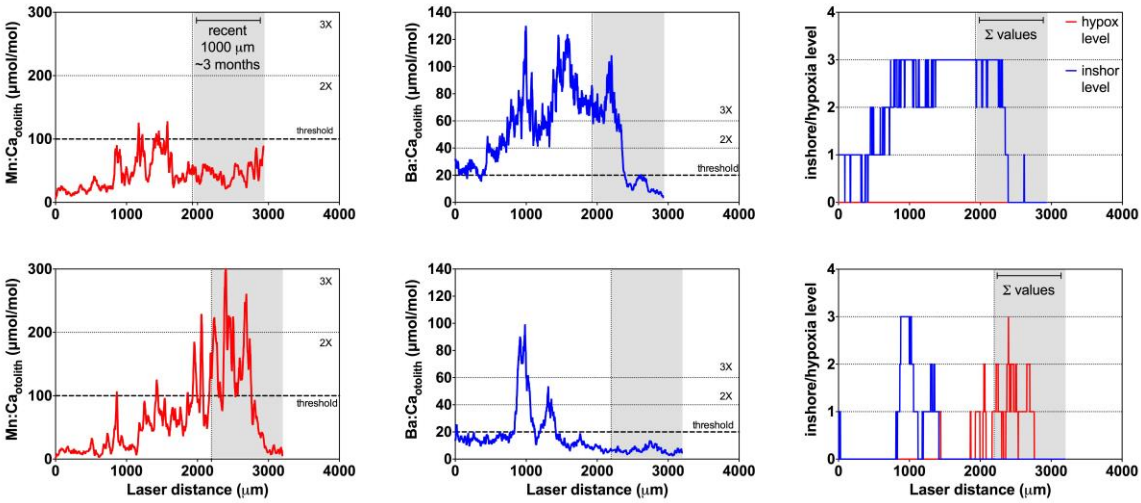


**Figure 5.3** Illustrative examples of raw data scans for fish clustered into groups at opposite extremes of the cluster tree type A (top row) and type D (bottom row). Otolith Mn:Ca (left columns), otolith Ba:Ca (middle columns) and standardized inshore/hypoxia level (right columns). Gray shaded area highlights last 1000 microns (~ 3 months) used in cluster analysis. Dashed bold line (**---**) indicates hypoxia/inshore threshold; dotted line (···) displays 2X and 3X above threshold limit.

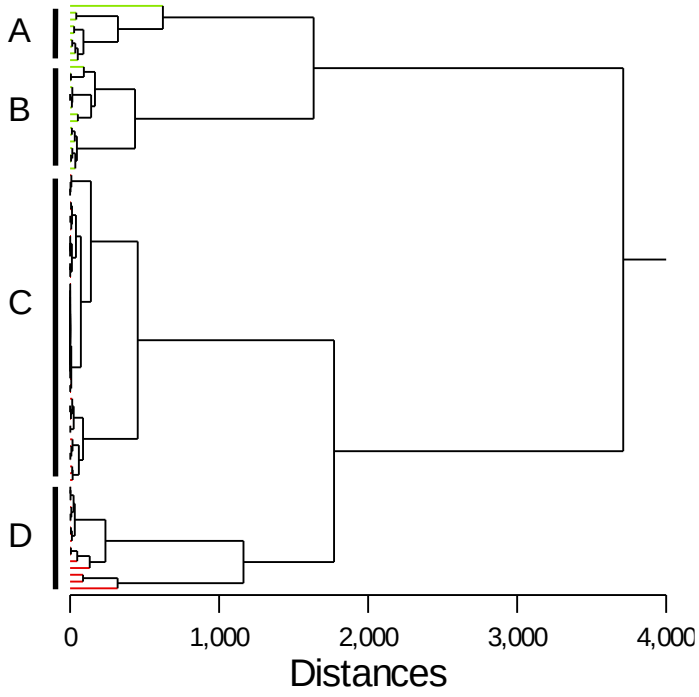


**Figure 5.4** Cluster tree produced using Wards method and recent hypoxia level (last 1000 μm of otolith edge) and recent inshore level of age 0&1 fish to classify individuals into four major groups (at distance ~1500).

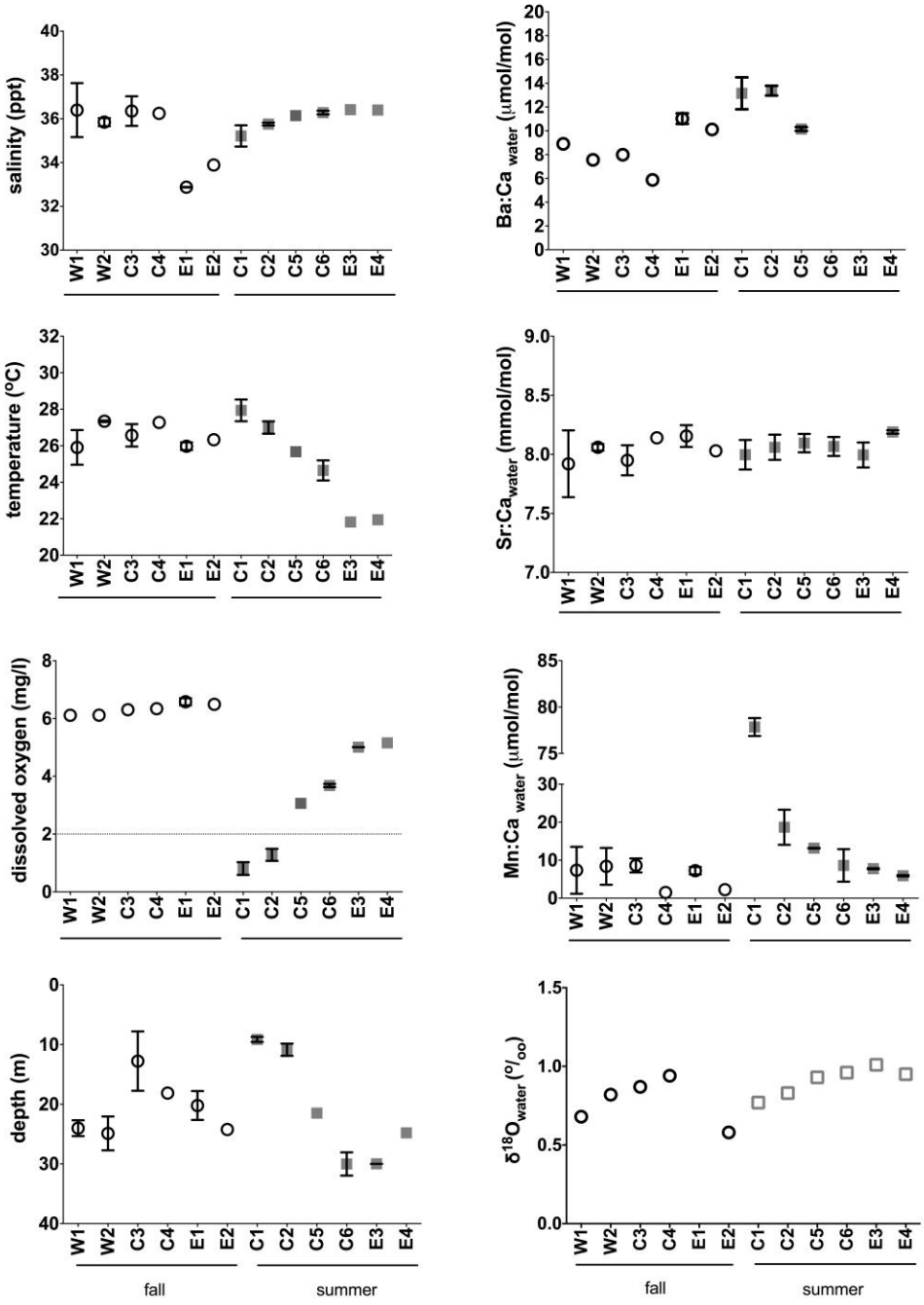


**Figure 5.5** Water quality parameters (left panels) and water chemistry (right panels) of bottom waters (~1 m above bottom) at each trawl site where demersal croaker where collected for the summer (open circles) and fall (gray squares).

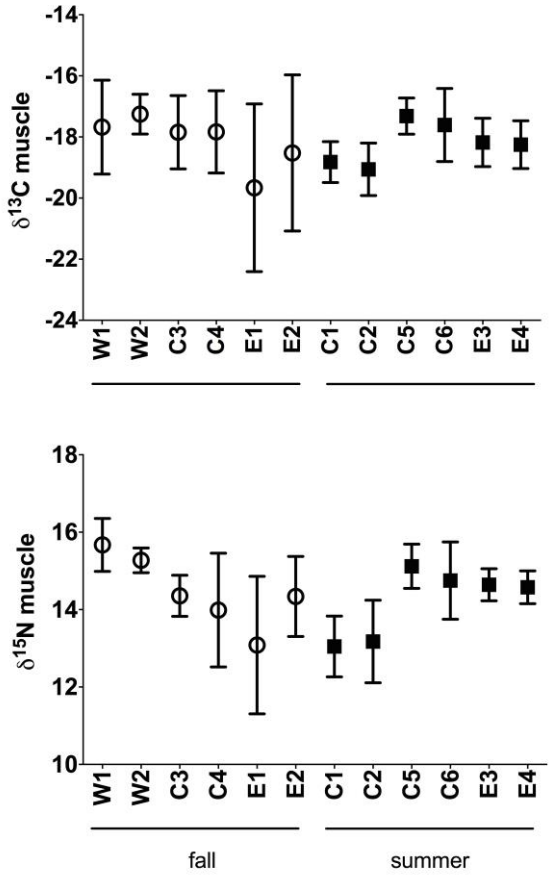


**Figure 5.6** Mean (± standard deviation) tissue stable isotope values for all fish (ages pooled) at each site (*n*=10 per site). Open circles = summer; filled squares = summer.

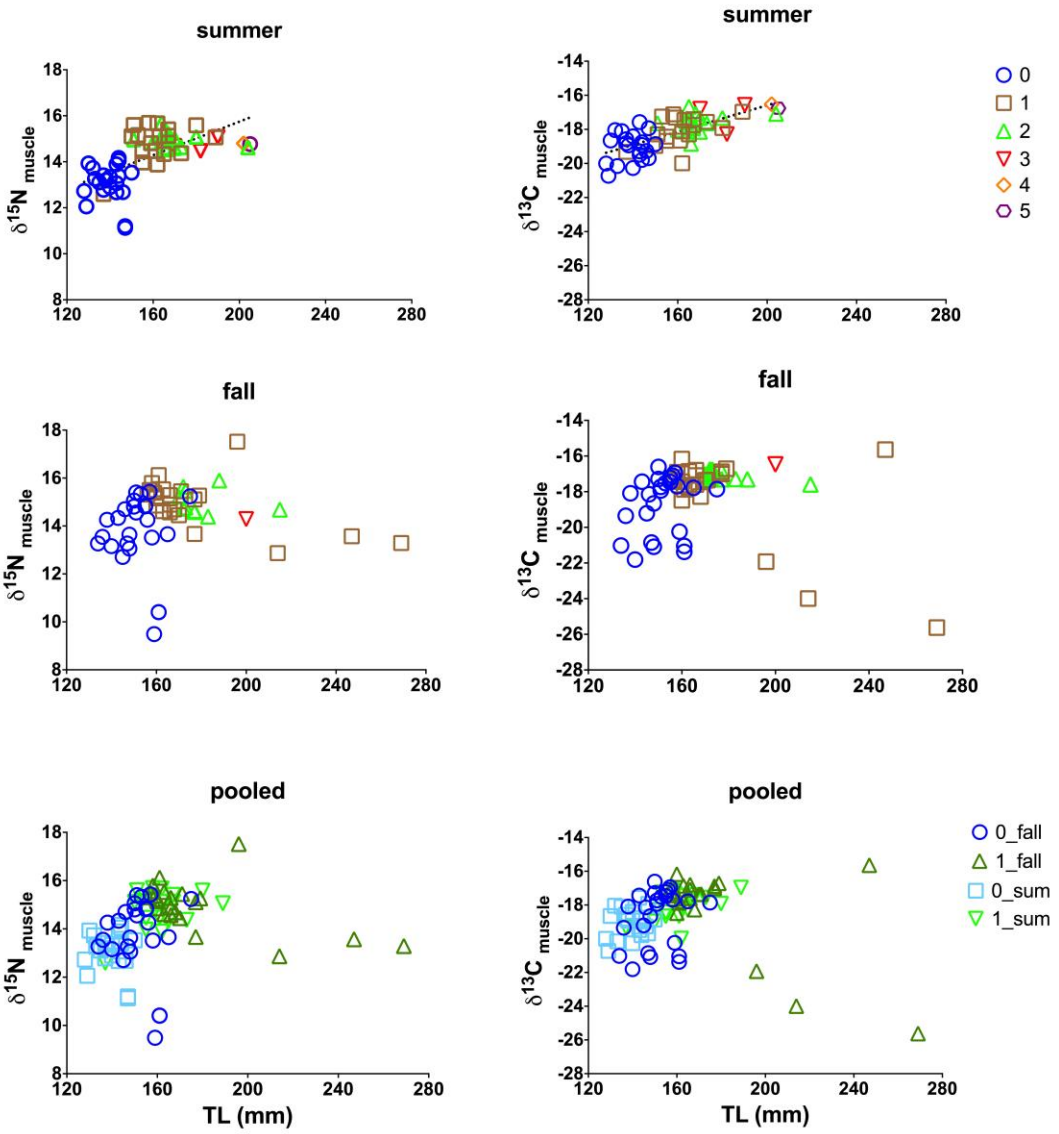


**Figure 5.7** Relationships between fish total length (TL) and muscle tissue isotope values for each age class (different colored symbols) for the summer (top panels) fall (middle panels) and pooled summer and fall age 0 and 1 only (bottom panels). Dashed line = significant linear regression.

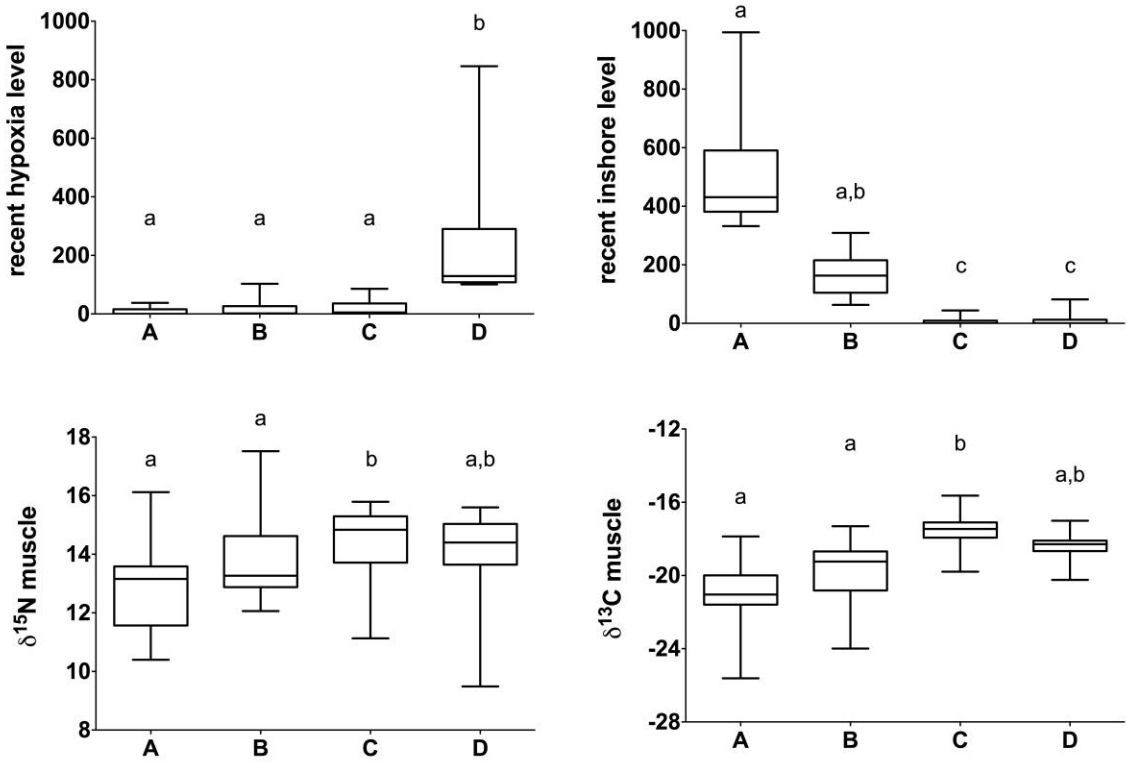


**Figure 5.8** Boxplots displaying recent hypoxia and inshore levels (top panels) and muscle tissue nitrogen and carbon isotope values (bottom panels) for each cluster. Lower case letters indicate significant difference detected with Kruskal Wallace and Dunn's multiple comparison statistics.

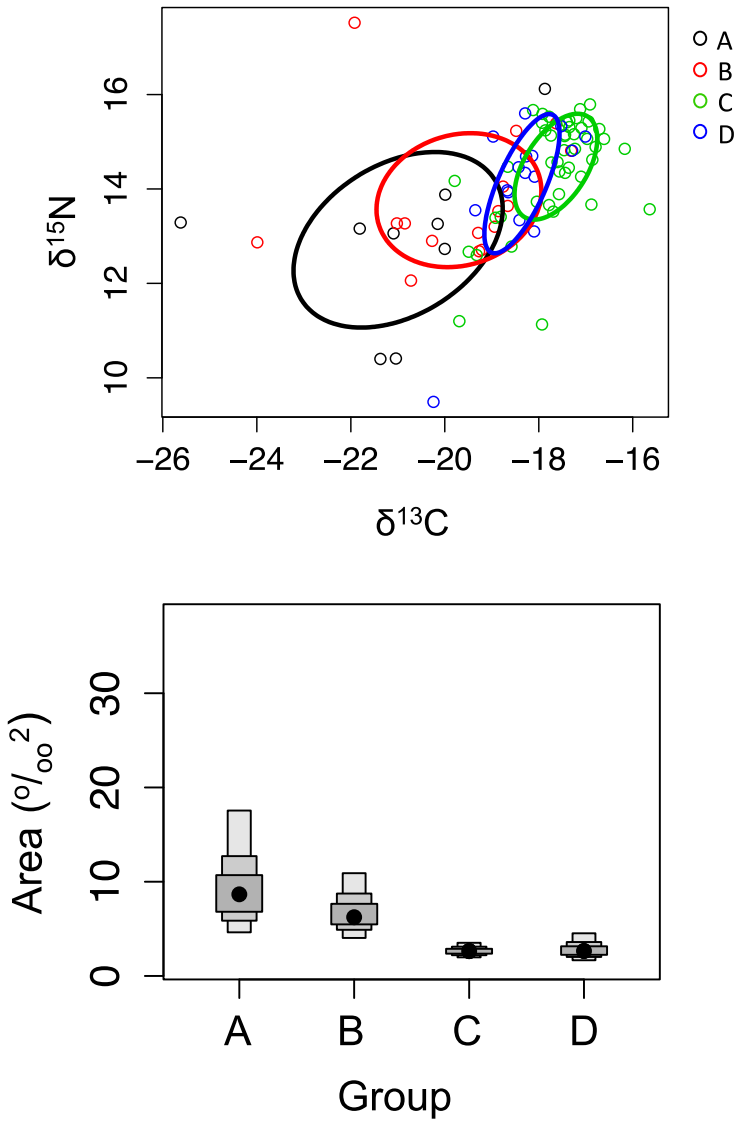


**Figure 5.9** Carbon-nitrogen isotope biplot (top panel) with individual fish in each cluster group indicated by colored circles. Dashed lines connecting points indicate convex hull area with colored solid lines displaying standard ellipse area. Bayesian estimated standard ellipse niche area (bottom panels) for each cluster group. Black dots indicate group modes with shaded boxes representing 50%, 75% and 95% credible intervals from dark to light shades. There is a 99% probability that groups A and B are significantly different than groups C and D.

# SYNTHESIS

Natural tags in fishes are useful for addressing ecological questions as they provide information on environmental histories and trophic interactions, across various ontogenetic life stages. A framework for using the multi-proxy approach developed here is presented in Figure 6.1. Otoliths record environmental history from early larval to late juvenile stages, thus otolith microchemistry can be used to address questions related to fish movement across salinity gradients and exposure to hypoxia at multiple life stages, as presented in Chapters 3 and 5. Additionally, otolith microstructure provides information on daily age, growth rates and hatch date that if combined with otolith microchemistry can expand the breadth of ecological questions addressed. In contrast to otoliths that provide discrete life history information, tissue stable isotopes of nitrogen and carbon provide an integrated signal of recently ingested food items. Combining multiple tissues and stable isotope ratios that have different turnover rates, can provide both short and long term diet histories for addressing specific ecological questions related to seascape migrations, connectivity, and resource dynamics (Figure 6.1). Chapter 3 presented the tissue-specific residual analysis for detecting recent movements of estuarine juvenile fish across salinity gradients and isoscapes and demonstrated agreement between independent otolith chemistry and tissue isotope proxies, which enhanced interpretation of the individual natural tags. In Chapter 5, groups of age 0 and 1 Atlantic croaker in the northern Gulf that experienced diverse environmental histories were identified and isotope niche areas based on muscle tissue isotope suggested trophic resilience to hypoxia

exposure. Application of natural tag approaches to address ecological questions first requires validation studies that examine element incorporation dynamics (Chapter 4) and isotope turnover rates (Chapter 2) and describe spatiotemporal variation in chemical gradients and isoscapes (Chapter 1).

There are limitations to the multi-proxy natural tag approach employed here that should be considered in future work. Although tissue stable isotope values provide recent dietary information, they lack information on earlier previous diet that fishes consumed before tissues were regenerated through growth and metabolism. Extracting chronological dietary information from otolith isotope values is an emerging area of research, and will expand the use of isotopes to address ecological questions in fishes. Additionally, stable isotope values of system-specific end members were not characterized in this study, which limited the ability to constrain percent contribution of various carbon sources to fish production using mixing models. Current progression in natural tag approaches entails greater specificity in diet source, which includes compound-specific stable isotope analysis of individual fatty acids and amino acids in soft and calcified tissues. Development and refinement of natural tag approaches through laboratory experiments and field surveys furthers our understanding of fish habitat use and resource needs, which are two essential factors that support resource management efforts to protect nursery habitats and quantify sub-lethal effects of hypoxia on mobile fish populations.

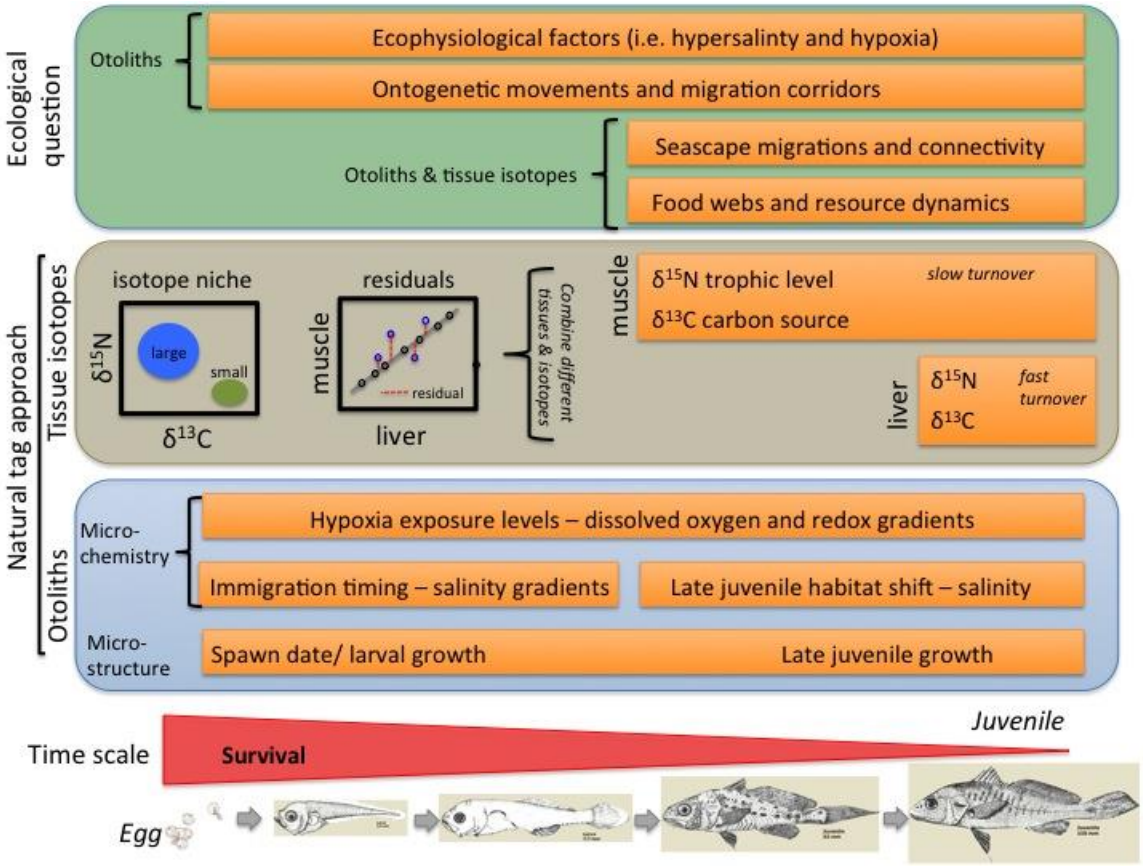


**Figure 6.1** Conceptual diagram illustrating the framework of the multi-proxy approach for answering ecological questions. Fish illustrations adapted from (Johnson 1978)

# APPENDIX A

control

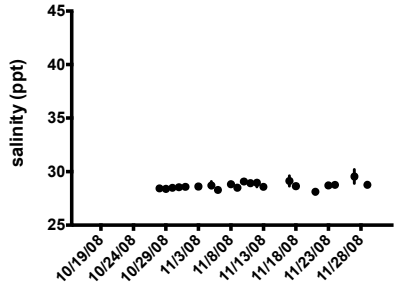


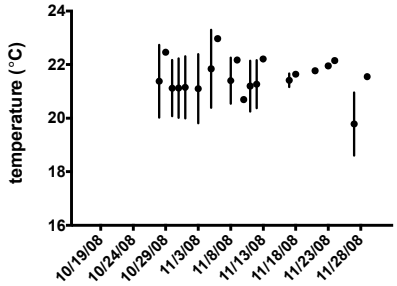


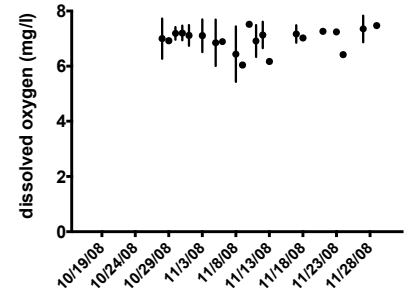


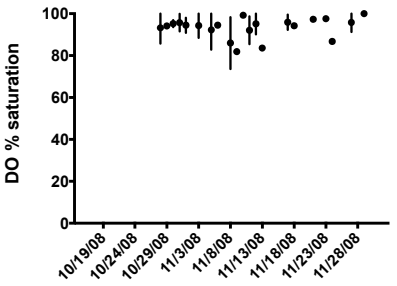


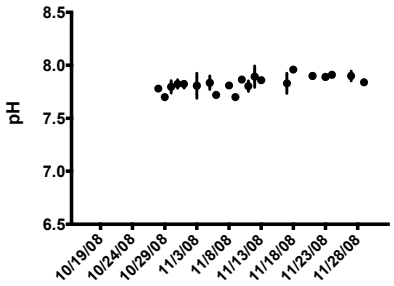


hypoxia

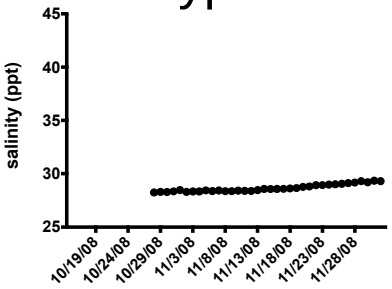


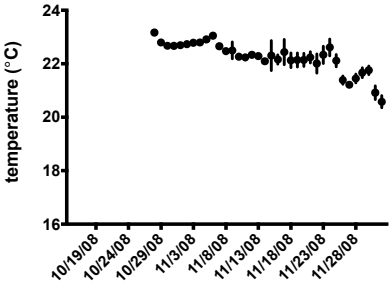


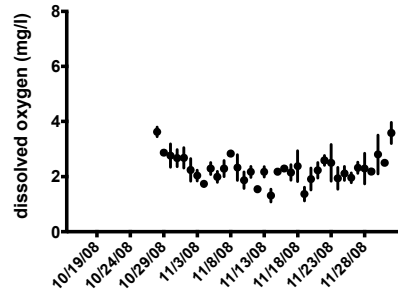


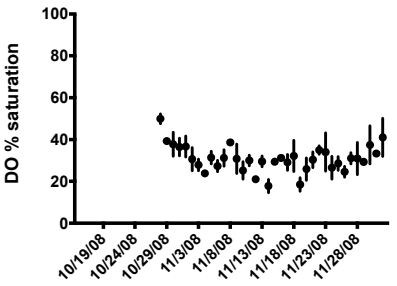


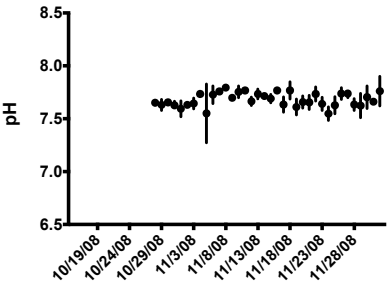

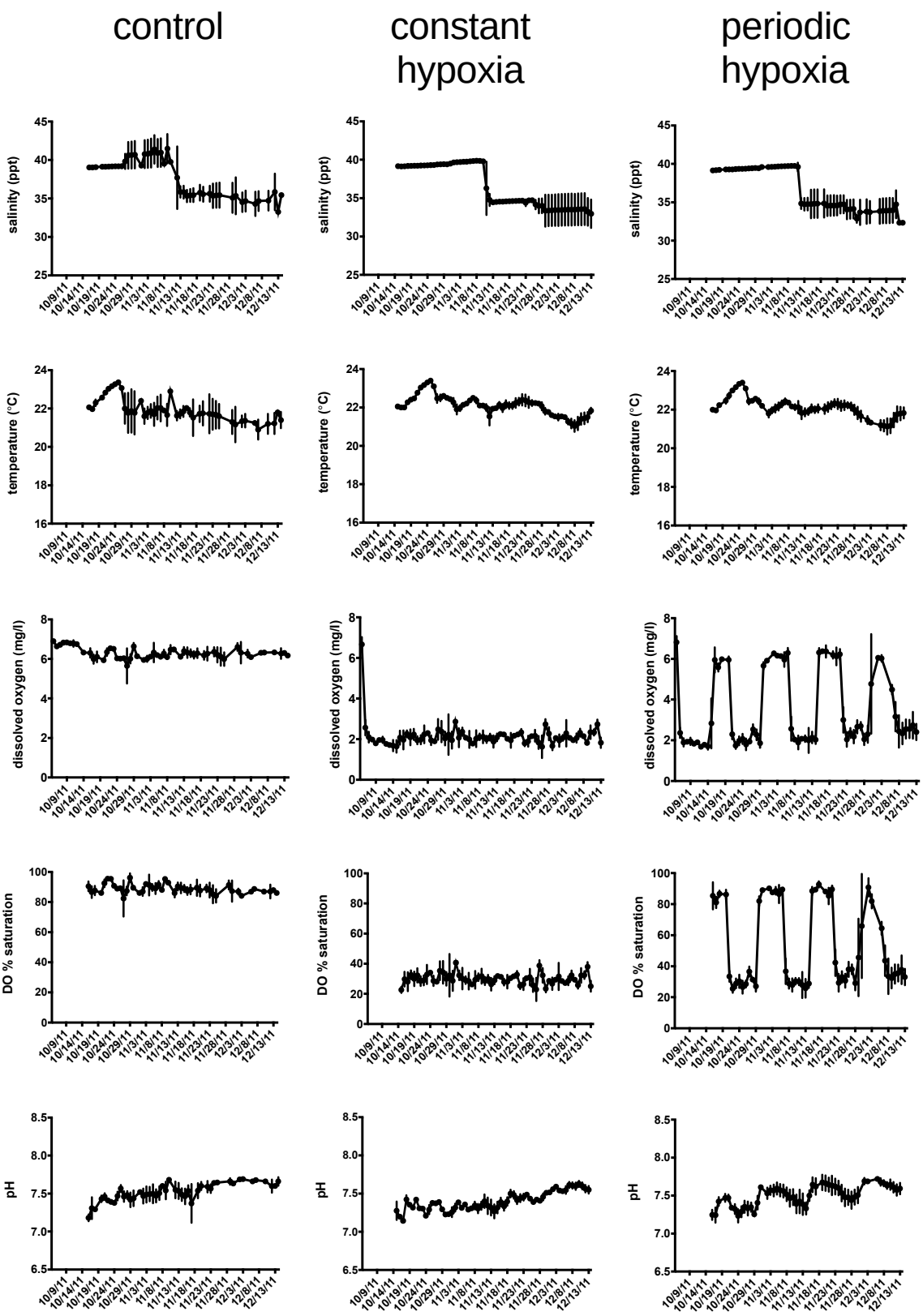
control
constant hypoxia
periodic hypoxia
salinity (ppt)
temperature (°C)
dissolved oxygen (mg/l)
DO % saturation
pH
10/9/11
10/14/11
10/19/11
10/24/11
10/29/11
11/3/11
11/8/11
11/13/11
11/18/11
11/23/11
11/28/11
12/3/11
12/8/11
12/13/11

**Figure A.1** Physiochemical parameters of experimental tanks measured daily during the 4 week and 10-week study. Mean values of 3 replicate tanks are presented, with error bars indicating standard deviation.

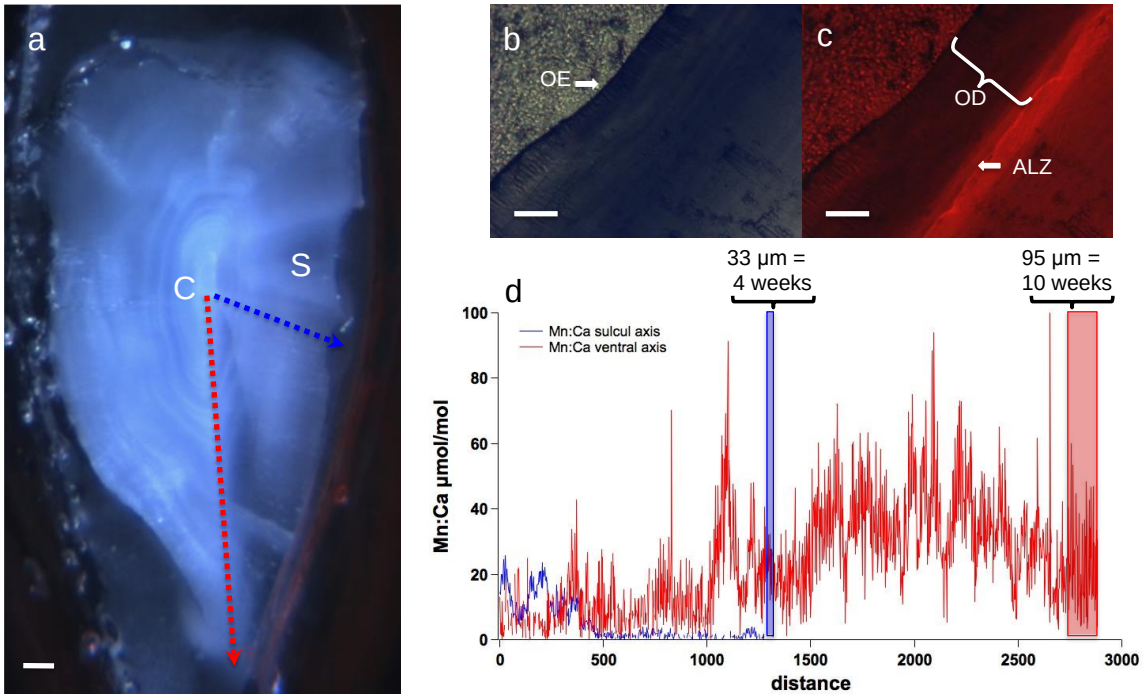


**Figure A.2** a) Transverse left sagittal otolith section depicting the core (C) and sulcal groove (S) with dashed blue line showing laser path along sulcal axis used in 4-week study and red dashed line laser path along ventral axis used in 10-week study; scale bar=300µm; b) digital image of an alizarin stained otolith under transmitted light showing the otolith edge (OE); c) same otolith in (b) under fluorescent light showing alizarin (ALZ) stain used to estimate the otolith distance (OD) of material precipitated during the 4-week or 10-week study; scale bar=15 µm; d) representative laser transect plot from core to edge showing Mn:Ca data collected along the sucal axis (blue line) or ventral axis (red line) with shaded boxes showing the otolith material representing the 4-week (33µm) and 10-week (95µm) experiments.

**Table A.1** Fish mass, total length (TL) at day 1 (beginning of study), day 29 (to estimate 4-week otolith precipitation), and day 70 (to estimate 10-week otolith precipitation). After being held for 24 hours in Alizarin red solution, fish were tagged with anchor tags (tag ID) to track individual growth. Otoliths were first weighed (in mg) and measured in width (mm), then embedded, sectioned, and polished to the core and viewed with fluorescent light to measure the distance from Alizarin stain to otolith edge (mean otolith width growth). Note that all fish lost weight (6-14 %) during the study due to low feeding and low densities, resulting in conservative estimates of otolith precipitation.

| tag ID | otolith | mean otolith growth (µm) | known age (days) | daily otolith precipitation (µm) | TL at day 1 (mm) | fish mass at day 1 (g) | TL at day 29 (mm) | fish mass at day 29 (g) | TL at day 71 (mm) | fish mass at day 71 (g) | final otolith mass (mg) | final otolith width (mm) | % body wt loss | K factor |
|---|---|---|---|---|---|---|---|---|---|---|---|---|---|---|
| NTG | left | 39.61 | 29 | 0.732 | 156 | 47.08 | 156 | 43.9 | | | 125 | 7.65 | 6.75 | 1.156 |
| | right | 36.11 | 29 | 0.803 | 156 | 47.08 | 156 | 43.9 | | | 126 | 7.66 | 6.75 | 1.156 |
| ORN | left | 29.34 | 29 | 0.988 | 147 | 37.46 | 147 | 33.2 | | | 98 | 7.29 | 11.37 | 1.045 |
| | right | 27.13 | 29 | 1.069 | 147 | 37.46 | 147 | 33.2 | | | 100 | 7.32 | 11.37 | 1.045 |
| BLU | left | 58.47 | 70 | 1.197 | 153 | 40.22 | 151 | 36.8 | 153 | 37.5 | 116 | 7.58 | 6.76 | 1.047 |
| | right | 77.82 | 70 | 0.900 | 153 | 40.22 | 151 | 36.8 | 153 | 37.5 | 116 | 7.54 | 6.76 | 1.047 |
| RED | left | 82.81 | 70 | 0.845 | 160 | 47.01 | 157 | 42.9 | 159 | 40.3 | 134 | 7.91 | 14.27 | 1.003 |
| | right | 86.30 | 70 | 0.811 | 160 | 47.01 | 157 | 42.9 | 159 | 40.3 | 135 | 7.87 | 14.27 | 1.003 |

# APPENDIX B

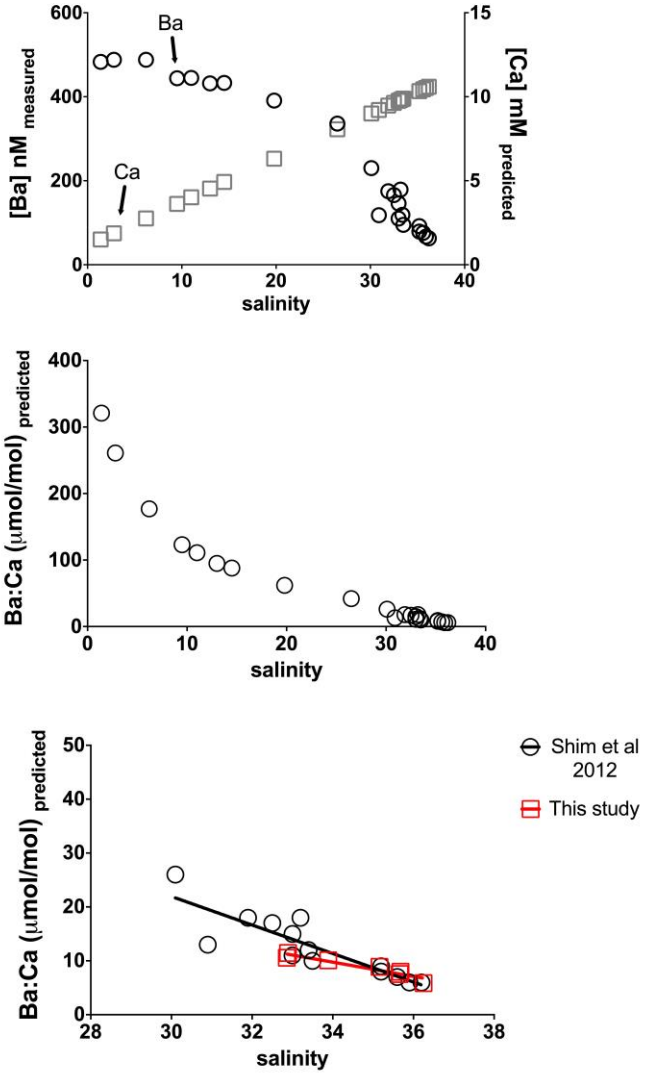


**Figure B.1** Predicted mixing curve for dissolved Ba:Ca in Mississippi River based on data adapted from Shim et al. (2012) and Cai (2003). Dissolved [Ba] (top panel) across salinity gradient in Miss. R.; dissolved [Ca] estimated using salinity and equation: [Ca2+ ] μM= 261.3* S + 1138.7 adapted from Cai 2003. Predicted dissolved Ba:Ca mixing curves (mid panel). Comparison of Ba:Ca-salinity relationship (bottom panel) exhibited in this study and Shim et al. (2012).

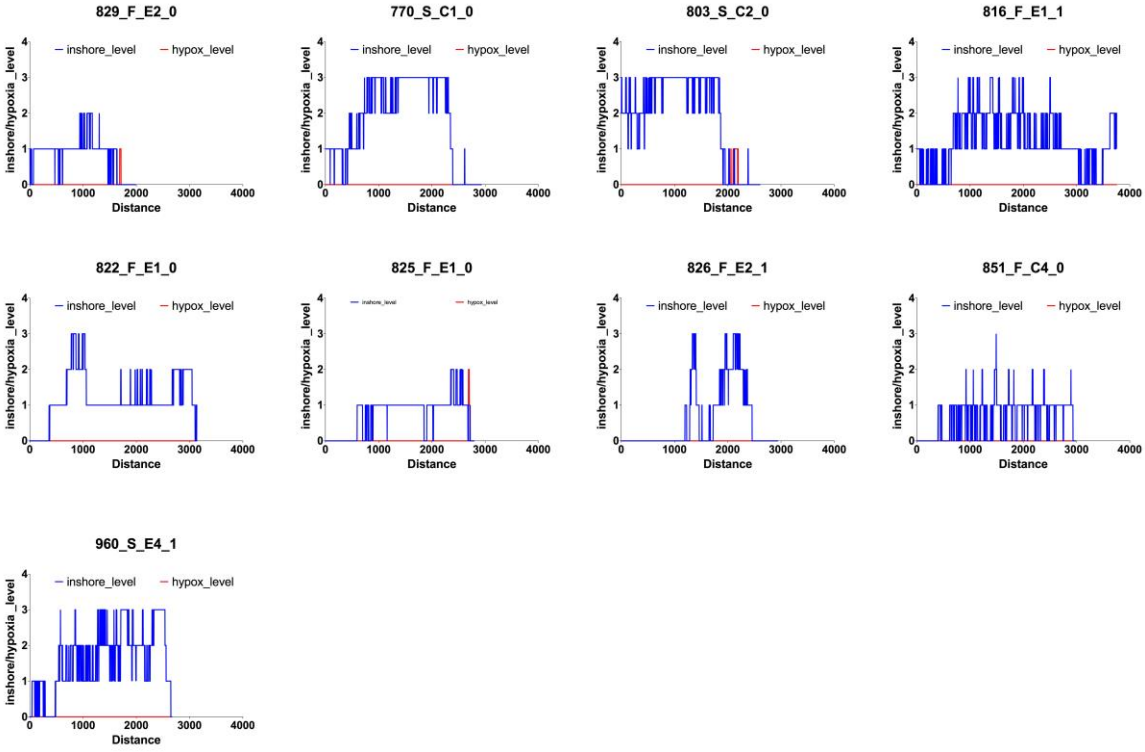


**Figure B.2** Threshold plots for all fish clustered in **Group A.**

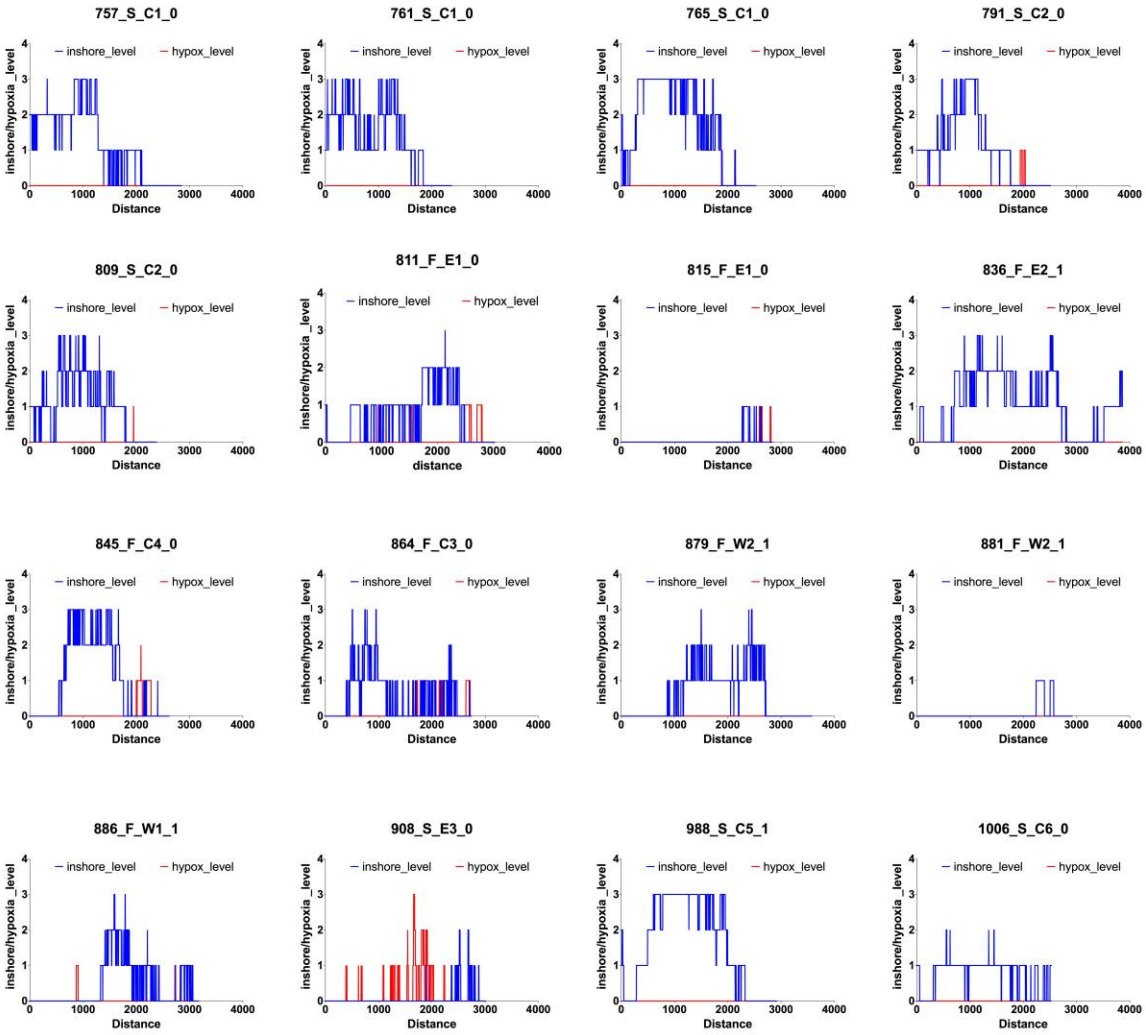


**Figure B.3** Threshold plots for all fish clustered in **Group B.**

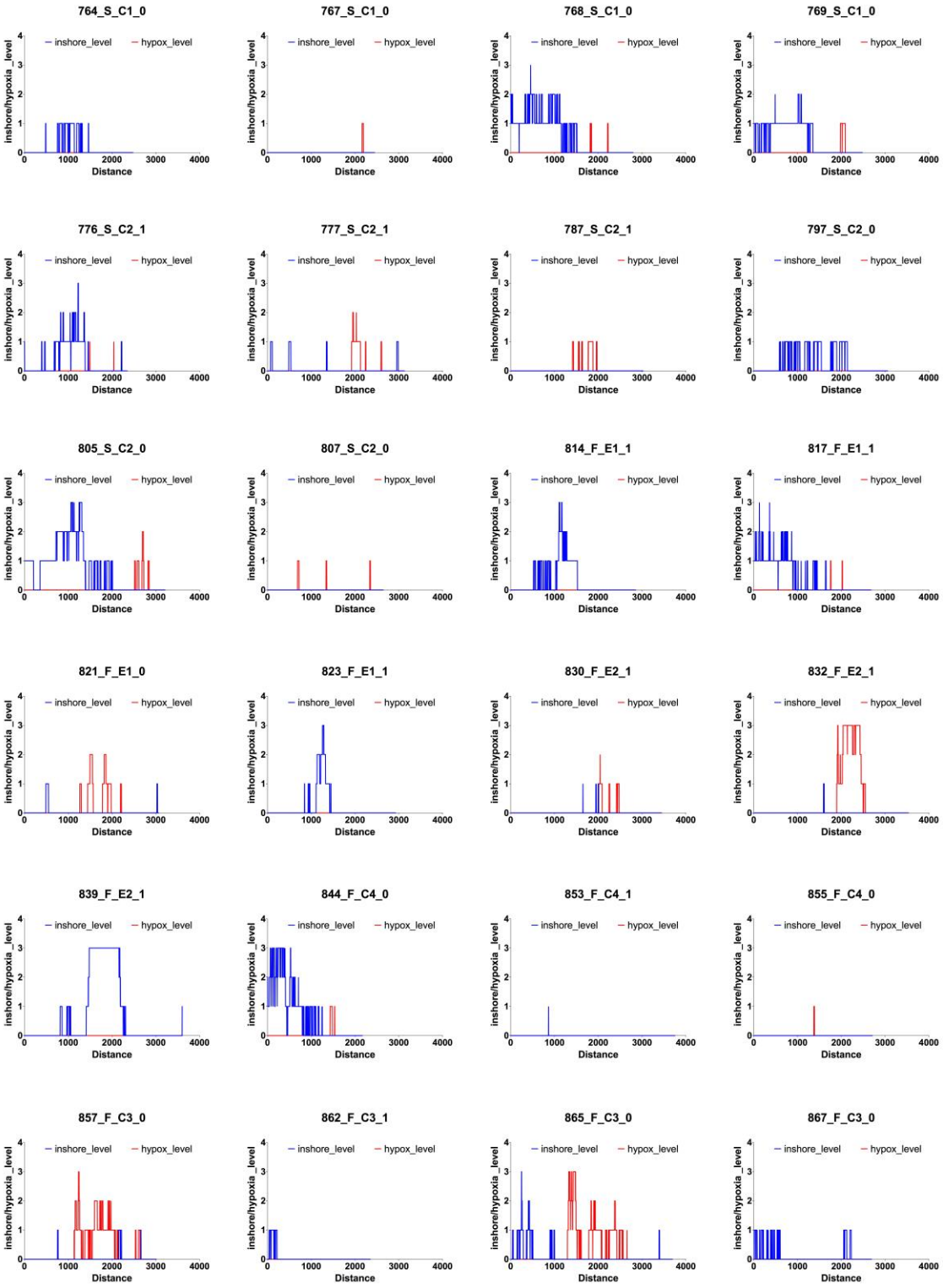


**Figure B.4.a** Threshold plots for all fish clustered in **Group C.**

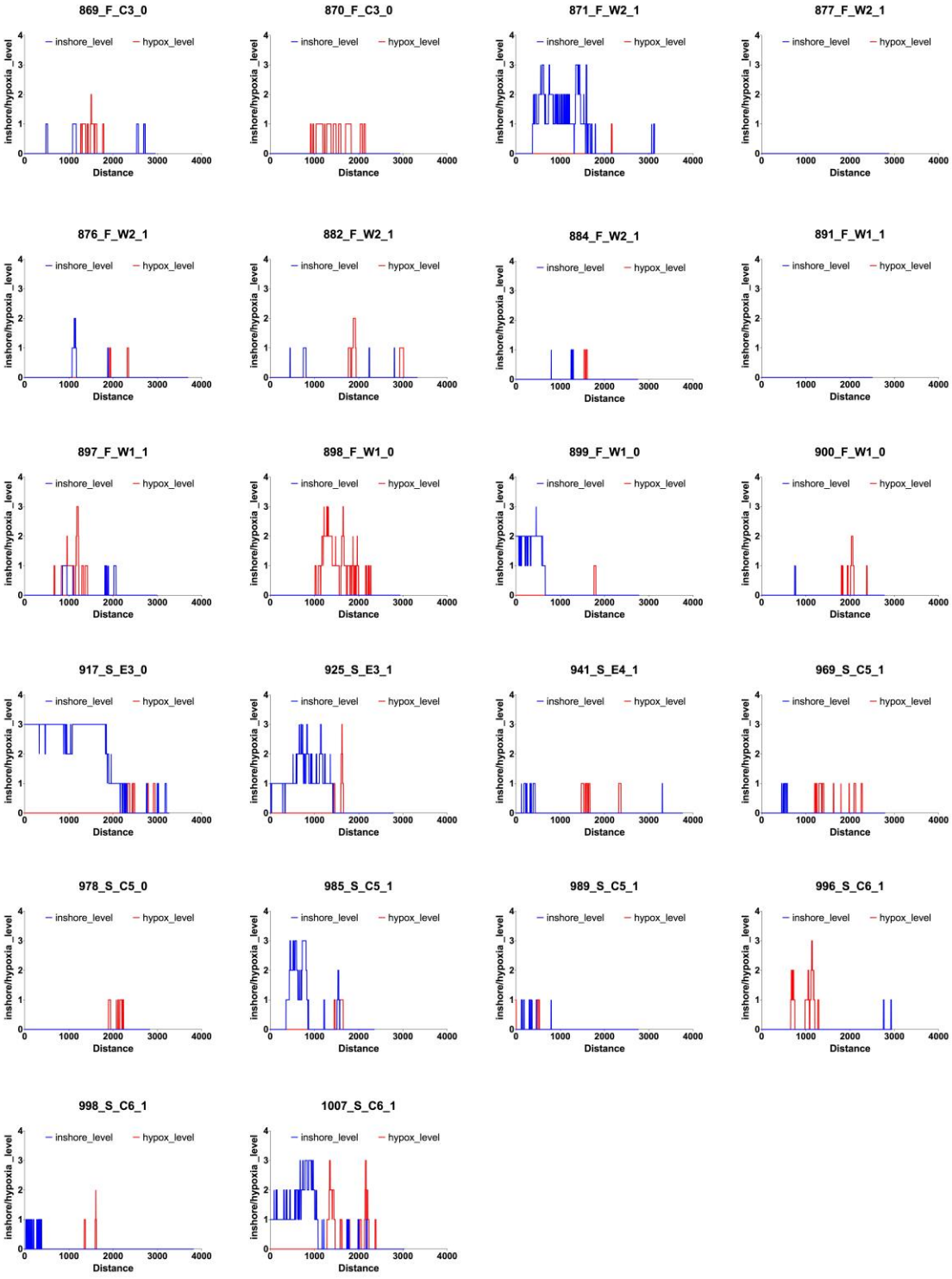


**Figure B.5.b** Threshold plots for all fish clustered in **Group C cont.**

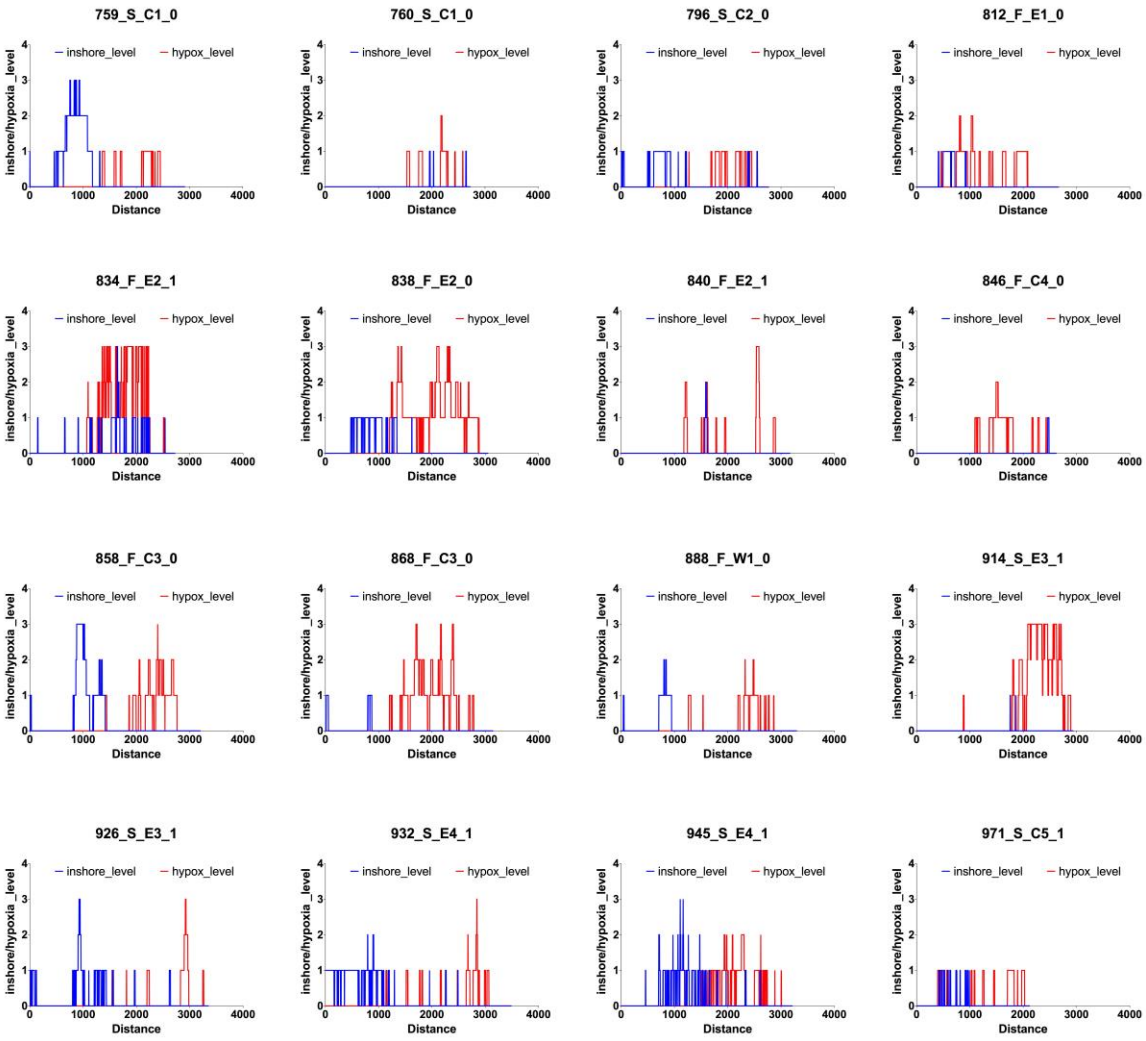


**Figure B.6** Threshold plots for all fish clustered in **Group D.**

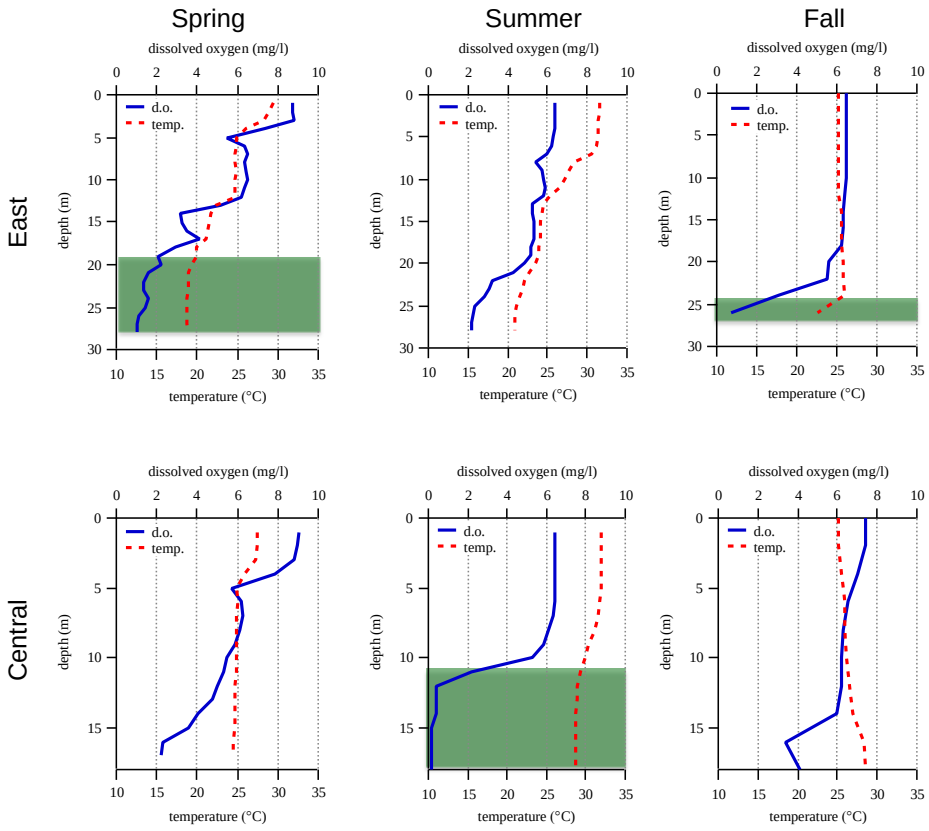


**Figure B.7** Depth profiles of DO and temperature from 2010 cruise demonstrating hypoxia occurring in eastern sites (relevant for strong hypoxic signals occurring in eastern sites in fall 2011 fish).

# REFERENCES


Able KW (2005) A re-examination of fish estuarine dependence: Evidence for connectivity between estuarine and ocean habitats. Estuar Coast Shelf Sci 64:5–17. doi: 10.1016/j.ecss.2005.02.002

Adams TS, Sterner RW (2000) The effect of dietary nitrogen content on trophic level $^{15}N$ enrichment. Limnol Oceanogr 45:601–607. doi: 10.4319/lo.2000.45.3.0601

Alteri AH, Gedan KB (2015) Climate change and dead zones. Glob Chang Biol 21:1395–1406. doi: 10.1111/gcb.12754

Atkinson CA, Jolley DF, Simpson SL (2007) Effect of overlying water pH, dissolved oxygen, salinity and sediment disturbances on metal release and sequestration from metal contaminated marine sediments. Chemosphere 69:1428–37. doi: 10.1016/j.chemosphere.2007.04.068

Baden SP, Eriksson SP, Gerhardt L (1999) Accumulation and elimination kinetics of manganese from different tissues of the Norway lobster *Nephrops norvegicus* (L.). Aquat Toxicol 46:127–137. doi: 10.1016/S0166-445X(98)00123-4

Baden SP, Eriksson SP, Weeks JM (1995) Uptake, accumulation and regulation of manganese during experimental hypoxia and normoxia by the decapod *Nephrops norvegicus* (L.). Mar Pollut Bull 31:93–102. doi: 10.1016/0025-326X(94)00257-A

Baden SP, Neil DM (2003) Manganese accumulation by the antennule of the Norway lobster *Nephrops norvegicus* (L.) as a biomarker of hypoxic events. Mar Environ Res 55:59–71. doi: 10.1016/S0141-1136(02)00216-7

Barnes C, Sweeting CJ, Jennings S, et al. (2007) Effect of temperature and ration size on carbon and nitrogen stable isotope trophic fractionation. Funct Ecol 21:356–362. doi: 10.1111/j.1365-2435.2006.01224.x

Bath G, Thorrold SR, Jones CM, et al. (2000) Strontium and barium uptake in aragonitic otoliths of marine fish. Geochim Cosmochim Acta 64:1705–1714.

Baustian MM, Craig JK, Rabalais NN (2009) Effects of summer 2003 hypoxia on macrobenthos and Atlantic croaker foraging selectivity in the northern Gulf of Mexico. J Exp Mar Bio Ecol 381:S31–S37. doi: 10.1016/j.jembe.2009.07.007

Beck M, Heck K, Able K, et al. (2001) The identification, conservation, and management of estuarine and marine nurseries for fish and invertebrates. Bioscience 51:633–641.

Benoit G, Oktay-Marshall S, Cantu II A, et al. (1994) Partitioning of Cu, Pb, Ag, Zn, Fe, Al, and Mn between filter-retained particles, colloids, and solution in six Texas estuaries. Mar Chem 45:307–336.

Bianchi TS, DiMarco SF, Cowan JH, et al. (2010) The science of hypoxia in the Northern Gulf of Mexico: a review. Sci Total Environ 408:1471–1484. doi: 10.1016/j.scitotenv.2009.11.047

Bianchi TS, Mitra S, McKee BA (2002) Sources of terrestrially-derived organic carbon in lower Mississippi River and Louisiana shelf sediments: Implications for differential sedimentation and transport at the coastal margin. Mar Chem 77:211–223. doi: 10.1016/S0304-4203(01)00088-3

Bickler PE, Buck LT (2007) Hypoxia tolerance in reptiles, amphibians, and fishes: life with variable oxygen availability. Annu Rev Physiol 69:145–70. doi: 10.1146/annurev.physiol.69.031905.162529

Bishop KA (2012) Freshwater contributions and nitrogen sources in a South Texas estuarine ecosystem: a time-integrated story from stable isotope ratios in the eastern oyster (*Crassostrea virginica*). MS Thesis, Unveristy of Texas

Bloomfield AL, Elsdon TS, Walther BD, et al. (2011) Temperature and diet affect carbon and nitrogen isotopes of fish muscle: Can amino acid nitrogen isotopes explain effects? J Exp Mar Bio Ecol 399:48–59. doi: 10.1016/j.jembe.2011.01.015

Boecklen WJ, Yarnes CT, Cook BA, James AC (2011) On the use of stable isotopes in trophic ecology. Annu Rev Ecol Evol Syst 42:411–440. doi: 10.1146/annurev-ecolsys-102209-144726

Brady D, Targett T (2013) Movement of juvenile weakfish *Cynoscion regalis* and spot *Leiostomus xanthurus* in relation to diel-cycling hypoxia in an estuarine tidal tributary. Mar Ecol Prog Ser 491:199–219. doi: 10.3354/meps10466

Brandt SB, Gerken M, Hartman KJ, Demers E (2009) Effects of hypoxia on food consumption and growth of juvenile striped bass (*Morone saxatilis*). J Exp Mar Bio Ecol 381:S143–S149. doi: 10.1016/j.jembe.2009.07.028

Breitburg DL, Hondorp DW, Davias LA, Diaz RJ (2009) Hypoxia, nitrogen, and fisheries: integrating effects across local and global landscapes. Ann Rev Mar Sci 1:329–349. doi: 10.1146/annurev.marine.010908.163754

Brown DT, Aday DD, Rice JA (2015) Responses of coastal Largemouth bass to episodic hypoxia. Trans Am Fish Soc 144:655–666. doi: 10.1080/00028487.2015.1024801

Buchheister A, Latour RJ (2010) Turnover and fractionation of carbon and nitrogen stable isotopes in tissues of a migratory coastal predator, summer flounder (*Paralichthys dentatus*). Can J Fish Aquat Sci 67:445–461. doi: 10.1139/F09-196

Burke JS, Peters DS, Hanson PJ (1993) Morphological indices and otolith microstructure of Atlantic croaker, *Micropogonias undulatus*, as indicators of habitat quality along an estuarine pollution gradient. Environ Biol Fishes 36:25–33.

Cai WJ (2003) Riverine inorganic carbon flux and rate of biological uptake in the Mississippi River plume. Geophys Res Lett 30:1032. doi: 10.1029/2002GL016312

Campana SE (1983) Calcium deposition and otolith check formation during periods of stress in coho salmon, *Oncorhynchus kisutch*. Comp Biochem Physiol Part A Physiol 75A:215–220.

Campana SE (1999) Chemistry and composition of fish otoliths: pathways, mechanisms and applications. Mar Ecol Prog Ser 188:263–297.

Caut S, Angulo E, Courchamp F (2009) Variation in discrimination factors (Δ 15 N and Δ 13 C): the effect of diet isotopic values and applications for diet reconstruction. J Appl Ecol 46:443–453. doi: 10.1111/j.1365-2664.2009.01620.x

Chan F, Barth J, Lubchenco J, et al. (2008) Emergence of anoxia in the California current large marine ecosystem. Science 319:920. doi: 10.1126/science.1149016

Coffey M, Dehairs F, Collette O, et al. (1997) The behaviour of dissolved barium in estuaries. Estuar Coast Shelf Sci 45:113–121.

Connolly RM, Hindell JS, Gorman D (2005) Seagrass and epiphytic algae support nutrition of a fisheries species, *Sillago schomburgkii*, in adjacent intertidal habitats. Mar Ecol Prog Ser 286:69–79. doi: 10.3354/meps286069

Cooper LW, Whitledge TE, Grebmeier J, Weingartner T (1997) The nutrient, salinity, and stable oxygen isotope composition of Bering and Chukchi Seas waters in and near the Bering Strait. J Geophys Res 102:12563–12573.

Coutant CC (1985) Striped bass, temperature, and dissolved oxygen: a speculative hypothesis for environmental risk. Trans Am Fish Soc 21:31–61.

Craig JK (2012) Aggregation on the edge: effects of hypoxia avoidance on the spatial distribution of brown shrimp and demersal fishes in the Northern Gulf of Mexico. Mar Ecol Prog Ser 445:75–95. doi: 10.3354/meps09437

Craig JK, Crowder LB (2005) Hypoxia-induced habitat shifts and energetic consequences in Atlantic croaker and brown shrimp on the Gulf of Mexico shelf. Mar Ecol Prog Ser 294:79–94.

Creekmore SB (2011) Modeling the population effects of hypoxia on Atlantic croaker (*Micropogonias undulatus*) in the northwestern Gulf of Mexico. MS Thesis, Louisiana State University

Davis DA, Arnold CR (1997) Response of Atlantic coraker fingerlings to practical diet formulations with varying protein and energy contents. J. World Aquac. Soc.

DeNiro M, Epstein S (1981) Influence of diet on the distribution of nitrogen isotopes in animals. Geochim Cosmochim Acta 45:341–351. doi: 10.1016/0016-7037(81)90244-1

DeNiro M, Epstein S (1977) Mechanism of carbon isotope fractionation associated with lipid synthesis. Science 197:261–263.

Diaz RJ, Rosenberg R (2008) Spreading dead zones and consequences for marine ecosystems. Science 321:926–9. doi: 10.1126/science.1156401

Diaz RJ, Rosenberg R (1995) Marine benthic hypoxia: A review of its ecological effects and the behavioural responses of benthic macrofauna. Oceanogr Mar Biol an Annu Rev 33:245–303.

Dierking J, Morat F, Letourneur Y, Harmelin-Vivien M (2012) Fingerprints of lagoonal life: Migration of the marine flatfish *Solea solea* assessed by stable isotopes and otolith microchemistry. Estuar Coast Shelf Sci 104-105:23–32. doi: 10.1016/j.ecss.2011.03.018

Diouf K, Panfili J, Labonne M, et al. (2006) Effects of salinity on stronitum:calcium ratios in the otoliths of the West African black-chinned tilapia *Sarotherodon melanotheron* in a hypersaline estuary. Environ Biol Fishes 77:9–20. doi: 10.1007/s10641-006-9048-x

Dorval E, Jones CM, Hannigan R (2005) Chemistry of surface waters: Distinguishing fine-scale differences in sea grass habitats of Chesapeake Bay. Limnol Oceanogr 50:1073–1083. doi: 10.4319/lo.2005.50.4.1073

Dorval E, Jones CM, Hannigan R, Montfrans J Van (2007) Relating otolith chemistry to surface water chemistry in a coastal plain estuary. Can J Fish Aquat Sci 424:411–424. doi: 10.1139/F07-015

Duan S, Bianchi TS, Sampere TP (2007) Temporal variability in the composition and abundance of terrestrially-derived dissolved organic matter in the lower Mississippi and Pearl Rivers. Mar Chem 103:172–184. doi: 10.1016/j.marchem.2006.07.003

Eby LA, Crowder LB, McClellan CM, et al. (2005) Habitat degradation from intermittent hypoxia: impacts on demersal fishes. Mar Ecol Prog Ser 291:249–261.

Elsdon T, Ayvazian S, Mcmahon K, Thorrold S (2010) Experimental evaluation of stable isotope fractionation in fish muscle and otoliths. Mar Ecol Prog Ser 408:195–205. doi: 10.3354/meps08518

Elsdon TS, Gillanders BM (2006) Temporal variability in strontium, calcium, barium, and manganese in estuaries: Implications for reconstructing environmental histories of fish from chemicals in calcified structures. Estuar Coast Shelf Sci 66:147–156. doi: 10.1016/j.ecss.2005.08.004

Elsdon TS, Gillanders BM (2003) Relationship between water and otolith elemental concentrations in juvenile black bream *Acanthopagrus butcheri*. Mar Ecol Prog Ser 260:263–272.

Elsdon TS, Gillanders BM (2002) Interactive effects of temperature and salinity on otolith chemistry: challenges for determining environmental histories of fish. Can J Fish Aquat Sci 1808:1796–1808. doi: 10.1139/F02-154

Elsdon TS, Gillanders BM (2005) Alternative life-history patterns of estuarine fish : barium in otoliths elucidates freshwater residency. Can J Fish Aquat Sci 1152:1143–1152. doi: 10.1139/F05-029

Elsdon TS, Gillanders BM (2004) Fish otolith chemistry influenced by exposure to multiple environmental variables. J Exp Mar Bio Ecol 313:269–284. doi: 10.1016/j.jembe.2004.08.010

Elsdon TS, Wells BK, Campana SE, et al. (2008) Otolith chemistry to describe movements and life-history parameters of fishes: Hypotheses, assumptions, limitations and inferences. Oceanogr Mar Biol an Annu Rev Vol 46 46:297.

Erhardt AM, Reimers CE, Kadko D, Paytan A (2014) Records of trace metals in sediments from the Oregon shelf and slope: Investigating the occurrence of hypoxia over the past several thousand years. Chem Geol 382:32–43. doi: 10.1016/j.chemgeo.2014.05.029

Falk-Petersen S, Pavlov V, Timofeev S, Sargent J (2007) Climate variability and possible effects on arctic food chains: The role of Calanus. In: Ørbaek J, Kallenborn R,

Hegseth E, et al. (eds) Arct. Alp. Ecosyst. people a Chang. Environ. Springer, pp 147–166

Flint RW (1985) Long-term estuarine variability and associated biological response. Estuaries 8:158–169.

Fodrie FJ, Herzka SZ (2013) A comparison of otolith geochemistry and stable isotope markers to track fish movement: describing estuarine ingress by larval and post-larval halibut. Estuaries and Coasts. doi: 10.1007/s12237-013-9612-5

Forrester GE (2005) A field experiment testing for correspondence between trace elements in otoliths and the environment and for evidence of adaptation to prior habitats. Estuaries 28:974–981.

France RL (1995) Differentiation between littoral and pelagic food webs in lakes using stable carbon isotopes. Limnol Oceanogr 40:1310–1313.

Froeschke JT, Stunz GW (2011) Hierarchical and interactive habitat selection in response to abiotic and biotic factors: The effect of hypoxia on habitat selection of juvenile estuarine fishes. Environ Biol Fishes 93:31–41. doi: 10.1007/s10641-011-9887-y

Fry B (2002) Conservative mixing of stable isotopes across estuarine salinity gradients: A conceptual framework for monitoring watershed influences on downstream fisheries production. Estuaries 25:264–271.

Fry B (1983) Fish and shrimp migrations in the Northern Gulf of Mexico analyzed using stable C, N, and S isotope ratios. Fish Bull 81:789–801.

Fry B, Anderson R, Entzeroth L, et al. (1984) $^{13}C$ enrichment and oceanic food web structure in the Northwestern Gulf of Mexcio. Contrib in Mar Sci 27:49–63.

Fry B, Arnold C (1982) Rapid $^{13}C/^{12}C$ turnover during growth of brown shrimp (*Penaeus aztecus*). Oecologia 54:200–204.

Fry B, Baltz DM, Benfield MC, et al. (2003) Stable isotope indicators of movement and residency for brown shrimp (*Farfantepenaeus aztecus)* in coastal Louisiana marshscapes. Estuaries 26:82–97. doi: 10.1007/BF02691696

Fry B, Scalan RS, Parker PL (1977) Stable carbon isotope evidence for two sources of organic matter in coastal sediments: seagrasses and plankton. Geochim Cosmochim Acta 41:1875–1877. doi: 10.1016/0016-7037(77)90218-6

Gaetani GA., Cohen AL (2006) Element partitioning during precipitation of aragonite from seawater: A framework for understanding paleoproxies. Geochim Cosmochim Acta 70:4617–4634. doi: 10.1016/j.gca.2006.07.008

Gillanders BM, Munro AR (2012) Hypersaline waters pose new challenges for reconstructing environmental histories of fish based on otolith chemistry. Limnol Oceanogr 57:1136–1148. doi: 10.4319/lo.2012.57.4.1136

Graham BS, Kock PL, Newsome SD, et al. (2010) Using isoscapes to trace the movements and foraging behavior of top predators in oceanic ecosystems. In: West JB, Bowen GJ, Dawson TE, Tu KP (eds) Isoscapes. Springer, pp 299–318

Grantham BA, Chan F, Nielsen KJ, et al. (2004) Upwelling-driven nearshore hypoxia signals ecosystem and oceanographic changes in the northeast Pacific. Nature 429:749–754. doi: 10.1038/nature02605

Greene CM, Blackhart K, Nohner J, et al. (2015) A national assessment of stressors to estuarine fish habitats in the contiguous USA. Estuaries and Coasts 38:782–799. doi: 10.1007/s12237-014-9855-9

Guelinckx J, Maes J, Driessche P Van Den, et al. (2007) Changes in $\delta^{13}C$ and $\delta^{15}N$ in different tissues of juvenile sand goby *Pomatoschistus minutus*: a laboratory diet-switch experiment. Mar Ecol Prog Ser 341:205–215.

Hanor J, Chan L (1977) Non-conservative behavior of barium during mixing of Mississippi River and Gulf of Mexico waters. Earth Planet Sci Lett 37:242–250.

Hazen EL, Craig JK, Good CP, Crowder LB (2009) Vertical distribution of fish biomass in hypoxic waters on the Gulf of Mexico shelf. Mar Ecol Prog Ser 375:195–207. doi: 10.3354/meps07791

Head P (1985) Practical estuarine chemistry: a handbook. Cambridge University Press

Herzka S (2005) Assessing connectivity of estuarine fishes based on stable isotope ratio analysis. Estuar Coast Shelf Sci 64:58–69. doi: 10.1016/j.ecss.2005.02.006

Herzka SZ, Holt SA, Holt GJ (2002) Characterization of settlement patterns of red drum Sciaenops ocellatus larvae to estuarine nursery habitat: a stable isotope approach. Mar Ecol Prog Ser 226:143–156.

Hesslein R, Hallard K, Ramlal P (1993) Replacement of sulfur, carbon, and nitrogen in tissue of growing broad whitefish (*Coregonus nasus*) in response to a change in diet traced by $\delta^{34}S$, $\delta^{13}C$, and $\delta^{15}N$. Can J Fish Aquat Sci 50:2071–2076.

Hobson KA, Barnett-Johnson R, Cerling T (2010) Using isoscapes to track animal migration. In: West JB, Bowen GJ, Dawson TE, Tu KP (eds) Isoscapes. Springer, pp 273–298.

Hobson KA, Clark RG (1992) Assessing avian diets using stable isotopes I: turnover of $^{13}C$ in tissues. Condor 94:181–188.

Hochachka PW, Buck LT, Doll CJ, Land SC (1996) Unifying theory of hypoxia tolerance: molecular/metabolic defense and rescue mechanisms for surviving oxygen lack. Proc Natl Acad Sci U S A 93:9493–8.

Holl CM, Villareal TA, Payne CD, et al. (2007) Trichodesmium in the western Gulf of Mexico : $^{15}N_2$-fixation and natural stable isotope evidence. Limnol Oceanogr 52:2249–2259.

Hoover RR, Jones CM, Grosch CE, Gillanders BM (2012) Estuarine ingress timing as revealed by spectral analysis of otolith life history scans. Can J Fish Aquat Sci 69:1266–1277. doi: 10.1139/f2012-058

Ingram BL, Conrad ME, Ingle JC (1996) Stable isotope and salinity systematics in estuarine waters and carbonates: San Francisco Bay. Geochim Cosmochim Acta 60:455–467. doi: 10.1016/0016-7037(95)00398-3

Izzo C, Doubleday ZA, Schultz AG, et al. (2015) Contribution of water chemistry and fish condition to otolith chemistry: comparisons across salinity environments. J Fish Biol 86:1680–1698. doi: 10.1111/jfb.12672

Jackson AL, Inger R, Parnell AC, Bearhop S (2011) Comparing isotopic niche widths among and within communities: SIBER - Stable Isotope Bayesian Ellipses in R. J Anim Ecol 80:595–602. doi: 10.1111/j.1365-2656.2011.01806.x

Johnson GD (1978) Development of fishes of the mid-Atlantic bight: an atlas of egg, larval and juvenile stages. Vol IV Carangidae through Ephippidae. Fish and Wildlife Service, US Department of the Interior

Joung D, Shiller AM (2013) Trace element distributions in the water column near the Deepwater Horizon well blowout. Environ Sci Technol 47:21612168. doi: 10.1021/es303167p

Joung D, Shiller AM (2014) Dissolved barium behavior in Louisiana Shelf waters affected by the Mississippi/Atchafalaya River mixing zone. Geochim Cosmochim Acta 141:303–313. doi: 10.1016/j.gca.2014.06.021

Kainz M, Fisk A (2009) Integrating lipids and contaminants in aquatic ecology and ecotoxicology. In: Arts M, Brett M, Kainz M (eds) Lipids Aquat. Ecosyst. Springer, New York, New York, pp 93–114

Kalish JM (1991) Determinants of otolith chemistry: seasonal variation in the composition of blood plasma, endolymph and otoliths of bearded rock cod *Pseudophycis barbatus.* Mar Ecol Prog Ser 74:137–159.

Kalish JM (1992) Formation of a stress-induced chemical check in fish otoliths. J Exp Mar Bio Ecol 162:265–277. doi: 10.1016/0022-0981(92)90206-P

Klinkhammer GP, McManus J (2001) Dissolved manganese in the Columbia River estuary: Production in the water column. Geochim Cosmochim Acta 65:2835–2841.

Knudsen E, Herke W (1978) Growth rate of marked juvenile Atlantic Croakers, *Micropogonias undulatus*, and length of stay in a coastal marsh nursery in southwest Louisiana. Trans Am Fish Soc 107:12–20.

Kodama K, Rahman MS, Horiguchi T, Thomas P (2012) Assessment of hypoxia-inducible factor-1α mRNA expression in mantis shrimp as a biomarker of environmental hypoxia exposure. Biol Lett 8:278–81. doi: 10.1098/rsbl.2011.0887

Kowalski N, Dellwig O, Beck M, et al. (2012) A comparative study of manganese dynamics in the water column and sediments of intertidal systems of the North Sea. Estuar Coast Shelf Sci 100:3–17. doi: 10.1016/j.ecss.2011.03.011

Kraus RT, Secor DH (2004) Incorporation of strontium into otoliths of an estuarine fish. J Exp Mar Bio Ecol 302:85–106. doi: 10.1016/j.jembe.2003.10.004

Layman C a., Quattrochi JP, Peyer CM, Allgeier JE (2007a) Niche width collapse in a resilient top predator following ecosystem fragmentation. Ecol Lett 10:937–944. doi: 10.1111/j.1461-0248.2007.01087.x

Layman CA, Arrington DA, Montana CG, Post DM (2007b) Can stable isotope ratios provide for community-wide measures of trophic structure? Ecology 88:42–48.

Lewis BL, Luther GW (2000) Processes controlling the distribution and cycling of manganese in the oxygen minimum zone of the Arabian Sea. Deep Res Part II Top Stud Oceanogr 47:1541–1561. doi: 10.1016/S0967-0645(99)00153-8

Limburg KE (1998) Anomalous migrations of anadromous herrings revealed with natural chemical tracers. Can J Fish Aquat Sci 55:431–437. doi: 10.1139/f97-219

Limburg KE, Olson C, Walther Y, et al. (2011) Tracking Baltic hypoxia and cod migration over millennia with natural tags. Proc Natl Acad Sci 108:E177–82. doi: 10.1073/pnas.1100684108

Limburg KE, Walther BD, Lu Z, et al. (2014) In search of the dead zone: Use of otoliths for tracking fish exposure to hypoxia. J Mar Syst 1–12. doi: 10.1016/j.jmarsys.2014.02.014

Litzow M, Bailey K, Prahl F, Heintz R (2006) Climate regime shifts and reorganization of fish communities: the essential fatty acid limitation hypothesis. Mar Ecol Prog Ser 315:1–11. doi: 10.3354/meps315001

Logan J, Haas H, Deegan L, Gaines E (2006) Turnover rates of nitrogen stable isotopes in the salt marsh mummichog, *Fundulus heteroclitus*, following a laboratory diet switch. Oecologia 147:391–395.

Logan JM, Jardine TD, Miller TJ, et al. (2008) Lipid corrections in carbon and nitrogen stable isotope analyses : comparison of chemical extraction and modelling methods. J Anim Ecol 77:838–46. doi: 10.1111/j.1365-2656.2008.01394.x

Long WC, Seitz RD (2008) Trophic interactions under stress: hypoxia enhances foraging in an estuarine food web. Mar Ecol Prog Ser 362:59–68. doi: 10.3354/meps07395

Macko S, Entzeroth L, Parker P (1984) Regional differences in nitrogen and carbon isotopes on the continental shelf of the Gulf of Mexico. Naturwissenschaften 991:8–9.

MacNeil MA, Drouillard KG, Fisk AT (2006) Variable uptake and elimination of stable nitrogen isotopes between tissues in fish. Can J Fish Aquat Sci 63:345–353. doi: 10.1139/f05-219

Madigan DJ, Litvin SY, Popp BN, et al. (2012) Tissue turnover rates and isotopic trophic discrimination factors in the endothermic teleost, Pacific Bluefin Tuna (*Thunnus orientalis*). PLoS One 7:1–13. doi: 10.1371/journal.pone.0049220

Maillet GL, Checkley DM (1990) Effects of starvation on the frequency of formation and width of growth increments in sagittae of laboratory-reared Atlantic menhaden *Brevoortia tyrannus* larvae. Fish Bull 88:155–165.

Malpica-Cruz L, Herzka SZ, Sosa-Nishizaki O, Lazo JP (2012) Tissue-specific isotope trophic discrimination factors and turnover rates in a marine elasmobranch: empirical and modeling results. Can J Fish Aquat Sci 69:551–564. doi: 10.1139/f2011-172

Martin G, Thorrold S (2005) Temperature and salinity effects on magnesium, manganese, and barium incorporation in otoliths of larval and early juvenile spot *Leiostomus xanthurus*. Mar Ecol Prog Ser 293:223–232. doi: 10.3354/meps293223

Martin G, Wuenschel M (2006) Effect of temperature and salinity on otolith element incorporation in juvenile gray snapper *Lutjanus griseus*. Mar Ecol Prog Ser 324:229–239.

Martínez del Rio C, Wolf N, Carleton SA, Gannes LZ (2009) Isotopic ecology ten years after a call for more laboratory experiments. Biol Rev 84:91–111. doi: 10.1111/j.1469-185X.2008.00064.x

McClelland JW, Valiela I, Michener RH (1997) Nitrogen-stable isotope signatures in estuarine food webs : A record of increasing urbanization in coastal watersheds. Limnol Oceanogr 42:930–937.

McNatt RA, Rice JA (2004) Hypoxia-induced growth rate reduction in two juvenile estuary-dependent fishes. J Exp Mar Bio Ecol 311:147–156. doi: 10.1016/j.jembe.2004.05.006

Van der Merwe N, Lee-Throp J, Thackeray J, et al. (1990) Source-area determination of elephant ivory by isotopic analysis. Nature 346:744–746.

Middelburg JJ, Weijden CHVDW, Woittiez JRW (1988) Chemical processes affecting the mobility of major, minor, and trace elements during weathering of granitic rocks. Chem Geol 68:253–273.

Miller J (2009) The effects of temperature and water concentration on the otolith incorporation of barium and manganese in black rockfish *Sebastes melanops*. J Fish Biol 75:39–60. doi: 10.1111/j.1095-8649.2009.02262.x

Miller J (2011) Effects of water temperature and barium concentration on otolith composition along a salinity gradient: Implications for migratory reconstructions. J Exp Mar Bio Ecol 405:42–52. doi: 10.1016/j.jembe.2011.05.017

Miller MB, Clough AM, Batson JN, Vachet RW (2006) Transition metal binding to cod otolith proteins. J Exp Mar Bio Ecol 329:135–143. doi: 10.1016/j.jembe.2005.08.016

Minagawa M, Wada E (1984) Stepwise enrichment of $^{15}N$ along food chains: Further evidence and the relation between $\delta^{15}N$ and animal age. Geochim Cosmochim Acta 48:1135–1140. doi: 10.1016/0016-7037(84)90204-7

Mintenbeck K, Brey T, Jacob U, et al. (2008) How to account for the lipid effect on carbon stable-isotope ratio ($\delta^{13}C$): sample treatment effects and model bias. J Fish Biol 72:815–830. doi: 10.1111/j.1095-8649.2007.01754.x

Mohan JA, Halden NM, Rulifson RA (2015) Habitat use of juvenile striped bass *Morone saxatilis (*Actinopterygii: Moronidae) in rivers spanning a salinity gradient across a shallow wind-driven estuary. Environ Biol Fishes 98:1105–1116. doi: 10.1007/s10641-014-0344-6

Mohan J, Rahman M, Thomas P, Walther B (2014) Influence of constant and periodic experimental hypoxic stress on Atlantic croaker otolith chemistry. Aquat Biol 20:1–11. doi: 10.3354/ab00542

Mohan J, Walther BD (2014) Spatiotemporal variation of trace elements and stable isotopes in subtropical estuaries: II. Regional, local, and seasonal salinity-element relationships. Estuaries and Coasts. doi: 10.1007/s12237-014-9876-4

Mohan JA, Rulifson RA, Corbett DR, Halden NM (2012) Validation of oligohaline elemental otolith signatures of striped bass by use of in situ caging experiments and water chemistry. Mar Coast Fish 4:57–70. doi: 10.1080/19425120.2012.656533

Mooney RF, McClelland JW (2012) Watershed export events and ecosystem responses in the Mission–Aransas National Estuarine Research Reserve, South Texas. Estuaries and Coasts 35:1468–1485. doi: 10.1007/s12237-012-9537-4

Morris A, Mantoura R, Bale A, Howland R (1978) Very low salinity regions of estuaries: important sites for chemical and biological reactions. Nature 274:678–680.

Moser ML, Carolina N, Gerry LR (1989) Differential effects of salinity changes on two estuarine fishes, *Leiostomus xanthurus* and *Micropogonias undulatus*. 12:35–41.

Nagelkerken I, Sheaves M, Baker R, Connolly RM (2013) The seascape nursery: A novel spatial approach to identify and manage nurseries for coastal marine fauna. Fish Fish 362–371. doi: 10.1111/faf.12057

Negrel P, Allegre CJ, Dupre B, Lewin E (1993) Erosion sources determined by inversion of major and trace element ratios and strontium isotopic ratios in river water: The Congo Basin case. Earth Planet Sci Lett 120:59–76.

Nielsen-Gammon J, Zhang F, Odins A, Myoung B (2005) Extreme rainfall in Texas: patterns and predictability. Phys Geogr 26:340–364. doi: 10.2747/0272-3646.26.5.340

Nikinmaa M, Rees BB (2005) Oxygen-dependent gene expression in fishes. Am J Physiol Regul Integr Comp Physiol 288:R1079–90. doi: 10.1152/ajpregu.00626.2004

Nims MK, Walther BD (2014) Contingents of Southern Flounder from Subtropical Estuaries Revealed by Otolith Chemistry. Trans Am Fish Soc 143:721–731. doi: 10.1080/00028487.2014.892535

Nixon SW, Jones CM (1997) Age and growth of larval and juvenile Atlantic croaker, *Micropogonias undulatus*, from the Middle Atlantic Bight and estuarine waters of Virginia. Fish Bull 95:773–784.

Nye JA, Loewensteiner DA, Miller TJ (2010) Annual, seasonal, and regional variability in diet of Atlantic croaker (*Micropogonias undulatus*) in Chesapeake Bay. Estuaries and Coasts 34:691–700. doi: 10.1007/s12237-010-9348-4

Overstreet RM, Heard RW (1978) Food of the Atlantic Croaker, *Micropogonias undulatus*, from Mississippi Sound and the Gulf-of-Mexico. Gulf Res Reports 6:145–152.

Pakhomova S V., Hall POJ, Kononets MY, et al. (2007) Fluxes of iron and manganese across the sediment–water interface under various redox conditions. Mar Chem 107:319–331. doi: 10.1016/j.marchem.2007.06.001

Le Pape O, Bonhommeau S (2013) The food limitation hypothesis for juvenile marine fish. Fish Fish 16:373–398. doi: 10.1111/faf.12063

Paton C, Hellstrom J, Paul B, et al. (2011) Iolite: Freeware for the visualisation and processing of mass spectrometric data. J Anal At Spectrom 26:2508–2518. doi: 10.1039/c1ja10172b

Paucot H, Wollast R (1997) Transport and transformation of trace metals in the scheldt estuary. Mar Chem 58:229–244. doi: 10.1016/S0304-4203(97)00037-6

Payan P, Edeyer A, De Pontual H, et al. (1999) Chemical composition of saccular endolymph and otolith in fish inner ear: lack of spatial uniformity. Am J Physiol 277:R123–R131.

Payan P, De Pontual H, Bœuf G, Mayer-Gostan N (2004a) Endolymph chemistry and otolith growth in fish. Comptes Rendus Palevol 3:535–547. doi: 10.1016/j.crpv.2004.07.013

Payan P, Pontual H De, Edeyer A, et al. (2004b) Effects of stress on plasma homeostasis, endolymph chemistry, and check formation during otolith growth in rainbow trout (*Oncorhynchus mykiss*). Can J Fish Aquat Sci 61:1247–1255. doi: 10.1139/f04-059

Pentreath R (1976) Some further studies on the accumulation and retention of $^{66}$Zn and $^{54}$Mn by the plaice, *Pleuronectes platessa* L. J Exp Mar Bio Ecol 21:179–189.

Pentreath R (1973) The accumulation and retention of $^{65}$Zn and $^{54}$Mn by the plaice, *Pleuronectes platessa* L. J Exp Mar Bio Ecol 12:1–18.

Petersen JK, Pihl L (1995) Responses to hypoxia of plaice, *Pleuronectes platessa*, and dab, *Limanda limanda*, in the south-east Kattegat: distribution and growth. Environ Biol Fishes 43:311–321. doi: 10.1007/BF00005864

Peterson BJ (1999) Stable isotopes as tracers of organic matter input and transfer in benthic food webs: A review. Acta Oecologica 20:479–487. doi: 10.1016/S1146-609X(99)00120-4

Peterson BJ, Fry B (1987) Stable isotopes in ecosystem studies. Annu Rev Ecol Syst 18:293–320.

Peterson MS, Comyns BH, Rakocinski CF, Fulling GL (1999) Does salinity affect somatic growth in early juvenile Atlantic croaker, *Micropogonias undulatus* (L.)? J Exp Mar Bio Ecol 238:199–207.

Pihl L, Baden SP, Diaz RJ, Schaffner LC (1992) Hypoxia-induced structural changes in the diet of bottom-feeding fish and Crustacea. Mar Biol 112:349–361.

Pinnegar J, Polunin N (1999) Differential fractionation of $\delta^{13}$C and $\delta^{15}$N among fish tissues: implications for the study of trophic interactions. Funct Ecol 13:225–231.

Post DM (2002) Using stable isotopes to estimate trophic position: Models, methods, and assumptions. Ecology 83:703–718.

Post DM, Layman CA, Arrington DA, et al. (2007) Getting to the fat of the matter: models, methods and assumptions for dealing with lipids in stable isotope analyses. Oecologia 152:179–89. doi: 10.1007/s00442-006-0630-x

Powers SP, Peterson CH, Christian RR, et al. (2005) Effects of eutrophication on bottom habitat and prey resources of demersal fishes. Mar Ecol Prog Ser 302:233–243. doi: 10.3354/meps302233

Prince ED, Luo J, Phillip Goodyear C, et al. (2010) Ocean scale hypoxia-based habitat compression of Atlantic istiophorid billfishes. Fish Oceanogr 19:448–462. doi: 10.1111/j.1365-2419.2010.00556.x

Rabalais N, Turner R (2001) Hypoxia in the Northern Gulf of Mexico: description, causes and change. In: Rabalais N, Turner R (eds) Coast. hypoxia consequences living Resour. Ecosyst. American Geophysical Union, Washington DC, pp 1–36

Radtke RL (1984) Cod fish otoliths: information storage structures. Flodevigen Rapp 1:273–298.

Radtke RL (1989) Strontium-calcium concentration ratios in fish otoliths as environmental indicators. Comp Biochem Physiol A Comp Physiol 92:189–193.

Rahman MS, Thomas P (2007) Molecular cloning, characterization and expression of two hypoxia-inducible factor alpha subunits, HIF-1alpha and HIF-2alpha, in a hypoxia-tolerant marine teleost, Atlantic croaker (*Micropogonias undulatus*). Gene 396:273–282. doi: 10.1016/j.gene.2007.03.009

Rahman MS, Thomas P (2012) Effects of hypoxia exposure on hepatic cytochrome P450 1A (CYP1A) expression in Atlantic croaker: molecular mechanisms of CYP1A down-regulation. PLoS One 7:e40825. doi: 10.1371/journal.pone.0040825

Ray GC (2005) Connectivities of estuarine fishes to the coastal realm. Estuar Coast Shelf Sci 64:18–32. doi: 10.1016/j.ecss.2005.02.003

Richard D, Sunby B, Mucci A (2013) Kinetics of manganese adsorption, desorption, and oxidation in coastal marine sediments. Limnol Oceanogr 58:987–996.

Robbins CT, Felicetti LA, Florin ST (2010) The impact of protein quality on stable nitrogen isotope ratio discrimination and assimilated diet estimation. Oecologia 162:571–579. doi: 10.1007/s00442-009-1485-8

Roberts JJ, Grecay PA, Ludsin SA, et al. (2012) Evidence of hypoxic foraging forays by yellow perch (*Perca flavescens*) and potential consequences for prey consumption. Freshw Biol 57:922–937. doi: 10.1111/j.1365-2427.2012.02753.x

Roberts JJ, Höök TO, Ludsin SA, et al. (2009) Effects of hypolimnetic hypoxia on foraging and distributions of Lake Erie yellow perch. J Exp Mar Bio Ecol 381:S132–S142. doi: 10.1016/j.jembe.2009.07.017

Rooker JR, Holt SA, Soto MA, Holt GJ (1998) Postsettlement patterns of habitat use by Sciaenid fishes in subtropical seagrass meadows. Estuaries 21:318–327.

Rooker JR, Kraus RT, Secor DH (2004) Dispersive behaviors of black drum and red drum: Is otolith Sr:Ca a reliable indicator of salinity history? Estuaries 27:334–341. doi: 10.1007/BF02803389

Rose KA, Adamack AT, Murphy CA, et al. (2009) Does hypoxia have population-level effects on coastal fish? Musings from the virtual world. J Exp Mar Bio Ecol 381:S188–S203. doi: 10.1016/j.jembe.2009.07.022

Rosenberg A, Bigford TE, Leathery S, et al. (2000) Ecosystem approaches to fishery management through essential fish habitat. Bull Mar Sci 66:535–542.

Sadovy Y, Severin KP (1992) Trace elements in biogenic aragonite: correlation of body growth rate and stronitum levels in the otoliths of the white grunt, *Haemulon plumieri* (Pisces: Haemulidae). Bull Mar Sci 50:237–257.

Sanchez-Jerez P, Gillanders BM, Kingsford MJ (2002) Spatial variability of trace elements in fish otoliths: comparison with dietary items and habitat constituents in seagrass meadows. J Fish Biol 61:801–821. doi: 10.1006/jfbi.2002.2109

Schlacher TA, Mondon JA, Connolly RM (2007) Estuarine fish health assessment: evidence of wastewater impacts based on nitrogen isotopes and histopathology. Mar Pollut Bull 54:1762–1776. doi: 10.1016/j.marpolbul.2007.07.014

Secor DH, Henderson-Arzapalo A, Piccoli PM (1995) Can otolith microchemistry chart patterns of migration and habitat utilization in anadromous fishes? J Exp Mar Bio Ecol 192:15–33.

Shaw T, Moore W, Kloepfer J, Sochaski M (1998) The flux of barium to the coastal waters of the southeastern USA: The importance of submarine groundwater discharge. Geochim Cosmochim Acta 62:3047–3054.

Sheaves M, Baker R, Nagelkerken I, Connolly RM (2014) True value of estuarine and coastal nurseries for fish: Incorporating complexity and dynamics. Estuaries and Coasts. doi: 10.1007/s12237-014-9846-x

Shiller AM (1997) Dissolved trace elements in the Mississippi River: Seasonal, interannual, and decadal variability. Geochim Cosmochim Acta 61:4321–4330. doi: 10.1016/S0016-7037(97)00245-7

Shim MJ, Swarzenski PW, Shiller AM (2012) Dissolved and colloidal trace elements in the Mississippi River delta outflow after Hurricanes Katrina and Rita. Cont Shelf Res 42:1–9. doi: 10.1016/j.csr.2012.03.007

Sigman DM, DiFiore PJ, Hain MP, et al. (2009) Sinking organic matter spreads the nitrogen isotope signal of pelagic denitrification in the North Pacific. Geophys Res Lett 36:1–5. doi: 10.1029/2008GL035784

Sinclair D (2005) Correlated trace element "vital effects" in tropical corals: A new geochemical tool for probing biomineralization. Geochim Cosmochim Acta 69:3265–3284. doi: 10.1016/j.gca.2005.02.030

Sinclair DJ, McCulloch MT (2004) Corals record low mobile barium concentrations in the Burdekin River during the 1974 flood: evidence for limited Ba supply to rivers? Palaeogeogr Palaeoclimatol Palaeoecol 214:155–174. doi: 10.1016/j.palaeo.2004.07.028

Slomp CP, Malchaert JFP, Lohse L, Van Raaphorst W (1997) Iron and manganese cycling in different sedimentary environments on the North Sea continental margin. Cont Shelf Res 17:1083–1117.

Slowey JF, Hood DW (1971) Copper, manganese and zinc concentrations in Gulf of Mexico waters. Geochim Cosmochim Acta 35:121–138.

Sotiropoulos M, Tonn W, Wassenaar L (2004) Effects of lipid extraction on stable carbon and nitrogen isotope analyses of fish tissues: potential consequences for food web studies. Ecol Freshw Fish 13:155–160.

Sponheimer M, Robinson T, Cerling T, et al. (2006) Turnover of stable carbon isotopes in the muscle, liver, and breath $CO_2$ of alpacas (*Lama pacos*). Rapid Commun Mass Spectrom 20:1395–9. doi: 10.1002/rcm.2454

Stalker JC, Price RM, Swart PK (2009) Determining spatial and temporal inputs of freshwater, including submarine groundwater discharge, to a subtropical estuary using geochemical tracers, Biscayne Bay, south Florida. Estuaries and Coasts 32:694–708. doi: 10.1007/s12237-009-9155-y

Statham PJ, Connelly DP, German CR, et al. (2005) Spatially complex distribution of dissolved manganese in a fjord as revealed by high-resolution in situ sensing using the autonomous underwater vehicle Autosub. Environ Sci Technol 39:9440–9445.

Stecher HA, Kogut MB (1999) Rapid barium removal in the Delaware estuary. Geochim Cosmochim Acta 63:1003–1012.

Stolpe B, Guo L, Shiller AM, Hassellöv M (2010) Size and composition of colloidal organic matter and trace elements in the Mississippi River, Pearl River and the northern Gulf of Mexico, as characterized by flow field-flow fractionation. Mar Chem 118:119–128. doi: 10.1016/j.marchem.2009.11.007

Strasser CA, Mullineaux LS, Walther BD (2008) Growth rate and age effects on *Mya arenaria* shell chemistry: Implications for biogeochemical studies. J Exp Mar Bio Ecol 355:153–163. doi: 10.1016/j.jembe.2007.12.022

Sturrock AM, Trueman CN, Darnaude AM, Hunter E (2012) Can otolith elemental chemistry retrospectively track migrations in fully marine fishes? J Fish Biol 81:766–95. doi: 10.1111/j.1095-8649.2012.03372.x

Sturrock AM, Trueman CN, Milton JA, et al. (2014) Physiological influences can outweigh environmental signals in otolith microchemistry research. Mar Ecol Prog Ser 500:245–264. doi: 10.3354/meps10699

Suzuki KW, Kasai A, Nakayama K, Tanaka M (2005) Differential isotopic enrichment and half-life among tissues in Japanese temperate bass (*Lateolabrax japonicus*) juveniles: implications for analyzing migration. Can J Fish Aquat Sci 62:671–678. doi: 10.1139/f04-231

Sweeting C, Polunin N, Jennings S (2006) Effects of chemical lipid extraction and arithmetic lipid correction on stable isotope ratios of fish tissues. Rapid Commun Mass Spectrom 20:595–601. doi: 10.1002/rcm.2347

Switzer TS, Chesney EJ, Baltz DM (2009) Habitat selection by flatfishes in the northern Gulf of Mexico: Implications for susceptibility to hypoxia. J Exp Mar Bio Ecol 381:S51–S64. doi: 10.1016/j.jembe.2009.07.011

Taylor JC, Rand PS, Jenkins J (2007) Swimming behavior of juvenile anchovies (Anchoa spp.) in an episodically hypoxic estuary: Implications for individual energetics and trophic dynamics. Mar Biol 152:939–957. doi: 10.1007/s00227-007-0745-6

Thamdrup B, Glud RN, Hansen JW (1994) Manganese oxidation and in situ manganese fluxes from a coastal sediment. Geochim Cosmochim Acta 58:2563–2570.

Thomas P, Rahman MS (2009a) Biomarkers of hypoxia exposure and reproductive function in Atlantic croaker: A review with some preliminary findings from the northern Gulf of Mexico hypoxic zone. J Exp Mar Bio Ecol 381:S38–S50. doi: 10.1016/j.jembe.2009.07.008

Thomas P, Rahman MS (2009b) Chronic hypoxia impairs gamete maturation in Atlantic croaker induced by progestins through nongenomic mechanisms resulting in reduced reproductive success. Environ Sci Technol 43:4175–4180.

Thomas P, Rahman MS, Khan IA, Kummer JA (2007) Widespread endocrine disruption and reproductive impairment in an estuarine fish population exposed to seasonal hypoxia. Proc Biol Sci 274:2693–2701. doi: 10.1098/rspb.2007.0921

Thomas P, Rahman S (2012) Extensive reproductive disruption, ovarian masculinization and aromatase suppression in Atlantic croaker in the northern Gulf of Mexico hypoxic zone. Proc Natl Acad Sci U S A 279:28–38. doi: 10.1098/rspb.2011.0529

Thorrold SR, Jones CM, Campana SE (1997) Response of otolith microchemistry to environmental variations experienced by larval and juvenile Atlantic croaker (*Micropogonias undulatus*). Limnol Oceanogr 42:102–111.

Thorrold SR, Shuttleworth S (2000) In situ analysis of trace elements and isotope ratios in fish otoliths using laser ablation sector field inductively coupled plasma mass spectrometry. Can J Fish Aquat Sci 57:1232–1242. doi: 10.1139/f00-054

Tieszen LL, Boutton TW, Tesdahl KG, Slade NA (1983) Fractionation and turnover of stable carbon isotopes in animal tissues: Implications for $\delta^{13}C$ analysis of diet. Oecologia 57:32–37.

Tolan JM (2007) El Niño-Southern Oscillation impacts translated to the watershed scale: Estuarine salinity patterns along the Texas Gulf Coast, 1982 to 2004. Estuar Coast Shelf Sci 72:247–260. doi: 10.1016/j.ecss.2006.10.018

Trefry J, Presley B (1982) Manganese fluxes from Mississippi Delta sediments. Geochim Cosmochim Acta 46:1715–1726.

Trueman CN, Mackenzie KM, Palmer MR (2012) Identifying migrations in marine fishes through stable-isotope analysis. J Fish Biol 81:826–847. doi: 10.1111/j.1095-8649.2012.03361.x

Trueman CN, McGill R a R, Guyard PH (2005) The effect of growth rate on tissue-diet isotopic spacing in rapidly growing animals. An experimental study with Atlantic salmon (*Salmo salar*). Rapid Commun Mass Spectrom 19:3239–3247. doi: 10.1002/rcm.2199

Uddameri V, Singaraju S, Hernandez EA (2014) Temporal variability of freshwater and pore water recirculation components of submarine groundwater discharges at Baffin Bay, Texas. Environ Earth Sci 71:2517–2533. doi: 10.1007/s12665-013-2902-1

Vasconcelos RP, Reis-Santos P, Costa MJ, Cabral HN (2011) Connectivity between estuaries and marine environment: Integrating metrics to assess estuarine nursery function. Ecol Indic 11:1123–1133. doi: 10.1016/j.ecolind.2010.12.012

Walther B, Nims MK (2015) Spatiotemporal variation of trace elements and stable isotopes in subtropical estuaries: I. Freshwater endmembers and mixing curves. Estuaries and Coasts 38:754–768.

Walther B, Thorrold S (2006) Water, not food, contributes the majority of strontium and barium deposited in the otoliths of a marine fish. Mar Ecol Prog Ser 311:125–130. doi: 10.3354/meps311125

Walther BD, Kingsford MJ, O'Callaghan MD, McCulloch MT (2010) Interactive effects of ontogeny, food ration and temperature on elemental incorporation in otoliths of a coral reef fish. Environ Biol Fishes 89:441–451. doi: 10.1007/s10641-010-9661-6

Walther BD, Limburg KE (2012) The use of otolith chemistry to characterize diadromous migrations. J Fish Biol 81:796–825. doi: 10.1111/j.1095-8649.2012.03371.x

Walther BD, Thorrold SR (2008) Continental-scale variation in otolith geochemistry of juvenile American shad (*Alosa sapidissima*). Can J Fish Aquat Sci 65:2623–2635. doi: 10.1139/F08-164

Walther BD, Thorrold SR, Olney JE (2008) Geochemical signatures in otoliths record natal origins of American shad. Trans Am Fish Soc 137:57–69. doi: 10.1577/T07-029.1

Wannamaker CM, Rice JA (2000) Effects of hypoxia on movements and behavior of selected estuarine organisms from the southeastern United States. J Exp Mar Bio Ecol 249:145–163. doi: 10.1016/S0022-0981(00)00160-X

Ward GH (2010) Inflows to San Antonio Bay. Austin, 91p

Ward J (1963) Hierarchical grouping to optimize an objective function. J Am Statisitical Assoc 58:236–244.

Warlen SM, Burke JS (1990) Immigration of larvae of fall/winter spawning marine fishes into a North Carolina estuary. Estuaries 13:453–461. doi: 10.1007/BF02689333

Watanabe Y, Seikai T, Tominaga O (2005) Estimation of growth and food consumption in juvenile Japanese flounder *Paralichthys olivaceus* using carbon stable isotope ratio δ13C under laboratory conditions. J Exp Mar Bio Ecol 326:187–198. doi: 10.1016/j.jembe.2005.05.020

Wen L, Santschi P, Gill G, Paternostro C (1999) Estuarine trace metal distributions in Galveston Bay : importance of colloidal forms in the speciation of the dissolved phase. Mar Chem 63:185–212.

White ML, Chittenden ME (1977) Age determination, reproduction, and population dynamics of the Atlantic croaker, *Micropogonias undulatus*. Fish Bull 75:109–123.

Woodcock SH, Munro AR, Crook DA, Gillanders BM (2012) Incorporation of magnesium into fish otoliths: Determining contribution from water and diet. Geochim Cosmochim Acta 94:12–21. doi: 10.1016/j.gca.2012.07.003

Woodland RJ, Secor DH (2011) Differences in juvenile trophic niche for two coastal fish species that use marine and estuarine nursery habitats. Mar Ecol Prog Ser 439:241–254. doi: 10.3354/meps09310

Wu RSS (2002) Hypoxia: from molecular responses to ecosystem responses. Mar Pollut Bull 45:35–45.

Xia B, Gao Q, Dong S, Wang F (2013a) Carbon stable isotope turnover and fractionation in grass carp *Ctenopharyngodon idella* tissues. Aquat Biol 19:207–216. doi: 10.3354/ab00528

Xia B, Gao Q, Li H, et al. (2013b) Turnover and fractionation of nitrogen stable isotope in tissues of grass carp *Ctenopharyngodon idellus*. Aquac Environ Interact 3:177–186. doi: 10.3354/aei00061

Yakupzack PM, Herke W, Perry WG (1977) Emigration of juvenile Atlantic croakers, *Micropogon undulatus*, from a semi-impounded marsh in southwestern Louisiana. Trans Am Fish Soc 106:538–544.

Zhang H, Ludsin SA, Mason DM, et al. (2009) Hypoxia-driven changes in the behavior and spatial distribution of pelagic fish and mesozooplankton in the northern Gulf of Mexico. J Exp Mar Bio Ecol 381:S80–S91. doi: 10.1016/j.jembe.2009.07.014

Zhang J (1995) Geochemistry of trace metals from Chinese river/estuary systems: an overview. Estuar Coast Shelf Sci 41:631–658. doi: 10.1006/ecss.1995.0082

Zuanon J, Pezzato A, Pezzato L, et al. (2006) Muscle $\delta^{13}C$ change in Nile tilapia (*Oreochromis niloticus*): effects of growth and carbon turnover. Comp Biochem Physiol Part B 145:101–7. doi: 10.1016/j.cbpb.2006.06.009

Zwolsman JJ., van Eck GT. (1999) Geochemistry of major elements and trace metals in suspended matter of the Scheldt estuary, southwest Netherlands. Mar Chem 66:91–111. doi: 10.1016/S0304-4203(99)00026-2